uOttawa

L'Université canadienne
Canada's university

FACULTÉ DES ÉTUDES SUPÉRIEURES ET POSTDOCTORALES

uOttawa

L'Université canadienne
Canada's university

FACULTY OF GRADUATE AND POSTDOCTORAL STUDIES

Helga Clare Halvorsen
AUTEUR DE LA THÈSE / AUTHOR OF THESIS

Ph.D. (Chemistry)
GRADE / DEGREE

Department of Chemistry
FACULTÉ, ÉCOLE, DÉPARTEMENT / FACULTY, SCHOOL, DEPARTMENT

Stabilization and Characterization of Pt Nano-Catalysts Formed on Highly Ordered Pyrolytic Graphite
TITRE DE LA THÈSE / TITLE OF THESIS

B. MacDougall
DIRECTEUR (DIRECTRICE) DE LA THÈSE / THESIS SUPERVISOR

CO-DIRECTEUR (CO-DIRECTRICE) DE LA THÈSE / THESIS CO-SUPERVISOR

EXAMINATEURS (EXAMINATRICES) DE LA THÈSE / THESIS EXAMINERS

S. Barry

D. Bryce

K. Kinoshita

D. Richeson

Gary W. Slater
Le Doyen de la Faculté des études supérieures et postdoctorales / Dean of the Faculty of Graduate and Postdoctoral Studies

Stabilization and Characterization of Pt Nano-catalysts formed on Highly Ordered Pyrolytic Graphite

Helga C. Halvorsen

Thesis submitted to the
Faculty of Graduate & Postdoctoral Studies
University of Ottawa
in partial fulfillment of the requirements for the
Ph. D. degree in the
Ottawa-Carleton Chemistry Institute

© Helga Halvorsen, Ottawa, Canada, 2009

Library and Archives Canada

Published Heritage Branch

395 Wellington Street
Ottawa ON K1A 0N4
Canada

Bibliothèque et Archives Canada

Direction du Patrimoine de l'édition

395, rue Wellington
Ottawa ON K1A 0N4
Canada

Your file Votre référence
ISBN: 978-0-494-61392-4
Our file Notre référence
ISBN: 978-0-494-61392-4

NOTICE:

The author has granted a non-exclusive license allowing Library and Archives Canada to reproduce, publish, archive, preserve, conserve, communicate to the public by telecommunication or on the Internet, loan, distribute and sell theses worldwide, for commercial or non-commercial purposes, in microform, paper, electronic and/or any other formats.

The author retains copyright ownership and moral rights in this thesis. Neither the thesis nor substantial extracts from it may be printed or otherwise reproduced without the author's permission.

AVIS:

L'auteur a accordé une licence non exclusive permettant à la Bibliothèque et Archives Canada de reproduire, publier, archiver, sauvegarder, conserver, transmettre au public par télécommunication ou par l'Internet, prêter, distribuer et vendre des thèses partout dans le monde, à des fins commerciales ou autres, sur support microforme, papier, électronique et/ou autres formats.

L'auteur conserve la propriété du droit d'auteur et des droits moraux qui protège cette thèse. Ni la thèse ni des extraits substantiels de celle-ci ne doivent être imprimés ou autrement reproduits sans son autorisation.

In compliance with the Canadian Privacy Act some supporting forms may have been removed from this thesis.

While these forms may be included in the document page count, their removal does not represent any loss of content from the thesis.

Conformément à la loi canadienne sur la protection de la vie privée, quelques formulaires secondaires ont été enlevés de cette thèse.

Bien que ces formulaires aient inclus dans la pagination, il n'y aura aucun contenu manquant.

Canada

Abstract

Platinum catalysts are prepared on highly ordered pyrolytic graphite (HOPG). Two different methods are used to deposit platinum onto HOPG; electrochemical deposition and impregnation followed by thermal decomposition. To increase interactions between the Pt deposits and the carbon support, HOPG is oxidized either electrochemically or with ozone gas. The combination two different deposition techniques and three different substrates (freshly cleaved, electrochemically, and ozone oxidized HOPG) results in six different Pt/carbon electrodes that are studied with respect to their particle morphology, activity towards electrochemically oxidizing adsorbed carbon monoxide (CO_{ads}), and electrochemical stability.

Oxidation of HOPG generated pits on the basal plane; ozone oxidation formed nano-pits, < 10 nm in diameter; electrochemical oxidation produced larger pits, > 85 nm in diameter. Regardless of the substrate pre-treatment, electrochemical deposition resulted in clusters of nanoparticles, while impregnation followed by thermal decomposition resulted in individual Pt nano-catalysts. Regardless of the deposition technique, Pt particles are confined to step edges on freshly cleaved HOPG, and dispersed over the basal plane on oxidized HOPG.

When comparing all six electrodes it became evident that substrate pre-treatment did not affect the electrochemical activity of the electrodes towards the oxidation of CO_{ads}, while the method of Pt deposition did significantly affect the measured activity. For example, Pt/HOPG electrodes prepared by electrochemical deposition using short deposition times,

< 10 s, show slower CO_{ads} electro-oxidation kinetics compared to polycrystalline Pt foil, while electrodes prepared by impregnation followed by thermal decomposition show faster kinetics compared to polycrystalline Pt foil.

For a given substrate, Pt/HOPG electrodes prepared by impregnation followed by thermal decomposition proved to be more electrochemically stable than electrodes prepared by electrochemical deposition. For a given deposition technique, ozone oxidized HOPG has the greatest stabilizing effect. The chemical interaction between the Pt catalyst and the carbon substrate was studied by XPS analysis. It was found that Pt 4f spectra of all six Pt/HOPG electrodes were shifted to higher binding energies indicating that Pt was interacting with the HOPG possibly forming Pt-C bonds. The XPS results indicate that the electrochemical stability is positively influenced by the interaction between the catalyst and the carbon support.

Acknowledgments

I would like to extend my gratitude to Dr. Barry MacDougall, my Supervisor, for his constant guidance and support over the last four years. Without a doubt this work would not have been completed at the same level of quality if Dr. MacDougall was not involved.

I would also like to praise Dr. Christina Bock for her day-to-day assistance. Dr. Bock provided a sounding board for many of my theories. She asked the needed questions that helped the theories to be more diligently tested so that they could be proved or disproved, as the case may be.

Over the time I worked on my thesis research I have had the pleasure to share lab space with several excellent scientists. In particular, Dr. Laurent Birry who provided guidance with both experimental and theoretical understanding of electrochemical impedance spectroscopy. Dr. Anne Co, always made herself available to discuss the many theories of electrochemistry. Dr. Yaser Abu-Lebdeh, Dr. Fabrice Courtel, Dr. Elena Baranova, in addition to Dr. Birry and Dr. Co provided a supportive scientific environment that only bettered the quality of my work.

I would like to extend my appreciation to David Kingston and Dr. Shery Chan for their assistance with X-ray photoelectron spectroscopy and high resolution transmission electron microscopy, respectively.

Curriculum Vitae

EDUCATION

Masters of Science; Chemistry (2004)

The University of Western Ontario; London, Ontario, Canada.

AWARDS

Ontario Graduate Scholarship (academic years 2006/2007, 2007/2008 & 2008/2009).

Safety Management Systems Health and Safety Challenge Award (2007).

University of Ottawa Excellence Scholarship (academic years 2006/2007, 2007/2008 & 2008/2009).

University of Ottawa Entrance Scholarship (academic years 2004/2005 & 2005/2006).

Ottawa-Carleton Chemistry Institute Day; Canadian Institute of Chemistry Local Award (2006).

Ontario Graduate Scholarship in Science and Technology (academic year 2002/2003).

Special University Scholarship (academic year 2001/2002).

South-Western Ontario University Student Chemistry Conference; Honourable Mention (2001).

University of Western Ontario Entrance Scholarship (academic year 1997/1998).

CONFERENCE PRESENTATIONS

H. Halvorsen, C. Bock, and B. MacDougall. "Stabilization and characterization of Pt nano-catalysts formed on oxidized HOPG" Canadian Symposium on Catalysis; Kingston, Canada. Oral presentation (2008).

H. Halvorsen, C. Bock, and B. MacDougall. "Stabilization and characterization of Pt nano-catalysts formed on oxidized HOPG" FCRC-NRC Fuel Cell Colloquium; Ottawa, Canada. Poster presentation (2007).

H. Halvorsen, C. Bock, B. MacDougall, and D. Wang. "Stabilization and characterization of Pt nanoparticles on HOPG." Electrochemical Society Meeting; Washington, USA. Oral Presentation (2007).

H. Halvorsen, C. Bock, and B. MacDougall. "Platinum nano-catalysts on oxidized highly ordered pyrolytic graphite." Ottawa-Carleton Chemistry Institute Nanochemistry Workshop; Ottawa, Canada. Oral Presentation (2007).

H. Halvorsen, C. Bock, and B. MacDougall. "Potentiostatic deposition of platinum onto unmodified and ozone modified HOPG." Gordon Research Conference; New London, USA. Poster presentation (2006).

H. Halvorsen, C. Bock, and B. MacDougall. "Electrochemical deposition of platinum on unmodified and ozone modified HOPG." FCRC-NRC Fuel Cell Colloquium; Kingston, Canada. Poster presentation (2006).

H. Halvorsen, C. Bock, and B. MacDougall. "Structure-activity relationships for nano-sized platinum-based catalyst." Ottawa-Carleton Chemistry Institute Day; Ottawa, Canada. Oral presentation (2006).

H. Halvorsen, C. Bock, and B. MacDougall. "Electrochemical deposition of platinum on modified and unmodified surfaces." Electrochemical Society: Canadian Section Fall Symposium; Sherbrooke, Canada. Poster presentation (2005).

H. Halvorsen and D.G. Leaist. "Aqueous polymer-micelle interactions. Canadian Society for Chemistry Conference; Vancouver, Canada. Poster presentation (2002).

H. Halvorsen and S. McIntyre. "Surface analysis of the initial stages of labradorite weathering." South-Western Ontario University Student Chemistry Conference; Toronto, Canada. Oral Presentation (2001).

PUBLICATIONS

H. Halvorsen, C. Bock, B. MacDougall, and D. Wang. "Stabilization and characterization of Pt nanoparticles on HOPG." In: G. Amatucci, A. Manthiram, W. Van Schalkwijk, R. Mantz, C. Bock, V. Ramani, editors. Nanomaterials for energy conversion and storage symposium. ECS Transactions, Electrochemical Society Inc. Vol 11. (2008).

C. Bock, B. MacDougall, and H. Halvorsen. "Catalysis synthesis techniques." In: J. Zhang editor. PEM Fuel Cell Electrocatalysts and Catalyst Layers - Fundamentals & Applications. Springer. (submitted 2007).

H. Halvorsen, E. Wygnal, M.R. MacIver, and D.G. Leaist. "Ternary Mutual Diffusion Coefficients from Error-Function Dispersion Profiles: Aqueous Solutions of Triton X-100 Micelles + Poly(ethylene glycol)" J. Chem. Eng. Data 52:442-448 (2007).

C. Bock, B. MacDougall, and H. Halvorsen. "Nano-technology related to electro-catalysis for energy conversion and environmental processes." In: Y. Lin, H.S. Nalwa, editors. Handbook of Electrochemical Nanotechnology. Amer. sci. pub. (accepted 2006).

H.C. Halvorsen and D.G. Leaist. "An electrostatic mechanism for the coupled diffusion of polymer molecules and ionic micelles. Aqueous poly(ethylene glycol) + sodium dodecyl sulfate solutions." Phys. Chem. Chem. Phys. 6:3515–3523 (2004).

P. Jakupi, H. Halvorsen and D.G. Leaist. "A thermodynamic Interpretation of the "excluded-volume effect" in coupled diffusion." J. Phys. Chem. B.108:7978–7985 (2004).

Table of Contents

Table of Figures

List of Tables

List of Abbreviations and Symbols

AFC	Alkaline fuel cell
C_{dl}	Double layer capacitance of the electrode
CE	Counter electrode
CO_{ads}	Adsorbed carbon monoxide
CO_{sol}	CO dissolved in solution
CVD	Chemical vapour deposition
DMFC	Direct methanol fuel cell
E^0	Thermodynamic cell voltage
E_H^0	Thermal cell voltage
E_R^a	Reversible potential of the anode
E_R^c	Reversible potential of the cathode
$E(i)$	Potential at a given current
F	Faraday's constant 96485 C mol^{-1}
ΔG^0	Change in free energy at standard state
h	Planck Constant
ΔH^0	Change in Enthalpy at standard state
H_{ads}	Adsorbed hydrogen
H_{des}	Desorbed hydrogen
HOPG	Highly ordered pyrolytic graphite
HOPG-E	Electrochemically oxidized HOPG
HOPG-FC	Freshly cleaved HOPG
HOPG-O_3	Ozone oxidized HOPG
HRTEM	High resolution transmission electron microscopy
I	Current, amps (A)
i	Current density, (A cm^{-2})
m	Number of moles of product formed (see Equation 2.7), mass of electron (Equation 2.26)
MCFC	Molten carbonate fuel cell
MSE	Mercury sulphate electrode; Hg/Hg_2SO_4, 0.5 M H_2SO_4

n	Number of electrons
OPD	Overpotential deposition
PAFC	Phosphoric acid fuel cell
PEG	Polyethylene glycol
PEMFC	Proton exchange membrane fuel cell
PVD	Physical vapour deposition
Q	Charge
Q_{COads}	CO_{ads} stripping charge (μC)
R	Roughness factor
RE	Reference electrode
ΔS^0	Change in Entropy at standard conditions
SCE	Saturated calomel electrode; Hg/Hg_2Cl_2 sat. KCl
SEM	Scanning electron microscopy
SOFC	Solid oxide fuel cell
STM	Scanning tunnelling microscopy
TEM	Transmission electron microscopy
UPD	Under potential deposition
V	Cell voltage
WE	Working electrode
XPS	X-ray photoelectron spectroscopy
z_i	Charge of species i
η	Overpotential
θ_B	Brags Angle
$\bar{\mu}_i$	Electrochemical potential of species i
μ_i	Chemical potential of species i
ξ_{load}	Load efficiency
ξ_{th}	Thermodynamic efficiency
υ	Sweep rate (mV s^{-1}); (frequency of photon in XPS)
Φ	Inner potential of a phase

List of Abbreviations and Symbols

AFC	Alkaline fuel cell
C_{dl}	Double layer capacitance of the electrode
CE	Counter electrode
CO_{ads}	Adsorbed carbon monoxide
CO_{sol}	CO dissolved in solution
CVD	Chemical vapour deposition
DMFC	Direct methanol fuel cell
E^0	Thermodynamic cell voltage
E_H^0	Thermal cell voltage
E_R^a	Reversible potential of the anode
E_R^c	Reversible potential of the cathode
$E(i)$	Potential at a given current
F	Faraday's constant 96485 C mol^{-1}
ΔG^0	Change in free energy at standard state
h	Planck Constant
ΔH^0	Change in Enthalpy at standard state
H_{ads}	Adsorbed hydrogen
H_{des}	Desorbed hydrogen
HOPG	Highly ordered pyrolytic graphite
HOPG-E	Electrochemically oxidized HOPG
HOPG-FC	Freshly cleaved HOPG
HOPG-O_3	Ozone oxidized HOPG
HRTEM	High resolution transmission electron microscopy
I	Current, amps (A)
i	Current density, (A cm^{-2})
m	Number of moles of product formed (see Equation 2.7), mass of electron (Equation 2.26)
MCFC	Molten carbonate fuel cell
MSE	Mercury sulphate electrode; Hg/Hg_2SO_4, 0.5 M H_2SO_4

n	Number of electrons
OPD	Overpotential deposition
PAFC	Phosphoric acid fuel cell
PEG	Polyethylene glycol
PEMFC	Proton exchange membrane fuel cell
PVD	Physical vapour deposition
Q	Charge
Q_{COads}	CO_{ads} stripping charge (μC)
R	Roughness factor
RE	Reference electrode
ΔS^0	Change in Entropy at standard conditions
SCE	Saturated calomel electrode; Hg/Hg_2Cl_2 sat. KCl
SEM	Scanning electron microscopy
SOFC	Solid oxide fuel cell
STM	Scanning tunnelling microscopy
TEM	Transmission electron microscopy
UPD	Under potential deposition
V	Cell voltage
WE	Working electrode
XPS	X-ray photoelectron spectroscopy
z_i	Charge of species i
—	
η	Overpotential
θ_B	Brags Angle
$\bar{\mu}_i$	Electrochemical potential of species i
μ_i	Chemical potential of species i
ξ_{load}	Load efficiency
ξ_{th}	Thermodynamic efficiency
υ	Sweep rate ($mV\ s^{-1}$); (frequency of photon in XPS)
Φ	Inner potential of a phase

Chapter One

Introduction

1.1 THE IMPORTANCE OF CATALYSIS

Chemical reactions can be controlled by varying the reaction temperature, pressure, contact time, as well as the concentration of reactants and products. Increasing reaction kinetics can be achieved by simply increasing the reaction temperature and pressure. However, this approach is energy intensive, non-selective, and results in corrosion or damage of industrial equipment. Another approach involves using a catalyst to increase reaction kinetics and/or selectivity. Catalysts have been used for centuries; for example, inorganic catalysts were used to produce soap while enzymes were used to produce cheeses, wines, and other foods and beverages. However, it was only in the early 1800's that catalysis developed as an area of chemical research. In 1875 the first industrial application of a catalyzed reaction, the large scale production of sulfuric acid utilizing platinum as a catalyst, was achieved.[1] Catalyzed reactions allow for lower reaction temperatures and pressures, thereby decreasing operational costs.

To understand the importance of catalysis one must understand the vast number of products that result from catalyzed process/reactions. To list these products would be tedious, however one can begin to appreciate the importance of catalysts by considering that in the Western world it would be impossible to live a single day without using a product that

somehow required a catalyst to be made or requires a catalyst to work. For example, since the early 1900s the synthesis of ammonia has been catalyzed by Fe/Al_2O_3.[2] This single reaction revolutionized the agriculture industry increasing food production and ensuring the capability of feeding the masses of the world. Another example of a catalyst having significant impact on an industry is the process of catalytically cracking petroleum crude feedstock.[1] This process allows refineries to increase gasoline yield and produce higher octane fuels. The chemical and polymer industries greatly benefited from the discovery that $AlCl_3$ catalysts could be used for the production of polypropylene at low pressures.[2] Environmental concerns regarding ground level smog caused by the automobile industry were addressed with the introduction of catalytic converters that remove carbon monoxide, un-reacted hydrocarbons, and nitrogen oxide from automobile emissions.[2]

When selecting or designing a catalyst it is important that the catalyst either allows for milder reaction conditions, or improves the selectivity of the desired product(s), or both. For example, lower reactions temperatures and pressures are desirable because they will translate into lower operational costs. Furthermore, side reactions that produce unwanted products should be avoided not only because they decrease the yield of the desired product, but they may also have negative effects on the reactor, e.g. corrosion, or they may pose environmental hazards.

Although the scientific community has been actively studying catalysis for 200 years there is still a need for further development. Three major areas of research have been identified[3] as: (1) enzymatic and homogeneous catalysis for the production of chemicals, drugs, and food products, (2) environmental catalysis to reduce pollution, and most importantly (3) catalysts that increase the production of energy (or energy fuels). As the world's population grows, new and more efficient methods of producing the products that we presently enjoy will need to be developed.

1.2 IMPORTANCE OF PLATINUM CATALYSIS

Platinum catalysts are used in a number of industrial processes. The following highlights some of these processes.

1.2.1 Platinum catalysis used for nitric acid production.

Nitric acid has a number of uses including the production of fertilizers, explosives, organic compounds, and polymers. One approach to synthesizing nitric acid begins by oxidizing ammonia to NO at 900 °C. After cooling, oxygen is reacted with NO to form NO_2, which is then absorbed in water to produce nitric acid. The equilibrium for the conversion of ammonia to NO is highly favourable with an equilibrium constant of about 10^{11}.[4] However, several side reactions also have favourable equilibrium constants. For example, the equilibrium constant associated with the oxidation of ammonia to form nitrogen gas and water is 10^{15}.[4] Furthermore, ammonia oxidation to form N_2O has a equilibrium constant of 10^{11}, and ammonia decomposition to nitrogen gas and hydrogen gas has a equilibrium constant of 10^{5}.[4] The use of platinum as a catalyst for this reaction highlights the importance of selectivity. For example, PtRh gauze has a very high selectivity towards NO (94 – 98%) and low selectivity towards N_2 (4 – 4.5%) and N_2O (1.5 – 2.5 %).[4] Platinum is the active species towards NO formation, while rhodium has been added to increase the durability of the gauze.

PtRh gauzes lose their activity with time. Poisoning due to SO_2 adsorption (originating from sulphur used in lubricating compounds) and adsorption of particulates (e.g. corrosion products from up-stream equipment) plug up the gauze. Furthermore, sprouting results in the enrichment of Rh oxide on the surface which is not as active as platinum. Sprouting is caused by the migration of metal oxides along grain boundaries to the surface. The metal oxides can be reduced to metal on the surface of the gauze, or as in the case of PtO_2, the product is volatilized. Sprouting during the first 3 – 5 days greatly increases the surface area of the gauze, however after several months, it results in overall losses of Pt from the surface of the gauze and therefore a decrease in catalytic activity.

1.2.2 Platinum catalysis used for hydrogen cyanide production.

Hydrogen cyanide is an important chemical used to produce methyl methacrylate and adiponitrile which are in turn used to make nylon. Hydrogen cyanide is produced by a highly endothermic reaction of ammonia and methane. In the Andrussow process, oxygen is added to the reaction chamber to simultaneously combust some of the methane.[5] This combustion reaction provides the required heat to convert the ammonia and methane to

hydrogen cyanide. A separate process, referred to as the Degussa or Blausäure-Methan-Ammoniak (BMA) method, reacts ammonia and methane inside a ceramic cylinder; outside the cylinder, a combustion reaction takes place to provide the required reaction temperature. Both methods require platinum as a catalyst; however, the platinum is used in different forms. For example, in the Andrussow methods, platinum gauze is used, whereas in the BMA method, platinum particles coat the inside of the ceramic tubes where the reaction takes place.

In both processes, i.e. the Andrussow and BMA processes, the platinum catalyst is poisoned during operation. For example, iron from up-stream corrosion deposits and fouls the Pt surface. Carbon deposits have similar effects on the Pt catalyst. Furthermore, in the Andrussow process, the high reaction temperatures (1000 °C) causes the platinum gauzes to sinter together.

1.2.3 Hydrogenation.

The catalysts generally used for hydrogenation reactions consist of group VIII transition base metals, i.e. Ni, Cu, Cr, and Co, and precious metals, i.e. Pd, Pt, Rh, and Ru.[6] The group VIII transition metals have lower activities, thus requiring higher reaction temperatures and pressures, than the precious metals. However, the precious metals are more costly and thus need to be recovered. Typically, catalysts for hydrogenation are formed by impregnation and reduction techniques (see Section 1.4.3) on carbon supports. Deactivation occurs via poisoning with sulphur, halogens, nitrogen, and phosphorous. Additionally, coke formed during the reaction can deposit onto the support blocking the pores and thus access to the catalysis. Mechanical attrition is also a problem for catalysts in hydrogenation as friction caused by mixing during the reaction results in gradual wear and tear of the catalyst/support surface.

1.2.4 Catalytic Converters.

In addition to carbon dioxide and water, the combusting engine of modern vehicles releases carbon monoxide (CO) and unburned hydrocarbons (HC) due to incomplete oxidation of the fuel. Furthermore, nitric oxides (NO_x) are also produced due to oxygen gas and nitrogen gas reacting together at high temperatures. In 1970 the Clean Air Act in the Unites States recognized the need to control vehicle emissions. The catalytic converter was

thus invented to remove carbon monoxide, unburned hydrocarbons, and nitric oxide from the exhaust stream. Oxidation is required to remove carbon monoxide and the unburned hydrocarbons. The nitric oxides are removed by reduction to form nitrogen and oxygen gas. Platinum or palladium are the catalysts of choice for the oxidation of CO and HC, while ruthenium shows the most activity towards reducing NO_x.[7] However, oxygen gas which aids the oxidation of CO and HC is found to deter the reduction of NO_x. This problem was solved by operating the engine close to the stoichiometric air-to-fuel ratio which allowed the simultaneous conversion of all three primary pollutants. The oxygen content of the exhaust is monitored electrochemically and the voltage signal is fed back to the fuel injector which adjusts the air-to-fuel ratio as needed. This type of catalytic converter is referred to as a three-way catalytic converter.

Presently, the average catalytic converter contains 2.2 g of Pt or Pd and 0.2 g of Rh.[7] The catalysts are deposited as nano-clusters within the pores of a support. Research into catalyst preparation techniques are on-going to maximize the dispersion of the noble metals. Moreover, durability, in particular sintering of particles, is a key aspect under study.

1.2.5 Catalytic Cracking.

Catalytic cracking is a petroleum refinery process where heavy petroleum, which has little value, is broken down into premium middle distillates. In 1936 the first catalytic cracking refinery opened replacing thermal cracking because it has higher selectivity to high octane components. In the early 1960s zeolites were introduced increasing catalytic activity and gasoline selectivity. Petro-refining is considered by some critics to be technologically mature. However, it is currently undergoing huge technological and economic changes due to trends of decreasing feed stock quality, increased fuel quality requirements, and increasing environmental restrictions. For example, increasingly restrictive emission standards have required refiners to address the control of sulphur oxides emission from catalytic crackers. Pt catalyst catalyzes the conversion of SO_2 to SO_3 which can then be trapped by an absorbent downstream.[8] Furthermore, Pt is used to convert excess CO to CO_2, thereby preventing uncontrolled afterburning.[9]

1.2.6 Platinum catalysis in fuel cells.

Within a fuel cell, oxidation of the fuel occurs at the anode and reduction of the oxidant (normally oxygen) occurs at the cathode. The anode and cathode are separated by a medium that prevents electron conductivity thereby forcing the electrical current to pass from the anode to the cathode via external wiring, thus, the chemical energy of the fuel and oxidant are converted into electrical energy. The driving force for fuel cells research is that fuel cells are an attractive alternative source of energy to the combustion of fossil fuels since, as an electrochemical power source, they are not subject to the Carnot limitations of combustion engines. Thermodynamic efficiencies of fuel cell reactions, as defined by

$$\xi_{th} = \frac{\Delta G}{\Delta H} \times 100\% = \left(1 - T\frac{\Delta S}{\Delta H}\right) \times 100\% \qquad (1.1)$$

Or

$$\xi_{th} = \frac{E^0}{E_H^0} \times 100\% \qquad (1.2)$$

(where $E_H^0 = -\Delta H/nF$ is the thermal cell voltage, and $E^0 = -\Delta G/nF$ is the thermodynamic cell voltage) can be greater than 100 % depending on the sign of the change in entropy during the reaction.[10] That is to say, if the overall fuel cell reaction results in an increase in disorder, $\Delta S^0 > 0$, then the thermodynamic efficiency will be greater than 100 %. Conversely, if the overall fuel cell reaction results in a decrease of disorder, $\Delta S^0 < 0$, then the thermodynamic efficiency will be less than 100 %. For example, for a hydrogen fuel cell, with overall reaction $H_2 + ½\ O_2 \rightarrow H_2O$, the reaction enthalpy at 25 °C is ΔH^0 – 286 kJ mol^{-1}, and the reaction entropy ΔS^0 is – 0.163 kJ mol^{-1} (i.e. $\Delta S^0 < 0$) . Thus the thermodynamic efficiency for the hydrogen fuel cell at 25 °C is

$$\xi_{th} = 1 - 273.15\frac{-0.163\ \text{kJ mol}^{-1}}{-286\ \text{kJ mol}^{-1}} \times 100\ \% = 83\ \% \qquad (1.3)$$

The change in entropy associated with the oxidation of formic acid at 25 °C is positive, ΔS^0 = 0.0510 kJ mol^{-1}. Given that the change in enthalpy is – 280.3 kJ mol^{-1}, the thermodynamic efficiency is 105.6 %.

Efficiencies when running an actual fuel cell are less than the thermodynamic efficiencies. That is to say the measured potential decreases from the reversible standard potential as the current is increased due to three main losses: (1) cell-potential losses due to activation overpotential (poor electro-catalysis), (2) internal resistance loss in the electrolyte, and (3) mass-transportation losses (see Figure 1.1). Despite these dramatic losses, useful current densities can be obtained for the hydrogen fuel cell at a cell voltage of 0.8 V. Thus the load efficiency, ξ_{load}, at 0.8 V can be calculated

$$\xi_{load} = \frac{E(i)}{E_H^0} = \frac{0.8\,V}{1.48\,V} = 54\,\% \tag{1.4}$$

Losses caused by internal resistance (2) and mass-transport (3) cannot be mitigated with the use of a more effective catalysis; intelligent engineering and materials development are required. Conversely, cell potential losses due to activation overpotentials (1) can be minimized by utilizing a highly active catalyst. The catalyst must also be cost effective and durable to allow for commercialization of fuel cells.

Fuel cell types are characterized by the type of electrolyte used to separate the fuel and the oxidant. The type of electrolyte will determine cell parameters such as hydration and more importantly temperature. The temperature of the cell in turn will dictate what type of catalyst is used. For example, the activity of Ni towards the oxidation of hydrocarbons at low temperatures does not make it a suitable catalyst for fuel cells operated at low, < 100 °C, and moderate, < 250 °C, temperatures. However, the high temperature required to ensure adequate conductivity through the solid oxide (SO) electrolyte increases the activity of hydrocarbon oxidation on Ni thereby making Ni an effective catalyst for SOFCs. Table 1.1 summarizes the prominent types of fuel cells. The operational temperature greatly influences what application a fuel cell will be designed for. For example, the high temperature fuel cells, e.g., SOFC and MCFC, are best suited for stationary applications where co-generation of heat can be used for co-generation of power and space/water heating. The high power output of PEMFC make them suitable for the automotive industry, while the lower power densities of DMFC are ideal for small electronic devices such as cell phones and laptop computers. Due to the high cost associated with platinum and platinum based alloys, e.g.

platinum-ruthenium, the amount of Pt used in low temperature fuel cells must be minimized. This in turn means that the activity for a particular amount of Pt catalyst must be increased.

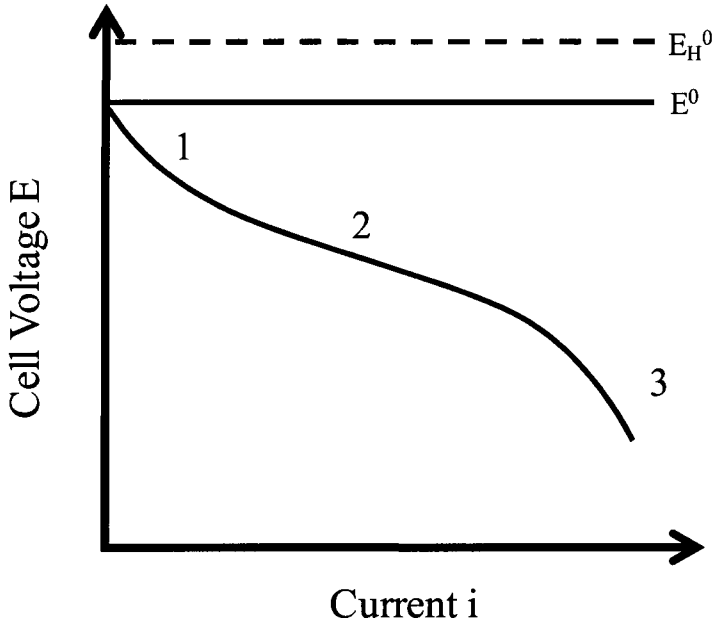

Figure 1.1 Schematic diagram depicting the voltage dependence of the electrochemical cell (with $\Delta S < 0$) on the current. (1) cell-potential losses due to activation overpotential, (2) internal resistance loss in the electrolyte, and (3) mass-transportation losses. E_H^0 is the thermal cell voltage, and E^0 is the thermodynamic cell voltage.

Table 1.1 Summary of the prominent types of fuel cells.

Fuel Cell	Electrolyte	Operating Temp. / °C	Catalyst
Proton exchange membrane (PEMFC)	Proton exchange membrane, e.g. Nafion	60 - 80	Pt
Direct methanol (DMFC)	Proton exchange membrane, e.g. Nafion	60 - 80	Pt, PtRu
Alkaline (AFC)	30 – 50 wt % KOH	65 – 220	Pt
Phosphoric acid (PAFC)	100 % Phosphoric acid	205	Pt
Molten Carbonate (MCFC)	Molten Carbonate, e.g. Na_2CO_3, K_2CO_3	650	Ni
Solid oxide (SOFC)	O^{2-}	600 - 1000	Perovskites, Ni

1.3 WHY WE NEED TO STUDY CATALYSIS

Although catalysis has been a subject of formal study for over two hundred years there is still more to be learnt. Research is motivated by practical needs to improve the durability and activity of catalysts. Increasing the catalyst activity will translate into decreases in the amount of catalyst needed, thus decreasing the cost of the system. Similarly, increases in durability will increase the lifespan of the catalyst, thus decreasing the frequency at which a catalyst needs to be replaced, thereby decreasing the operational cost of the system. In addition to these particular reasons of why catalysts need to be studied, there is a more fundamental motivation; the need to broaden our understanding of how things work.

1.4 METHODS OF SYNTHESIZING PLATINUM NANO-CATALYSTS

This section presents a general overview of the most common synthetic methods to fabricate both supported and unsupported catalysts. An unsupported catalyst consists of bare catalysts suspended in a media (i.e., in solution or in Nafion). Catalysts are said to be supported if they are adsorbed onto a material (referred to as the support). In fuel cell

applications, carbon supports are the most prevalent. Although no single synthesis method is superior to the others, one method may be advantageous over another depending on the end application of the catalyst and the instrumentation available. Therefore, Section 1.4.9 will discuss the catalysis synthesis methods selected to prepare nano-catalysts for this work and why they were selected.

1.4.1 Chemical Precipitation.

Platinum and platinum-based nano-catalysts can be made by chemical precipitation at low temperatures. The process is generally simple and involves the addition of a reducing agent to a platinum-salt solution. Once the platinum salt is reduced to the metallic state it precipitates out of solution forming unsupported catalysts. To form supported catalyst, powdered carbon is added prior to the reduction of the metal-salts. Unsupported particles grow more quickly than supported particles; typically they are almost twice the size of supported particles.[11] Despite this limitation, unsupported platinum electrocatalysts as small as 3 nm have been fabricated, with $[Pt_3(CO)_6]_{\sim 10}^{2-}$ as the platinum source and using dihydrogen gas (bubbled through the solution) as the reducing agent.

1.4.2 Colloidal.

The colloidal method of generating nano-catalysts is similar to the low temperature chemical precipitation method, but with the added benefit of a capping agent. The primary role of the capping agent is to stabilize the nanoparticles, thus preventing agglomeration, and thus allowing particle size control. Any molecule that adsorbs onto the reduced metal can act as a capping agent. The experimental procedure is as simple as combining the metal source, a reducing agent, and a capping agent together and mixing. As with chemical precipitation, a powdered carbon support is added to the mixture to synthesize supported catalysts.[16] If a fast reducing agent is used, the reactions can be completed in less than 30 min..[12] Conversely, slow reducing agents like dihydrogen gas at room temperature require longer reactions times and are generally allowed to react over night or for at least 12 h.[12]

An interesting example of colloidal Pt nanoparticle synthesis is the combination of colloidal synthesis and the formation of cross linked Pt networks.[13] The Pt colloids were prepared by first dissolving $Pt(acac)_2$ in toluene. A separate solution of $Al(CH_3)_3$ in toluene was added to the platinum solution slowly (over a period of 4 h). This formed a colloidal

platinum powder. Spacer molecules terminated with —OH groups were cross-linked to the colloids resulting in well spaced Pt nanoparticles assembled into a three-dimensional network. The ratio of methylaluminum groups in the colloid to hydroxyl groups in the molecular spacer was found to be 1:1. Transmission electron microscopy (TEM) analysis showed well distributed Pt nano-crystals 1.2 nm in diameter.[13] It should be noted that the intricate network-spacers have the potential to negatively affect the catalytic activity of the prepared Pt nano-catalysts.

1.4.3 Impregnation.

Due to the ease of preparation, impregnation is one of the most commonly used techniques to fabricate catalysts. High-surface-area carbon black can be impregnated with catalyst precursors by mixing the two in an aqueous solution.[14] Another method of impregnating a substrate involves depositing an aliquot of solution which contains the catalyst precursor onto a substrate and allowing it to air dry.[15] Following the impregnation step, a reduction step is required to reduce the catalyst precursor to its metallic state. As reduction occurs after the impregnation step, the nature of the support plays a crucial role in controlling particle size.[16] Common liquid phase reducing agents are $Na_2S_2O_3$, $NaBH_4$, $Na_4S_2O_5$, N_2H_4, or formic acid. H_2 is the dominant gas phase reducing agent.

The most common platinum precursors used for impregnation are chloride salts; however, it has been argued that the metal chloride salts might lead to chloride poisoning which could affect the catalytic activity of the particles.[17] To avoid chloride poisoning, metal sulphite salts, metal carbonyl complexes, and metal nitrate salts have been used instead.[16] Metal carbonyl complexes are particularly attractive as precursors since they can be easily made by direct reduction of the metal chloride salt with carbon monoxide. Additionally, an external reducing agent is not required as nano-particles can then be formed by impregnation and thermal decomposition of the metal carbonyl complexes impregnated onto carbon supports.[18,19]

The impregnation technique is a comparatively green method to synthesize catalysts; reduction reactions occur either at low or room temperatures minimizing energy consumption and organic solvents are avoided by using aqueous media. Drawbacks of the impregnation technique are related to using liquids solutions as the processing medium. In

solution, particles can easily agglomerate. Furthermore, the high surface tension of liquid solutions can cause fragile supports, such as aerogels, to collapse.[20]

1.4.4 Microemulsions.

Emulsions are dispersions of one type of liquid in another liquid.[21] Emulsions used to make nano-catalysts generally consist of a protic phase (normally water) and an aprotic phase (some type of oil). The two liquids can be emulsified by shaking them together. However, to stabilize the emulsified solution, an emulsifying agent such as an amphiphile (typically a surfactant) must be added to the solution. At high water concentrations, the emulsion consists of small oil droplets surrounded by surfactants in a continuous water phase. At high oil concentrations, the emulsion consists of small water droplets surrounded by surfactants in a continuous oil phase. Since most metal precursors are inorganic salts, they are soluble in water and not oil. Therefore, emulsions with high oil concentrations and low water concentrations are almost exclusively used. The metal salt is reduced by either adding a reducing agent into the microemulsion system, or by mixing a microemulsion system that contains a reducing agent with a microemulsion system that contains the metal salt.[16,22] Once the nano-catalysts are formed, they can be deposited onto a support. To deposit the catalyst onto a support, a solvent like tetrahydrofuran is added, in conjunction with the support powder, to the microemulsion.[22] The solvent destabilizes the microemulsion by competing with the surfactant to adsorb onto the particles, in the destabilized system the particles will adsorb onto the support. The majority of residual surfactant molecules can be removed by heat-treatment.[16] Emulsion systems are very sensitive to temperature, and therefore the oil and surfactant must be selected with care.[22] Unfortunately, catalyst fabrication by microemulsion is costly, since expensive surfactants and oils are needed. Furthermore, surfactants and oils can have a negative environmental impact.

The method of size control during microemulsion synthesis appears to be much more complicated than preliminary research indicated. Originally, the water droplets containing dissolved metal salts stabilized by a surfactant were often described as a "micro-reactor" or "nano-cage".[23] Since the reduction is confined inside the nano-scaled microemulsion, it was originally believed that the catalyst size was exclusively controlled by the size of the water

droplets in the microemulsion. [16] However, it has been found that particle size control is a more complicated phenomenon involving the nature of the reducing agent, as well as the size of the water droplets in the microemulsion. For example, it has been found that small particles are formed by fast nucleation caused by a fast or efficient reducing agent.[22] Hydrazine is an example of a fast reducing agent, while dihydrogen gas is a relatively slow reducing agent.

The size of the water droplet is influenced by (1) the ratio of water to surfactant and (2) the surfactant concentration (at fixed water/oil ratios). As the ratio of water to surfactant increases, the size of the water droplet increases, and consequently, the catalyst-size also increases. However, a maximum particle size is reached and further increases of the water to surfactant ratio does not cause the catalyst size to increase further.[24,25,26] For example, in a microemulsion system of water/*n*-heptane with the surfactant sodium dioctyl sulfosuccinate, the Pt-Ru particle size increases from 2.4 ± 0.1 to 3.2 ± 0.1 nm when the ratio of water to sodium dioctyl sulfosuccinate increased from four to eight.[26] However, increasing the water to dioctyl-sulfosuccinate ratio to 10 did not result in any further increase in catalyst size.[26] Droplet size can also be controlled by varying the surfactant concentration while keeping the concentration of water and oil constant. For example, increasing the surfactant concentration, with constant water and oil concentration, increases the number of droplets. As a result, droplet size decreases resulting in fewer metal ions per droplet and consequently particle size decreases.

Droplet size, however, does not directly or absolutely control particle size. For example, it was estimated that there are five $PtCl_6^{2-}$ ions in each water droplet in the microemulsion system of water in hexane stabilized by the surfactant pentaethyleneglycol dodecylether.[22,27] However, TEM analysis indicated that the platinum catalyst formed had an average diameter of 3.5 nm which corresponds to 1000–1500 metal atoms (depending on the shape of the particle). This example illustrates how the final particle is not formed inside the droplet. It is likely that the formation of catalysts via the microemulsion process proceeds by two steps: (1) nucleation of the metal catalyst inside the droplet, followed by (2) aggregation of multiple nuclei via collision and coalescence of droplets to form the final nano-catalyst.[22]

1.4.5 Sol-Gel Technique.

Platinum nanoparticles as small as 2 nm have been prepared by the sol-gel technique.[28] The sol-gel technique begins with the formation of a liquid solution of suspended particles, a sol, that is aged and dried to form a semi-solid suspension of particles in a liquid, a gel, and finally calcified resulting in a mesoporous solid. There are four distinct steps to the sol-gel technique;[29] (1) formation of the sol. (2) aging, to allow fine-tuning of the gel properties. (3) drying, to remove solvent from the gel. (4) calcination, to permanently change the physical/chemical properties of the solid. Controlling experimental parameters such as time, temperature, heating rate, and pore-liquid composition during the aging and calcination steps allows for fine control of pore size distribution and volume.

Metallic nano-catalysts can be incorporated into the mesoporous structure by a variety of methods. Prefabricated nanoparticles can be incorporated into mesoporous solids by incorporating the particles into the sol-gel mixture or, if the particles are formed by microemulsions (see Section 1.4.4), the microemulsion can be incorporated into the preformed mesoporous structure. Alternatively, metal salts can be added during the gel formation or after the mesoporous structure has formed.[30] An example of the former is the synthesis of WO_x and WO_x/Pt films that were made by first synthesizing $W(OC_2H_5)_6$ and H_2PtCl_6 sol-gel solutions followed by aging and calcination.[31] A possible drawback associated with this method is that the catalytic nanoparticles will not necessarily form in the pores, but rather may form within the structure. If the particles are not located in the pore, they will not be accessible to reactants and therefore will not be efficient catalysts.

Adding nano-catalysts after the mesoporous structure has formed, i.e. after calcination, ensures that the particles form in the pores. This can be accomplished by impregnating the structure with the metal ions followed by a reduction step.[30] The impregnation technique allows for controlled particle growth as the pore size limits particle growth. Impregnation can be facilitated by functionalizing the mesoporous structure with organic groups that anchor metal compounds and/or interact with the surface of the growing nanoparticles. For example, a gel containing acidic functionality on its backbone was required to facilitate doping an organic gel with $Pt(NH_3)_4Cl_2$.[32] Functionalizing pores with cationic surfactants allows for ion exchange; i.e. metal cations can replace the cationic surfactants.[30] Since monovalent surfactant cations are replaced with multivalent metal cations, entropy drives

this efficient ion exchange. Once the ion exchange is completed, the metal cations are reduced to form nano-catalysts. Chemical vapour deposition, (see Section 1.4.8.1) is another method to add nano-catalysts to prefabricated mesoporous structures.[30] This method should be restricted to thin films or particles (i.e., not to monolithic samples) to prevent uneven distribution of the metal compounds within the material.

1.4.6 Electrochemical.

Electrochemical deposition has been used to deposit Pt and Pt based nanoparticles on a wide variety of substrates including glassy carbon,[33] highly ordered pyrolytic graphite (HOPG),[34,35] carbon black inside Nafion,[36] carbon nanotubes,[37] and Pan-based carbon fibres[38]. Electrochemical deposition occurs at the interface of an electronically conductive substrate and an electrolyte solution which contains the salt of the metal to be deposited. There are five stages to electrochemical deposition of metals; [39,40] (1) diffusion of metal ion in solution to the electrode surface, (2) electron transfer, (3) the formation of metal adatoms via adsorption, (4) nucleation and growth, two- or three-dimensional, of metal particles, (5) growth to form a three-dimensional bulk metal phase. Nano-catalysts are formed if the growth process is stopped after the fourth step. Conversely, if the particles are allowed to grow, a metal film is formed.

Deposition occurs by supplying the substrate, called the working electrode, with sufficient potential to reduce the metal salt to its zero valent state; $M^{z+} + ze^- \rightarrow M^0$. The substrate is therefore immersed in a metal salt solution that usually contains a supporting electrolyte to decrease the resistivity of the solution. The anode, where the oxidation half reaction occurs, and a reference electrode, used to monitor the reaction, are also immersed in the metal salt solution. If the binding energy of the metal adatom to substrate is lower than the binding energy of the metal adatom to itself, then 3D growth of the nuclei occurs. Conversely, if the binding energy of the metal adatom to the substrate is higher than the binding energy of the metal adatom to itself, then 2D growth of the nuclei occurs. 2D and 3D growth can also be influenced by the deposition potential via the use of either underpotential deposition (UPD) or overpotential deposition (OPD), respectively. UPD refers to deposition initiated by applying a potential that is less cathodic the Nernst

equilibrium potential of the M/M^{z+} metal ion electrode, while OPD occurs when a more cathodic than the Nernst equilibrium potential is applied.[39]

Electrochemical deposition offers the advantages that stabilizers and or capping agents, which should be avoided as residues of stabilizers likely influence the catalytic activity of the nanoparticles, are not required. Furthermore, particle size can be controlled by varying the length and the amplitude of the potential pulse. Additionally, nuclei density can be increased by electrodepositing with a large overpotential,[35,35] however, increasing the overpotential may result in other reaction occurring in addition to the metal reduction, i.e., hydrogen adsorption and evolution. If metal reduction is not the only process occurring, then it is not possible to extract valuable information, such as the type of nucleation or the amount of platinum deposited, from current-time transients.

Platinum nano-catalysts have been electrochemically deposited onto highly ordered pyrolytic graphite (HOPG) from an aqueous H_2PtCl_6 solution containing HCl as the supporting electrolyte. The nano-catalyst size is varied by varying the time the deposition potential is applied. Atomic force microscopy revealed that 10 ms deposition time generated particles 2.5 ± 0.9 nm in height, and that increasing the deposition time to 100 ms generated particles 7.2 ± 3.2 nm in height.[34] The large size distribution in this example indicates that nucleation is progressive, i.e., the number of nuclei increases with deposition time. Ideally, the deposition process would occur in an instantaneous fashion, i.e. the number of nuclei is constant and equal to that at time t = 0 of the deposition process. Assuming that all the nuclei grow at the same rate, instantaneous nucleation results in mono-size-dispersed particles and is therefore preferred in fabricating nano-catalyst of a specific size. It has been shown that increasing the deposition overpotential or increasing the electrolyte conductivity (with chloride, sulphate and perchlorate) causes a shift from progressive to instantaneous nucleation.[35]

1.4.7 Spray Pyrolysis.

The experimental procedure of spray pyrolysis is conceptually simple[41]: First, an aqueous solution containing the metal precursor is atomized into a carrier gas that is passed through a furnace. Second, the atomized precursor solution deposits onto a substrate where it reacts and forms the final product. The process has many advantages compared to other metal

forming techniques.[42] (1) It is very easy to dope films or form alloys in any proportion by manipulating the spray solution. (2) High purity targets, substrates, and vacuum set-ups are not required. (3) Deposition rates, and therefore, film thickness can easily be controlled by controlling the spray parameters. (4) Moderate operation temperatures (100 – 500 °C) allow for deposition on temperature sensitive substrates and ensure that the overall process is less energy intensive. (5) The technique has relatively limited environmental impact since the precursor solution is aqueous. (6) The process is easily scalable with production rates as high as to 1.1 kg of deposited metal per hour.[43]

Ultrasonic nebulizers[42] can be used to form micrometer and submicrometer sized droplets. Droplets formed by ultrasonic waves have very small sizes and size distributions. To deposit onto a substrate the aerosol is transported to the heated substrate, where the solvent vaporizes. A heterogeneous reaction occurs that leads to the formation of thin solid films. The spray jet can be scanned continuously to coat a large area. To form nanoparticles the aerosol is pyrolyzed. To improve the deposition efficiency, i.e. the ratio of atoms effectively deposited to those supplied, a corona discharge is used to control the transport of aerosol droplets towards the substrate.[42] Electrostatic spray pyrolysis is another method used to control the transportation of the atomized precursor solution from the atomizer to the substrate. It is accomplished by applying a positive voltage, up to 12.5 kV, to the spray nozzle forming a positively charged spray. Electrostatic forces guide the spray to the hot substrate where pyrolysis takes place.

Although spray pyrolysis is usually used to form thin films of metals, it can also be used to form nanoparticles. Pt-Ru/C catalysts have been formed by spray pyrolysis using H_2PtCl_6 and $RuCl_3$ as the precursors dissolved in an aqueous solution containing carbon black and various molecular lengths of polyethylene glycol (PEG). Once atomized, the droplets of precursor solution in the carrier gas pass through a quartz tube that was heated by a tube furnace at 180 °C. Solvent evaporation and precursor decomposition results in nanoparticles forming on the carbon black. Interestingly, PEG plays an integral role in particle stability against agglomeration. If the PEG chain is too short (PEG with average molecular weight 200 g mol^{-1} PEG200) the Pt-Ru particles agglomerate. If the PEG chain is too long, e.g. PEG1000, the PEG molecules aggregate and do not protect the particles from agglomeration.

However, at intermediate PEG lengths, e.g. PEG600, the precursors mixed well with the polymer and agglomeration is prevented.

1.4.8 Vapour deposition.

1.4.8.1 Chemical Vapour Deposition (CVD).

CVD is an ideal method to form thin metal films. A typical CVD process[44] begins by vaporizing the precursor, an inorganic compound containing the desired metal(s). The substrate is placed in a reaction chamber into which the vaporized precursor, mixed with a carrier gas and any other gaseous reactants, is introduced. The precursors diffuse to, and adsorb onto the substrate surface where they decompose thermally, forming a metallic film. The precursor is designed to ensure that any reaction by-products are gaseous and desorbs into the gas phase.

Although CVD is typically used to form thin films, it can also be used to make nanoparticles. Pt-Ru particles 2 nm in diameter have been formed by vapour deposition using platinum(II) acetylacetonate and ruthenium(III) acetylacetonate.[45] While particle size was virtually independent of sublimation temperature, the Pt:Ru ratio increased as sublimation temperature decreased. Particle composition was effected by sublimation temperature because the vapour pressure of the two precursors changed with sublimation temperature. This example illustrates how vapour pressure of the precursors can act as a limitation of CVD alloy formation.[20] CVD is also limited by processing temperature and mass-transfer-limited kinetics. [20] One final disadvantage of CVD that should be noted is that many of the precursors used are highly toxic and therefore difficult to work with.[46]

1.4.8.2 Physical vapour deposition (PVD).

Mechanical methods such as cathodic sputtering, and thermal methods like evaporation, are grouped together under the term physical vapour deposition.[47] All PVD experiments have four essential components: (1) they occur in vacuum, (2) they have (i) a source to supply the material, called a target, (ii) a substrate on which the film is deposited, and (iii) an energy supply to transport the material from a source to substrate. The types of PVD vary in how energy is imparted to the particles and how the energized particles are transported to the substrate.

Evaporation PVD occurs by heating the material to be deposited. Under vacuum, a molecular beam of the catalyst material is formed thermally. In a molecular beam, atoms and molecules move in a well-defined direction without colliding with each other.[48] When the system is oil free and the substrate is atomically clean before deposition, molecular beam epitaxial deposition is possible.

Cathodic sputtering occurs by generating a plasma between the substrate and a target, made of the material to be deposited. The target acts as the cathode emitting atoms to the substrate which acts as the anode. Nickel coatings were developed as the anode for SOFCs based on $BaCe_{0.9}Y_{0.1}O_3$ as the electrolyte.[49] By utilizing a pulsed cathodic sputtering technique, the microstructure and adhesion of the thin film anode to the ceramic electrolyte lead to higher quality anodes and therefore longer stack life of the fuel cell. The main disadvantage associated with cathodic sputtering are the low deposition rates.[44]

1.4.9 Selection of catalysis synthesis methods used in this work.

The purpose of all catalyst research is to study and improve the stability and activity of the prepared catalyst systems. To test the electrochemical activity of these nano-catalysts, they must be prepared on a conductive support that is stable and catalytically inactive towards the test reactions. Additionally, for a catalyst system to be truly model, it must be free from all possible sources of interference during catalytic activity testing.[34] For example, the catalysts must be free from agglomeration during formation and catalytic testing.

Reviewing the methods to synthesize Pt nano-catalysts presented in this chapter with respect to the above mentioned guidelines quickly narrows the number of possible synthesis methods to a select few. For example, chemical precipitation techniques (Section 1.4.1) are not feasible as they do not allow for easy size control, i.e. there is no parameter that can be varied to produce particles of a specific size in one experiment and particles of a different size in another experiment. Colloidal methods (Section 1.4.2) of synthesizing catalysts are not preferable as residues of stabilizers may influence the catalytic activity of the nanoparticles. Similarly, microemulsion preparation techniques (Section 1.4.4) are avoided as residual surfactants may have the same effect. Sol-gel techniques (Section 1.4.5) are generally avoided as the resulting mesoporous structures are notoriously fragile and would not withstand the harsh electrochemical testing environment. Additionally, as the catalyst

would be located within the mesoporous structure, mass-transportation effects could possibly adversely affect the measured activity. Spray Pyrolysis (Section 1.4.7) is more suitable for film formation than nano-particle formation. When using spray pyrolysis to form nanoparticles, stabilizers are required to prevent particle agglomeration during particle formation. Thus, as with colloidal and microemulsion techniques, this method is not suitable as residual stabilizer may affect the activity of the prepared nano-catalysts. High vacuum experimental conditions and high purity targets needed for physical vapour deposition (Section 1.4.8.1) add unnecessary experimental cost and complications. The elevated temperatures, > 100 °C, associated with chemical vapour deposition (Section 1.4.8.2) are not feasible for many of the carbon supports typically used in electrochemical analysis.

In this work, we investigate two synthesis methods for Pt nano-catalysts; (1) electrochemical deposition and (2) impregnation followed by thermal decomposition. Electrochemical deposition offers several advantages over other techniques. For example, stabilizers are not required, and particle size can be controlled by varying the length and the amplitude of the potential pulse. Additionally, electrochemical deposition is an "information rich" technique. For instance, analysis of the measured current-time transients of the Pt electrodeposited process gives insight into the type of nucleation (instantaneous vs. progressive) and the amount of platinum deposited. Synthesizing nanoparticles by impregnation of the substrate followed by thermal decomposition also avoids the use of stabilizers. Unfortunately, this method does not allow for nucleation studies. In the following chapters, Pt nano-catalysis synthesized by these two techniques will be studied with respect to their morphology, physical stability, electrochemical stability, and their activity towards electrochemically oxidizing adsorbed carbon monoxide.

1.5 MOTIVATION AND CHOICE OF SYSTEM

The motivation for this work is to study the effects of particle deposition techniques and substrate pre-treatment on the morphology, activity towards electro-oxidation of adsorbed carbon monoxide, and the electrochemical stability of the prepared electrodes. The system selected for study for this thesis is platinum deposited onto highly ordered pyrolytic graphite (HOPG). Platinum was selected as the catalyst because of its wide application as a catalyst

in many different industrial processes. Advancing the understanding of platinum nanoparticles and the interactions of these particles with their support, will therefore improve the use of catalysts in these fields. Although the majority of experiments performed for this work are electrochemical in nature, the findings are not limited to electrochemical applications of platinum.

HOPG was selected as the support for the platinum particles because due to its highly crystalline nature and atomically smooth basal planes HOPG can be considered a model carbon electrode. It is electrically conductive, which is necessary for the electrochemical analysis of the prepared electrodes. As a carbon support is studied, this work is directly applicable to low temperature fuel cells, since carbon supports are commonly used in low temperature fuel cells. Due to HOPG's well defined surface structure it is more stable than other carbons such as carbon blacks. The surface chemistry is significantly simpler than that of other carbons; this facility studying HOPG surface modifications as well as carbon platinum interactions. Furthermore, it is catalytically inert for the electrochemical reactions studied in this thesis. And finally, it is easy to work with since a clean surface can be easily obtained by simply cleaving the top layer by the "adhesive tape" method.

1.6 THESIS ORGANIZATION

This thesis focuses on the preparation and characterization of platinum on carbon electrodes. Chapter Two of this thesis presents the reader with an overview of the various experimental techniques used for this research. Chapters Three, Four, and Five, discuss in detail the morphology of the prepared Pt/HOPG electrodes. Chapters Six and Seven compare the activity of the different Pt/HOPG electrodes towards the electro-oxidation of adsorbed carbon monoxide and the electrochemical stability of the electrodes, respectively. Chapter Eight reviews the major conclusions of the work as well as proposing future work in this area. Chapter Nine presents the claims to original research.

1.6.1 Pt catalysts prepared on freshly cleaved HOPG by electrochemical deposition.

Chapter Three presents Pt/HOPG electrodes prepared by electrochemical deposition of a platinum salt in an aqueous solution with supporting electrolyte onto freshly cleaved HOPG. The reduction was achieved by applying a constant potential sufficiently cathodic to reduce

the Pt salt and measuring the resulting reduction current. Electrochemical deposition of Pt is an 'information rich' technique; by analyzing various parameters, such as the current-time transients, information regarding how much platinum is deposited, as well as the nature of the nucleation process can be determined. The nucleation of Pt onto freshly cleaved HOPG is extensively studied. Transmission electron spectroscopy (TEM) of the prepared Pt/HOPG electrodes gives further insight to the nature of the nucleation sites on the HOPG surface.

1.6.2 Pt catalysts prepared on oxidized HOPG by electrochemical deposition.

In Chapter Four, the influence of oxidizing the HOPG substrate on the electrochemical deposition process is discussed. Two different oxidation techniques are presented in Chapter Four; electrochemical oxidation and ozone gas oxidation. The effect of the oxidizing treatment on the HOPG surface morphology is studied using scanning electron microscopy and scanning tunnelling microscopy. Furthermore, the roughening of the HOPG substrates was studied electrochemically by measuring the double layer capacitance of the oxidized surfaces. The effect of oxidizing the HOPG substrate on nucleation was determined by analyzing current – time transients and TEM images.

1.6.3 Pt catalysts prepared on freshly cleaved and oxidized HOPG by impregnation followed by thermal decomposition.

Chapter Five introduces the technique of impregnation followed by thermal decomposition. Platinum deposits are prepared in this manner onto freshly cleaved and oxidized (electrochemically or with ozone gas) HOPG. Pt nano-catalyst morphology is studied by TEM.

1.6.4 Analysis of the activity of the prepared Pt/HOPG electrodes towards the electro-oxidation of adsorbed carbon monoxide.

The combination of two deposition techniques, electrochemical deposition and impregnation followed by thermal decomposition, and three types of substrates, freshly cleaved, ozone oxidized and electrochemically oxidized HOPG, results in six different types of Pt/HOPG electrodes. In Chapter Six, the activity of all six electrodes towards the electro-oxidation of adsorbed carbon monoxide is studied giving insight into the surface structure of the electrodes.

1.6.5 Analysis of the electrochemical stability of the prepared Pt/HOPG.

In Chapter Seven, the electrochemical stability of the six different electrodes is presented. The stability was studied by comparing the measured stripping charge of successive CO_{ads} stripping voltammograms. Since the stripping charge is proportional to the Pt surface area, changes in stripping charge reflect changes in Pt surface area. The interactions between the platinum catalyst and the HOPG substrate was studied by X-ray photoelectron spectroscopy.

Chapter Two

Experimental Methods

Throughout this thesis many experimental methods were used repeatedly. In order to minimize repetition, this chapter highlights these main experimental techniques. As not all research scientists, or all chemists, utilize these techniques on a regular basis, it is the authors opinion that a brief discussion of the chemical and theoretical background should be presented. Without understanding how a method works, one cannot appreciate the information that it generates.

2.1 THE FUNDAMENTALS OF ELECTROCHEMISTRY

Electrochemical techniques are used throughout this thesis to prepare and characterize various Pt catalyst electrodes. Thus, this section will introduce some fundamental concepts of electrochemistry.

2.1.1 The Driving Force for Electrochemical Reactions.

The gradient in electrochemical potential is the driving force for electrochemical reactions

$$\text{driving force} = -\text{grad}\ \bar{\mu}_i \tag{2.1}$$

where the electrochemical potential is given by

$$\bar{\mu}_i = \mu_i + z_i F\Phi \tag{2.2}$$

and μ_i is the standard chemical potential given by

$$\mu_i = \mu_i^o + RT\ln(a_i) \tag{2.3}$$

a_i and z_i are the activity and charge associated with species i, respectively. F is Faraday's constant which has the value 96485 C mol^{-1}, and Φ is the inner potential of a phase. Note that if a given species does not have an associated charge, then the electrochemical potential reduces to the chemical potential. Although the electrochemical potential of a species can be

measured, the chemical and electrical components can neither be measured nor calculated independently.

2.1.2 The Two Electrode System.

In a heterogeneous electrochemical process, electrode reactions involve the transfer of electrons to or from a surface. The electrode reaction may be an anodic reaction where a species is oxidized by loss of electrons to the electrode. For example, $Cl_{2(g)}$ evolution, i.e., $2Cl^- \rightarrow Cl_{2(g)} + 2e^-$, and corrosion, i.e., $Fe \rightarrow Fe^{2+} + 2e^-$ are both anodic reactions. Or, the electrode reaction may be cathodic in nature where a species is reduced by gaining electrons from the electrode. The electron transfer reaction between two species in solution $Fe^{3+} + e^- \rightarrow Fe^{2+}$, and electrodeposition of a species from solution onto the electrode $Pt^{4+} + 4e^- \rightarrow Pt^0$ are two example of cathodic reactions. By definition, the current associated with an anodic process is positive and the current associated with a cathodic process is negative.

The simplest electrochemical system is a two electrode system. A classic example of a two electrode system is the system used in the chlor-alkali industry. In this cell, chlorine gas is evolved at the anode, and hydroxyl anions are produced at the cathode, $2H_2O + 2e^- \rightarrow H_{2(g)} + 2OH^-$. Since the overall charge must be balanced, the amount of oxidation at the anode and reduction at the cathode must be equal. The overall cell reaction is the combination of the two half cell reactions

Oxidation half reaction: $$2Cl^- \rightarrow Cl_{2(g)} + 2e^- \quad (2.4)$$

Reduction half reaction: $$2H_2O + 2e^- \rightarrow H_{2(g)} + 2OH^- \quad (2.5)$$

Overall cell reaction: $$2Cl^- + 2H_2O \rightarrow Cl_{2(g)} + H_{2(g)} + 2OH^- \quad (2.6)$$

In order to maintain electrical neutrality at all points in the system, ions pass through the solution from one electrode to the other and electrons travel from the anode to the cathode externally through a electron-conductive wire. The rate at which electrons travel through the external wire is termed the current, I, and has units amps, A. Commonly, the current is

normalized to the geometric surface area of the electrode and is termed current density, i, and has units A cm^{-2}. The total amount of chemical reaction which has taken place is quantified by the charge, which is calculated by integrating the measured current with respect to time, t, using Faraday's Law

$$Q = \int_0^t idt = mnF \tag{2.7}$$

where n is the number of electrons involved in the reaction, and m is the number of moles of the product formed.

When two electrodes are connected by an external circuit, the cell reaction will only proceed if the free energy change associated with the overall cell reaction is negative. If the reaction is not spontaneous, it can be made to proceed by applying a potential between the two electrodes. This applied potential must be greater than the difference between the reversible potentials of the cathode, E_R^c, and the reversible potential of the anode E_R^a

$$\Delta G = -nF(E_R^c - E_R^a) \tag{2.8}$$

It should be highlighted that even though a reaction may be thermodynamically favourable, the rate of reaction is dependent on the kinetics of the reaction at the anode and cathode. An overpotential, η, can be applied to the electrode to increase the rate of reactions. Additionally, energy is required to move ions through the electrolyte, the media between the two electrodes. Thus, the total cell voltage, V, required for an electrochemical reaction is given by

$$V = (E_R^c - E_R^a) - (|\eta_a| - |\eta_c|) - iR \tag{2.9}$$

where R is the resistance of the media between the two electrodes.

The potential difference at a single electrode immersed in a solution, i.e., the potential difference at a single metal-solution interface

$$^{M}\Delta^{S}\Phi = \Phi^{M} - \Phi^{S} \tag{2.10}$$

is impossible to measure. For example, consider the system of a platinum wire in a solution. If the platinum wire were connected at one end to a voltmeter, the terminal connected to the voltmeter would be assigned the potential Φ^M. The potential of the solution, Φ^S, can only be measured by connecting another platinum wire into the other terminal of the meter and dipping that wire into the solution. This, however, creates a second metal-solution interface, and the meter would show the sum of the two metal-solution potential differences. Although $\Delta\Phi$ cannot be measured, changes in $\Delta\Phi$ (i.e., caused by passing a current) can be easily measured.

2.1.3 The Three Electrode System.

When a two electrode cell is used, a plot of *I* vs. *V* does not generate useful information regarding the electron transfer processes at the electrodes since both the reaction over potentials and the *iR* term (from Equation 2.9) change with the current. Typically a three electrode system is used that allows for only one electrode to be monitored. The third electrode is the reference electrode, RE; this electrode is placed in a Luggin probe. The Luggin probe is placed in the cell in such a way that the tip is positioned very close to the working electrode, WE, thereby minimizing the overpotential loss due to solution resistance, i.e., *iR*. The potential of the working electrode is controlled with respect to the reference electrode using a potentiostat. Figure 2.1 shows a simplified circuit diagram of a potentiostat. The feedback circuit drives the current between the working and counter electrode, CE, while ensuring that no current passes through the reference electrode. To minimize excessive polarisation of the counter electrode, the working electrode should have a much smaller (many order of magnitude) surface area compared to the counter electrode.

The terms working and counter electrodes are specifically selected so that they don't indicate an anodic or cathodic process. This is because depending on the half reaction being studied, one may wish the working electrode to act as an anode or a cathode. For example, when studying metal corrosion ($Fe \rightarrow Fe^{2+} + 2e^-$) the working electrode would be the anode and the counter electrode would be the cathode. If, on the other hand, one wanted to study the deposition of Pt metal ($Pt^{4+} + 4\ e^- \rightarrow Pt^0$) the working electrode would be the cathode, and the counter electrode would be the anode.

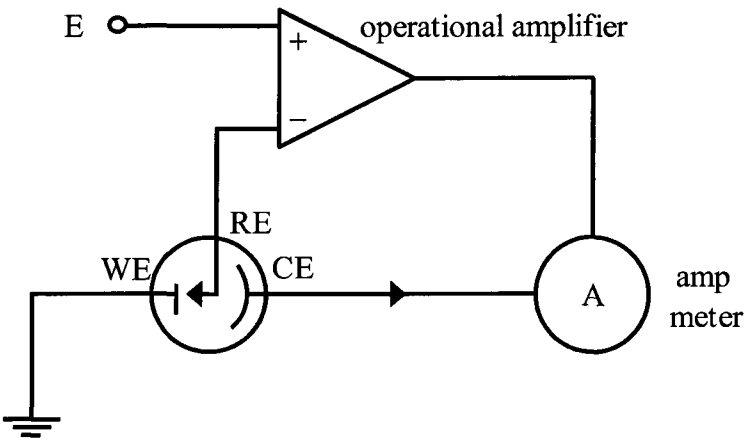

Figure 2.1 A simplified circuit diagram of a potentiostat.

2.2 ELECTROCHEMICAL SOLUTIONS, CELLS, AND ELECTRODES

2.2.1 Solutions.

In order to ensure that only the target species is reduced or oxidized (as the case may be) in an electrochemical experiment, the solution must be free from all other species that may change oxidation state at the experimental potential. Thus, all electrochemical solutions were made, using high resistivity 18 MΩ water. As dissolved oxygen in the solution may facilitate oxidation of the electrodes and/or species in solution, all solutions were deoxygenated with high purity argon prior to electrochemical experiments.

2.2.2 Cells and Electrodes.

A three compartment cell with the reference electrode separated from the working- and counter-electrode by a Luggin capillary was employed for all electrochemical experiments. A large surface area Pt mesh was used as the counter electrode. Two different reference electrodes were used; Hg/Hg_2Cl_2, sat. KCl (SCE), and Hg/Hg_2SO_4, 0.5 M H_2SO_4 (MSE). The reference electrodes were monitored regularly using a second SEC to ensure that potential drift, due to electrode degradation, did not occur.

2.2.3 Instrumentation.

Electrochemical experiments were performed using an EG&G 273 potentiostat driven by CorrWare software program (Scribner, Assoc.).

2.3 ELECTROCHEMICAL TESTING

2.3.1 Cyclic Voltammetry.

Cyclic voltammetry is one of the most commonly used methods to conduct preliminary investigations on an electrochemical system. This technique generates an 'electrochemical spectrum' indicating the potentials at which electrochemical processes occur. A cyclic voltammogram is obtained by varying the applied potential, in a cyclic manner, and measuring the resulting current. For example, the potential is swept from the initial potential E_1 to a second potential E_2 at a known sweep rate, υ (mV s^{-1}); the sweep direction is then reversed, normally at the same sweep rate, until E_1 is once again reached. Cyclic voltammetry allows comparison between the current measured at a particular potential on the anodic sweep (sweeping from low potential to high potential) to the current measured on the cathodic sweep (sweeping from high potential to low potential).

The measured current represents the rate of reaction of the electrochemical processes which occur at a given potential. Electrochemical processes can be (1) purely capacitive, (2) pseudo capacitive, or (3) Faradic. For a pseudo capacitive process, there is a specific coverage of the electrode by an adsorbed species that corresponds to an equilibrium condition at each potential. Upon potentiostatic polarization (i.e. the electrode potential is held at a specific value), once the coverage of adsorbed species determined by the equilibrium condition is attained the electrochemical process cannot proceed further (i.e. the coverage cannot be increased) and the current falls to zero. Conversely, the reaction currents for Faradic processes do not fall to zero upon potentiostatic polarization. That is to say, although some Faradic processes involve adsorbed specie the adsorbed species react forming a bulk species and thus the current is not limited by the coverage of adsorbed species.

A cyclic voltammogram of polycrystalline platinum foil in a solution of dilute sulphuric acid (see Figure 2.2) is an excellent example of how this techniques can be used to generate an electrochemical spectrum of the electrode, i.e. Pt foil. Polycrystalline Pt foil is an especially good example since all three different types of electrochemical processes (purely capacitive, pseudo capacitive, and Faradic) can be readily measured.

An example of a purely capacitive process is double layer charging. Double layer charging occurs whenever a potential is applied to an electrode, however if it is the only process occurring within a given potential region (i.e. between E_1 and E_2), the region is

referred to as the double layer region. Sweeping the potential of the polycrystalline Pt foil anodically (to more positive potentials) the region where double layer charging is the only electrochemical process to occur is between – 0.27 V and 0.10 V vs. MSE (see Figure 2.2). Within this potential window, the electrochemical process is purely capacitive and the measured current represents solely double layer charging. On the cathodic sweep, the region where the only electrochemical process to occur is purely capacitive is smaller (between – 0.27 V and – 0.1 V vs. MSE) than on the anodic sweep. This is due to the reduction of platinum oxide and is discussed below.

There are two regions in the cyclic voltammogram of polycrystalline Pt foil that represent the combination of double layer charging and a pseudo capacitive electrochemical process (see Figure 2.2): (1) Hydrogen desorption (peaks a and b) and adsorption (peaks e and f). (2) Oxygen adsorption, i.e. Pt oxidation, (plateau c) and desorption, i.e. Pt reduction, (peak d). These regions will be discussed in the following.

Sweeping the potential from – 0.27 V vs. MSE to more cathodic potentials (sweeping from positive potentials to negative potentials) the pseudo capacitive electrochemical process of hydrogen adsorption

$$Pt + H^+ + e^- \rightarrow PtH \qquad (2.11)$$

occurs and is represented by the two cathodic peaks, peaks e and f, located at – 0.44 and – 0.58 V vs. MSE (see Figure 2.2). The fact that there are two peaks represents the fact that there are two types of adsorbed hydrogen. The more strongly bound hydrogen is formed at the less cathodic potential (peak e), while the less strongly bound hydrogen is formed at the more cathodic potential (peak f). Switching the direction of the sweep at – 0.6 V vs. MSE changes the pseudo capacitive process from hydrogen adsorption to hydrogen desorption

$$PtH \rightarrow Pt + H^+ + e^- \qquad (2.12)$$

Oxidative desorption of the weaker Pt–H occurs at less anodic potentials (peak a), while the stronger Pt–H is removed at more anodic potentials (peak b). It should be highlighted that the potential at which the strongly bound hydrogen is adsorbed (peak e), is the same as the

potential at which the strongly bound hydrogen is removed (peak b); moreover, the potential at which the more weakly bound hydrogen is formed (peak f) is the same as the potential at which it is removed (peak a). The high degree of symmetry in the hydrogen adsorption/desorption peaks indicates that this pseudo capacitive process is highly reversible.

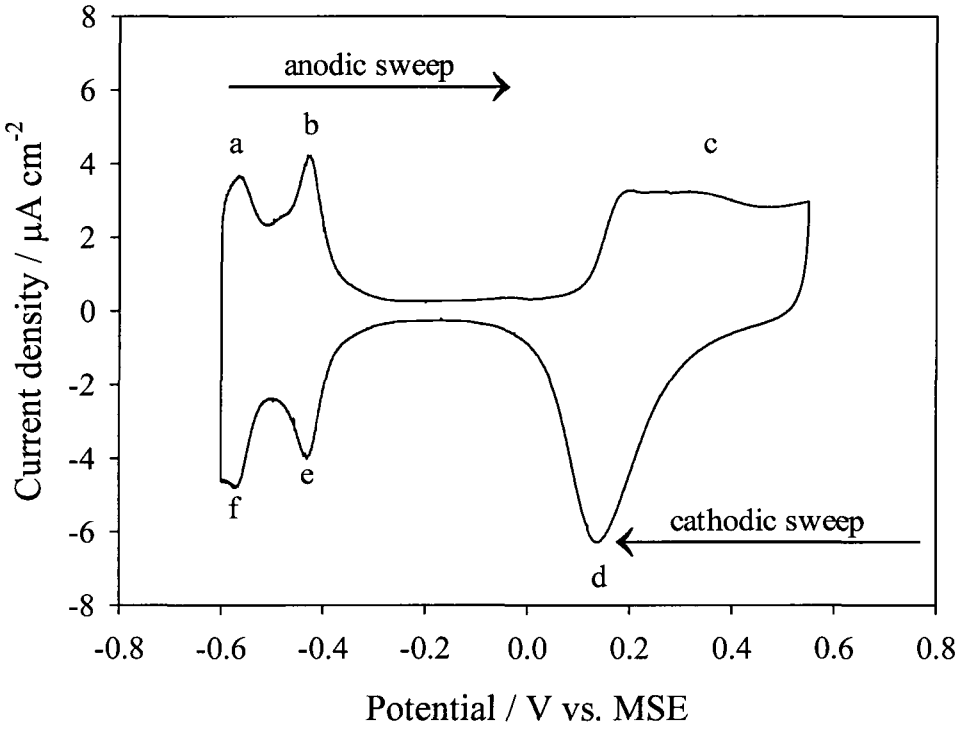

Figure 2.2 Cyclic Voltammogram of polycrystalline bulk platinum in 0.5 M H_2SO_4 vs. MSE. Sweep rate 10 mV s^{-1}.

Sweeping the potential anodically (see Figure 2.2) past 0.1 V vs. MSE causes the measured anodic current to increase and plateau (plateau c). The measured current of plateau c represents the combination of double layer charging and the adsorption of oxygen. As mentioned above, double layer charging is a purely capacitive process. Platinum oxidation, on the other hand, is a pseudo capacitive electrochemical process.

$$Pt + H_2O \rightarrow PtOH + H^+ + e^- \qquad (2.13)$$

On the cathodic sweep, a large peak (d) centered at 0.13 V vs. MSE represents the desorption of oxygen, i.e., reduction of the Pt-O_x layer:

$$PtOH + H^+ + e^- \rightarrow Pt + H_2O \qquad (2.14)$$

It should be noted that the potential at which the oxide is formed is different than the potential at which it is removed, i.e. plateau c and peak d are not symmetrical. This suggests that the oxidation and reduction of platinum (when the platinum electrode is cycled to the anodic potential shown in Figure 2.2) is a less reversible process than the adsorption and desorption of hydrogen.

Oxygen gas evolution, which occurs at potentials more positive than 0.55 V vs. MSE (not shown in Figure 2.2), and hydrogen gas evolution, which occurs at potentials more negative than – 0.6 V vs. MSE (not shown in Figure 2.2), are two examples of Faradic processes.

One of the useful experimental parameter that can be obtained from a cyclic voltammogram of platinum is the surface area of platinum, which can be determined from the measured charge associated with the adsorption or desorption of hydrogen. The charge associated with the adsorption or desorption of a monolayer of hydrogen on polycrystalline Pt is known to be 210 $\mu C\ cm^{-2}$.[50] For example, the hydrogen adsorption charge calculated from the measured current in Figure 2.2, using Equation 2.7, is 70 μC. Thus, the surface area of platinum used in the experiment run to obtain Figure 2.2 is 70 $\mu C/210\ \mu C cm^{-2} = 0.33\ cm^2$.

Cyclic voltammograms are used throughout this thesis as a means to determine (1) if platinum was successfully deposited onto the substrate; (2) to test the stability of platinum, i.e., to see if the platinum surface area changes during and after electrochemical testing; and (3) to give insight into the type of platinum that has been formed, i.e. how easily it oxidizes.

2.3.2 Electrochemical Impedance Spectroscopy.

Electrochemical impedance spectroscopy, EIS, was used to determine the double layer capacitance of the substrates, i.e. freshly cleaved, ozone oxidized, and electrochemically oxidized HOPG. EIS is a technique where a small amplitude alternating (ac) voltage is applied to the working electrode, thus the potential is given by

$$E = \Delta E sin(\omega t) \tag{2.15}$$

Where E is the instantaneous potential, ΔE is maximum potential, and ω is the angular frequency in hertz given by

$$\omega = 2\pi f \tag{2.16}$$

Impedance is a general term for resistance. All circuit elements, i.e. resistors, capacitors, and inductors, that impede current flow are referred to as impedance. For example, a pure resister (R) obeys ohms law ($i = \Delta E/R$) and therefore the resulting current of an applied sinusoidal potential is given by

$$i = \frac{\Delta E}{R} sin(\omega t) \tag{2.17}$$

When a sinusoidal potential is applied to a capacitor (C), the resulting current is determined from the definition of a capacitor;

$$q = CE \tag{2.18}$$

Where q is the charge passed through the capacitor. Differentiating the charge (Equation 2.18) with respect to time gives the current response

$$i = \frac{dq}{dt} = C\frac{dE}{dt}$$

$$i = C\frac{d(\Delta E sin(\omega t))}{dt}$$

$$i = \omega C \Delta E sin(\omega t + \pi/2)$$

$$i = \frac{\Delta E}{X_c} sin(\omega t + \pi/2) \tag{2.19}$$

Where $X_c = 1/\omega C$ is referred to as the capacitive resistance. A pure capacitor causes a phase shift in the current of $\pi/2$ compared to the potential. The impedance response caused by a resistor and a capacitor are shown in the Phasor diagrams in Figure 2.3 and the Nyquist diagrams in Figure 2.4. Phasor diagrams are constructed by considering the voltages and currents as rotating vectors. The x-axis of the Nyquist diagram is Z' which is the ohmic resistance, and the y-axis is the Z", which is the capacitive impedance $-jX_c$. Z' is the "real" or "in-phase" component and Z" is the "imaginary" or "out-of-phase" component of the impedance.

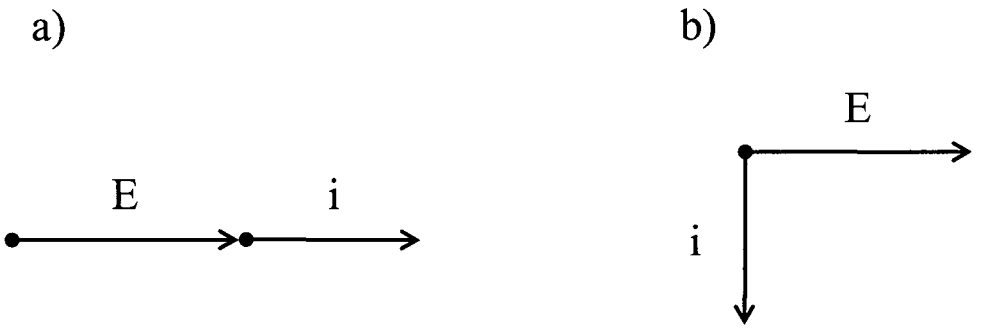

Figure 2.3 Phasor diagrams of a) a pure resistor and b) a pure capacitor.

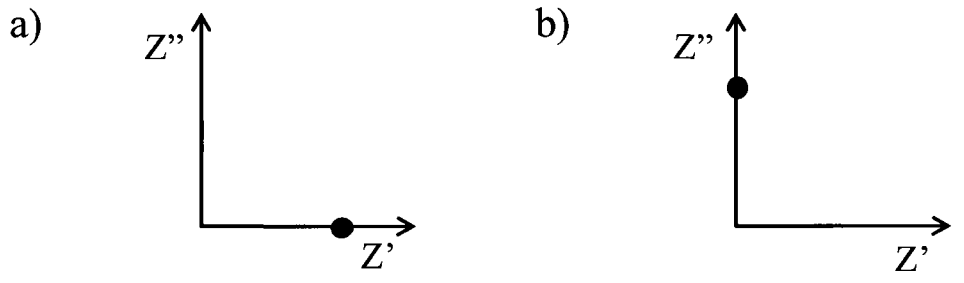

Figure 2.4 Nyquist Diagrams of a) a pure resistor and b) a pure capacitor measured at a single angular frequency.

The equivalent circuit for the charging of the double layer of HOPG is given by a resistor and capacitor in series (see Figure 2.5). The resistor, R_s, represents the resistance of the

system and the capacitor, C_{dl}, is the double layer capacitance. Since the circuit elements are in series the impedance is additive,

$$E = E_R + E_C$$

$$E = i(R - jX_C) \tag{2.20}$$

The Phasor and Nyquist diagrams for a resistor and capacitor in series is presented in Figure 2.6. It is important to emphasize that the Nyquist diagram in Figure 2.6 represents the impedance that results from a particular angular frequency. In EIS the impedance is measured for a series of angular frequencies. Figure 2.7 shows a Nyquist plot for a resistor and capacitor in series. As you can see from Figure 2.7, the impedance decreases with increasing frequency. As the frequency increases, the capacitive impedance decreases which makes the circuit behave more like a resistor.

Figure 2.5 The equivalent circuit diagram to represent the double layer charging of HOPG in a dilute sulfuric acid solution.

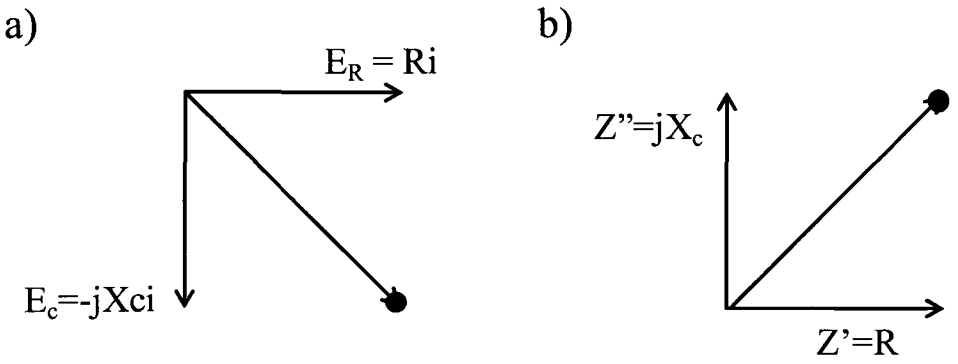

Figure 2.6 a) The Phasor and b) Nyquist Diagram for a resistor and capacitor in series measured for a single angular frequency.

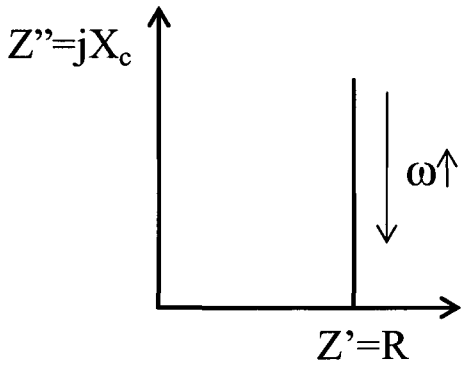

Figure 2.7 The Nyquist plot for a resistor and capacitor in series.

Figure 2.7 is the Nyquist plot for an ideal resistor and ideal capacitor in series. Real systems, however, are rarely ideal. The measurement of the double layer capacitance for HOPG in dilute sulfuric acid did not produce a Nyquist plot as show in Figure 2.7. Rather, instead of the impedance generating a perpendicular line to the imaginary axis the impedance was set at a slight angle. This deviation from ideal behaviour is caused by non-homogeneity on the surface, i.e. variations in the surface chemistry of the HOPG electrode. To determine the capacitance of this non-ideal system a constant phase element was used to replace the capacitor element in the circuit.

A Solartron Frequency Response analyzer 1260 driven by ZPlot was employed for the electrochemical impedance spectroscopy measurements. Measurements were taken at three different potentials within the double layer charging region; 0.22, 0.32 and 0.42 V vs. MSE. Double layer capacitance values were similar at all three potentials. The potential amplitude was set to 3 mV. The Impedance was measured for angular frequencies ranging from 0.1 to 10000 s^{-1}.

2.4 SURFACE CHARACTERIZATION

Various surface characterization techniques were utilized for this research. Scanning tunnelling microscopy, STM, and scanning electron microscopy, SEM, were used to analyze the carbon substrate before and after oxidation (see Chapter Four). Transmission electron microscopy, TEM, was utilized to study the as prepared particle morphology as well as the morphology after various electrochemical tests were performed (see Chapters Three, Four,

and Five). Finally, X-ray photoelectron spectroscopy, XPS, was used to study the interactions between the prepared catalysts and the substrate that they were deposited upon (see Chapter Seven). The following sections introduce these surface characterization techniques. The purpose of this section is to provide the reader with sufficient information as to understand the interpretation of the results gained by using these techniques; it is not meant to be an all inclusive description of how the instrument operates.

2.4.1 Transmission Electron Microscopy.

Transmission electron microscopy, TEM, was used to generate images of the prepared Pt nano-catalysts on the carbon substrate. From these images the size of the prepared nano-catalyst size and their distribution over the substrate was easily determined. TEM images are presented in Chapters Three through Six. This section will highlight the principals of operation as well as the basic instrumental components needed to generate a TEM image. Additionally, the method of sample preparation, which is unique to HOPG (the carbon substrate used in this work) will also be reviewed.

2.4.1.1 Principles of operation.

In transmission electron microscopy a beam of electrons is passed through a thin slice of a sample. The electrons that are transmitted through the sample are then analyzed by a detector. The resulting images shows differences in atomic composition (heavier elements appear darker in the image) as well as some topographic information (thicker regions in the sample also appear darker in the image). In order to understand how the transmission of electrons through a sample can generate such an image, it is important to understand the different possible fates of an electrons that passes through a sample. The three most significant possible fates are:[51] (1) The electron can transmit through the sample without interacting with any atoms. (2) The electron is elastically scattered. Or (3) the electron is inelastically scattered (i.e., it loses a significant amount of energy) resulting in the transfer of energy to secondary electrons or in the emission of X-rays. If all three types of transmitted electrons were to be collected at the detector, the resulting image would not have any contrast. In order to generate an image with contrast, the (elastically or inelastically) scattered electrons must be separated from the electrons that didn't interact with the sample at all. Contrast is generated by the use of an aperture that stops electrons that scatter, for

a) Electron transmission through sample

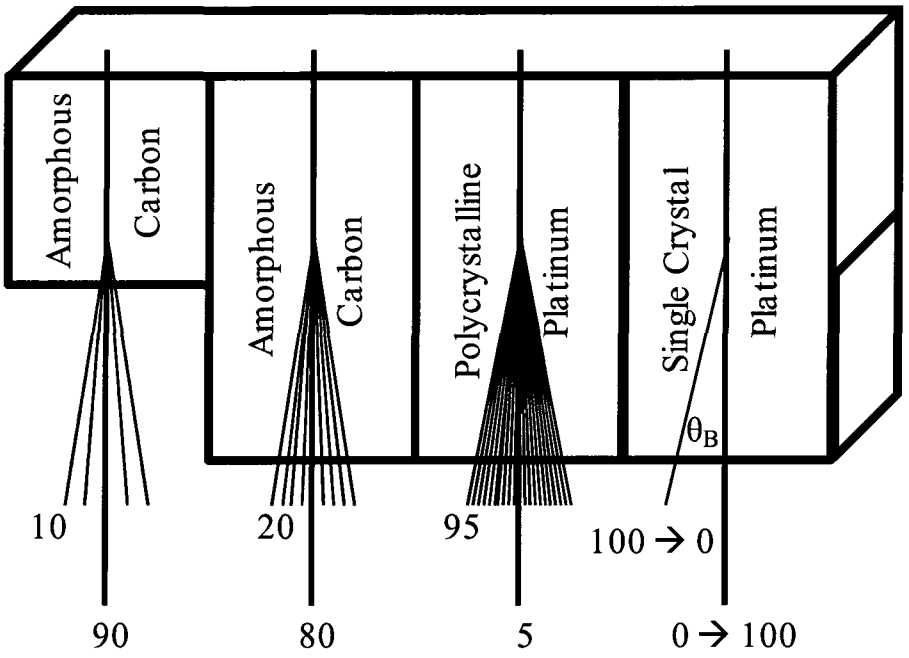

b) Resulting TEM image

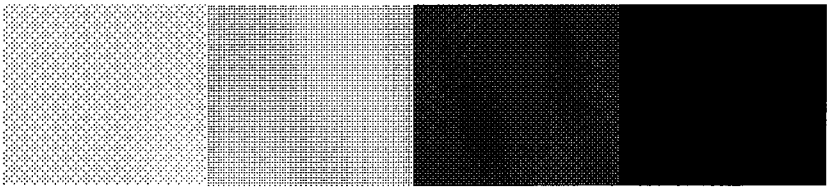

Figure 2.8 a) Schematic representation of electrons transmitting through four different media. The numerical values represent the percent of electrons deflected by 0.5° or more, and the percent that are un-scattered. b) Schematic representation of the resulting TEM image from the sample in part a.

example, by more than 0.5°, from the incident bream from transmitting to the detector. This concept is best described by comparing the scatter that results from different materials.[51] For example, Figure 2.8a is a schematic representation of the percent of electrons scattered and unscattered as they pass through four different media. When electrons are transmitted through amorphous carbon, only a small amount of electrons are scattered by more than 0.5° since carbon is a very light atom. If, however, electrons are transmitted through a thicker

layer of amorphous carbon, then a greater percentage of electrons will be scattered. Due to the higher molecular mass of platinum compared to carbon, a much larger number of electrons will be scattered by 0.5° or more when transmitted though polycrystalline platinum, compared to the same thickness of amorphous carbon. The last media represented in Figure 2.8a is crystalline platinum. In a single crystal media, scattered electrons will be reinforced at certain angles, and cancelled out in other angles. Thus, the majority of the scattered electrons will travel at a specific angle from the unscattered beam know as the Bragg angle, θ_B. The number of electrons emerging from the specimen in the unscattered and diffracted beams is dependent on the specimen orientation, and thickness and can range from almost zero to 100 %.

If the TEM detector measured all of the electrons transmitted through the sample represented in Figure 2.8 then there would be no contrast in the resulting image. However, if an aperture was placed between the sample and the detector that prevented electrons that were deflected by more than 0.5° from traveling to the detector, then a different number of electrons would transmit to the detector for each of the different materials. For example, in Figure 2.8, the thin region of amorphous carbon would transmit the greatest number of electrons, followed by the thicker region of amorphous carbon, and polycrystalline platinum would transmit the least number of electrons. The amount of electrons transmitted by the platinum single crystal would depend on the crystal face and sample orientation, in this example let's assume that almost all of the electrons are deflected greater than 0.5°, and therefore almost zero electrons are transmitted through the aperture to the detector. Since the thin region of amorphous carbon would transmit the greatest number of electrons through the aperture, it would generate the brightest region in the TEM image (see Figure 2.8b) the thicker region of amorphous carbon transmits comparatively less electrons and is therefore darker than the thin region of amorphous carbon. The region of polycrystalline platinum, which transmits far less electrons than either carbon region, will have a darker TEM image than either carbon region. And finally, the single crystal TEM image, which in this example has almost no transmission of electrons, will have an almost black TEM image.

Most TEM instruments, including the one used for this work, use a thermionic triode electron gun that produces an intense beam of high energy electrons which is directed down the microscope column. Electromagnetic lenses are used to change the magnification or

focus of the electron microscope. The lenses work by exerting an electromagnetic field symmetrically around the optical axis of the microscope. This can be easily achieved by winding a coil around the optical axis of the TEM. A condenser lens focuses the electron bean to a spot size around 1 μm onto the sample. Below the sample lies an objective lens that focuses on the specimen and forms an intermediate image at a magnification of about 50 x. After the objective lens a series of lenses are used to magnify the central part of the image.

2.4.1.2 Sample preparation and instrumentation.

TEM samples were prepared by gluing a Cu grid to the surface of the HOPG substrate upon which platinum was deposited using a small amount of Vishay Micro-measurements 610 bond. After curing the glue for one hour at 100 °C, the Cu grids were peeled off the HOPG surface. Small amounts of HOPG remained attached to the grid and TEM analysis was performed on the HOPG flakes. To determine if heating the sample at 100 °C for one hour affected the platinum nanoparticles, one sample was prepared using Krazy Glue® cured at room temperature. Comparison of the sample prepared using 610 bond and Krazy Glue® indicated that heating the sample to 100 °C for one hour had no effect on platinum morphology. 610 bond allowed for easier sample preparation, and therefore, was used for all TEM analysis. Due to the destructive nature of the TEM sample preparation, the same sample could not be imaged before and after electrochemical analysis. A Philips CM 20 TEM was employed.

2.4.2 Scanning Electron Microscopy.

Scanning electron microscopy, SEM, was used to study the topography of oxidized HOPG the carbon support upon which Pt nano-catalysts were deposited. Additionally, some Pt deposits were analyzed by SEM. SEM results are presented and analyzed in Chapter Four.

2.4.2.1 Principles of operation.

An electron beam that impinges a surface and interacts with the atoms of the surface can produce auger electrons, secondary electrons, backscattered electrons, characteristics X-rays, continuous X-rays, and Fluorescent X-rays. The number of secondary electrons emitted from a surface is dependent on the incident angle of the electron beam to the surface. Thus,

the collection and analysis of secondary electrons can generate topographical information of a surface. During analysis an electron beam, generated from an electron gun, is finely focused on the sample's surface. As the beam is scanned over the sample's surface in the x_i and y_i directions, secondary electrons and backscattered electrons are ejected from the surface and detected by the SEM instrument.

The electron beam used in SEM instruments can be generated by either a thermionic emission gun or a field emission gun. The instrument used in this work uses a thermionic emission gun. The electron bean is focused on the sample by a series of lenses. The secondary electrons emitted from the surface are detected and used to generate a topographical image of the sample. Emitted backscattered electrons can also be detected and generate images that show a contrast depending on the mean atomic number of the atoms in the sample. X-rays emitted from the sample during SEM analysis can generate qualitative and quantitative elemental information of the sample's composition. However, elemental analysis was not required and therefore backscattered electrons and X-rays were not analyzed.

2.4.2.2 Instrumentation.

Samples were analyzed by scanning electron microscopy using a JEOL 840A scanning electron microscope. All photos were taken using an accelerating voltage of 20 kV at a working distance of 15 mm.

2.4.3 Scanning Tunnelling Microscopy.

Scanning tunnelling microscopy, STM, is a surface analysis techniques commonly used to detect changes in surface topography. During analysis, a probe that measures changes in surface electron density is rastered across a surface. If the surface has relatively uniform electronic properties, the resulting STM image effectively represents the surface topography. STM was used extensively to study the effects of oxidizing HOPG which are discussed in Chapter Four. This section will review the concept of quantum mechanical tunnelling as applied to STM operation, introduce the two modes of operation, and finally highlight the STM probe requirements and methods of probe preparation.

2.4.3.1 Principles of operation.

Quantum mechanical tunnelling.

STM operates by measuring electrons that travel between the sample and the STM probe, which is commonly called a tip. This highlights the biggest restriction of STM analysis; STM analysis of a sample is only possible if the sample is electron-conducting. Electrons travel between the sample and the STM tip via quantum mechanical tunnelling. Quantum mechanical tunnelling is the penetration of a potential barrier by an electron wave function. In the case of STM the barrier is the material between the STM tip and the sample. The type of material that makes up the barrier is determined by how the STM analysis is completed. For example, if STM analysis is done in vacuum then the barrier is a vacuum gap, or if analysis done in solution (i.e., for some biological applications) then the barrier is the solution. For the work presented in this thesis, all of the STM analysis was done in ambient air, and therefore, the barrier that electrons must pass through is ambient air.

Although STM analysis is done in the real three dimensional world, the process of quantum tunnelling is best described, and most easily understood, by considering the simple case of one-dimensional tunnelling.[52] For example, consider the system of an electron that is traveling towards an infinitely thick potential barrier of height V (see Figure 2.9).

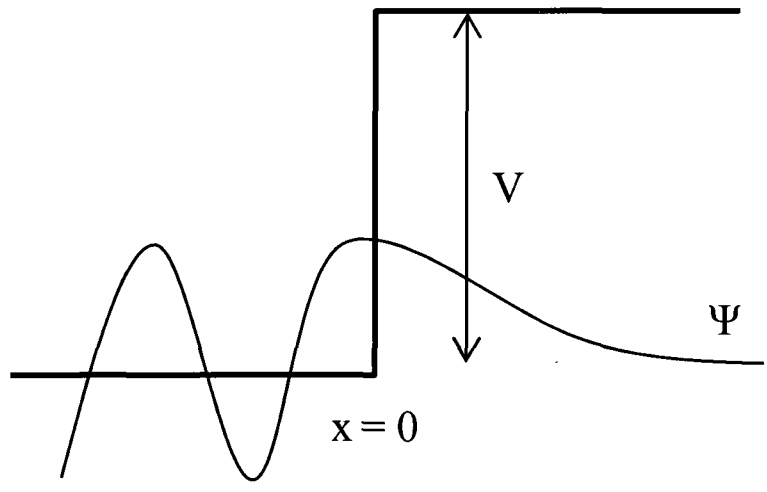

Figure 2.9 A schematic representation of a one dimensional potential barrier, of height V, position at x = 0.

The Schrödinger equation has two components for this system, at $x < 0$

$$\hat{H}\Psi = -(h^2/2m)\left(d^2\Psi/dx^2\right) \tag{2.21}$$

and at x > 0

$$\hat{H}\Psi = -(h^2/2m)\left(d^2\Psi/dx^2\right) + V\Psi \tag{2.22}$$

Where m is the mass of the particle (an electron in this case), and h is the well known Planck constant. The solutions of Equations 2.21 and 2.22 are

$$\psi = A^{ikx} + B^{-kx},\ k = (2mE/h^2) \text{ at } x < 0 \tag{2.23}$$

And

$$\psi = C^{ik'x} + D^{-k'x},\ k = (2m(E-V)/h^2)^{1/2} \text{ at } x > 0 \tag{2.24}$$

Inside the barrier, (x > 0) the wave function has an imaginary part that rises to infinity (and is thus ignored) and a real part that decays exponentially with increasing x. The physical meaning of Equation 2.24 is that there is a finite probability of finding the electron past the barrier, i.e. the electron can tunnel through the barrier, which is strictly forbidden by classical theory. Moreover, Equation 2.24 indicates that the probability of finding the electron decreases with increasing distance past the barrier.

A closer approximation of the one-dimensional analogy to an actual STM apparatus is when two of the above described barriers are combined so that there are two electrodes with given work functions, Φ_1 and Φ_2, separated by a distance, d, (see Figure 2.10). When the two electrodes are separated by a relatively large distance, then the effective overlap of the Fermi level wavefunctions is negligible due to the exponential decay of the wave functions of the two electrodes. However, when the electrodes are brought sufficiently close together to allow for a minimum amount of overlap of the two electrodes' wavefunctions then quantum mechanical tunnelling occurs. Under these conditions, if an potential difference is

applied then a measurable current will pass between the two electrodes. Within the STM application, one of the electrodes is the sample and the other electrode is the STM tip.

Figure 2.10 is still a one dimensional representation of quantum tunnelling. A three dimensional representation is required to more accurately depict the quantum mechanical tunnelling between an STM tip and the sample under analysis. Tersoff and Hamann are most commonly quoted for the full expression of the tunnelling current.[53] The full expression, however, is beyond the scope of this chapter. What is important to understand when analyzing STM data is that the relationship between the measured current, and the distance between the tip and the sample is as follows:

$$I \propto e^{-2\kappa d} \tag{2.25}$$

$$\kappa = (2m\phi/h^2)^{1/2} \tag{2.26}$$

The above equations indicate that the magnitude of the measured current is a exponentially proportional to the distance between the STM tip and the sample. For example, as the distance between the STM tip and the sample increases, the measured current decreases (at constant applied potential). Equation 2.26 emphasizes that STM instruments measure electron density, which is dependant on the work function of the STM tip and sample.

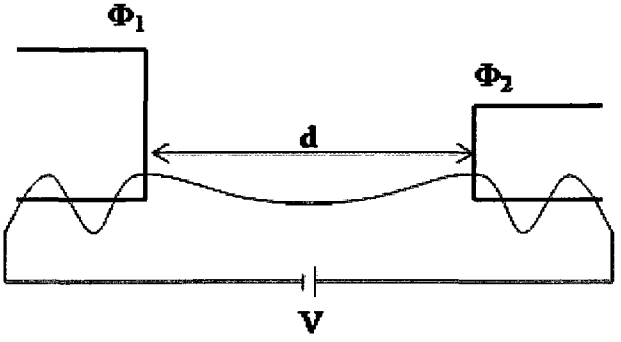

Figure 2.10 Schematic representation of one dimensional quantum mechanical tunnelling between two electrodes with two different work functions, Φ_1 and Φ_2, separated by a distance, d. When a potential, V, is applied between the two electrodes the resulting current can be measured.

STM operational modes.

The distance between the STM tip and the sample, as well as the (x_i, y_i) position of the STM tip on the sample is varied by a piezoelectric crystal on which the tip is mounted. (The same effect is achieved if the sample is mounted onto a piezoelectric crystal.) Piezoelectric crystals move in a well defined manner in each of the three directions (x_i, y_i and z_i directions) when a potential difference is applied in each of the directions. STM instruments generally operate under one of two modes; either constant-current or constant-voltage. In constant-current operation, the tunnelling current is measured at each position (x_i, y_i) and the voltage, termed the bias voltage, is adjusted via a computer-controlled feedback loop to ensure that the tunnelling current re–assumes the pre-set value. The STM image that results from constant-current operation, therefore, represents the variation in the bias voltage with respect to coordinate (x_i, y_i). Conversely, in constant-voltage mode, a bias voltage is applied between the STM tip and sample and the resulting current measured. Thus, in constant-voltage mode the resulting STM image represents the variation of the measured current with respect to the coordinate (x_i, y_i). The disadvantage of constant-voltage mode is that there is no fail-safe mechanism in place to prevent the STM tip from crashing into the sample, whereas in constant-current mode the occurrence of tip crashing is minimized since the distance between the STM tip and sample is continually changed (via the feed-back loop) to maintain a constant-current. Most STM instruments, including the instrument used in this work, operate in constant-current mode.

The STM tip.

To achieve atomic imaging, the STM tip must have a single atom situated at its apex. However, for nano-scale images, as are presented in this thesis, a single atom apex is not required. STM tips can be prepared mechanically or by electrochemical etching. Mechanical tip preparation techniques, which is by far simpler and less time consuming than electrochemical etching, involved cutting a platinum-iridium wire on a 45° angle with a sharp pair of wire-cutters. To prepare a tip by electrochemical etching, a solution of NaOH is used as the electrolyte in which a tungsten wire is electrochemically etched. Once the wire is placed in the center of a thin meniscus of the electrolyte, an anodic potential is applied. Due to diffusion effects, the wire etches predominantly at the center of the meniscus. Once

the wire has been etched through, the lower portion of the wire drops off generating two very sharp tips. The experimental difficulty of electrochemically etching tips lies in terminating the applied potential at the exact instance that the lower portion of the tungsten detaches. If the potential continues to be applied after the lower portion has detached the upper portion of the wire will continue to etch resulting in a dull and unusable tip.

2.4.3.2 Instrumentation.

STM studies were performed at room temperature and in ambient air using a Pico SPM from Molecular Imaging. STM tips were prepared by both mechanical and electrochemical etching techniques for this work.

2.4.4 X-ray Photoelectron Spectroscopy.

X-ray photoelectron spectroscopy, XPS, is a powerful ex-situ analysis technique for the characterization of the platinum electrodes prepared in this work. XPS was used to test for the presence of platinum, to ensure that the deposited platinum was in the metallic form, and to study the relative strength of the interactions between the prepared platinum nano-catalysts and the support that they were deposited onto. This section will briefly highlight the results of interactions between X-rays and matter, introduce the concepts of initial and final state effects, and finally, present an overview of how an typical XPS instruments generates data.

2.4.4.1 Principles of Operation.

X-ray interactions with matter.

The first step to understanding XPS is to understand that when a photon impinges upon an atom three different events may occur: (1) The photon can pass through the atom without interacting with the atom. (2) The photon can be scattered by an atomic orbital electron causing a partial energy loss. Or finally, (3) the photon may interact with an atomic orbital electron resulting in a total transfer of the photon energy to the electron that in turn causes an electron to be emitted from the atom. The latter describes the basis of XPS. The physics of this process can be described by the Einstein equation:

$$E_B = h\nu - \mathrm{KE} \tag{2.27}$$

Where E_B is the binding energy of the electron in the atom, hv is the energy of the X-ray source (a known value), and KE is the kinetic energy of the emitted electron (measured in the XPS spectrometer). Hence, E_B that gives information regarding the type of atom and its environment can easily be determined from the measured kinetic energy of the emitted electron and the known energy of the X-ray source. The challenge of XPS lies in interpreting the binding energy values. Photo-emitted electrons cannot easily travel through solids. Typically the photo-emitted electrons will only penetrate approximately 10 nm, making XPS a surface-characterization technique.

Initial and final state effects on binding energy, i.e. chemical shifts.

An incident photon that interact with an atomic orbital electron and results in a total transfer of its energy to a core-level electron and in turn causes an electron to be emitted from the atom is the basis of XPS. This process is illustrated schematically in Figure 2.11a. After the electron has been photo-emitted, the atom will re-arrange its electrons to minimize its energy. Figure 2.11b illustrates how an electron can move within the atom to a lower energy level. The excess energy, due to rearrangement, can be released in the form of an Auger electron or X-ray photon emission, referred to as X-ray fluorescence, Figure 2.11c. Auger electron analysis is a separate surface analysis technique that is not used in this work, and therefore, will not be discussed. Since XPS involves the analysis of photo-emitted electrons, Figure 2.11a, it is tempting to ignore the rearrangement process, Figure 2.11b. However, rearrangement is very important to XPS as it defines the final state. The binding energy of the emitted photo electron is the difference between the $(n-1)$-electron final state and the (n)-electron initial state, i.e.,

$$E_B = E_f(n-1) - E_i(n) \tag{2.28}$$

The initial state is the ground state of the atom before photo-ejection, and the final state is the state of the atom after rearrangement. If either the initial or final state changes, then Equation 2.28 indicates that the binding energy will also change, ΔE_B, which is referred to as a chemical shift.

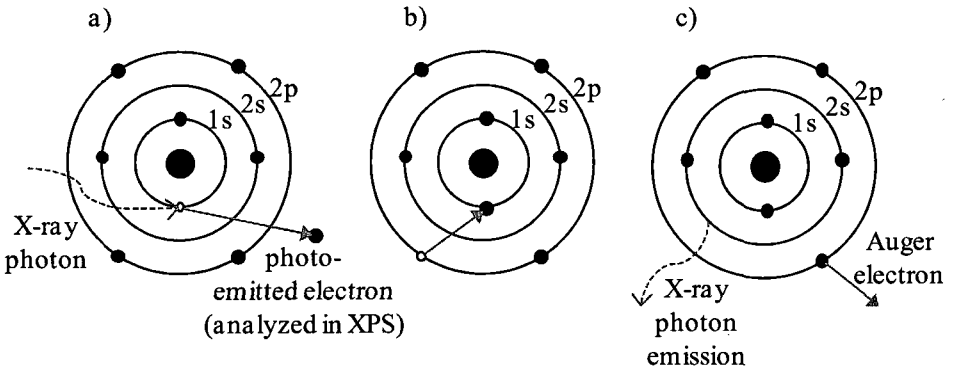

Figure 2.11 A schematic representation of a) the incident photon interaction with an core-level electron resulting in a total transfer of energy that in turn causes an electron to be emitted from the atom (it is the kinetic energy of this electron that is measured and used to calculate the binding energy Equation 2.27); b) rearrangement to minimize energy; c) the excessive energy released as an Auger electron and also possibly the emission of an X-ray photon.

The formation of chemical bonds with other atoms can alter the initial state of an atom. For example, as the formal oxidation state of an element increases, the E_B of the photo-emitted electrons from that element will also increase. For most samples, ΔE_B is interpreted solely in terms of changes in initial state. However, electron rearrangement, which occurs after photoemission, always results in the lowering of E_B. When rearrangement involves the movement of inner shell electrons, that have larger E_B than the emitted photo electron, the contribution to the atomic relaxation energy is small and can be ignored. However, most of atomic relaxation results from outer shell electrons, which have a smaller E_B than the emitted photoelectron and should not be ignored.

A particular final state effect that is worth discussion, since it pertains to platinum metal and this thesis pertains to the preparation and study of platinum nano-catalysts, is spin-orbit coupling (or $j-j$ coupling). Spin-orbit coupling arises when there is an open shell (of quantum number $l > 0$) with two states of the same energy (orbital degeneracy). A magnetic interaction between the spin of the electron (up or down), see Figure 2.12, and its orbital angular momentum may lead to a splitting of the degenerate states into two components.

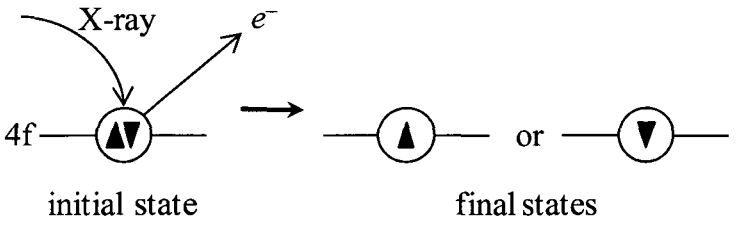

Figure 2.12 Schematic representation of the initial and final states of an electron photo-emitted from a platinum 4f orbital. The final state has two equivalent states, either the spin-up or spin-down state.

The ratio of the respective degeneracies, $2j + 1$, determines the intensities of the components. Quantification of the amount of platinum on a surface is done using the sum of the two spin-orbit peaks.

The experiment.

XPS experiments must be done under vacuum conditions to allow the emitted photoelectrons to travel from the sample to the detector without colliding with gas phase particles, X-ray sources require vacuum conditions to remain operational, and the surface composition of the sample must not change during analysis. In addition to a vacuum system, an X-ray source, an energy analyzer, and a data system are all required to perform XPS analysis of a sample.

X-rays in an XPS experiment are produced by impinging a high-energy electron beam on a target. This creates core holes in the target material (see Figure 2.11a), which in turn causes rearrangement in the target, (see Figure 2.11b), and finally fluorescence X-rays and electrons are emitted (see Figure 2.11c). Fluorescing X-rays from the target are used to generate photo-emitted electrons in the sample (see Figure 2.11a). Several difficulties arise if the fluorescing X-rays are allowed to directly strike the sample. For example, the resolution will be limited to the natural width of the fluorescence line (1 – 2 eV). An X-ray monocromator, normally one or more quartz crystals, can be used to optimize the resolution of the fluorescence lines. Other disadvantages of allowing the fluorescing X-rays to directly hit the sample are; (1) satellite peaks appear in the XPS spectrum due to satellite X-ray fluorescence lines also striking the sample, and (2) sample degradation can result from high energy electrons also hitting the sample. These two problems can be eliminated by placing a

thin Al foil between the target and the sample that prevents the passing of electrons and satellite X-ray lines.

2.4.4.2 Instrumentation.

XPS spectra were obtained using a Kratos Axis Ultra spectrometer equipped with a monochromatized AlKα source. For each catalyst, a survey spectrum was collected before high-resolution spectra of the C 1s, O 1s, and Pt 4f core level regions were collected. After Shirley background removal, the peaks were separated using CasaXPS Version 2.3.12. Shifting that may have arisen due to charging was compensated by setting the major C 1s peak to 284.7 eV, which is typical for HOPG.[54] All the remaining high-resolution spectra were corrected accordingly.

Chapter Three

Electrochemical Deposition onto Freshly Cleaved HOPG

3.1 ABSTRACT

The electrochemical deposition of Pt onto freshly cleaved HOPG has been studied in detail. Analysis of current – time transients indicates that the growth of Pt deposits occurred via a 3D nucleation process. Nucleation analysis indicates that the deposition process is highly irreproducible, varying from a progressive to instantaneous nucleation process. TEM analysis indicates that Pt clusters are formed during the deposition process. The clusters are either agglomerates of nanoparticles or dendrite structures. The clusters are located predominately along step edges on the HOPG surface, indicating that the step edges are acting as nucleation and/or stabilization sites.

3.2 INTRODUCTION

Platinum is used to catalyze a vast number of heterogeneous reactions including hydrogenation, dehydrogenation, isomerisation, reduction, and oxidation reactions.[55] It is platinum's high activity towards oxidizing hydrogen and simple organics such as methanol, as well as reducing oxygen, that renders it an important catalyst for low temperature energy conversion technologies such as polymer electrolyte membrane fuel cells (PEMFCs) and direct methanol fuel cells (DMFCs). Platinum nano-catalysts are generally deposited onto a carbon support, typically high surface area carbons such as carbon black, when the catalysts are used in a low temperature fuel cell system. Unfortunately, these types of support do not allow for easy characterization of the Pt catalysts, thus other carbon supports, such as highly ordered pyrolytic graphite, HOPG, have been investigated as an alternative support to study various Pt catalyst phenomenon such particle-support interactions. HOPG has been selected as an alternative carbon support since it has well-defined surface characteristics and it is catalytically inactive for a number of reactions of interest.

Platinum deposited potentiostatically onto HOPG is a promising method to fabricate a Pt/HOPG electrode suitable for catalytic activity testing. Electrochemical deposition offers the advantages that stabilizers (which should be avoided as residues of stabilizers likely influence the catalytic activity of the nanoparticles) are not required, and that the particle size can be controlled by varying the length and the amplitude of the potential pulse. Other

studies have utilized potentiostatic deposition to generate a Pt/HOPG catalyst system. However, early attempts have not shown much success.

For example, electrodeposition of Pt, using a solution of H_2PtCl_6 + HCl, onto HOPG resulted in large Pt agglomerates containing flat crystallites located around HOPG step edges.[56] In another study,[57] also using H_2PtCl_6 as the platinum source, Pt nanoparticle growth on HOPG could be changed from 3D growth to 2D growth by removing $HClO_4$ which was used as a supporting electrolyte. Regardless of the absence or presence of supporting electrolyte, Pt nanoparticle aggregation was observed.[57] Electrochemical deposition at relatively large overpotentials has been found to result in individual non-agglomerated nanoparticles, however, particle size distributions were too large for accurate catalytic activity testing.[34,58]

In this chapter, we investigate potentiostatic electrochemical deposition of Pt onto HOPG. Current-time transients are analyzed to deduce the nature of platinum nucleation. Finally, the morphology of the platinum deposits are examined by transmission electron microscopy.

3.3 EXPERIMENTAL

3.3.1 Solutions, Cells, and Electrodes.

Chapter Two, Section 2.2 describes the solutions, cells, and electrodes used in this work. A Hg/Hg_2SO_4, 0.5 M H_2SO_4 (MSE) electrode was used as the reference electrode for electrochemical deposition of Pt.

3.3.2 Substrate Pre-Treatment.

Grade SPI-1 HOPG from SPI supplies were used as substrates in all experiments. Pt was deposited onto freshly cleaved HOPG. The HOPG was freshly cleaved using the adhesive-tape method.

3.3.3 Platinum Deposition Method.

Electrochemical deposition of Pt onto freshly cleaved HOPG was carried out in a solution of 1 mM $PtCl_4$ (Alfa Aesar, 99.9 % purity) with 0.1 M H_2SO_4 as supporting

electrolyte. All solutions were deoxygenated with high purity argon gas prior to electrochemical deposition. Electrochemical deposition occurred at – 0.475 V vs. MSE.

3.3.4 Particle Size/Morphology Determination.

The size and morphology of platinum catalysts on HOPG were determined by transmission electron microscopy, TEM. Sample preparation was completed as described in Chapter 3, Section 3.4.1.3. Due to the destructive nature of the TEM sample preparation, the same sample could not be imaged before and after electrochemical analysis.

3.4 RESULTS AND DISCUSSIONS

3.4.1 Electrochemical Deposition of Platinum onto Freshly Cleaved HOPG.

A pulsed deposition technique was selected to deposit Pt onto HOPG. The potential was stepped from a protective anodic potential to a cathodic potential and then back to the anodic protective potential (see Figure 3.1). The HOPG substrate was immersed and removed from the platinum salt solution while the protective potential is applied. The protective potential was selected in order to prevent "spontaneous" deposition of Pt onto the HOPG surface before and/or after the deposition potential was applied.

Spontaneous deposition of Pt on HOPG refers to the formation of Pt^0 on HOPG by simply immersing the HOPG substrate into a platinum salt solution, i.e., the reaction is not initiated by applying a reduction potential or adding a reducing reagent, rather the reaction occurs spontaneously. To conserve charge neutrality, for the Pt salt to be reduced something must be oxidized. It is generally believed that surface groups on the HOPG are oxidized as the Pt salt reduces. Specifically, it has been suggested that electron-rich incompletely oxidized functionalities located at the step edges and other defects of the graphite layer are available to reduce the Pt salt.[34] Another possible explanation for the spontaneous deposition of Pt onto HOPG is that the carbon atoms located at defect sites and along step edges may be hydrogen-terminated, and that these hydrogen atoms act as reducing agents.[59] Finally, it has also been proposed that a disproportionation reaction of $PtCl_2$ to Pt(0) and Pt(IV) is also a possible source of Pt metal.[60] However, the disproportionation reaction is a bulk reaction and does not necessarily involve the HOPG surface. Thus, it is unlikely that disproportionation plays a significant role in the spontaneous deposition of Pt onto HOPG.

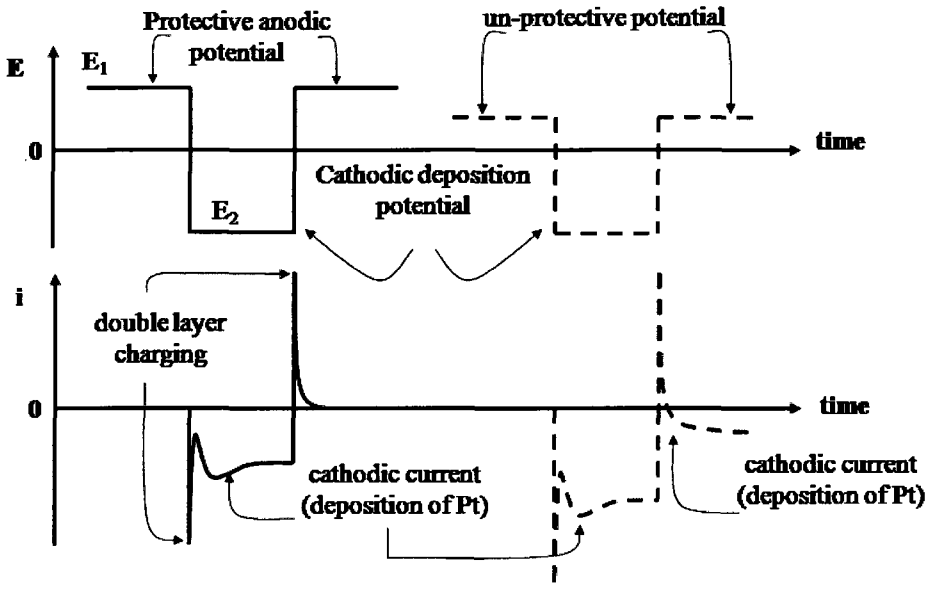

Figure 3.1 Schematic representation of the applied potential and resulting measured current.

It is important that spontaneous deposition of Pt onto HOPG is avoided to ensure that we have absolute control over the amount of platinum deposited onto the surface. As spontaneous deposition is a redox reaction that does not involve the counter electrode, electrons do not flow through the external circuit of the cell. Thus, there is no measured current associated with spontaneous deposition.

In addition to preventing spontaneous deposition, the protective potential applied after the deposition potential must prevent electrochemical deposition. This is because it is easier to reduce additional platinum onto the already deposited platinum. Figure 3.1 illustrates the effect of a protective potential which is not sufficiently anodic; as you can see there is a measured reduction current after the deposition potential is applied.

To select a suitable deposition potential for Pt, a linear potential sweep voltammogram was run. Figure 3.2, which shows the first sweep of the voltammogram, indicates a large increase in cathodic current that occurs at around – 0.2 V vs. MSE and a current plateau that ends at – 0.56 V vs. MSE. At the end of the current plateau, the cathodic current increases dramatically. XPS analysis indicates that the current plateau corresponds to the reduction of platinum ions to platinum metal onto the HOPG surface. The increase in current that begins at – 0.56 V vs. MSE is believed to correspond to the evolution of hydrogen gas. $H_{2(g)}$

evolution occurs at higher cathodic potentials (– 0.68 V vs. MSE) for polycrystalline platinum foil, (see the dotted line in Figure 3.2). However, the assignment of the cathodic current increase at – 0.56 V vs. MSE to $H_{2(g)}$ evolution is a likely explanation, since, as the potential was swept to even higher cathodic potentials, the cathodic current never decreased nor levelled off. It may be that H_2 evolution occurs more easily on a freshly-deposited Pt surface, like the one generated here on HOPG.

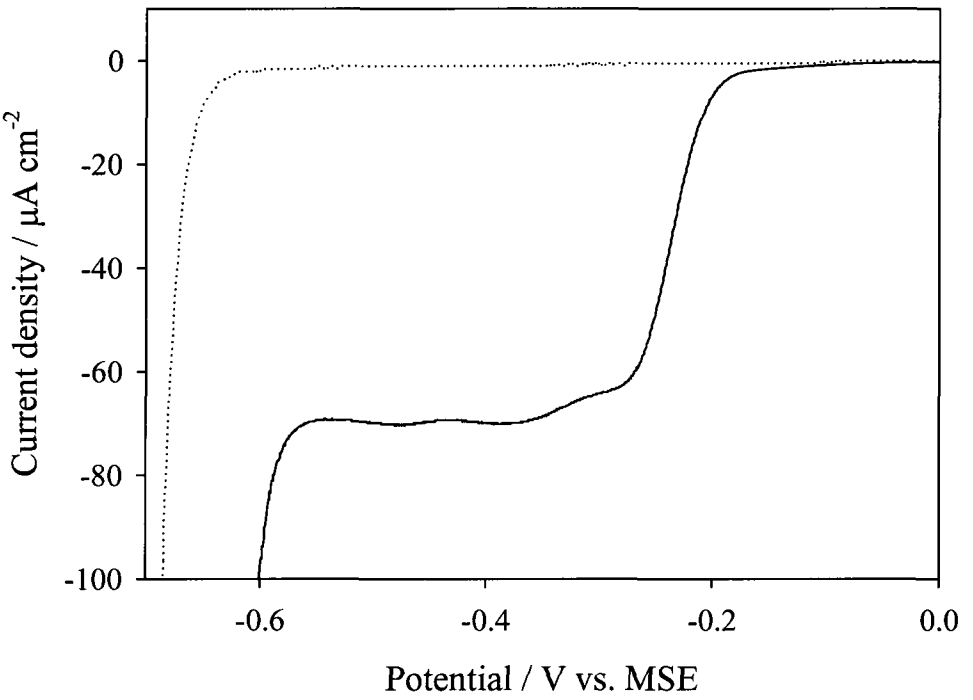

Figure 3.2 Linear sweep voltammograms recorded at 1 mV s^{-1} for freshly cleaved HOPG in 0.1 M H_2SO_4 + 1 mM $PtCl_4$ (_____). Included for reference is the linear sweep voltammogram recorded at 1 mV s^{-1} of polycrystalline platinum foil in 0.1 M H_2SO_4 (.....).

The deposition potential was selected to be – 0.475 V vs. MSE as XPS analysis indicated that metallic Pt is deposited onto the HOPG substrate at this potential . Additionally, since this potential is sufficiently more positive (by almost 100 mV) than the potential where $H_{2(g)}$ evolution begins, one can be confident that the measured current reflects exclusively the formation of Pt metal. The current-time transients can therefore be used to determine the

amount of Pt metal deposited, as well as the type of nucleation process occurring (discussed in Section 3.4.2).

In this chapter, deposition times between 2.5 and 7.5 s are employed. It has been reported that particles with heights as small as 1.5 nm were formed using shorter, e.g., 1 ms, deposition times.[35] However, the previous work was done at significantly higher overpotentials where the Pt reduction kinetics are more rapid. For the reasons discussed above, we have selected a lower overpotential for the Pt deposition, thus requiring longer deposition times. It was found in preliminary work that an insufficient amount of platinum was deposited using reduction times less than 2.5 s (and a deposition potential of – 0.475 V vs. MSE) to allow for electrochemical as well as TEM characterization of the deposits.

3.4.2 Pt Nucleation onto Freshly Cleaved HOPG.

Analysis of current-time transients for the electrochemical deposition of Pt onto freshly cleaved HOPG substrates, shown in Figure 3.3, indicates that Pt deposition occurs via a 3-D nucleation process. The transient can be divided into three regions: Region (1) is due to double layer charging, while regions (2) and (3) reflect the deposition of Pt.[61,62,63] The rise in cathodic current after the double layer charging, region (2), is caused by the increase in electro-active area due to (i) each independent nucleus growing in size; (ii) the number of nuclei increasing; or (iii) a combination of the two. During this initial stage of growth the nuclei develop hemispherical mass-transfer diffusion zones (see Figure 3.4). As the diffusion zones grow in size, they eventually overlap resulting in linear mass-transfer diffusion to an effectively planar surface (see Figure 3.4). Once the diffusion process becomes linear, the cathodic current falls exponentially as predicted by the Cottrell equation (3).

For the majority of nucleation processes, the empirical law

$$\frac{dN}{dt} = AN_0e^{-At} \tag{3.1}$$

describes the rate of nuclei formation.[64] N is the number of nucleation sites, N_0 is the number of sites at the beginning of the deposition process ($t = 0$), and A is the nucleation rate constant.

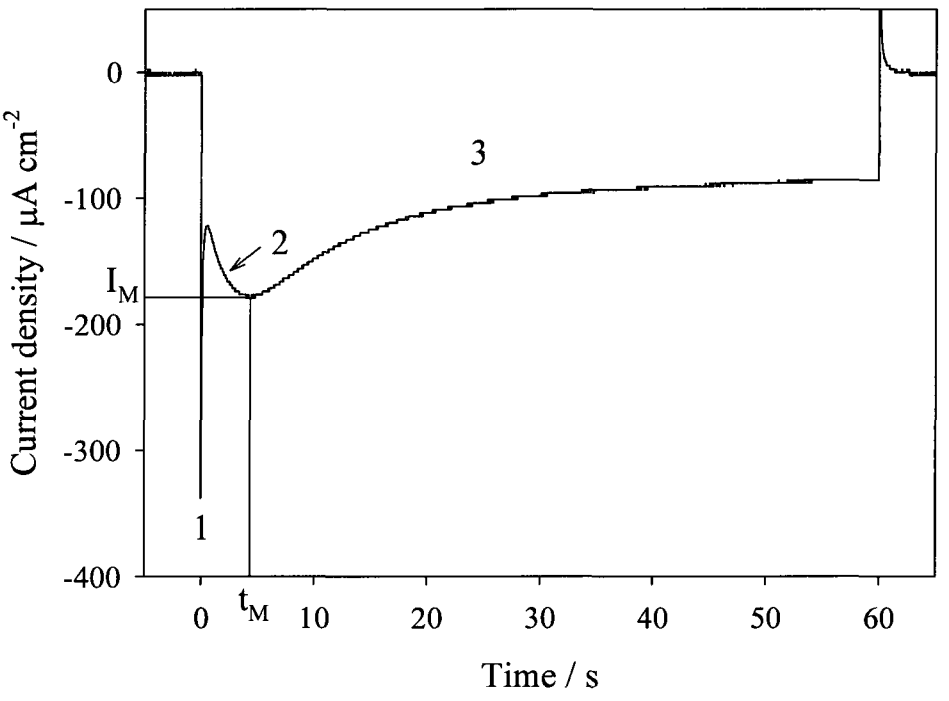

Figure 3.3 Potentiostatic reduction of $PtCl_4$ onto freshly cleaved HOPG at – 0.475 V vs. MSE in 1 mM $PtCl_4$ + 0.1 M H_2SO_4. At 60 s the deposition reaction is terminated by stepping the potential from the reduction potential (– 0.475 V vs. MSE) to the protective potential (+0.25 V vs. MSE).

If the nucleation rate is very large, integrating the rate law gives

$$N = N_0 \tag{3.2}$$

i.e., the number of nuclei is constant throughout the deposition experiment. In this case, nucleation is termed instantaneous since all the nuclei are formed instantaneously at the beginning of the experiment. Conversely, if the nucleation rate is very slow, integrating the rate law gives

$$N = AN_0t \tag{3.3}$$

and the number of nuclei is a function of deposition time. When a nucleation process has a slow nucleation rate, it is referred to as progressive nucleation, since the number of nuclei increases progressively with time. Assuming that all the nuclei grow at the same rate, instantaneous nucleation results in mono-size-dispersed particles. Thus, instantaneous nucleation is the preferred case in this work.

As mentioned above, regions (2) and (3) in Figure 3.3 reflect the nature of the deposition of Pt. For example, if the current maximizes (makes the transition from region (2) to region (3)) at shorter times for one sample, compared to another sample, then it could be concluded that the hemispherical diffusion zones have overlapped more quickly for the sample where the current maximizes at shorter time. This indicates that either the density of nuclei is larger or the growth rate of the nuclei is greater for the sample where the current maximizes at shorter times. Several mathematical models have been developed to characterize the electrochemical nucleation process. The theory which is most commonly utilized is one developed by Scharifker and Hills.[61]

The main obstacle in modeling the electrochemical nucleation of a substance on a planar surface is that although nucleation occurs on the plane of the electrode surface, the growth of nuclei and the diffusion of depositing species extends into the bulk of the electrolyte. Scharifker and Hills[61] solved this problem by considering the equivalent area of the planar surface towards which diffuses (by linear diffusion) the same amount of material that would be transferred, through spherical diffusion, to a hemispherical growing centre. Thus, the overlap of diffusion fields of individual nuclei is reduced to a two dimensional problem to which the Avrami theorem can be applied.

Using the theory developed by Scharifker and Hills,[61] the current transients can be plotted in reduced variables, $(I/I_M)^2$ vs. t/t_M, to easily determine if nucleation is instantaneous or progressive. Although reduced variable plots hide some of the finer details of current-transients, for example N_0 and A, they are useful to qualitatively compare experimental data with the limiting cases of progressive and instantaneous nucleation. The reduced variable equation for the limit of instantaneous nucleation[61] is

$$\frac{I^2}{I_m^2} = \frac{1.9542}{t/t_m}\{1 - exp[-1.2564(t/t_m)]\}^2 \qquad (3.4)$$

and the equation for the limit of progressive nucleation[61] is

$$\frac{I^2}{I_m^2} = \frac{1.2254}{t/t_m}\{1 - exp[-2.3367(t/t_m)^2]\}^2 \quad (3.5)$$

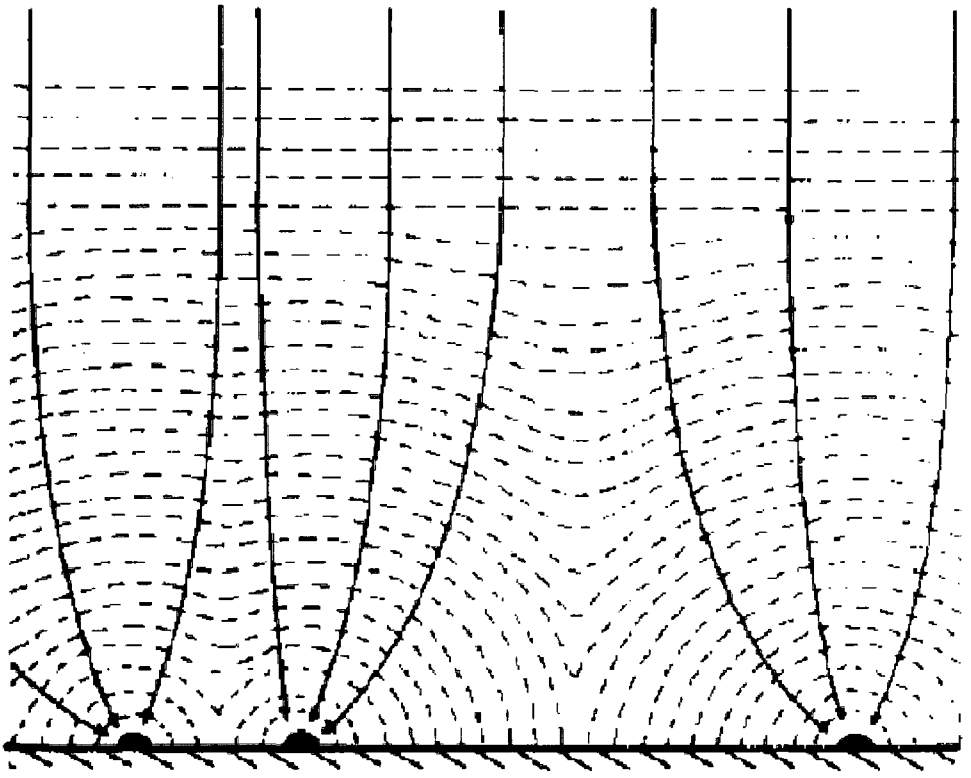

Figure 3.4 Schematic representation of the growth of diffusion zones and their eventual overlap.[61]

Reduced variable plots for three separate experiments of potentiostatic reduction onto HOPG in 1 mM $PtCl_4$ + 0.1 M H_2SO_4 at -0.475 V vs. MSE, run under the same experimental conditions, are plotted in Figure 3.5. It is seen that the three separate experiments give three different results. In one case nucleation was progressive, while in another case it was almost instantaneous. Such large variations in the nucleation process indicate a large variation in the number of nucleation sites on different HOPG substrates. Particles formed under progressive nucleation conditions will have a wider size dispersion than particles formed under instantaneous nucleation conditions. Furthermore, the

nucleation process varies between instantaneous and progressive between samples, hence the particle size distribution will also be sample dependant. Thus, analysis of the reduced variable plots, Figure 3.5, indicates that these conditions will not form Pt particles in a reproducible manner.

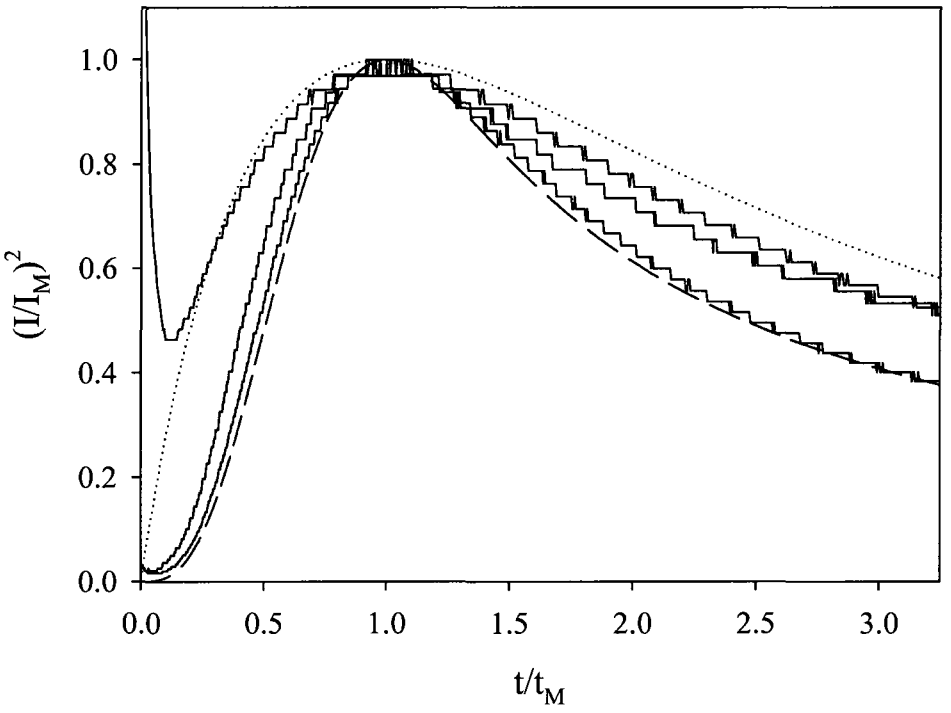

Figure 3.5 Reduced variable plots (see text) of potentiostatic Pt deposition onto freshly cleaved HOPG in 1 mM $PtCl_4$ + 0.1 M H_2SO_4 at – 0.475 vs. MSE. (_____) experimental data, (.....) theoretical instantaneous nucleation, and (_ _ _) theoretical progressive nucleation.

3.4.3 Platinum Morphology on Freshly Cleaved HOPG.

Figure 3.6 shows TEM images of Pt potentiostatically deposited for 5 s onto freshly cleaved HOPG. Figure 3.6a suggests that the average size of the Pt deposits is 80 ± 37 nm. Higher resolution images (a typical example is shown in Figure 3.6b) indicate the deposits are in fact clusters consisting of platinum particles that are on average 3.5 ± 0.4 nm in diameter. Whether or not these clusters are agglomerates of individual nanoparticles or represents dendrite structures will be discussed in Chapter 4, Section 4.4.3.

As seen in Figure 3.6a, the platinum deposits form along lines. As previous work[34,35,93] shows that electrochemically deposited platinum forms preferentially along step edges, the lines of platinum clusters observed here are assumed to coincide with step edges of the HOPG substrate. Defects in the basal plane can also act as nucleation sites, but on a typical HOPG surface they are far less numerous than step edges.

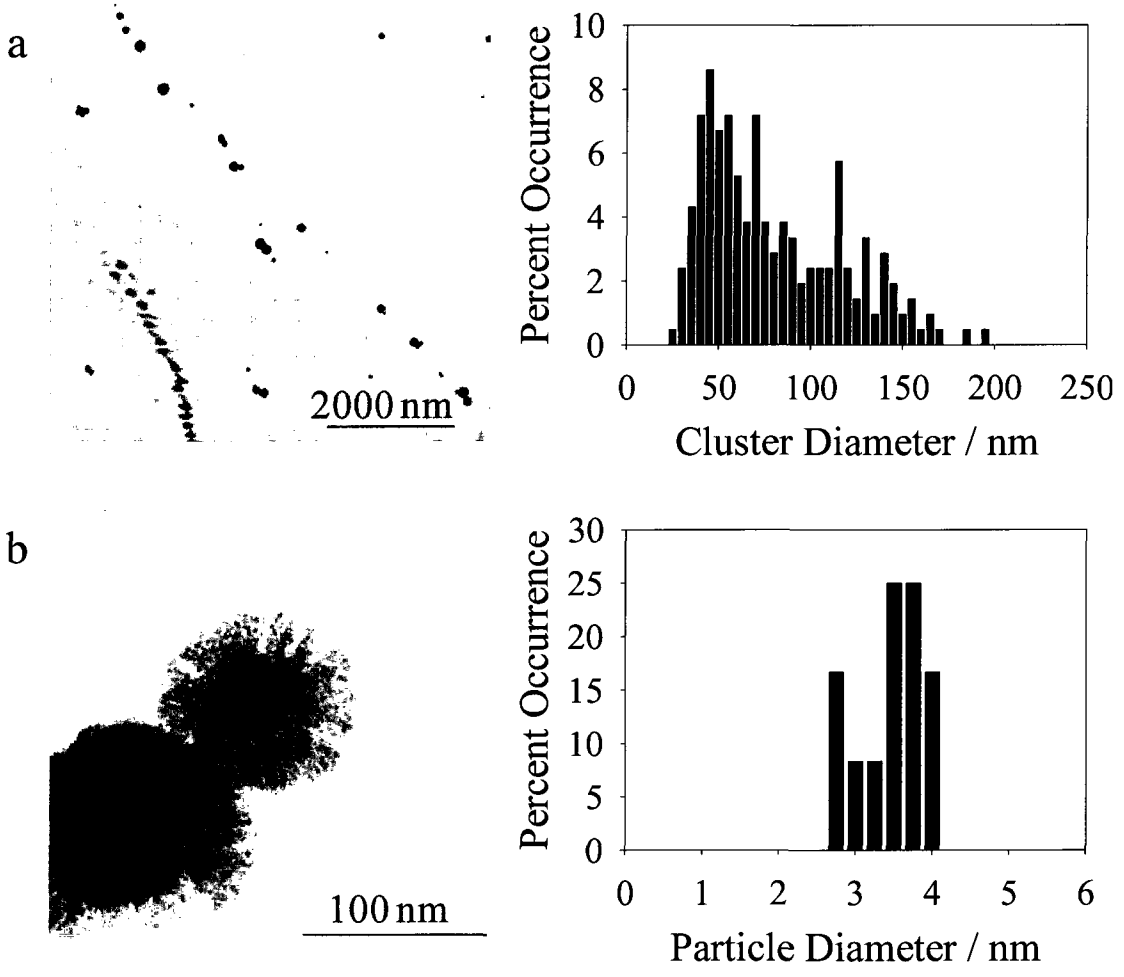

Figure 3.6 a) TEM images of Pt deposits on freshly cleaved HOPG. The Pt was deposited at – 0.475 V vs. MSE for 5 s in 0.1 M H_2SO_4 + 1 mM $PtCl_4$, b) shows a higher resolution TEM image of the same sample.

Table 3.1 lists the average reduction charges with their corresponding standard deviations for potentiostatically deposited platinum onto freshly cleaved HOPG. The large standard deviations for the deposition charge indicates that there is a large variability in the amount of

platinum deposited onto these substrates. As discussed above, TEM results indicate preferential deposition along the step edges. Given that the amount of Pt deposited varies between samples, and that Pt is formed along step edges, we can infer that the number of step edges (i.e., the number of nucleation sites) is sample dependant. The fact that the amount of platinum deposited is inconsistent between samples suggests these experimental conditions and HOPG pre-treatment is not providing a method to deposit Pt in a reproducible way.

Table 3.1 Deposition charges (Q_{DepPt}) for potentiostatically deposited platinum onto freshly cleaved HOPG.

Deposition* time / s	**(Q_{DepPt}) / μC cm^{-2}**
2.5	386 ± 255
5.	839 ± 311
7.5	1310 ± 290

* Pt was deposited at – 0.475 V vs. MSE in a 0.1 M H_2SO_4 + 1 mM $PtCl_4$ solution.

3.5 CONCLUSIONS

Electrochemical deposition under the conditions presented in this chapter (– 0.475 V vs. MSE in 1 mM $PtCl_4$ + 0.1 M H_2SO_4) onto freshly cleaved HOPG resulted in the formation of Pt clusters. Current-time analysis indicates that Pt deposit growth occurred via a 3D nucleation process. Reduced variable plots indicated that the nucleation process was highly variable; in some cases nucleation occurred instantaneously, in other cases progressive nucleation was observed. Analysis of average deposition charges and the large corresponding standard deviations supports the finding of an inconsistent deposition process.

TEM analysis revealed the important role that nucleation sites play in causing the observed inconsistency in the Pt deposition process. It was found that the Pt deposits were nucleating almost exclusively along step edges. As the number of step edges on an HOPG substrate changes each time the substrate is cleaved, the number of nucleation sites also changes. It was concluded that the variability in the number of step edges, and thus, the

number of nucleation sites, is the cause of the variability in the observed nucleation process and amount of deposited platinum.

It was determined by TEM analysis that electrochemical deposition results in the formation of Pt clusters. The clusters consist of what appears to be smaller nanoparticles. It is possible that the clusters from by agglomeration, i.e. surface diffusion of Pt nano-catalysts gives rise to agglomeration. However, it is equally possible that the clusters represent dendrite structures.

Chapter Four

Electrochemical Deposition onto Oxidized HOPG

4.1 ABSTRACT

Platinum was potentiostatically deposited onto ozone oxidized and electrochemically oxidized highly ordered pyrolytic graphite (HOPG-O_3 and HOPG-E, respectively). Both oxidation methods increased the roughness of the HOPG surface; electrochemical oxidation had the greater oxidizing effect. Oxidation generated pits on the basal plane; ozone oxidation formed nano-pits, < 10 nm in diameter; electrochemical oxidation produced larger pits, > 85 nm in diameter. Ozone oxidation increased electrochemical deposition reproducibility while electrochemical oxidation increased electrochemical deposition variability. Ozone oxidation has many positive effects on the electrochemical deposition of platinum onto HOPG: (1) Platinum nucleation density increased with increasing ozone oxidation of the HOPG surface; (2) Instantaneous Pt nucleation is favoured on ozone oxidized HOPG; and (3) The reproducibility of the Pt deposition process is substantially increased with increasing ozone oxidation time. The Pt deposits formed on oxidized HOPG consisted of clusters of nanoparticles. On ozone oxidized HOPG, the Pt cluster size was controlled by controlling the Pt deposition time. High resolution transmission electron microscopy results indicate that the clusters formed by diffusion and agglomeration.

4.2 INTRODUCTION

As discussed in Chapter Three, step edges on the surface of freshly cleaved HOPG act as nucleation sites for electrochemically deposited platinum. Furthermore, the number of step edge sites varies between HOPG samples, hence, the number of nucleation sites also varies between samples. This results in an irreproducible Pt deposition process. Consistency in the number of nucleation sites from one sample to the next, as anticipated for "treated" surfaces, would be expected to increase the reproducibility of Pt deposition. Furthermore, a large number of nucleation sites should encourage instantaneous nucleation, and therefore yield a narrow particle-size distribution.[65,66,107] While a large nucleation site density may seem ideal, it is important that the site density is sufficiently low to ensure that during particle growth neighbouring particles do not overlap.

It is likely that the atomically smooth basal plane and hydrophobic nature of HOPG prevents good adhesion between the Pt nano-catalysts and the HOPG surface. Therefore, it

is reasonable to assume that oxidizing HOPG, which will simultaneously increase the surface roughness and the hydrophilic nature of the HOPG surface, will increase adhesion between Pt nano-catalyst and the HOPG surface. The most common method of HOPG oxidation reported in the literature is thermal oxidation,[66,67] which consists of oxidizing the HOPG surface in air at elevated temperatures, normally between 570 – 770 °C. This results in the formation of pits ranging in size from tens of nanometres to several microns in diameter depending on the experimental conditions. Ozone oxidation of HOPG forms nanometre sized pits distributed randomly over the basal plane.[66] Electrochemical oxidation of HOPG[68,69,70,71] has also been studied and is found to result in exfoliation of the HOPG surface. Other methods such as radio-frequency plasma etching,[72] as well as sputtering with oxygen[73] or argon[74,75,76,77] ion beams, have been investigated. There is only one study known to the author where the morphological stability of Pt nano-catalysts deposited onto oxidized HOPG was tested. This study showed that Pt nano-catalysts prepared by impregnation and thermal decomposition onto thermally oxidized HOPG agglomerated when cycling the Pt nano-catalyst between the regions of hydrogen and oxygen evolution.[92] Regardless of the fact that thermally oxidized HOPG failed to stabilize Pt nano-catalysts, other methods of HOPG oxidation should be investigated to determine if they can form a HOPG surface that is capable of stabilizing Pt nano-catalysts.

The introduction of pits to facilitate random deposition of Pt and also possibly stabilize the Pt particles from agglomeration appears to be feasible. Thermal oxidation of HOPG, however, is not an appropriate oxidation method since it generates pits at point defects on the basal plane, thus resulting in a low surface density of micrometer-sized pits. However, O_3-oxidation should cause pit formation at point defects and in areas that are defect-free, resulting in a high surface density of nanometre-sized-pits.[66] It is hypothesized that particles will be effectively deposited, and possibly stabilized, in pits if the pits are approximately the same size as the particles. O_3 oxidation allows for pit size and density control by varying the O_3 concentration, reaction time, and substrate temperature. Nanometre sized pits will effectively introduce sites for Pt nucleation on the basal plane. Increasing the nucleation site density is further expected to have the beneficial effect of encouraging instantaneous Pt nucleation. A more instantaneous nucleation process favours a narrow size distribution of the deposited platinum particles.

Chapter Three discussed electrochemical deposition onto freshly cleaved HOPG. The deposition process resulted in Pt clusters forming along step edges on the HOPG surface. From the TEM analysis, it was not possible to determine if the clusters formed by individual nano-catalysts diffusing over the surface of the HOPG substrate and agglomerating together, or if they represent a dendrite structure. If the clusters form by agglomeration, it is likely that the atomically smooth basal plane did not stabilize the individual nano-catalysts. Thus, the introduction of defects on the basal plane by oxidation could potentially stabilize the nano-catalysts. If, however, the clusters are dendrite structures, then substrate oxidation will have little effect on the deposit morphology.

In this chapter, Pt is electrochemically deposited onto ozone or electrochemically oxidized HOPG. The effect of oxidizing HOPG on the substrate surface morphology is studied by scanning electron microscopy (SEM), and scanning tunneling microscopy (STM). X-ray photoelectron spectroscopy (XPS) is used to monitor chemical changes in the HOPG surface caused by oxidation. Additionally, double layer capacitance measurements are made as a function of oxidation extent to determine the roughness of the oxidized HOPG. The effect of oxidizing HOPG on Pt electrochemical nucleation is studied with the use of reduced variable plots. Pt deposit morphology is analyzed by transmission electron microscopy (TEM).

4.3 EXPERIMENTAL

4.3.1 Solutions, Cells, and Electrodes.

Chapter Two, Section 2.2 describes the solutions, cells, and electrodes used in this work. A Hg/Hg_2SO_4, 0.5 M H_2SO_4 (MSE) electrode was used as the reference electrode for electrochemical deposition of Pt and electrochemical oxidation of HOPG. A Hg/Hg_2Cl_2, sat. KCl (SCE) was used for the CO_{ads} stripping voltammetry.

4.3.2 Substrate Pre-Treatments.

Grade SPI-1 HOPG from SPI supplies were used as substrates in all experiments. Pt was deposited onto ozone-oxidized (denoted HOPG-O_3), and electrochemically-oxidized (denoted HOPG-E) HOPG.

The ozone oxidation of the HOPG were carried out according to work by Tracz, et al.[66] A Model 49C ozone analyzer equipped with an optional ozone generator was used to generate 0.15 ppm O_3 in air. Zero air was fed into the ozone analyzer generating an ozone/air mixture, which then flowed to the reaction chamber (a quartz tube of 22 mm inner diameter that was placed in the center of a 300 °C tube furnace). Teflon tubing was used to transport the ozone/air mixture to the tube furnace. The flow of ozone/air could be switched from flowing to the reaction chamber or to a vent using a three way glass stopcock, thus allowing precise control of the oxidation times. The HOPG substrates were heated at 300 °C in an air atmosphere for 5 min. prior to O_3 oxidation. Following the oxidation period, the oven was switched off and the ozone/air mixture was flushed out of the tube furnace with zero air for an additional 5 min.. The samples were allowed to cool to room temperature at the edge of the tube furnace. In air scanning tunneling microscopy (STM) analysis of the oxidized HOPG samples were carried out on the same day of preparation.

HOPG was electrochemically-oxidized in a 0.1 M H_2SO_4 solution at + 1.55 V vs. MSE. Oxidation times were varied between 30 and 180 s.

4.3.3 XPS Analysis of Substrates.

See Chapter Two, Section 2.4.4.2 for details regarding acquisition and analysis of XPS spectra.

4.3.4 Double Layer Capacity Measurements.

The double layer capacities of freshly cleaved, ozone-oxidized, and electrochemically-oxidized HOPG were measured by electrochemical impedance spectroscopy. See Chapter Two, Section 2.3.3.

4.2.5 Platinum Deposition Method.

Platinum was electrochemically deposited onto oxidized HOPG using the same conditions as for freshly cleaved HOPG discussed in Chapter Three, Section 3.3.3.

4.3.6 Particle Size/Morphology Determination.

The size and morphology of platinum catalysts on HOPG were determined by transmission electron microscopy, TEM. Sample preparation was completed as described in Chapter 3, Section 3.4.1.3. Due to the destructive nature of the TEM sample preparation, the

same sample could not be imaged before and after electrochemical analysis. A sample prepared by electrochemical deposition onto ozone oxidized HOPG was sent for high resolution TEM (HRTEM) (on a aberration corrected Titan @300kV) analysis at the Brockhouse Institute for Materials Research and Centre for Emerging Device Technologies at McMaster University.

4.3.7 Adsorbed CO Stripping Voltammetry.

Adsorbed CO (CO_{ads}) stripping voltammetry is used as a test reaction to determine if the electrode morphology changes after electrochemical use. Chapter Six, Section 6.3.4 describes the method of CO_{ads} stripping voltammetry and Section 6.4.1 describes the process of electrochemical oxidation of CO_{ads} onto polycrystalline Pt foil.

4.4 RESULTS AND DISCUSSIONS

4.4.1 Oxidation of HOPG.

4.4.1.1 Surface imaging of oxidized HOPG.

The HOPG substrates were modified by either ozone gas oxidation or electrochemical oxidation with the dual aim of increasing platinum particle stability and encouraging instantaneous nucleation (and therefore small particle size distributions). Previous work[66] has shown that nano-scale pits can be formed on HOPG by an ozone oxidation process. Tracz et. al. proposed that ozone molecules are adsorbed onto and diffuse along the HOPG surface and after an average time, which is dependent on reaction temperature and ozone concentration, are consumed by a reaction which generates the first defect which will then grow into a pit.[66] The pit size and density can be controlled by varying the O_3 concentration, reaction time, and temperature; it does not appear to be dependent on the 'defect-status' of the HOPG surface. HOPG pitting by O_3 was tested in this work. Consistent with the literature,[66] ozone oxidation of HOPG resulted in nanometre-sized pits that are randomly distributed over the basal plane of the surface. Within this chapter, the discussion is limited to HOPG samples oxidized at 300 °C in an ozone/air mixture with an ozone concentration of 0.15 ppm. The ozone concentration is limited to 0.15 ppm since work by Tracz et. al showed that this concentration results in pits < 10 nm that are one monolayer deep.[66] The temperature is kept at 300 °C since atomic force microscopy analysis, not shown, indicates

that at higher temperatures HOPG undergoes oxidation in an air atmosphere, i.e., without the participation of O_3. During air oxidation on its own, large micrometer sized pits that nucleate at point defects are formed, and since the objective of this work is to make small pits, < 10 nm, air oxidation on its own must be avoided.

STM images and corresponding histograms of HOPG surfaces oxidized for varying lengths of times at 300 °C and 0.15 ppm O_3 are shown in Figure 4.1. As expected,[66] the average pit density and diameter increased with increasing oxidation time. Oxidation times of 7.5, 10, and 15 min. were found to result in average pit diameters of 1.7 ± 0.4, 2.3 ± 0.7, and 3.8 ± 0.9 nm, respectively. For the O_3 concentration and oxidation times studied in this work, the size distribution of the pits was found to increase with an increase in oxidation time indicating that new pits are continually formed during the oxidation process.

Electrochemical oxidation proved to be a much more damaging and complicated process compared to ozone oxidation. Electrochemical oxidation caused parts of the HOPG to flake away from the substrate. HOPG substrates that have undergone electrochemical oxidation at 1.55 V for 30 and 90 s in 0.1 M H_2SO_4 were analyzed by scanning electron microscopy (SEM) and are shown in Figure 4.2. From Figure 4.2, it appears as though these flakes originated along step edges. The longer electrochemical oxidation time reveals cracking of the HOPG surface, which probably occurs along grain boundaries, while the shorter electrochemical oxidation time does not (see Figures 4.2c and 4.2a, respectively).

Higher magnification images, Figures 4.2b and 4.2d, show that electrochemical oxidation of the HOPG substrate results in the formation of pits on the surface. What is particularly interesting is that the pits observed on the sample oxidized for 30 s have an average diameter of 127 ± 32 nm, while the pits observed on the sample oxidized for 90 s are found to be only 85 ± 20 nm in diameter. By considering pit size alone, it might appear as though the sample oxidized for 30 s is 'more' heavily oxidized than the one oxidized for 90 s because the former has larger pits than the later. However, the measured oxidation charge for the sample oxidized for 30 s is 16 mC cm^{-2}, while the sample oxidized for 90 s has a measured oxidation

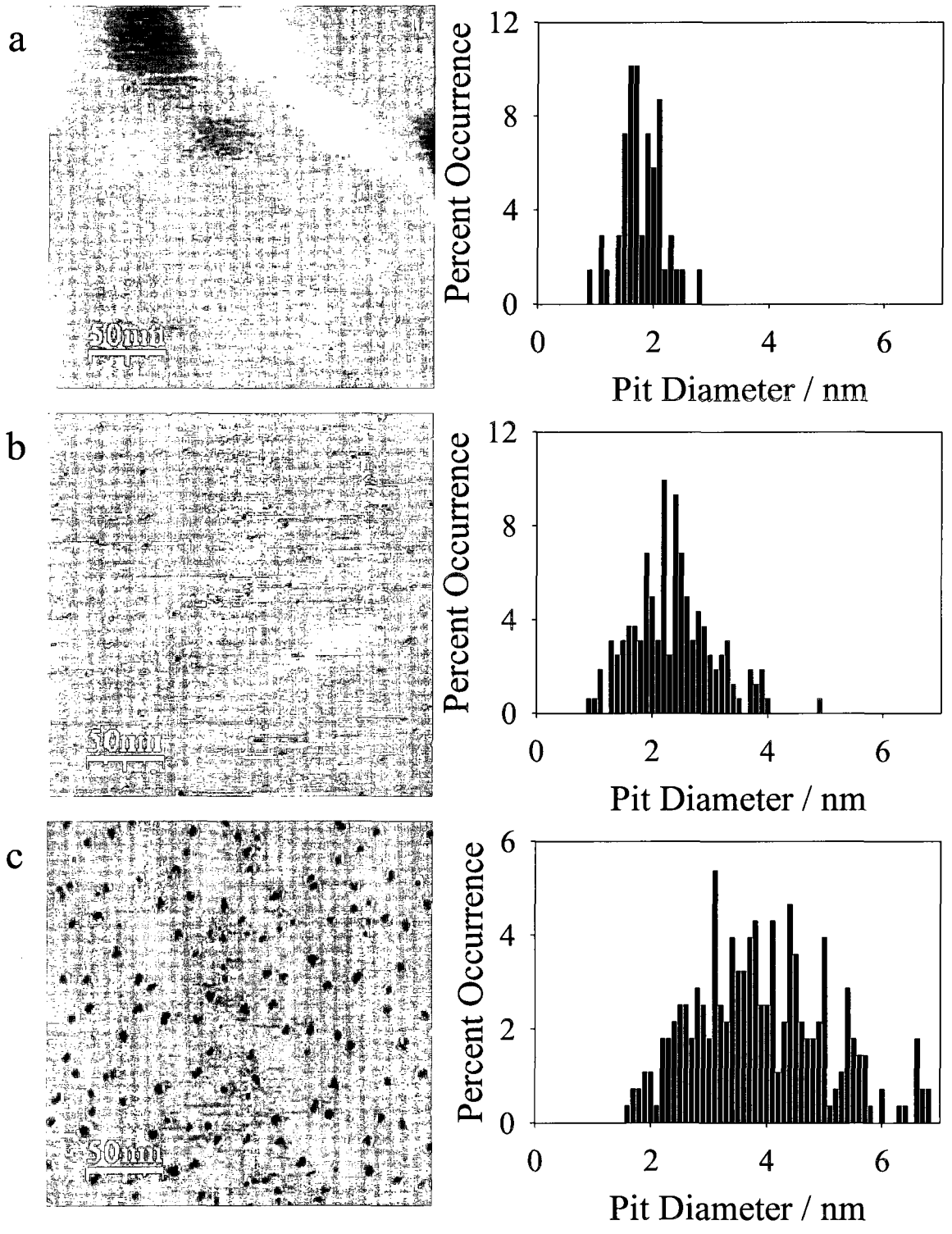

Figure 4.1 STM images of HOPG surfaces oxidized in 0.15 ppm O_3 at 300 °C for a) 7.5, b) 10, and c) 15 min. The corresponding pit diameter histograms are also shown.

charge of 56 mC cm^{-2}, indicating that the sample oxidized for 90 s is indeed more oxidized than the sample oxidized for 30 s. During the electro-oxidation process, once a pit forms it will grow in size, thus the fact that the sample analyzed after 30 s of electro-oxidation has larger pits than the sample electro-oxidized for 90 s must be reflective of the samples used, and not the oxidation process. The explanation for the discrepancy in pit size is found when analyzing the density of pit. Figure 4.2 shows that the sample oxidized for 30 s has a much smaller pit density than the sample oxidized for 90 s. In fact, the sample oxidized for 30 s has 2.9 ± 0.3 pits per μm^{-2}, while the sample oxidized for 90 s has 5. ± 1.3 pits per μm^{-2}. The fact is that electrochemical oxidation of HOPG occurs predominantly at edge and defect sites.[94] Thus, analysis of Figure 4.2 suggests that the particular sample oxidized for 30 s had a lower density of defect sites to begin with, in comparison to the sample oxidized for 90 s. As mentioned above, it appears that in the "electrochemical-oxidation-treatment" technique, pits are predominately formed at "pre-existing" surface defects. This approach therefore reveals any irreproducibility in the "density-of-defects" from sample to sample. Electrochemical oxidation of a HOPG substrate (for the same amount of charge passed) with a smaller density of defect sites results in a larger average pit diameter compared to a sample with a lower density of defect sites. Thus, the "extent of oxidation" of HOPG needs to be considered in terms of both pit size and density.

SEM analysis of electrochemically oxidized HOPG reveals that electrochemical oxidation is a complicated and variable process in terms of the number of surface sites participating in the oxidation process. To reiterate, when O_3 is used to oxidize and "etch" the HOPG surface, it is not the "pre-existing" sample defects that dictates the density of the sites at which pitting begins, but the O_3 itself "generates" the sites where pits initiate.

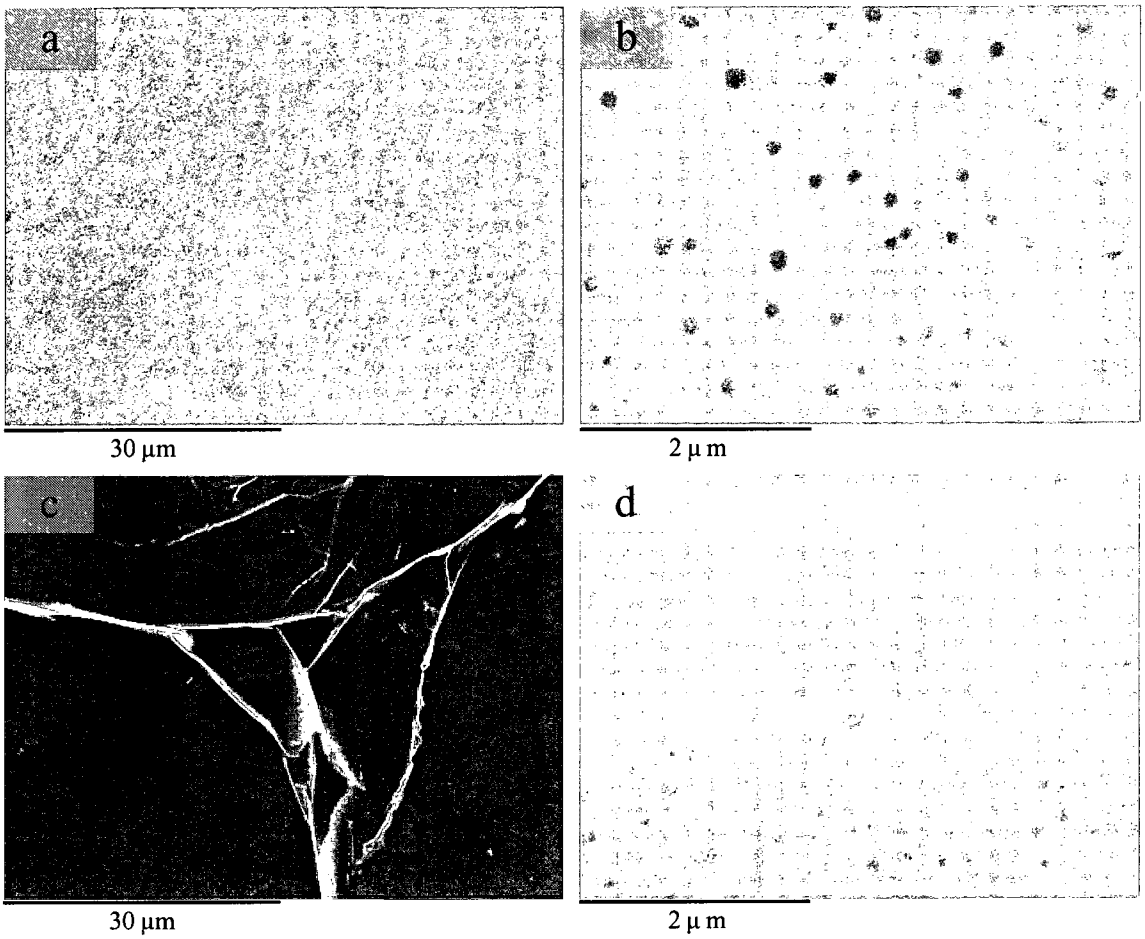

Figure 4.2 Scanning electron images of HOPG electrochemically oxidized at 1.55 V vs. MSE in 0.1 M H_2SO_4. Sample oxidized for 30 s; a) low resolution image 2000 × mag., b) high resolution image 25000 × mag.. Sample oxidized for 90 s; c) low resolution image 2000 × mag., d) high resolution image 25000 × mag..

4.4.1.2 X-ray photoelectron spectroscopy analysis of HOPG pre-treatments.

The three different substrate pre-treatments (freshly cleaved, ozone oxidation, and electrochemical oxidation) were analyzed by X-ray photoelectron spectroscopy (XPS). Table 4.1 lists the elemental composition of the surfaces. As expected, only carbon and oxygen are present on the freshly cleaved and ozone oxidized surfaces. In addition to carbon and oxygen, electrochemically oxidized HOPG also has a measured sulfur contribution. This sulfur results from intercalated H_2SO_4 either as $(HSO_4)^-$ or $(S_2O_8)^{2-}$.[78]

All three samples are composed predominantly of carbon. Less than one percent of the freshly cleaved HOPG surface is comprised of oxygen, while slightly more than one percent

of the ozone oxidized HOPG surface is oxygen (see Table 4.1). Conversely, 10.2 ± 0.4 % of the electrochemically oxidized HOPG surface is comprised of oxygen. According to the sulfur content, and the association of sulfur with oxygen when intercalated as $(HSO_4)^{2-}$ or $(S_2O_8)^{2-}$, we can say that 6.7 ± 1.1 % of the oxygen is associated with sulfur and not carbon for the electrochemically oxidized HOPG and the remaining oxygen (3.5 ± 1.4 %) is associated with carbon; i.e. roughly 65 % of the measured oxygen is associated with the intercalated H_2SO_4 and 35 % is associated with oxidized HOPG. From STM and SEM analysis (above), we know that both ozone and electrochemical oxidation results in the formation of pits on the surface. Since the oxidized samples do not have a large increase in oxygen content, it can be concluded that almost all of the oxidized carbon is removed from the surface either as CO_2 or CO.

Table 4.1 Summary of the elemental composition of freshly cleaved and oxidized HOPG. *

Substrate pre-treatment	% C	% O	% S
Freshly cleaved	99.2 ± 0.6	0.8 ± 0.6	0
Ozone oxidized†	98.9 ± 0.1	1.1 ± 0.1	0
Electrochemically oxidized‡	88. ± 0.8	10.2 ± 0.4	1.7 ± 0.3

* Three different areas of the HOPG surface were analyzed and averaged.

† Ozone oxidation occurred at 300 °C in 0.15 ppm O_3 for 15 min.

‡ Electrochemical oxidation occurred in 0.1 M H_2SO_4 for 30 s at 1.55 V vs. MSE.

The measured amount of carbon that is oxidized is sufficiently low that analysis of the C 1s peak to determine the form of oxidized carbon is not practical. For example, less than one percent of the carbon signal represents oxidized carbon for the freshly cleaved HOPG substrate; therefore the peak area of the deconvoluted peak representing carbon associated to carbon would be less than one percent of the entire envelop and essentially in the noise of the signal. The same conclusion is drawn for ozone oxidized HOPG (1.1 ± 0.8 % O on HOPG) and electrochemically oxidized HOPG (3.5 ± 1.4% O associated with carbon). Therefore the nature of oxygen on HOPG is drawn exclusively from the oxygen signal. This does not mean that the C 1s peaks do not provide insight into the effect of oxidation of HOPG on the chemical structure of HOPG. Figure 4.3 show the C 1s peak for freshly cleaved, ozone

oxidized and electrochemically oxidized HOPG. From Figure 4.3 it can be seen that there is very little difference between the chemical nature of ozone oxidized HOPG compared to freshly cleaved HOPG, in fact the spectra lines so closely resemble one another that it is very difficult to separate them in Figure 4.3. Conversely, HOPG which has undergone electrochemical oxidation had a very different C 1s spectra compared to freshly cleaved HOPG. The C 1s peak for electrochemically oxidized HOPG is significantly wider compared to that for freshly cleaved HOPG indicating that there is a wider distribution of chemical states for carbon atoms in electrochemically oxidized HOPG. The increase in the C 1s peak width for electrochemically oxidized HOPG supports the SEM observations that electrochemical oxidation induces intense structure damage in the form of cracking and pitting of the HOPG surface. Conversely, ozone oxidation only pits the surface.

The O 1s signals for the freshly cleaved and ozone oxidized substrates were relatively weak compared to the electrochemically oxidized HOPG and therefore they were not interpreted. Conversely, the O 1s signal for electrochemically oxidized HOPG was significantly stronger and thus can be analyzed confidently. Figure 4.4 shows the deconvoluted O 1s peak for electrochemically oxidized HOPG. Table 4.2 list the O 1s XPS data for all three substrate pre-treatments. As discussed above, 65 % of the oxygen signal represent oxygen associated with sulfur in $(HSO_4)^{2-}$ or $(S_2O_8)^{2-}$ groups, and 35 % of the oxygen signal represents oxygen associated with carbon. Thus, the O 1s peak was deconvoluted into two peaks. Peak B was set to 532.5 eV (the binding energy of O 1s in H_2SO_4)[79] and was constrained to represent 65% of the signal. Peak A was manipulated to give the best fit. The result of the O 1s peak fit for electrochemically oxidized HOPG are presented in Table 4.2 and Figure 4.4. The position of peak A, the oxygen that is associated with carbon, is close to, yet slightly lower than, the value expected for aromatic C=O groups.[80]

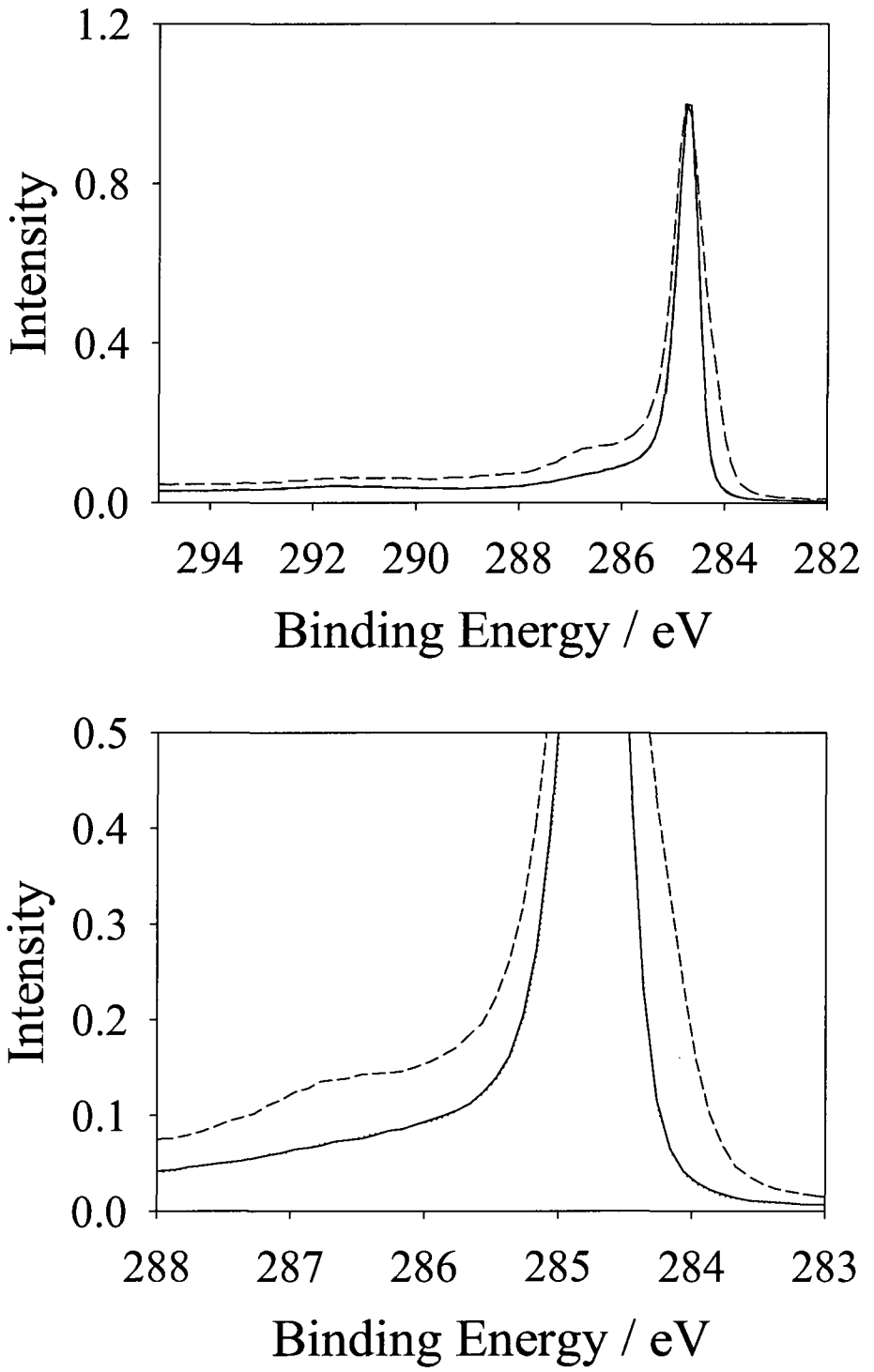

Figure 4.3 C 1s peak for freshly cleaved (——) ozone oxidized (.....) and electrochemically oxidized (- - - -) HOPG. a) full spectra, b) magnification of the lower binding energy region.

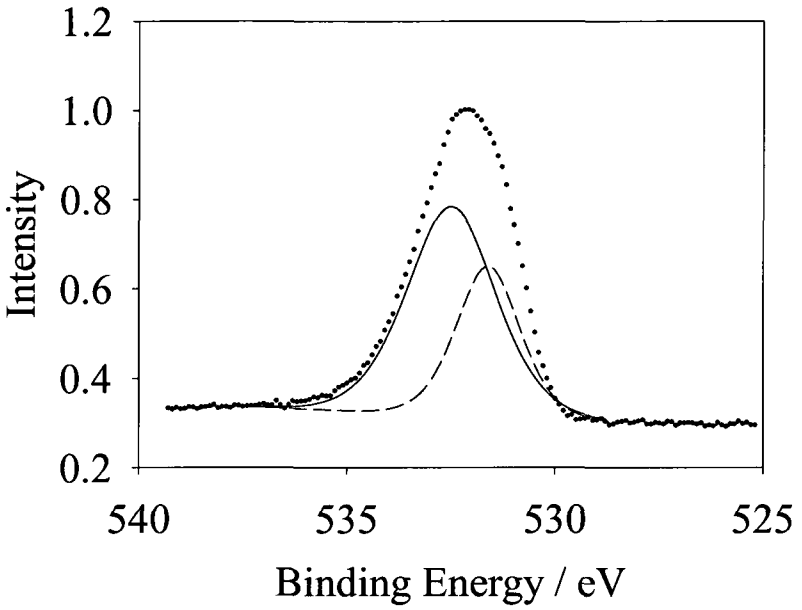

Figure 4.4 Deconvoluted O 1s spectra for a) freshly cleaved, b) ozone (0.15 ppm, 15 min, 300 °C) oxidized, and c) electrochemically (30 s at 1.55 V vs. MSE in 0.1 M H_2SO_4) oxidized HOPG. • Data, peak A (——), and peak B (– – – –). See text for explanation of peaks.

Table 4.2 Oxygen 1s XPS data for electrochemically oxidized HOPG. *

	Peak Position / eV	Peak Width / eV	% Contribution
A‡	531.75 ± 0.2	1.86 ± 0.1	35
B‡	532.5	2.57 ± 0.13	65

* Three different areas of the HOPG surface were analyzed.

† Electrochemical oxidation occurred in 0.1 M H_2SO_4 for 30 s at 1.55 V vs. MSE.

‡ See text.

4.4.1.3 Roughness analysis of oxidized HOPG.

It is assumed that a rougher surface will provide additional nucleation sites for Pt nano-catalyst deposition, and more importantly it is believed that the additional HOPG edge sites (surrounding the pits) created by oxidation will help stabilize the Pt nano-catalysts against agglomeration. Thus, it is necessary to determine to what extent the HOPG surface is roughened by the two different oxidation processes under investigation. To help in this

analysis, it is useful to consider the term roughness factor, "R". In this application, R is defined as the ratio between the real surface area of the oxidized HOPG to the real surface area of freshly cleaved HOPG. R can be directly calculated from measured values of the double layer capacitance, C_{dl}, of the HOPG substrates.

At the interface between the electrode and electrolyte solution there exists a segregation of positive and negative charge in a direction perpendicular to the phase boundary. The term "double layer" is used to describe the arrangement of charges and oriented dipoles in the interphase region. As the interphase does not extend more than about 0.5 nm in a direction perpendicular to the surface,[81] the measured capacitance depends on the structure of this very thin region. The double layer follows the surface curvature of the electrode down to atomic dimensions, and therefore the measured capacitance is proportional to the real surface area of the electrode. Thus, by measuring the double layer capacitance of the substrate we are in effect measuring the real surface area of the substrate. The ratio of the C_{dl} value of the oxidized HOPG surface to the freshly cleaved HOPG surface gives the roughness factor, R, of the oxidized HOPG surface, as follows:

$$R = \frac{C_{dl}(\text{oxidized})}{C_{dl}(\text{freshly cleaved})} = \frac{\text{real surface area (oxidized)}}{\text{real surface area (freshly cleaved)}} \qquad (4.1)$$

Experimentally determined R values of ozone-oxidized and electrochemically-oxidized HOPG with respect to the substrate oxidation time are shown in Figure 4.5a and Figure 4.5b, respectively. It is clear that electrochemical oxidation at +1.55 V vs. MSE in 0.1 M H_2SO_4 roughens the surface to a much greater extent than ozone oxidation at 0.15 ppm O_3 and 300 °C. The average roughness factor increases from 4 ± 2 to 31 ± 26 to 103 ± 21 for electrochemical oxidation times of 30, 90, and 180 s, respectively. Such large roughness factors indicate that the HOPG substrate is being exfoliated, which is not surprising as it is known that electrochemical oxidation follows a three step exfoliation process.[68,71] The first step of exfoliation is the intercalation of water and electrolyte. Intercalation, which strains the top-most layer of the atomically flat surface of HOPG, occurs at defect sites. The C–C bonds, which are still intact, become further strained as protrusions begin to appear. Finally,

some of the C–C bonds on the top area of the protrusions begin to fracture forming graphite oxide and pits on the HOPG surface.

Previous work[68] showed that during electrochemical oxidation, damage occurs preferentially at defect sites and along step edges. The number of naturally occurring defects on a HOPG basal plane varies for each sample. Furthermore, due to the nature of cleaving HOPG, every time an HOPG substrate is cleaved the freshly cleaved surface has a different number of step edges. As each HOPG sample will have a different number of step edges and a different number of naturally occurring defect sites, each sample will be oxidized to a different extent. Thus, there is an inherent variability in the extent of electrochemical oxidation from one HOPG sample to the next. A good measure of the electrochemical oxidation variability is to compare the average measured oxidation charges and their corresponding standard deviations. It was found that electrochemical oxidation at 1.55 V vs. MSE of freshly cleaved HOPG for 30, 90, and 180 s has corresponding oxidation charges of 20 ± 7, 125 ± 60, and 875 ± 280 mC cm^{-2}. Standard deviations that range from 33 – 48 % of the total oxidation charge for a particular oxidation time reveal a significantly variable oxidation process.

Analysis of the roughness factors, Figure 4.5, indicate that ozone oxidation is much less "severe" than electrochemical oxidation. For example, the roughness factor is less than two for all of the ozone-oxidized samples. STM analysis indicates that ozone-oxidation does not cause exfoliation.[65,66] Rather, ozone oxidation causes pit formation simultaneously at both existing point defects and in areas that are defect-free. Thus, ozone oxidation results in a high surface density of randomly distributed pits that are less than 10 nm in diameter[66] (see Figure 4.1). It is important to highlight that while electrochemical oxidation roughens the HOPG surface to a greater extent than ozone oxidation, it also amplifies the differences between samples. Conversely, since ozone oxidation generates its own defects on the basal plane, it minimizes the differences between samples.

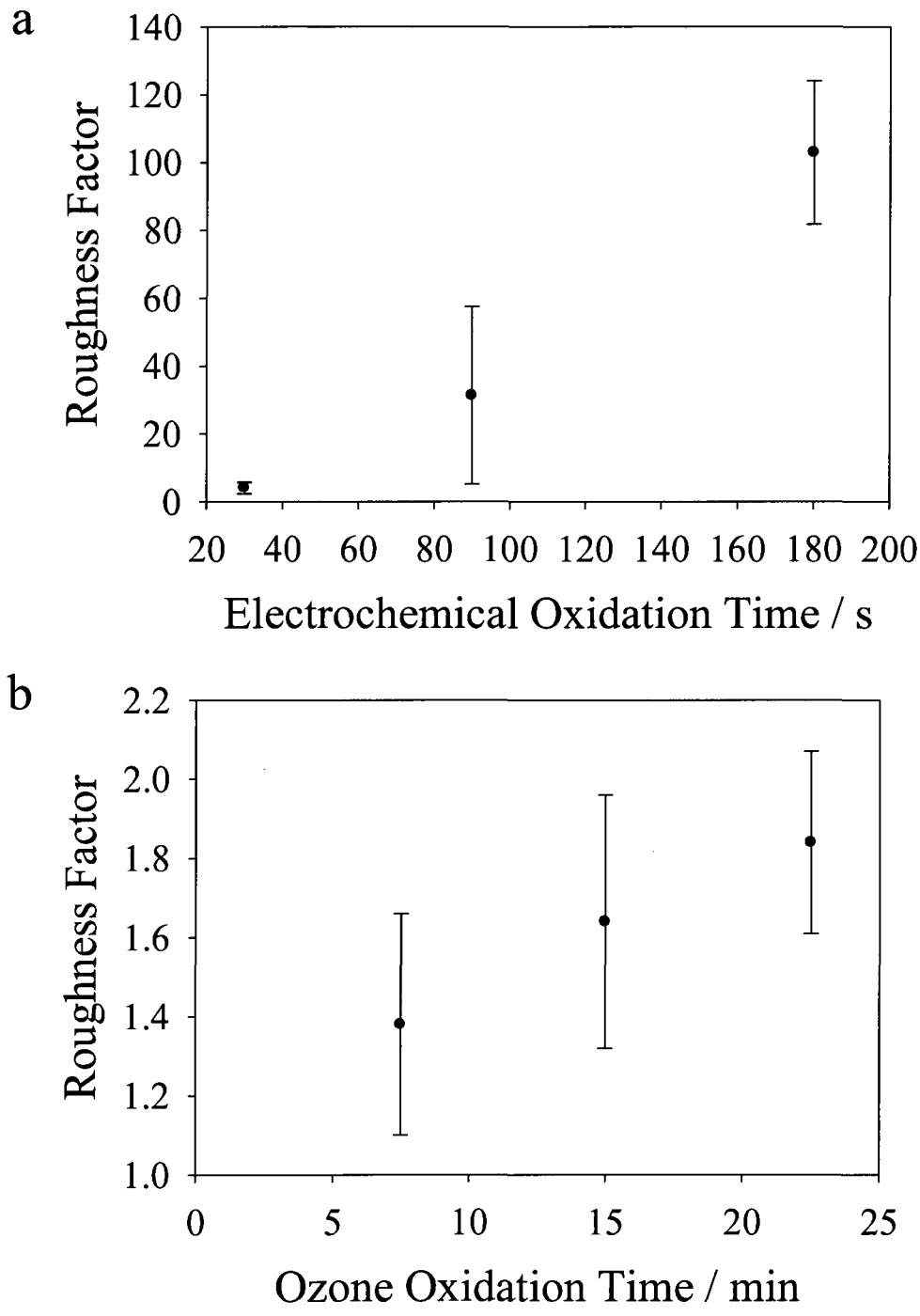

Figure 4.5 Roughness factor, R, calculated from experimental C_{dl} values using Equation 4.1 for a) electrochemically-oxidized and b) ozone-oxidized pre-treatments of HOPG substrates.

4.4.2 Electrochemical Deposition onto Oxidized HOPG.

Platinum was electrochemically deposited onto oxidized HOPG using the same conditions as for freshly cleaved HOPG discussed in Chapter Three, Section 3.3.3. Current-time transients were analyzed to determine the effect of increasing the surface roughness on the extent and mechanism of Pt nucleation. Current-time transients of deposition onto ozone oxidized HOPG (for a typical example see Figure 4.6a) are very similar to those for deposition onto freshly cleaved HOPG (see Figure 3.3). The deposition current-time transients, on both freshly cleaved and ozone oxidized HOPG, are typical of a 3D nucleation process. As discussed in Chapter Three, Section 3.4.2, the transient can be divided into three regions: Region (1) is due to double layer charging, while regions (2) and (3) reflect the deposition of Pt.[61,62,63] At long times, i.e., greater than 30 s, the deposition current falls to that as predicted by the Cottrell equation. As the current-time transient for deposition onto ozone oxidized HOPG is typical of a 3D nucleation process, it was analyzed in reduced variable plots, as in Section 3.4.2, to determine the nature of the nucleation process on ozone oxidized HOPG.

Figure 4.6b is a typical plot of a current-time transient for electrochemical deposition onto electrochemically oxidized HOPG. Comparing Figure 4.6a and Figure 4.6b, it is clear that electrochemical deposition onto electrochemically oxidized HOPG is different than electrochemical deposition onto ozone oxidized HOPG. The initial current spike, region (4), which represents the double layer charging, is more than a factor of 10 larger than the double layer charging measured for ozone oxidized HOPG. This signifies that electrochemically oxidized HOPG has a larger surface area than the ozone oxidized HOPG, which supports the observed larger increase in the roughness factor for electrochemically oxidized HOPG compared to that of ozone oxidized HOPG (see Figure 4.5). In Figure 4.6b, the current-time transient does not increase again after the double layer charging, i.e., the current maxima, I_M, is not observed. Instead, the cathodic current decreases as time increases falling to that predicted by the Cottrell equation, region (5). This could indicate that nucleation is not occurring via a 3D process. Conversely, 3D nucleation could be occurring, but due to data acquisition limitations, the current maxima may not be resolved separately from the current associated with the double layer charging. As the current maxima is not observed for

electrochemical deposition onto electrochemically oxidized HOPG, nucleation analysis is unfortunately not possible for these samples.

Reduced variable plots of platinum electrodeposition onto HOPG oxidized using 0.15 ppm O_3 at 300 °C for 7.5 and 15 min. are illustrated in Figure 4.7a and Figure 4.7b, respectively. Comparing reduced variable plots for electrodeposition onto freshly cleaved (Figure 3.5) and ozone modified (Figure 4.7) HOPG exemplifies the shift from progressive nucleation, on freshly cleaved HOPG, towards instantaneous nucleation, on ozone modified HOPG. A further shift towards instantaneous nucleation with increasing ozone oxidation time takes place, particularly at deposition times before the current maxima, as shown in Figure 4.7b vs. Figure 4.7a. This improvement towards instantaneous nucleation can be explained by the increase in pit density that accompanies the increase in ozone oxidation time. Oxidation with 0.15 ppm O_3 at 300 °C for 7.5 min. resulted in the formation of approximately 695 ± 190 pits per μm^2. Increasing the oxidation time to 15 min., while keeping the O_3 concentration and reaction chamber temperature constant, increased the pit density to 2000 ± 140 pits per μm^2. When comparing the TEM images of Pt electrochemically deposited onto O_3-oxidized HOPG (Figure 4.9) to Pt electrochemically deposited onto freshly cleaved HOPG (Figure 3.6), it is evident that the pits generated by O_3-oxidation on the basal plane are acting as platinum nucleation sites. Therefore, increasing the number of pits is equivalent to increasing the number of nucleation sites. Comparing the reduced variable plots for nucleation onto freshly cleaved HOPG (Figure 3.5) to the reduced variable plots for nucleation onto HOPG oxidized with ozone gas for 7.5 min. (Figure 4.7a) and 15 min. (Figure 4.7b) indicates that increasing the number of nucleation sites (by ozone oxidation) increases the nucleation rate constant, i.e., the process becomes more instantaneous. Since instantaneous nucleation results in narrow particle size distribution, electrodeposition onto ozone oxidized HOPG, which has a comparably more instantaneous nucleation process, is expected to produce an electrode with catalyst deposits that display greater size consistency than electrodeposition onto freshly cleaved HOPG.

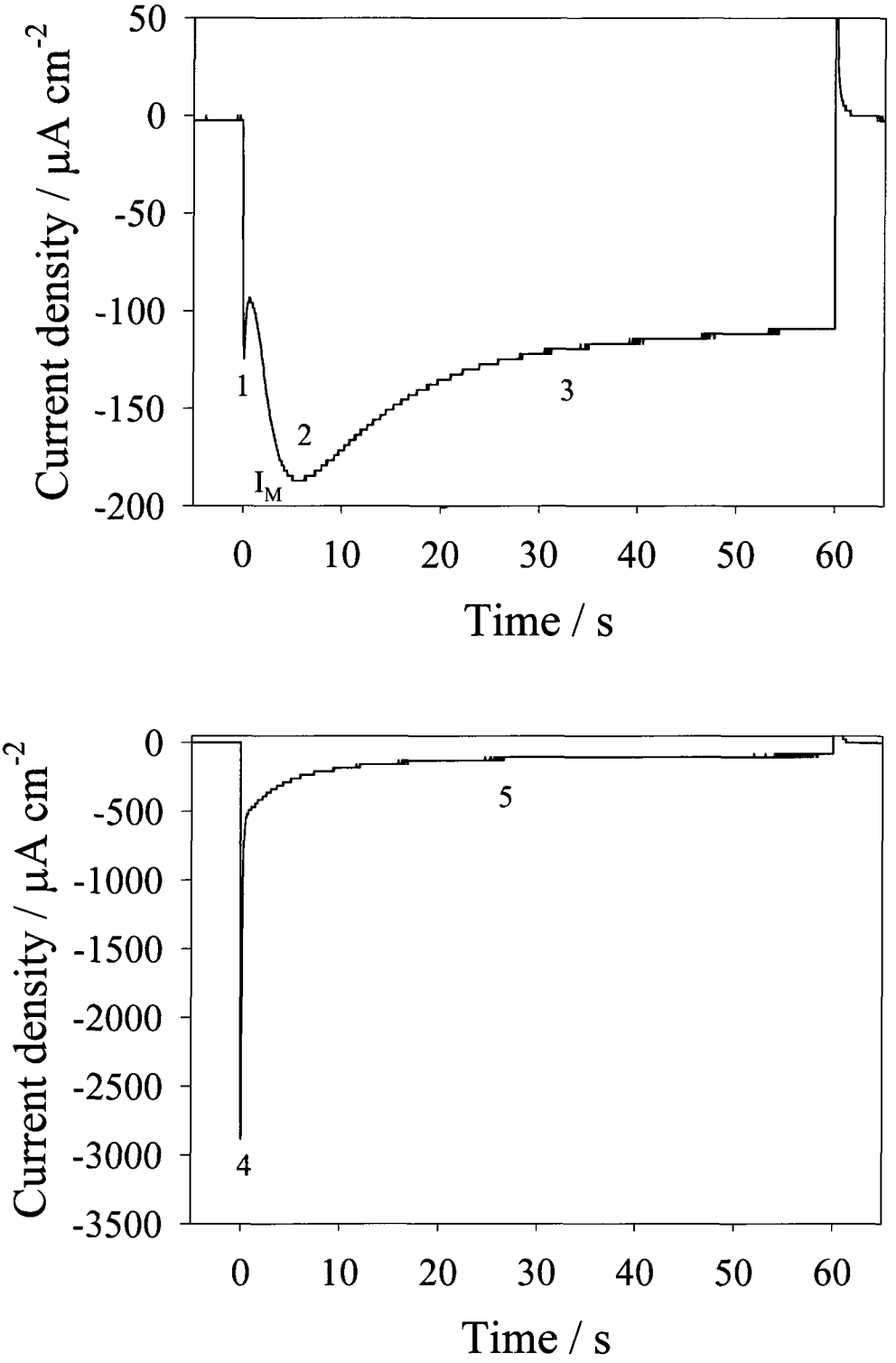

Figure 4.6 Potentiostatic reduction (at – 0.475 V vs. MSE in 0.1 M H_2SO_4 + 1 mM $PtCl_4$) onto a) ozone oxidized (0.15 ppm O_3, 15 min, 300 °C) b) electrochemically oxidized (90 s at 1.55V vs. MSE) HOPG.

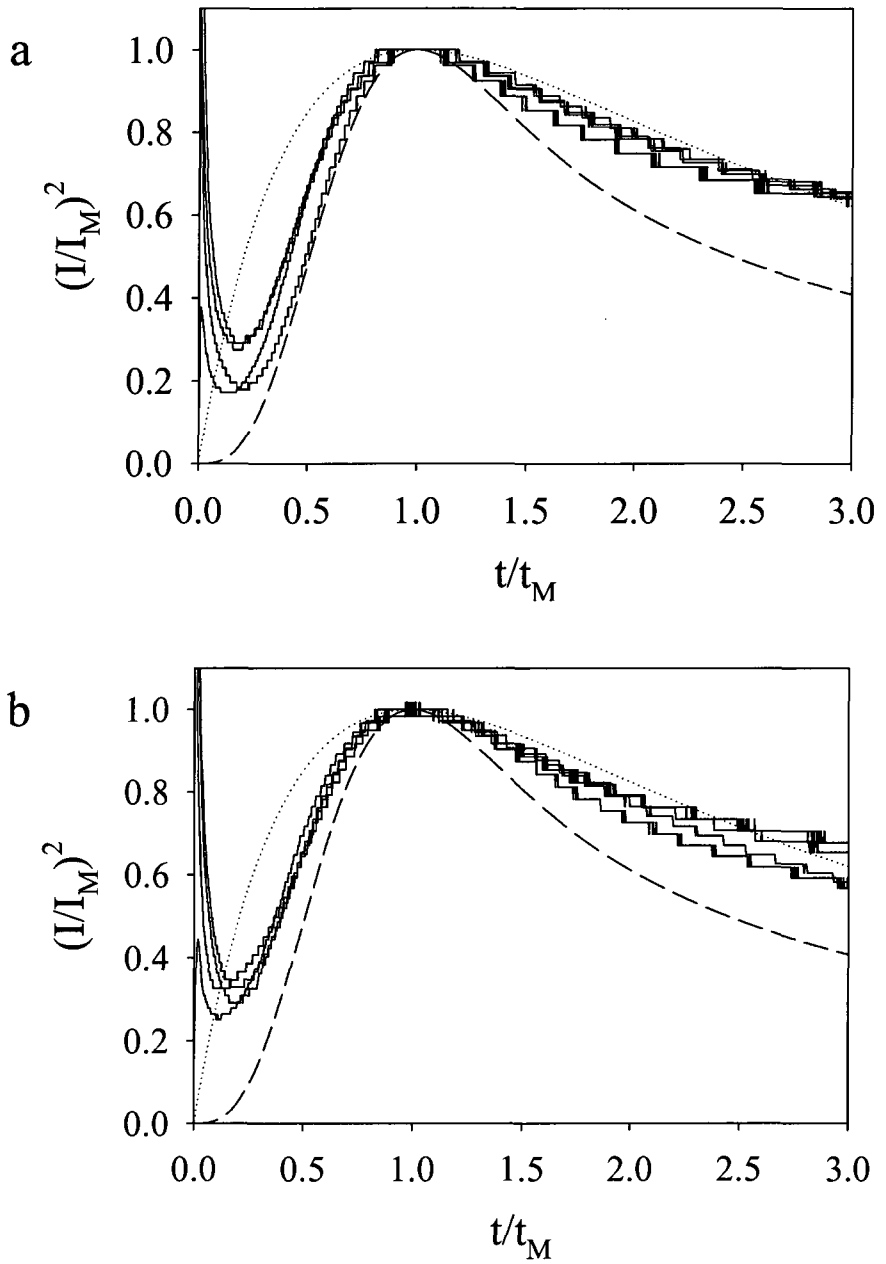

Figure 4.7 Reduced variable plots of potentiostatic Pt deposition onto O_3 oxidized HOPG in 0.1 M H_2SO_4 + 1 mM $PtCl_4$ at – 0.475 V vs. MSE. Oxidation condition: a) 0.15 ppm O_3, 300 °, 7.5 min. and b) 0.15 ppm O_3, 300 °, 15 min. ——— experimental data, ... theoretical instantaneous nucleation, and – – – theoretical progressive nucleation.

Another advantage of oxidizing HOPG with ozone gas is that electrodeposition onto ozone oxidized HOPG is more reproducible compared to deposition onto freshly cleaved HOPG. This increase in reproducibility is illustrated when comparing reduced variable plots of platinum electrodeposition onto ozone oxidized (Figure 4.7) and onto freshly cleaved (Figure 3.5) HOPG. Improved reproducibility is also illustrated in Table 4.3, which shows the reduction charges and the corresponding standard deviations for Pt deposition onto freshly cleaved and O_3 oxidized HOPG. The increase in reproducibility is likely due to the larger number of nucleation sites introduced randomly across the basal plane when using ozone oxidation treatments. By creating pits on the basal plane of the HOPG substrate, platinum can deposit onto pits in addition to step edges. As the density of pits increases, the proportion of nucleation sites on step edges to nucleation sites on pits decreases, and consequently the importance of step edges as nucleation sites decreases. Therefore, the variations in the number of step edges between HOPG substrates becomes less important for nucleation compared to the larger number of pits. Thus, ozone oxidation of the HOPG substrate results in a more reproducible Pt deposition process.

Table 4.3 Deposition charges (Q_{DepPt}) for potentiostatically deposited platinum onto freshly cleaved (Pt/HOPG), O_3 oxidized (Pt/HOPG-O_3), and electrochemically oxidized (Pt/HOPG-E) HOPG.

	(Q_{DepPt}) / mC cm^{-2}				
Deposition*			**Pt/ HOPG-E§**		
time/ s	**Pt/HOPG-FC†**	**Pt/HOPG-O_3‡**	**Electrochemical-Oxidation Time / s**		
			30	**90**	**180**
2.5	0.39 ± 0.26	0.43 ± 0.16	—	—	—
5.	0.84 ± 0.31	0.80 ± 0.18	1.6 ± 0.1	2.9 ± 0.9	18.9 ± 7.5
7.5	1.31 ± 0.29	1.28 ± 0.07	—	—	—

* Pt was deposited at – 0.475 V vs. MSE in 0.1 M H_2SO_4 + 1 mM $PtCl_4$ solution.

† Pt was deposited onto freshly cleaved HOPG.

‡ Pt was deposited onto HOPG-O_3. The HOPG was oxidized for 15 min. at 300 °C using 0.15 ppm O_3.

§ Pt was deposited onto HOPG-E. The HOPG was oxidized in 0.5 M H_2SO_4 at 1.55 V.

Unlike ozone oxidation, oxidizing HOPG electrochemically did not improve the reproducibility of the electrochemical deposition procedure (see Table 4.3). The variability in electrochemical deposition charge was found to increase with increasing electrochemical oxidation time. For example, the average deposition charge measured when applying a deposition pulse for 5 s onto HOPG that has been electrochemically oxidized at 1.55 V vs. MSE for 30, 90, and 180 s resulted in an average measured charge of $1.6 \pm 6\%$, $2.9 \pm 31\%$, and $18.9 \pm 39\%$ mC cm^{-2}, respectively. It is interesting to note that the Pt deposition charge increases with increasing the substrate electrochemical-oxidation time. This is different than what was observed for electrochemical deposition onto ozone oxidized HOPG: Oxidizing HOPG with ozone gas did not greatly increase the amount of platinum deposited, i.e., the deposition charge was roughly the same for ozone oxidized and freshly cleaved HOPG, see Table 4.3. The measured increase in deposition charge for electrochemically oxidized HOPG compared to ozone oxidized HOPG reflects the fact that electrochemical oxidation is a much more severe oxidation process which generates a much larger surface area, thus facilitating a greater amount of platinum to be electrochemically deposited.

As discussed in Section 4.4.1.3, the standard deviations of the electrochemical oxidation charges for cleaved HOPG samples are large compared to the total oxidation charge due to oxidation occurring preferentially along step edges and at naturally occurring defect sites on the HOPG surface. Since the measured oxidation charge is the 'real' indication of "extent-of-oxidation", as opposed to time-of-oxidation, the former will be used to discuss the amount of electrochemically deposited platinum with respect to the true extent of HOPG electrochemical oxidation, i.e., the oxidation charge. The measured deposition charges that correspond to 5 s deposition pulses onto electrochemically oxidized HOPG are plotted with respect to the electrochemical oxidation charges for several samples electrochemically oxidized for different lengths of time in Figure 4.8.

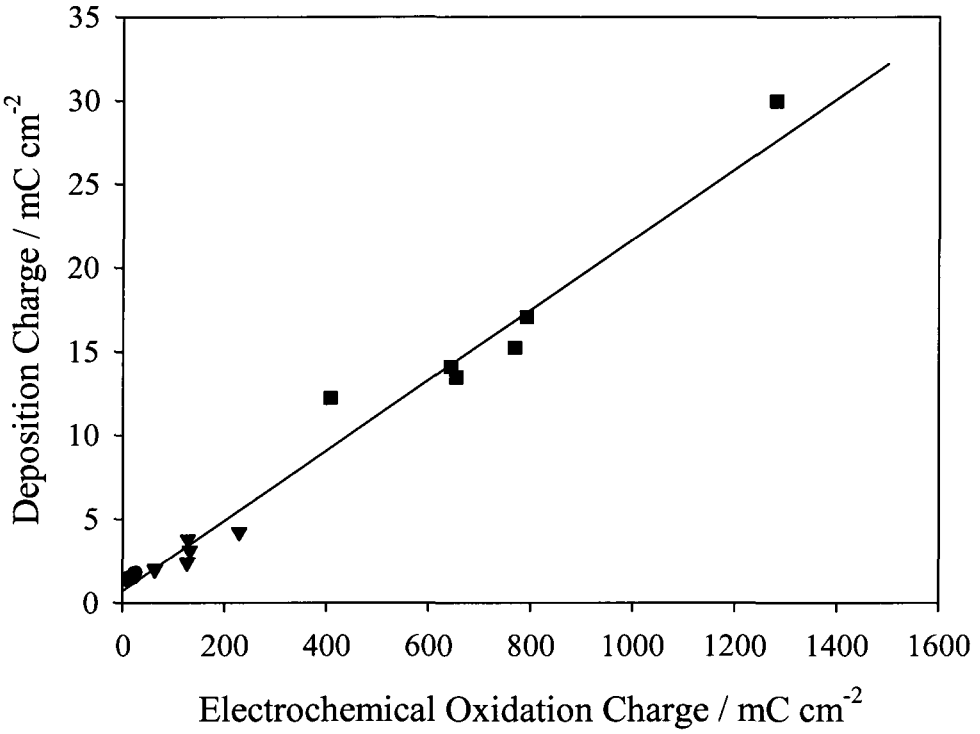

Figure 4.8 Measured charge of Pt electrochemically deposited onto electrochemically oxidized HOPG plotted with respect to the measured electrochemical oxidation charge of the HOPG. ● 30, ▼ 90, and ■ 180 s electrochemical oxidation times. The Pt was electrochemically deposited at – 0.475 V vs. MSE for 5 s, the HOPG was pre-treated at + 1.55 V vs. MSE in 0.1 M H_2SO_4.

Figure 4.8 clearly shows that the amount of platinum deposited (deposition charge) is linearly dependent on the extent of electrochemical oxidation (oxidation charge). What is striking about Figure 4.8 is that the measured data fits a straight line very well, as demonstrated by a calculated R^2 value of 0.98. The calculated intercept of the line is found to be 710 μC cm^{-2}. Theoretically, this intercept represents the deposition charge that corresponds to electrochemical deposition onto an HOPG substrate that has had zero oxidation charged passed, i.e. a freshly cleaved HOPG substrate. In fact, the calculated intercept value lies very close to the average and well within the standard deviation of the deposition charge onto freshly cleaved HOPG, 839 ± 311 μC cm^{-2}, measured under the same experimental deposition conditions. (see Table 4.4). The high degree of linearity of the data

plotted in Figure 4.8, combined with the fact that the intercept is very close in value to the measured deposition charge onto freshly cleaved HOPG, strongly indicates that the amount of platinum deposited onto HOPG is directly proportional to the roughness, or extent of oxidation, of the HOPG surface.

4.4.3 Platinum Particle Morphology.

4.4.3.1 Pt Electrochemically Deposited onto Ozone Oxidized HOPG.

The morphology of Pt deposits prepared by electrochemical deposition onto freshly cleaved HOPG was discussed in Chapter Three. To summarize, it was found that during deposition Pt nano-catalysts formed clusters that are located along step edges. Whether these clusters resulted from individual particles agglomerating together or if they represent a dendrite structure was not determined.

In the present chapter, ozone treatment of the HOPG surface is shown to have significant advantages over simply cleaving in regards to deposition of Pt. Of the three ozone-oxidation times presented in Section 4.4.2, the most reproducible deposition process was found to take place using HOPG substrates oxidized for 15 min. in 0.15 ppm O_3 at 300 °C; therefore, these conditions will be used for the remainder of this chapter. Figure 4.9 shows TEM images of Pt electrochemically deposited onto ozone oxidized HOPG, using these treatment conditions. Three different deposition times are shown Figure 4.9; 2.5, 5, and 7.5 s. In all three cases, Pt nano-catalysts form clusters homogeneously distributed on the HOPG surface.

The presence of Pt clusters on the basal plane indicates that the introduction of nanometre-sized pits onto the basal plane by ozone oxidation successfully introduces nucleation sites for Pt deposition. This supports our theory, as discussed in Section 4.4.2, that the nucleation process becomes more instantaneous on ozone oxidized HOPG compared to freshly cleaved HOPG because the generation of pits on the HOPG surface increases the number of nucleation sites. Similar to the case of deposition onto freshly cleaved HOPG, deposition onto ozone oxidized HOPG results in the formation of Pt clusters.

Pt clusters formed on ozone oxidized HOPG after 5 s of deposition time are on average 30 nm in diameter less than clusters formed on freshly cleaved HOPG. Additionally, the size distribution of these clusters decreased by a factor of almost two when using the ozone oxidized HOPG substrates. TEM analysis (Figure 4.9) shows that the average diameter of Pt deposits increases from 37 ± 20 to 55 ± 20 to 100 ± 49 nm for samples deposited for 2.5, 5,

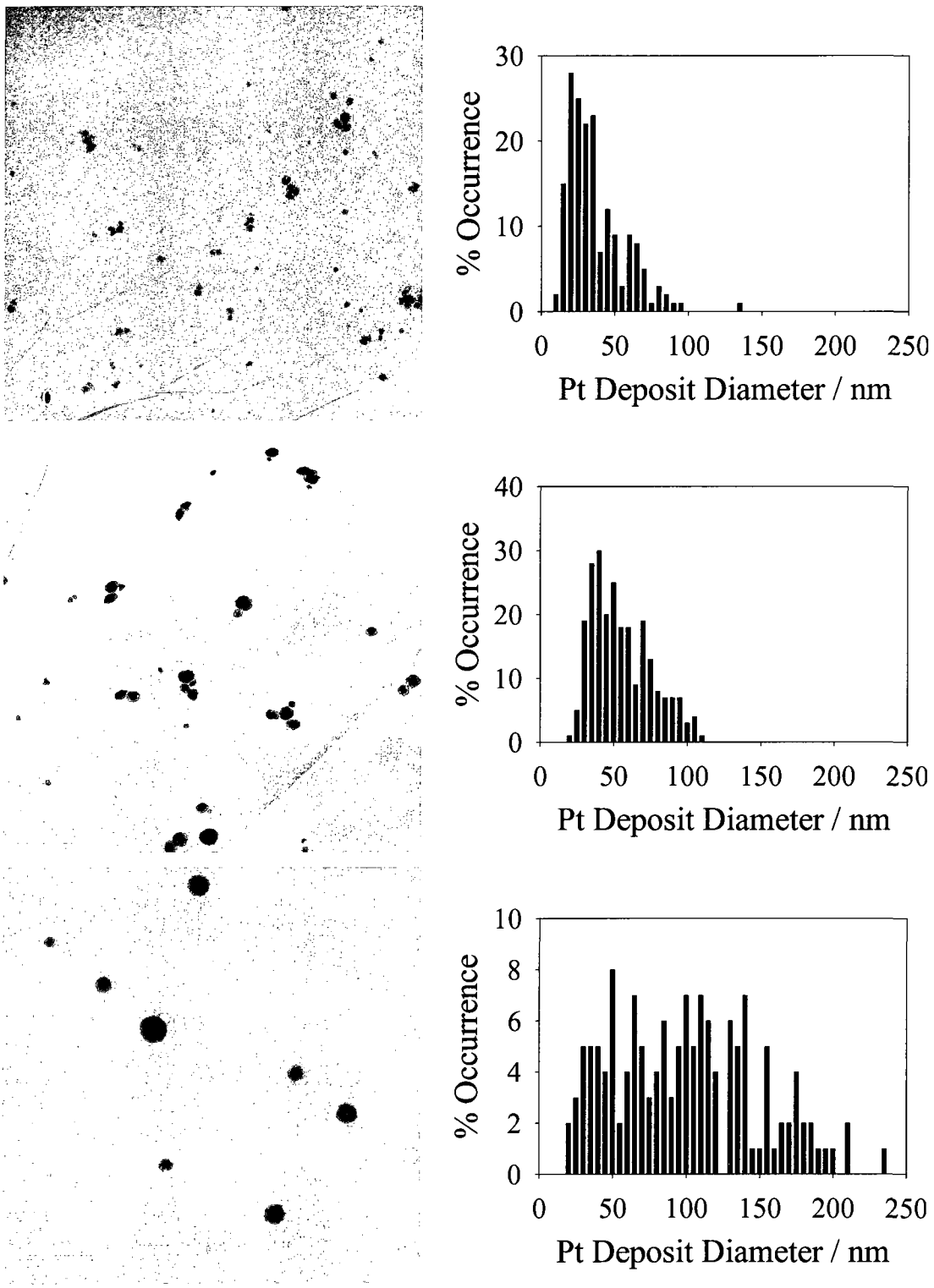

Figure 4.9 TEM images of Pt deposits on O_3 oxidized HOPG (15 min., 300 °C, 0.15 ppm O_3) a) 2.5, b) 5, c) 7.5 s deposition in 0.1 M H_2SO_4 + 1 mM $PtCl_4$ at – 0.475 V vs. MSE. Histograms for the corresponding Pt cluster diameters are also shown.

and 7.5 s, respectively, on ozone oxidized HOPG. This suggests that the cluster size can be controlled by varying the Pt deposition time. Similar to the case of Pt electrodeposition onto freshly cleaved HOPG, the deposits are in fact clusters consisting of nanometre platinum particles.

Table 4.4 shows the size of Pt clusters for deposition times of 2.5, 5, and 7.5 s before and after a CO_{ads} stripping experiment determined by TEM analysis. For all three deposition times, the average size of the Pt clusters is similar (i.e., within the standard deviation of the average value) after CO_{ads} stripping to the average size before CO_{ads} stripping. The size dispersion of the Pt deposits formed after 2.5 s of deposition time is seen to almost double for the sample examined after performing a CO_{ads} stripping voltammogram compared to the sample examined that did not undergo CO_{ads} stripping voltammetry. The same comparison for the 5 s deposition sample indicates only a slight increase in dispersion. Conversely, the dispersion of the 7.5 s deposition sample that was CO_{ads} stripped is found to be less than the dispersion of the "as-prepared" sample. One could interpret the slight increase in cluster size and size dispersion observed for Pt clusters which are less than 60 nm in size as resulting from surface diffusion of the clusters, and thus agglomeration during the CO_{ads} stripping voltammetry. Continuing with this line of reasoning, one could also conclude that Pt clusters larger than 60 nm are comparatively more stable, and thus do not diffuse along the surface of the HOPG surface and agglomerate during CO_{ads} stripping. However, as the size dispersion represents a large fraction of the average cluster size, it is much more likely that the changes in the average Pt cluster size and size dispersion reflects the variability in the deposition process.

Transmission electron microscopy (TEM) analysis of the Pt deposits prepared by electrochemical deposition onto ozone oxidized HOPG indicated that this deposition technique resulted in the formation Pt clusters rather than individual nano-particles. These clusters are either agglomerates of individual nano-particles, or they may be dendrites. Although dendrite structures and agglomerates may appear the same when using low resolution TEM or scanning electron microscopy, they are formed by drastically different mechanisms; i.e, an agglomerate is formed by surface diffusion, collision, and adhesion of individual nanoparticles on the HOPG surface, whereas dendrite structures grow by the addition of individual atoms to the parent structure.

Table 4.4 Size of Pt deposit* on HOPG-O_3† determined from TEM images.

Deposition* time / s	As prepared cluster size / nm	Cluster size after CO_{ads} stripping‡ experiment / nm
2.5	37 ± 20	38 ± 37
5.	55 ± 20	57 ± 26
7.5	100 ± 49	70 ± 30

* Pt was deposited at – 0.475 V vs. MSE in 0.1 M H_2SO_4 + 1 mM $PtCl_4$ solution.

† The HOPG was oxidized for 15 min. at 300 °C using 0.15 ppm O_3..

‡ The CO_{ads} stripping voltammograms were carried out at 10 mV s^{-1} in 0.5 M H_2SO_4.

The following four aspects can be analyzed to determine if the prepared cluster is an agglomerate of smaller clusters or a dendrite structure (as indicated in ref. 82): (1) If the cluster is formed by agglomeration, then one would expect to find, in addition to the clusters, individual nano-particles on the substrate surface. (2) High cluster size control is achieved with dendrite structures, but not with agglomerates. (3) Dendrite structures are more robust than agglomerate structures, thus, physical stresses such as washing, drying, and presumably electro-oxidation of adsorbed carbon monoxide, will not alter the morphology of dendrites where as it may with agglomerates. (4) HRTEM indicates that dendrites have a single-crystalline nature, whereas within an agglomerate the crystal structure of the individual particles will be randomly orientated.

Considering the clusters formed in this work with respect to the above mentioned differences between agglomerates and dendrites, we can conclude the following: (1) The lack of individual nanoparticles on the HOPG surface indicates that our cluster may be dendrites. (2) Large standard deviations of the cluster size ranging from 40 % to 100 % of the average the cluster size show very poor size control indicating that they may actually be agglomerates. (3) It is difficult to comment on the robustness of the prepared clusters because cluster size was determined by TEM, which is a destructive technique and therefore the same sample could not be analyzed before and after CO_{ads} stripping voltammograms. Points (1), (2), and (3) do not conclusively determine, for this system, if the clusters are dendrite structures or if they are agglomerates, only HRTEM (4) can make this distinction.

Figure 4.10 shows a HRTEM image of a Pt cluster formed on ozone oxidized HOPG. The figure clearly shows that the crystal orientation of the smaller particles in the cluster are randomly orientated. This indicates that the clusters are formed by surface diffusion and agglomeration of nanoparticles and are therefore not dendrite structures. Thus, it appears that the clusters are indeed formed by agglomeration based on the random crystal orientation of the particles within the cluster.

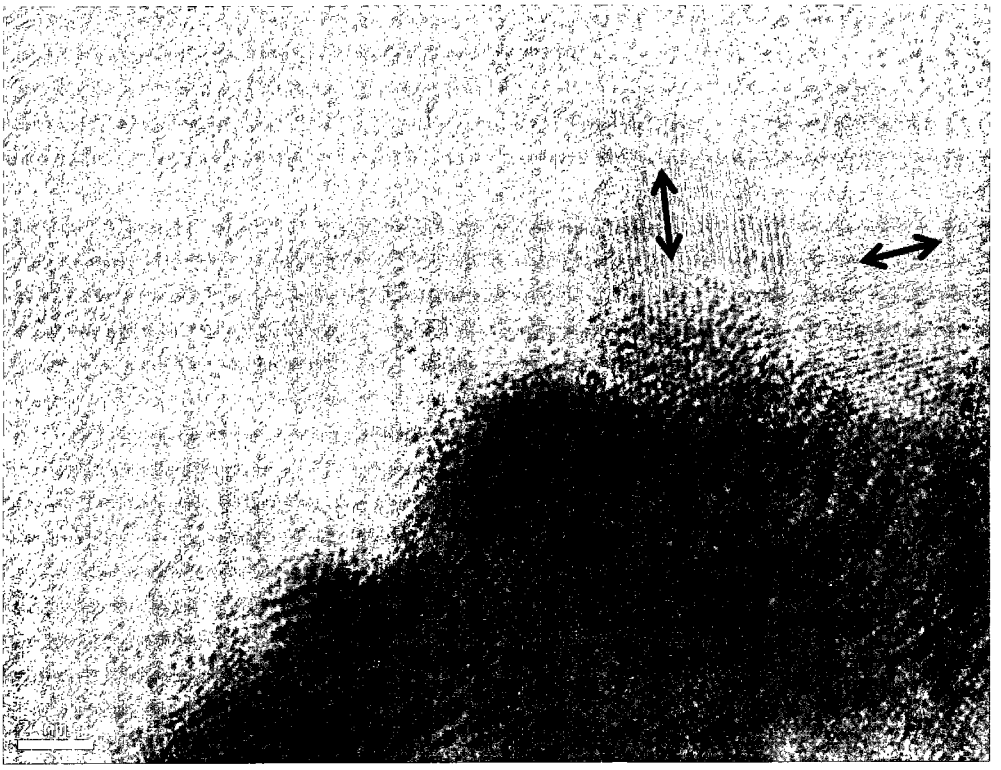

Figure 4.10 High resolution TEM image of a Pt cluster formed by electrochemical deposition (– 0.475 V vs. MSE in 1 mM $PtCl_4$ + 0.1 M H_2SO_4) onto ozone oxidized (0.15 ppm O_3 at 300 °C for 15 min.) HOPG. Atomic resolution at cluster fringe indicates that that the cluster is an agglomerate of individual nanoparticles.

4.4.3.2 Pt Electrochemically Deposited onto Electrochemically Oxidized HOPG.

TEM images of Pt electrochemically deposited for 5 s onto HOPG, which has undergone electrochemical oxidation for 30, 90 and 180 s, are shown in Figure 4.11a, Figure 4.11b, and Figure 4.11c, respectively. Table 4.5 lists selected electrochemical and morphological data for the Pt/HOPG electrodes presented in Figure 4.11. As with the Pt/HOPG electrodes prepared onto freshly cleaved and ozone oxidized HOPG, electrochemical deposition of Pt

onto electrochemically oxidized HOPG results in the formation of Pt clusters – not individual particles. The random distribution of Pt clusters in Figure 4.11 indicates that electrochemical oxidation, like ozone oxidation, creates Pt nucleation sites on the basal plane of the HOPG substrate.

From Table 4.5 and Figure 4.11 we can see that the cluster density is not proportional to the extent of electro-oxidation. For example, the samples electro-oxidized for 30 , 90, and 180 s (which have the corresponding electro-oxidation charges of 0.14, 43, and 290 mC cm^{-2}, respectively) have measured cluster densities of 3.4 ± 1.1, 0.7 ± 0.5, and 21.5 ± 2.8 μm^{-2}. The cluster density is expected to be proportional to the nucleation density. On electrochemically oxidized HOPG, the nucleation sites are step edges and pits that are formed by the electrochemical oxidation process. In Section 4.4.1 we discussed how the density of pits formed by electrochemical oxidation is proportional to the number of defect sites on the HOPG surface, and not the electro-oxidation time or charge. Thus, since the number of pits is dependent on the number of naturally occurring defect sites, it follows that the number of nucleation sites is also dependent on the number of naturally occurring defects sites. That is to say, the cluster density is proportional to the number of naturally occurring defect sites on the HOPG surface and not the extent of electro-oxidation of the HOPG substrate. Analysis of Table 4.5 indicates that in the early stages of electrochemical oxidation of HOPG, the linear correlation between electrochemical oxidation charge and electrochemical deposition charge is not observed.

As previously discussed (see Figure 4.8), the measured Pt reduction charge increases with increasing electrochemical oxidation extent of the HOPG substrate. For example, the measured reduction charges (for a 5 s deposition pulse) corresponding to the samples presented in Figure 4.11a, Figure 4.11b, and Figure 4.11c (which were oxidized for 30, 90, and 180 s, respectively) are 0.8, 1.1, and 6.7 mC cm^{-2}, respectively (see Table 4.5). The sequential increase in reduction charge does not, however, result in a sequential increase in the average deposit size. Analysis of the TEM images indicates that the average Pt cluster size formed from a 5 s deposition pulse onto HOPG substrates electrochemically oxidized for 30, 90, and 180 s is 23 ± 8, 94 ± 40, and 44 ± 21 nm, respectively (see Table 4.5). Although there is considerably more Pt deposited on the HOPG substrate oxidized for 180 s, compared to the HOPG substrate oxidized for 90 s, the larger Pt cluster density on the latter likely

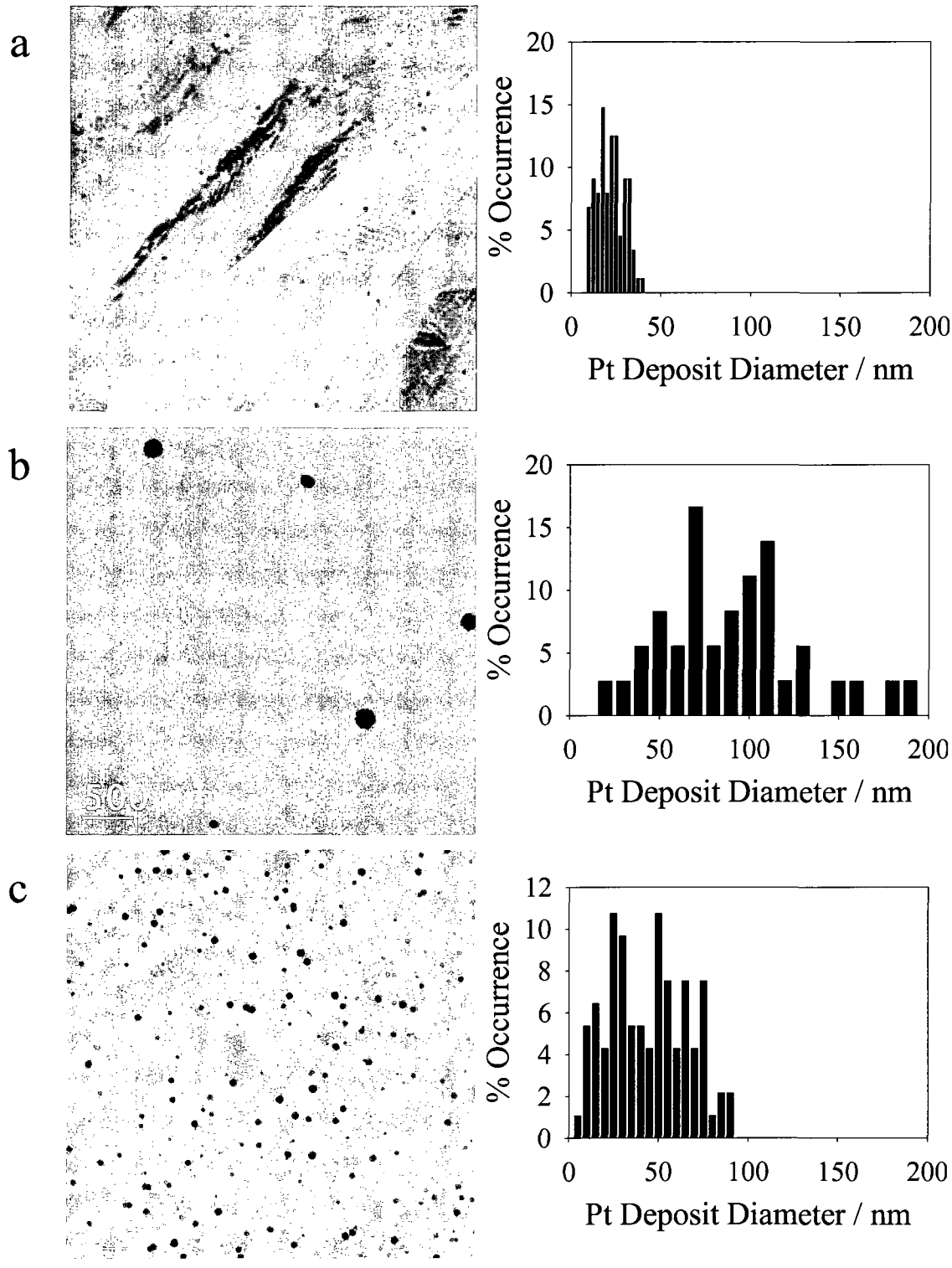

Figure 4.11 TEM images of Pt electrochemically deposited (5 s at – 0.475 V in 1 mM $PtCl_4$ + 0.1 M H_2SO_4) onto HOPG which has undergone electrochemical oxidation at 1.55 V for a) 30, b) 90 and c) 180 s. Histograms for the corresponding Pt cluster diameters are also shown.

causes the smaller measured average Pt cluster size. From Figure 4.11, it is clear that electrochemically oxidizing the HOPG substrate increases the variability of the reduction process, compared to ozone oxidized HOPG.

Table 4.5 Selected electrochemical and morphological data for the samples presented in Figure 4.11.

Electro-oxidation time / s	Electro-oxidation charge* / mC cm^{-2}	Electro-deposition charge† / mC cm^{-2}	Cluster size / nm	Cluster density / μm^{-2}
30	0.2	0.8	23 ± 8	3.4 ± 1.1
90	43	1.1	94 ± 40	0.7 ± 0.5
180	290	6.7	44 ± 21	21.5 ± 2.8

* The HOPG was oxidized in 0.1 M H_2SO_4 at 1.55 V vs. MSE.

† Pt was deposited at – 0.475 V vs. MSE for 5 s in 0.1 M H_2SO_4 + 1 mM $PtCl_4$ solution.

4.5 CONCLUSIONS

Platinum nano-catalysts were electrochemically deposited onto ozone or electrochemically oxidized HOPG. Both oxidation methods introduced pits on the basal plane of HOPG. Measured roughness factors indicate that electrochemical oxidation is a much more severe oxidation process compared to ozone oxidation. For example, electrochemical oxidation produces large pits, > 85 nm in diameter, originating at naturally occurring defect sites on the HOPG surface, as well as flaking of the substrate along step edges, whereas ozone oxidation produced nano-meter sized pits which were randomly distributed over the basal plane of HOPG. As the number of defect sites and step edges differ for each HOPG substrate, electrochemical oxidation amplifies the differences between HOPG samples. Conversely, as ozone oxidation creates defects, it minimizes the differences between HOPG samples.

Oxidizing the HOPG substrate with ozone shifts the nucleation process from progressive towards instantaneous, compared to Pt nucleation onto freshly cleaved HOPG (which was

observed to be predominantly progressive). Instantaneous nucleation is preferred since it results in a narrower cluster size distribution. Pt is believed to nucleate on the nano-pits on ozone oxidized HOPG, forming a random distribution of Pt clusters over the basal plane.

TEM analysis revealed that oxidizing HOPG with either ozone gas, or electrochemical methods, results in Pt depositing on the basal plane of the substrate. Electrochemically depositing onto ozone oxidized HOPG resulted in an increase in deposition reproducibility compared to freshly cleaved HOPG. Conversely, electrochemical deposition onto electrochemically oxidized HOPG proved to be highly irreproducible as is was highly dependent on the extent of electrochemical oxidation, which is in turn dependant on the number of step edges and naturally occurring defects found on the HOPG substrate. The size of Pt nano-catalyst clusters formed on ozone oxidized HOPG is controlled by the deposition time. HRTEM analysis indicates that the Pt clusters formed on ozone oxidized HOPG are agglomerates on nano-particles, and not dendrite structures.

Chapter Five

Impregnation and Thermal Decomposition of Pt onto Freshly Cleaved and Oxidized HOPG

5.1 ABSTRACT

Platinum nano-catalysts were deposited by impregnation followed by thermal decomposition onto highly ordered pyrolytic graphite (HOPG). To help stabilize the prepared nano-catalysts, the HOPG substrate was oxidized. Two methods of oxidation, electrochemical or ozone gas oxidation, were studied. As a point of comparison, Pt was also deposited onto freshly cleaved HOPG. These three types of Pt/HOPG electrodes are compared to one another with respect to their particle morphology. Impregnation and thermal decomposition onto oxidized HOPG resulted in individual Pt nano-catalysts that are well dispersed over the basal plane. Conversely, Pt deposits are confined to step edges on freshly cleaved HOPG. TEM analysis reveals that ozone oxidized HOPG stabilizes Pt nano-catalysts prepared by impregnation and thermal decomposition from agglomerating during CO_{ads} stripping voltammetry. Freshly cleaved and electrochemically oxidized HOPG, on the other hand, either do not stabilize the Pt nano-catalysts against agglomeration during CO_{ads} stripping voltammetry or do not allow for a reproducible process to form Pt nano-catalysts by impregnation and thermal decomposition.

5.2 INTRODUCTION

Chapters Three and Four discussed the electrochemical deposition of Pt onto freshly cleaved and oxidized HOPG. Electrochemical deposition resulted in the formation of Pt clusters on the HOPG surface. As the interest of this work lies in the formation of nano-catalysts, the fabrication methods discussed in Chapters Three and Four are inadequate. Thus, it was decided to explore a different method of nano-catalyst preparation. Chapter One provides a detailed discussion of the various methods available to prepare Pt catalysts. Section 1.4.9 discusses the advantages and disadvantages of the different catalyst preparation methods. To reiterate, it was concluded that impregnation followed by thermal decomposition is a catalyst preparation method worthy of investigation since it did not involve the use of stabilizers that can affect the electrochemical activity of the prepared nano-catalysts.

Experimental techniques used to prepare nano-catalysts from impregnation followed by thermal decomposition are relatively simple. Carbon supports, such as high-surface-area

carbon black, are commonly impregnated with catalyst precursor salts by mixing the two in an aqueous solution.[14] However, as the substrate used in this work is not a powder, impregnation involves depositing an aliquot of solution that contains the catalyst precursor onto a HOPG substrate and allowing it to air dry.[15] It has been found in other work that the Pt(IV) precursor salt reduces to the Pt(II) state after a redox reaction with the partially oxidized carbon surface.[83] Pt(II) is found to be anchored to the HOPG surface through the formation of π-complexes with the surface >C=C< groups on the support.[84,85,92]

Following the impregnation step, a reduction step is required to reduce the catalyst precursor to its metallic state. When powdered carbon is used as the support, a liquid phase reducing agent is commonly used. However, if the reduction process were to occur when the HOPG substrate was submerged in the platinum salt solution, platinum metal would not be confined to the top surface of the HOPG substrate. Instead, platinum would deposit on all exposed surfaces. This catalyst preparation technique was to be tested on oxidized HOPG as well as freshly cleaved HOPG. Since electrochemical oxidation is confined to the top surface of the HOPG sample, impregnation and thermal decomposition under a hydrogen gas atmosphere was used to confine the Pt salt to the top surface of the HOPG substrate.

Previous studies utilized impregnation and $H_{2(g)}$ reduction to prepare Pt/HOPG samples. One study successfully controlled the Pt catalyst size by varying the Pt metal concentration in the precursor solution; Pt catalysts 4.5 and 8 nm in diameter were produced using a 2 and 5 wt% H_2PtCl_6 solution.[86] Unfortunately, that study showed a poor size distribution, specifically particles with an average diameter of 4.5 nm ranged in size from 2 – 8 nm, and particles with an average diameter of 8 nm ranged in size from 5 – 11 nm.[86] Another study found that impregnation followed by thermal decomposition under $H_{2(g)}$ formed Pt clusters, instead of individual particles, the size of which could also be controlled by Pt concentration in the precursor solution.[87]

The above mentioned studies utilized high reducing temperatures. HOPG will oxidize in air at temperatures of 350 °C and greater. Air oxidation results in the formation of micrometer-sized pits that initiate at naturally occurring defect sites in the HOPG surface. Thus, reducing Pt precursor salts onto HOPG at temperatures of 350 °C or greater, which will change the surface morphology of the HOPG, can in turn affect the morphology of the Pt catalysts. In fact, one study analyzed the change of crystallite morphology with time

while using a decomposition temperature of 600 °C.[88] It was found that short decomposition times formed rod-like particles that decomposed to crystallites with ellipsoidal shape. Further treatment resulted in the Pt particles developing box-like morphology with well developed facets.

The majority of studies where Pt is impregnated and reduced onto HOPG are mainly surface-science studies. That is to say, in the majority of studies the Pt/HOPG electrodes were prepared and the surface structure of the electrodes were studied; however, they were never tested to determine their electrochemical activity. One study tested the morphological stability of Pt nano-catalysts impregnated and thermally decomposed onto air oxidized HOPG, although it again did not test the electrocatalytic activity of the prepared Pt/HOPG electrode.[92,107] This study showed that Pt nano-catalysts prepared by impregnation and thermal decomposition onto thermally oxidized HOPG agglomerated when cycling the Pt nano-catalyst between the regions of hydrogen and oxygen evolution. It was determined that the Pt nano-catalyst had agglomerated, as opposed to growth due to Ostwald ripening, because the size distribution before cycling shows a Gaussian-type profile with an average particle size of 3.4 nm, while the post potential cycling size distribution was polymodal with an average size distribution of 6.4 nm.[92,107] The study found that Pt deposit nucleated at the edge of the pits introduced by air oxidation, however, the pits failed to stabilize the Pt catalyst from agglomeration. It is possible that the pits introduced by air-oxidation were too large to effectively stabilize the Pt particles (these pits were 10 to 100 times larger than the thermally decomposed particles).

In this chapter, Pt/HOPG electrodes prepared by combining impregnation and thermal decomposition in a $H_{2(g)}$ atmosphere will be presented as a method to prepare catalysts. To increase the interaction between the Pt nano-catalysts and the HOPG substrate, we decided to oxidize the HOPG substrate utilizing either ozone gas or electrochemical methods, as discussed in Chapter Four. We hypothesize that particles will nucleate and possibly be stabilized in the pits, especially if the pits are approximately the same size as the particles. To assess the effects of oxidizing HOPG, Pt/HOPG electrodes prepared by impregnation and thermal decomposition in an $H_{2(g)}$ atmosphere using freshly cleaved HOPG are also discussed. Thus, three different types of Pt/HOPG electrodes will be examined in this chapter.

5.3 EXPERIMENTAL

5.3.1 Solutions, Cells, and Electrodes.

Chapter Two, Section 2.2 describes the solutions, cells, and electrodes used in this work. A Hg/Hg_2SO_4, 0.5 M H_2SO_4 (MSE) electrode was used as the reference electrode for electrochemical oxidation of HOPG. A Hg/Hg_2Cl_2, sat. KCl (SCE) was used for the CO_{ads} stripping voltammetry.

5.3.2 Substrate Pre-Treatments.

Grade SPI-1 HOPG from SPI supplies were used as substrates in all experiments. Pt was deposited onto freshly cleaved (denoted HOPG-FC), ozone-oxidized (denoted HOPG-O_3), and electrochemically-oxidized (denoted HOPG-E) HOPG.

HOPG was freshly cleaved using the adhesive-tape method.

Ozone oxidation of the HOPG is described in detail in Chapter Four Section 4.3.2. Ozone oxidized HOPG substrates discussed in this chapter were oxidized at 300 °C for 15 min in 0.15 ppm O_3.

HOPG was electrochemically-oxidized in a 0.1 M H_2SO_4 solution at + 1.55 V vs. MSE. The oxidation time was 90 s, unless otherwise noted.

5.3.3 Platinum Deposition Method.

Impregnation and thermal decomposition was used to form platinum nanoparticles onto freshly cleaved and oxidized HOPG. Aqueous solutions of H_2PtCl_4 in HCl of various concentrations (ranging from 2.6×10^{-5} M H_2PtCl_4 + 6.5×10^{-5} M HCl to 2.6×10^{-4} M H_2PtCl_4 + 6.4×10^{-4} M HCl) were pipetted onto the substrate surface and allowed to dry in air. Thermal decomposition of the Pt precursor salt was carried out by heating the substrate to 250 °C under a hydrogen atmosphere for 2 h. XPS analysis indicated that 2 h were sufficient to form platinum metal. All samples were kept in a desiccator until analysis.

5.3.4 Particle Size/Morphology Determination.

The size and morphology of platinum catalysts on HOPG were determined by transmission electron microscopy (TEM). Sample preparation was completed as described in Chapter Two, Section 2.4.1.2. Due to the destructive nature of the TEM sample preparation, the same sample could not be imaged before and after electrochemical analysis.

A sample prepared by impregnation and thermal decomposition onto ozone oxidized HOPG was sent for HRTEM (on a aberration corrected Titan @300kV) analysis at the Brockhouse Institute for Materials Research and Centre for Emerging Device Technologies at McMaster University.

5.3.5 Adsorbed CO Stripping Voltammetry.

Adsorbed CO (CO_{ads}) stripping voltammetry is used as a test reaction to determine if the electrode morphology changes after electrochemical use. Chapter Six, Section 6.3.4 describes the method of CO_{ads} stripping voltammetry and Section 6.4.1 describes the process of electrochemical oxidation of CO_{ads} onto polycrystalline Pt foil.

5.4 RESULTS AND DISCUSSIONS

5.4.1 Platinum Particle Morphology.

Impregnation and thermal decomposition of the Pt precursor salt H_2PtCl_4 onto HOPG was investigated as an alternative method of forming Pt nano-catalysts. Figure 5.1 shows TEM images of Pt nano-catalysts prepared by impregnation and thermal decomposition onto (a) freshly cleaved, (b) ozone oxidized, and (c) electrochemically oxidized HOPG. Analysis of Figure 5.1 reveals that impregnation and thermal decomposition results in the formation of nano-catalysts that are randomly dispersed over the basal plane of both the ozone and electrochemically oxidized HOPG substrates. Conversely, Pt nanoparticles prepared by impregnation and thermal decomposition onto freshly cleaved HOPG appear to be localized along step edges. It was also observed that Pt nanoparticles formed predominantly along step edges when deposited electrochemically onto freshly cleaved HOPG, see Chapter Three.

The TEM images presented in Figure 5.1 highlight that fact that the surface of HOPG must undergo oxidation to create nucleation sites on the basal plane, as discussed in Chapter Four. From Figure 5.1, it appears that the substrate pre-treatment does not directly control the size of the Pt nanoparticles prepared by impregnation and thermal decomposition. For example, impregnation and thermal decomposition of a 175 μL aliquot of 2.6×10^{-5} M H_2PtCl_4 in 6.5×10^{-5} M HCl results in average Pt particle sizes of 3.8 ± 0.8, 4.2 ± 1, and 2.3 ± 0.5 nm on freshly cleaved, ozone oxidized, and electrochemically oxidized HOPG, respectively. Particles prepared on freshly cleaved and ozone oxidized HOPG are of similar

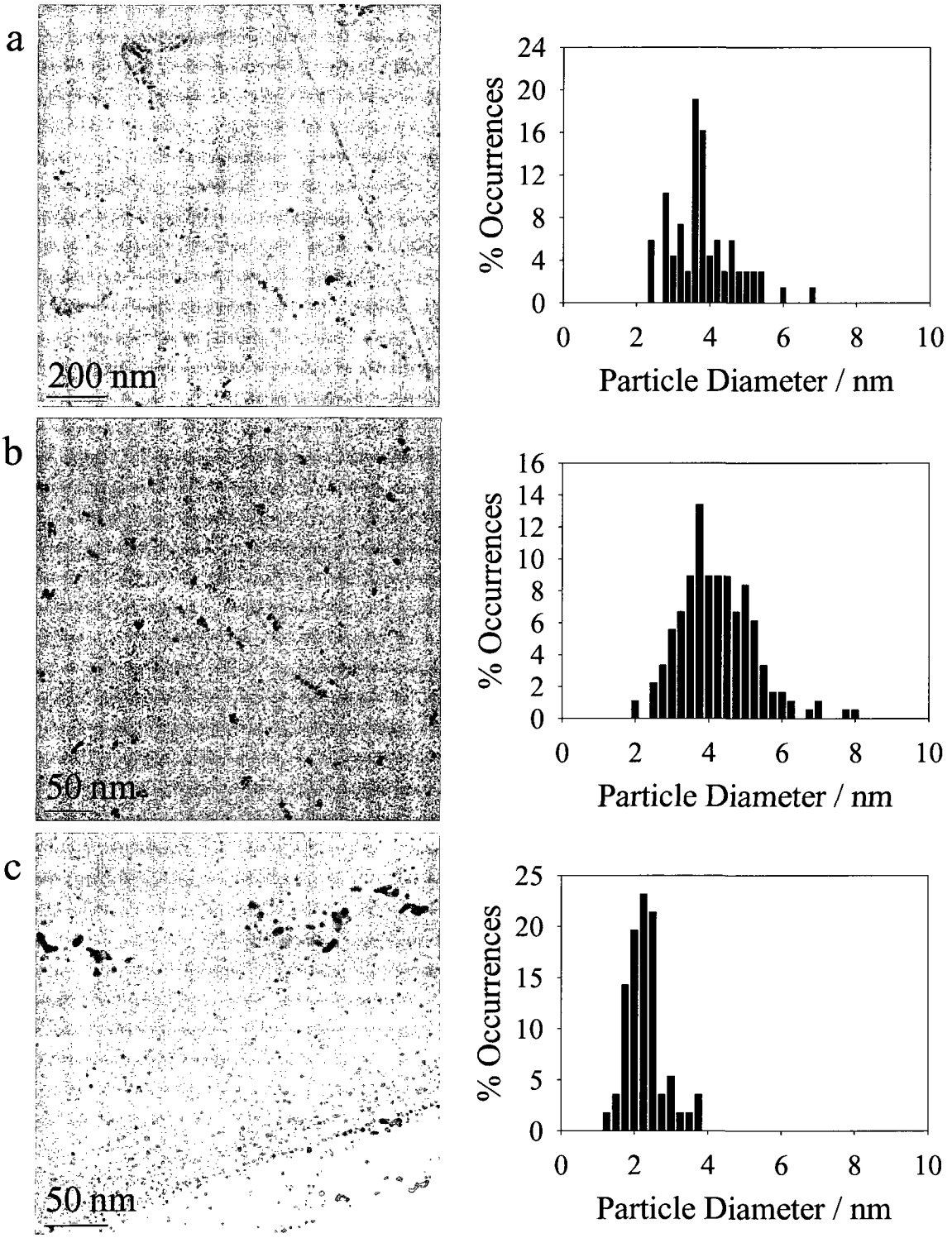

Figure 5.1 TEM image of Pt nano-catalysts prepared by impregnation and thermal decomposition (175 μL 2.6×10^{-5} M H_2PtCl_4 + 6.5×10^{-5} M HCl) onto a) freshly cleaved HOPG, b) O_3 oxidized HOPG, and c) electrochemically oxidized HOPG. Histograms for the corresponding particle diameters are also shown.

size and fall within each other's standard deviation. Pt nanoparticles prepared on electrochemically oxidized HOPG, however, are almost half the size of the particles prepared on freshly cleaved or ozone oxidized HOPG. It is possible that the smaller particle size observed on electrochemically oxidized HOPG results from the greater roughness of electrochemically oxidized HOPG compared to either freshly cleaved or ozone oxidized HOPG. A surface which is rougher would have more nucleation sites. As the amount of Pt precursor is the same for all three samples, it is reasonable that the sample with the largest number of nucleation sites would form the smallest particles.

High resolution (HR)TEM analysis indicates that the individual nano-particles are irregular in shape; there are no clear facets on the particles (see Figure 5.2). This is a unique result; i.e. platinum generally forms truncated octahedral particles, since truncated octahedral allows for a minimum surface energy.[89]

As mentioned previously, impregnation and thermal decomposition is known to make nano-catalysts on HOPG, however, the nano-catalysts reported in the literature agglomerated when the Pt/HOPG electrode was cycled between the regions of hydrogen and oxygen adsorption.[107] TEM analysis was carried out after the prepared Pt/HOPG electrodes underwent stripping voltammetry of adsorbed carbon monoxide (CO_{ads}) to probe if oxidizing HOPG, either with ozone gas or by electrochemical methods, stabilizes the Pt nano-catalysts prepared by impregnation and thermal decomposition against agglomeration. Figure 5.3 shows TEM images of Pt/HOPG samples prepared by impregnation and thermal decomposition onto (a) freshly cleaved, (b) ozone oxidized, and (c) electrochemically oxidized HOPG after CO_{ads} stripping voltammetry.

TEM analysis of the Pt/HOPG samples prepared by impregnation and thermal decomposition onto freshly cleaved HOPG that underwent CO_{ads} stripping proved to be particularly difficult as it was not easy to find the platinum catalyst on the substrate. Several areas on many different samples were analyzed and although platinum could be found, it was never found in the same density as found on the "as-prepared" samples. Analysis of successive CO_{ads} stripping charges (discussed in more detail in Chapter Seven) indicate that approximately 20 % of the platinum surface area is lost after the first CO_{ads} stripping experiment. This measured decrease in stripping charge could result from either agglomeration of the Pt nanoparticles or dissolution of Pt into the solutions. Agglomeration

of particles would decrease the number individual particles on the surface, which would in turn make it more difficult to find the particles on the HOPG surface. Similarly, if dissolution was severe enough to dissolve some particles completely, dissolution would decrease the number of particles on the surface and therefore make it more difficult to find the particles on the HOPG surface. Analysis of the Pt particles prepared by impregnation and thermal decomposition onto freshly cleaved HOPG after CO_{ads} stripping voltammetry indicated an average particle size of 6.5 ± 3.4 nm. The increase in particle size and particle size distribution (compared to the as-prepared sample; 3.8 ± 0.8 nm) probably reflects the agglomeration of neighbouring particles. This result strongly supports the findings presented in reference 107.

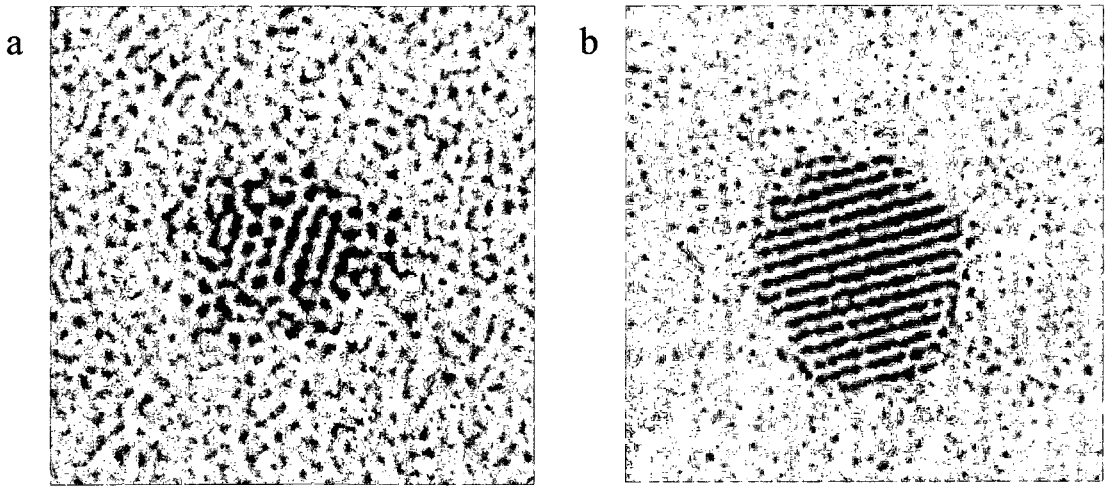

Figure 5.2 High resolution TEM images of individual nanoparticles. Sample prepared by impregnation and thermal decomposition (250 μL 2.6 x 10^{-4} H_2PtCl_4 + 6.4 x 10^{-4} HCl onto ozone oxidized) (0.15 ppm, 300 °C and 15 min) HOPG a) particle size is 2.6 nm, b) particle size is 3.5 nm.

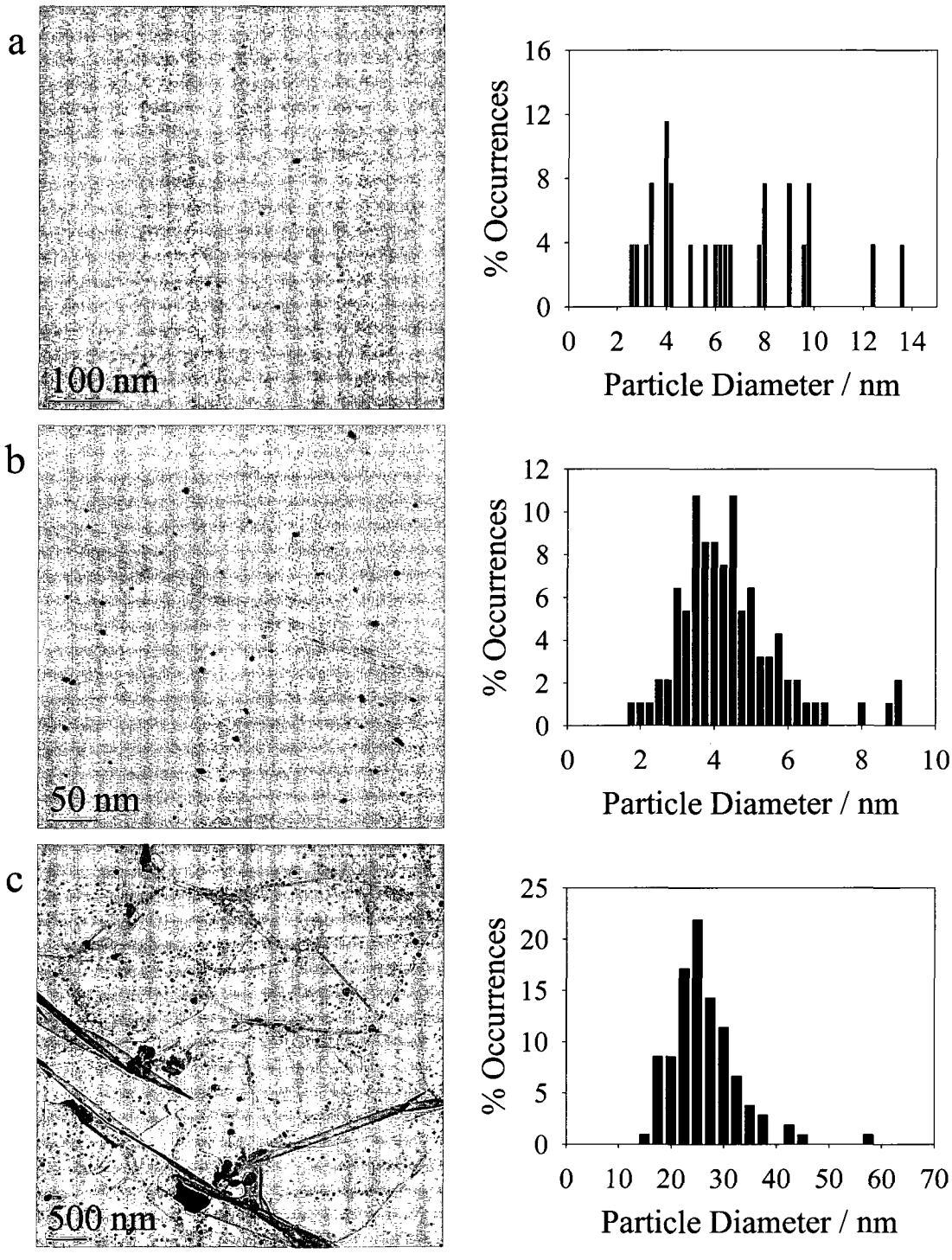

Figure 5.3 TEM image of Pt/HOPG samples prepared by impregnation and thermal decomposition (175 μL 2.6×10^{-5} M H_2PtCl_4 + 6.5×10^{-5} M HCl) onto a) freshly cleaved HOPG, b) O_3 oxidized HOPG, and c) electrochemically oxidized HOPG and which had undergone CO_{ads} stripping voltammetry. Histograms for the corresponding particle diameters are also shown.

Pt nano-catalysts thermally decomposed onto electrochemically oxidized HOPG that have undergone CO_{ads} stripping voltammetry were found to have an average diameter of 26.2 ± 6.5 nm. This indicates a more than 10 times larger size than found for the "as-prepared" nano catalyst prepared by impregnation and thermal decomposition onto electrochemically oxidized HOPG. It is important to re-emphasize that the TEM analysis procedure is a destructive technique. Thus, it is impossible to image the same sample before and after stripping voltammetry. Consequently, we cannot determine with absolute certainty if stripping voltammetry causes the platinum nano-catalysts to agglomerate, or if there is scatter in the reproducibility of the deposition technique. Regardless, the results show that HOPG which has been electrochemically oxidized does not facilitate the production of a catalyst system suitable for study.

Pt nano-catalysts prepared by impregnation and thermal decomposition onto ozone oxidized HOPG after CO_{ads} stripping voltammetry are essentially the same size, namely 4.4 $\pm$ 1.4 nm, compared to the "as-prepared" sample of 4.2 $\pm$ 1 nm. This indicates, that oxidizing HOPG with ozone gas successfully stabilizes the thermally decomposed Pt nano-catalysts against agglomeration and dissolution during CO_{ads} stripping voltammetry. The striking similarity in particle size between the two samples indicates that oxidizing HOPG with ozone gas allows for the reproducible preparation of platinum nano-catalysts. Figure 5.3b shows that impregnation and thermal decomposition in combination with ozone oxidation of HOPG generates the superior Pt nano-catalyst electrode.

5.5 CONCLUSIONS

In this chapter, impregnation and thermal decomposition was studied as a alternative method to electrochemical deposition to form Pt nano-catalysts. The nano-catalysts were prepared on freshly cleaved, ozone oxidized, and electrochemically oxidized HOPG. The morphology before and after CO_{ads} electro-oxidation were studied.

Impregnation and thermal decomposition of the Pt precursor salt onto freshly cleaved and oxidized HOPG produced well dispersed nano-catalysts that did not agglomerate during the deposition process. Pt nano-catalysts were confined to step edges on the freshly cleaved HOPG while they were distributed randomly over the basal plane on the oxidized HOPG.

This supports our finding presented in Chapter Four that oxidation is required to produce nucleation sites on the basal plane of HOPG.

TEM analysis after CO_{ads} stripping voltammetry of Pt nano-catalysts formed on freshly cleaved and electrochemically oxidized HOPG indicates that the catalysts were larger compared to the "as-prepared" samples. This indicates that either the catalysts agglomerate during CO_{ads} stripping voltammetry or deposition is not a reproducible process on freshly cleaved and electrochemically oxidized HOPG. Impregnation and thermal decomposition onto ozone oxidized HOPG, however, produced Pt nano-catalysts that are stable against agglomeration during CO_{ads} stripping voltammetry. Moreover, impregnation and thermal decomposition onto ozone oxidized HOPG is a reproducible "nano-catalyst" preparation technique.

Chapter Six

Adsorbed Carbon Monoxide Stripping Voltammetry

6.1 ABSTRACT

The electrochemical activity of Pt/HOPG electrodes prepared by electrochemical deposition or impregnation followed by thermal decomposition onto freshly cleaved, ozone oxidized, or electrochemically oxidized HOPG towards the electro-oxidation of adsorbed carbon monoxide (CO_{ads}) were tested. When comparing all six electrodes it became evident that substrate pre-treatment did not affect the activity, while the method of Pt deposition did significantly affect the measured activity. For example, Pt/HOPG electrodes prepared by electrochemical deposition using short deposition times, < 10 s, showed slower CO_{ads} electro-oxidation kinetics compared to polycrystalline Pt foil, while electrodes prepared by impregnation followed by thermal decomposition show faster electro-oxidation kinetics. The electro-oxidation of CO_{ads} involves three steps; (1) the adsorption of activated water, (2) the surface diffusion of CO_{ads}, and finally (3) the reaction of adsorbed activated water with CO_{ads} to form CO_2. Stripping voltammetry cannot determine which of the above three reactions is the rate determining step (RDS). Thus, it is not known if the RDS is different for the Pt/HOPG electrodes prepared by the two different deposition techniques, or if the RDS is the same for both types of electrodes but faster for the electrode prepared by impregnation followed by thermal decomposition. The activity of Pt/HOPG electrodes prepared by electrodeposition could be controlled by controlling the deposition. It was found that electrodes prepared using a long deposition time, e.g. 900 s, had faster CO_{ads} electro-oxidation kinetics than polycrystalline Pt foil, illustrating the versatility of this deposition technique.

6.2 INTRODUCTION

Chapters Three through Five describe in detail the preparation and characterization of six different types of electrodes. In these chapters, it was found that oxidizing the HOPG substrate was necessary to facilitate nucleation of Pt catalysts on the HOPG basal plane; on freshly cleaved HOPG Pt was located predominantly along step edges regardless of the deposition technique. Ozone oxidation, which formed nanometre sized pits randomly distributed on the basal plane of HOPG was found to increase the reproducibility of Pt deposition for both electrochemical deposition and impregnation followed by thermal

decomposition. Electrochemical oxidation, which only formed pits where naturally occurring defect sites occurred on the HOPG surface, decreased the reproducibility of the deposition process for both deposition methods. Electrochemical deposition resulted in the formation of Pt clusters regardless of substrate pre-treatment; whereas, impregnation followed by thermal decomposition produced well dispersed individual nanoparticles.

In addition to characterizing these electrodes with respect to their morphology, their electrochemical activity was also studied. When selecting a "test reaction" for the prepared electrodes I wanted to select a reaction that is relevant to low temperature fuel cell applications. There are many different types of low temperature fuel cells and they vary mainly in the type of fuel that is used. Hydrogen fuel cells, probably one of the most well studied fuel cells, utilize platinum catalyst to oxidize hydrogen gas at the anode. However, the kinetics of hydrogen oxidation and the platinum loadings required to oxidize hydrogen gas are not in need of improvement (compared to other aspects of hydrogen fuel cells), and thus this reaction was not selected. Oxidizing other fuels like methanol or formic acid were considered for the test-reaction. However, oxidizing these fuels is considerably more complicated than oxidizing hydrogen gas, and they have been found to oxidize best on platinum alloys. Since bi-metallic catalysts are not prepared in this thesis, methanol and formic acid would be inappropriate test-reactions. In most low temperature fuel cells, oxygen gas is reduced at the cathode. Pt catalysts are among the best for oxygen reduction and therefore the electrodes prepared in this work could be used to test the oxygen reduction reaction. However, the oxygen reduction reaction is highly complicated. Many reaction pathways have been proposed, and normally it is a mix of theses different reaction pathways that occur at a given time.[90] It was decided a simpler reaction would be a more prudent choice for an exploratory test-reaction.

The electrochemical oxidation of adsorbed carbon monoxide (CO_{ads}) was selected as the test-reaction. This reaction is applicable to most low temperature fuel cells. For example, CO is a common intermediate formed in the oxidation of methanol, formic acid, and other carbon based fuels. CO is also commonly found in hydrogen gas because it is a by-product of the reforming of hydrocarbons, which is a common method to make hydrogen gas. CO binds onto the Pt catalyst surface acting as a poison because it effectively blocks platinum sites making them not available to catalyze the oxidation of the fuel. Thus, the development

of a Pt catalyst which can easily remove CO_{ads}, by oxidation, would result in the formation of a more active catalyst.

It was decided to oxidize CO_{ads} by stripping voltammetry. This involves cycling the potential of the Pt/HOPG electrode (onto which CO was previously adsorbed) from the adsorption potential to more anodic potentials. Once a potential sufficiently anodic to initiate the electro-oxidation of CO_{ads} is reached the anodic current rises due to the measured oxidation current. Once all of the CO_{ads} has been removed from the electrode the current falls to the values typical of the electrode without CO_{ads}. The potential of the electrode is then cycled in the opposite direction towards (but not reaching) the potential of hydrogen evolution. This represents the first sweep of a stripping voltammetry experiment. The second & third sweeps are essentially a repeat of the first. Assuming all of the CO_{ads} was removed in the first sweep, the second and third sweeps will represent the cyclic voltammogram of the electrode in an electrolyte solution. If not all of the CO_{ads} was removed on the first sweep an anodic oxidation peak will appear on the second (and possibly third) sweep. If this occurs the sweep rate and maximum anodic potential are adjusted to ensure that all of the CO_{ads} is removed in the first sweep. An added benefit of this method of oxidizing CO_{ads}, is that in one CO_{ads} stripping experiment, Pt/HOPG cyclic voltammograms (the second and third sweeps) are obtained. Thus, in addition to data regarding the electro-oxidation of CO_{ads} the electrochemical spectrum of the Pt/HOPG electrode is also obtained.

In this chapter, electrochemical oxidation of adsorbed carbon monoxide by stripping voltammetry is performed on all six different types of Pt/HOPG electrodes prepared and discussed in this thesis, since useful in situ electrochemical information can be gained about Pt catalysts from this experimental technique.[91]

6.3 EXPERIMENTAL

6.3.1 Solutions, Cells, and Electrodes.

Chapter Two, Section 2.2 describes the solutions, cells, and electrodes used in this work. A Hg/Hg_2SO_4, 0.5 M H_2SO_4 (MSE) electrode was used as the reference electrode for electrochemical deposition of Pt and electrochemical oxidation of HOPG. A Hg/Hg_2Cl_2, sat. KCl (SCE) was used for the CO_{ads} stripping voltammetry.

6.3.2 Substrate Pre-Treatments.

Grade SPI-1 HOPG from SPI supplies were used as substrates in all experiments. Pt was deposited onto freshly cleaved (denoted HOPG-FC), ozone-oxidized (denoted HOPG-O_3), and electrochemically oxidized (denoted HOPG-E) HOPG.

HOPG was freshly cleaved using the adhesive-tape method.

Ozone oxidation of the HOPG is described in detail in Chapter Four Section 4.3.2. Ozone oxidized HOPG substrates discussed in this chapter were oxidized at 300 °C for 15 min in 0.15 ppm O_3.

HOPG was electrochemically oxidized in a 0.1 M H_2SO_4 solution at + 1.55 V for 30 s.

6.3.3 Platinum Deposition Method.

Electrochemical deposition occurred at – 0.475 V vs. MSE in 1 mM $PtCl_4$ + 0.1 M H_2SO_4. Details of the deposition procedure are described in Chapter Three, Section 3.3.3.

Impregnation and thermal decomposition was carried out as described in Chapter Five, details of the deposition procedure are described in Chapter Five, Section 5.3.3.

6.3.4 Adsorbed CO Stripping Voltammetry.

The experimental procedure involves adsorbing CO onto the Pt nano-catalysts at – 0.10 V vs. SCE by bubbling CO gas (Matheson purity, Matheson gas) through the 0.5 M H_2SO_4 electrolyte solution, which the Pt/HOPG electrode is immersed in, for 10 min. The solution is then purged of CO by bubbling argon gas for 30 min, while maintaining the potential at – 0.10 V vs. SCE. It is important to remove all CO dissolved in solution, CO_{sol}, to ensure that once the CO_{ads} has been electro-oxidized from the Pt surface, additional CO_{sol} does not adsorb onto the surface. To remove the CO_{ads}, the potential was cycled from – 0.10 to 0.86 V vs. SCE at 10 mV s^{-1}. The positive potential scan was limited to 0.86 V vs. SCE to prevent the Pt catalyzed surface oxidation of the substrate which the nano-catalysts were deposited onto.[92,93,94] Furthermore, at 0.86 V vs. SCE one monolayer of $Pt(OH)_{ads}$ will have formed on polycrystalline Pt foil. Two additional oxidation/reduction cycles were completed to ensure that the CO_{ads} was completely removed during the first cycle. If any CO_{ads} remained, then a CO_{ads} oxidation peak, similar to that in the first cycle, would be present in the second and possibly third cycles.

6.4 RESULTS AND DISCUSSION

6.4.1 Stripping Voltammetry of CO_{ads} onto Polycrystalline Pt foil.

The mechanism of electrochemical oxidation of CO_{ads} follows a Langmuir-Hinshelwood mechanism. In order to electro-oxidize CO_{ads} from platinum, it must first be adsorbed on the surface of the Pt catalysts

$$Pt + CO_{sol} \leftrightarrows Pt(CO)_{ads} \tag{6.1}$$

CO is allowed to adsorb onto the Pt surface until the platinum is saturated with adsorbed carbon monoxide. A saturated surface does not necessarily mean that every Pt atom has a CO molecule bound to it. A saturated surface simply means that increasing the exposure time does not result in the coverage of carbon monoxide increasing. In fact, the coverage of CO_{ads} is normally found to be between 80 – 95 %, i.e. CO is adsorbed onto 80 – 95 % of Pt atoms. The model by which the electro-oxidation of CO_{ads} proceeds utilizes a two state "active site" model of the platinum surface. That is to say, all Pt surface atoms can be labelled as either "active" or "inactive". Adsorption of carbon monoxide can occur onto either active or inactive sites on the Pt surface.

The first electrochemical step is the adsorption of "activated-water" on an active site on the surface of the platinum catalyst. Although the exact form of activated water is not known, it is commonly accepted that the oxygenated species needed to oxidized CO_{ads} is $Pt(OH)_{ads,}$ which is formed by water splitting.[95]

$$Pt + H_2O \leftrightarrows Pt(OH)_{ads} + H^+ + e^- \tag{6.2}$$

Once $Pt(OH)_{ads}$ has formed it can react with a neighbouring CO_{ads} to form carbon dioxide in the following recombination reaction,

$$Pt(CO)_{ads} + Pt(OH)_{ads} \rightarrow 2Pt + CO_2 + H^+ + e^- \tag{6.3}$$

The overall electro-oxidation reaction involves two electrons per molecule of adsorbed CO. As the recombination reaction proceeds and the coverage of CO_{ads} decreases, Pt surface sites

become exposed to the electrolyte solution. Some of these newly exposed sites will be active sites and will adsorb activated water. Thus, the electrochemical oxidation of CO_{ads} is auto catalytic.

At the beginning of the electrochemical oxidation of CO_{ads}, when the coverage of CO_{ads} is high, the distance between an active site on Pt where activated water can adsorb and a Pt site (active or inactive) where CO_{ads} had previously been adsorbed is small. However as the reaction proceeds, and the coverage of CO_{ads} decreases, the distance between $Pt(OH)_{ads}$ and $Pt(CO)_{ads}$ increases, and thus, diffusion of the adsorbed species becomes an important consideration. It is known that CO_{ads} can diffuse along the surface more easily than OH_{ads}.[96] Therefore, a third process in the electro-oxidation of CO_{ads}, which is particularly important at low CO_{ads} coverage, is the surface diffusion of CO_{ads} from its adsorption site to a site adjacent to adsorbed activated water

$$Pt^a(CO)_{ads} + Pt^b \rightleftharpoons Pt^a + Pt^b(CO)_{ads} \qquad (6.4)$$

Where $*_a$, $*_b$ are neighbouring sites on the Pt surface and can be either active or inactive.

Figure 6.1 shows the CO_{ads} stripping voltammogram for CO adsorbed onto polycrystalline bulk platinum. On the first sweep, it can be seen that the typical hydrogen desorption peaks (see Chapter Two, Figure 2.2) are suppressed. This is because the adsorption of CO_{ads} prevents the adsorption of hydrogen and/or displaces the PtH_{ads} already there. As the potential is swept anodically, a pronounced peak, I, begins at 0.39 V vs. SCE. This is the onset of CO_{ads} electro-oxidation. In this work, the onset of CO_{ads} electro-oxidation is determined to occur when the measured current first becomes more anodic than the current measured in the second cyclic voltammogram (assuming that all the CO_{ads} is removed during the first cycle). At 0.70 V vs. SCE, all of the CO_{ads} has been removed from the platinum surface and the measured current returns to that of a platinum cyclic voltammogram (compare the second cycle of Figure 6.1 to Figure 2.2 in Chapter Two).

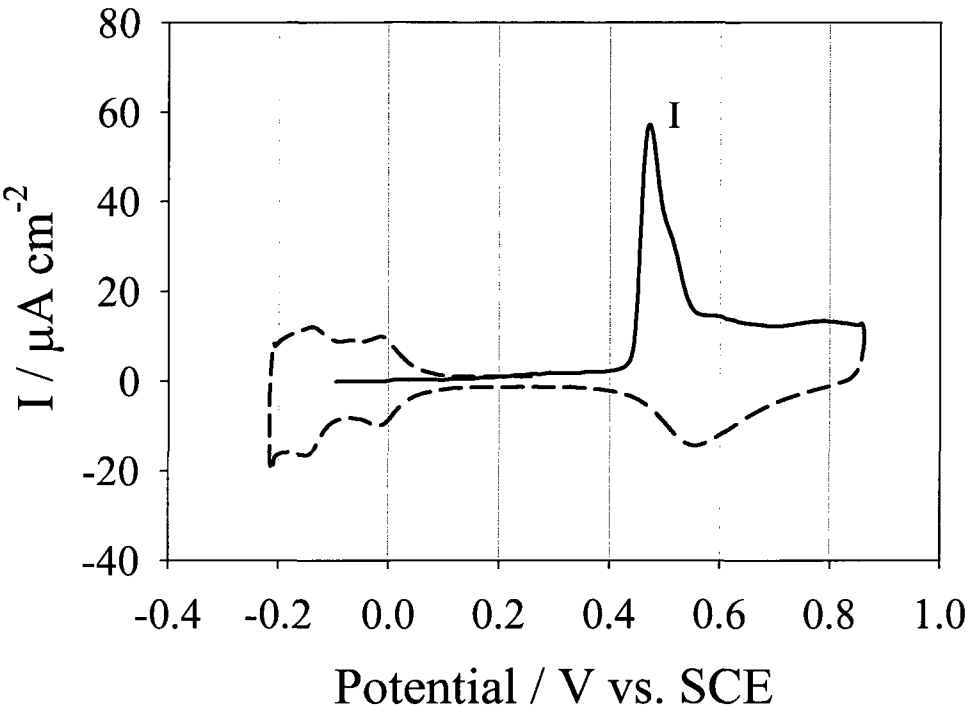

Figure 6.1 CO_{ads} stripping voltammograms for a polycrystalline bulk platinum foil electrode recorded at 10 mV s^{-1} in 0.5 M H_2SO_4 with the current normalized by the geometric surface area of the sample. First anodic sweep to electro-oxidized CO_{ads} (——), second sweep showing the typical CV for polycrystalline bulk platinum (– – –).

As with the adsorption or desorption of hydrogen in a cyclic voltammogram, the carbon monoxide electro-oxidation charge can be used to calculate the surface area of Pt covered by CO_{ads}. The charge associated with oxidizing a monolayer (100% coverage) of CO_{ads} is known to be 420 μC cm^{-2}.[97] This allows for the real surface area of platinum (covered by CO_{ads}) to be measured. For example, the CO_{ads} oxidation charge measured in Figure 6.1 using

$$Q = \int_0^t i dt \tag{6.5}$$

Q_{COads} = 138 μC, and therefore the platinum surface area covered by CO_{ads} is 138 μC/420 μC cm^{-2} = 0.33 cm^2. The Pt surface area calculated by the hydrogen adsorption

peak is 80 μC/210 μC cm^{-2} = 0.38 cm^2, indicating that the percent coverage by CO_{ads} is 0.33 cm^2/0.38 cm^2 × 100 % = 87 %.

Electrochemical oxidation of CO_{ads} is a kinetically controlled process, thus thermodynamic information cannot be obtained by the absolute position of the CO_{ads} electro-oxidation peak. Furthermore, it is not known with any certainty which step in the electrochemical oxidation of CO_{ads} is the rate determining step (RDS). That is to say, analysis of the stripping voltammogram will not reveal if it is the adsorption of activated water (Equation 6.2), the recombination reaction (Equation 6.3), or the surface diffusion of CO_{ads} (Equation 6.4) which is the RDS. However, qualitative kinetic information of the electro-oxidation of CO_{ads} can be obtained by comparing the stripping voltammograms of the prepared Pt/HOPG electrodes to one another and to polycrystalline foil.

6.4.2 Stripping Voltammetry of CO_{ads} onto Electrochemically Deposited Pt.

Typical CO_{ads} stripping voltammograms are shown in Figure 6.2 for Pt deposited electrochemically for 7.5 s onto freshly cleaved HOPG. A series of subsequent CO_{ads} stripping experiments carried out on the same sample is shown. Typical CO_{ads} stripping voltammograms are shown in Figure 6.3 for Pt electrodeposited for 2.5, 5, and 7.5 s on HOPG that was oxidized for 15 min. in 0.15 ppm O_3 at 300 °C. Figure 6.4 show an example of a CO_{ads} stripping voltammogram of Pt electrodeposited onto electrochemically oxidized HOPG. The variability in the electrochemically oxidized HOPG surface (see Chapter Four, Section 4.4.1), and the consequent irreproducibility of the electrochemical deposition process (see Chapter Four, Section 4.4.2), made it impractical to study the electro-oxidation characteristics of CO_{ads} on Pt/HOPG-E either as a function of substrate oxidation time or Pt electrodeposition time. Both the first and second sweeps are plotted in Figure 6.3 and Figure 6.4. The first sweep in a CO_{ads} stripping voltammogram experiment gives insight into the electrochemical activity of the catalyst towards oxidizing CO_{ads}. The second sweep, which is conducted to ensure that all of the CO_{ads} was oxidized in the first sweep, also generates an 'electrochemical spectrum' indicating the potentials at which electrochemical processes occur. Since Figure 6.2 show three successive stripping voltammograms, the second sweep is omitted for clarity. Average CO_{ads} peak width at half height and average CO_{ads} peak onset

potential for Pt/HOPG-FC, Pt/HOPG-O_3, and Pt/HOPG-E samples, are summarized in Table 6.1.

Comparison of Figure 6.2, Figure 6.3, and Figure 6.4 shows that the stripping characteristics for the Pt/HOPG electrodes prepared by electrochemical deposition are remarkably similar to one another despite the different pre-treatments of the HOPG substrate. This indicates that the substrate does not significantly influence the activity of the Pt/HOPG electrodes prepared by electrochemical deposition towards the electrochemical oxidation of CO_{ads}.

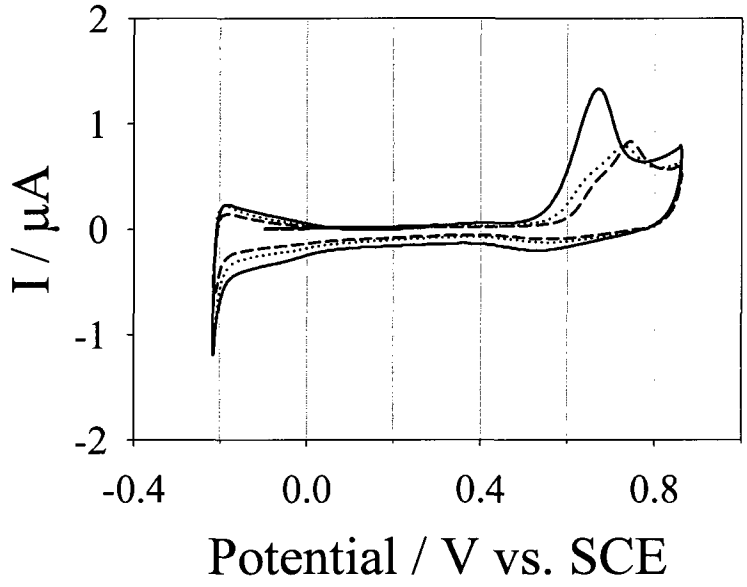

Figure 6.2 CO_{ads} stripping voltammograms recorded at 10 mV s^{-1} with the current normalized by the geometric surface area of the sample. Three CO_{ads} stripping voltammograms for the same Pt/HOPG electrode recorded successively are shown; (——) first, (.....) second, and (– – –) third CO_{ads} stripping CV. CO was adsorbed onto the Pt deposits before each stripping voltammogram. The Pt/HOPG electrode was prepared by depositing Pt for 7.5 s in 0.1 M H_2SO_4 + 1 mM $PtCl_4$ at – 0.475 V vs. MSE onto HOPG-FC.

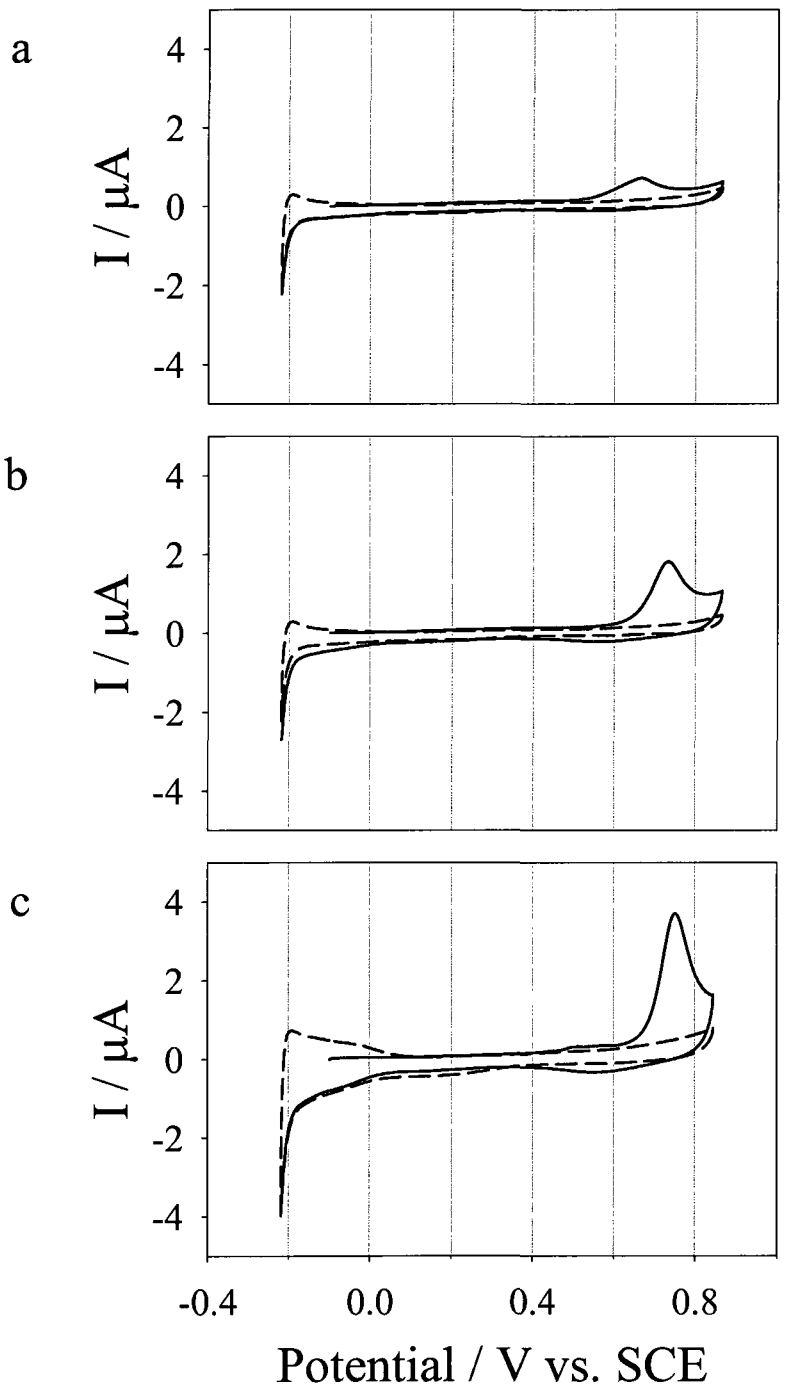

Figure 6.3 CO_{ads} stripping voltammograms recorded at 10 mV s^{-1} in 0.5 M H_2SO_4. Pt/HOPG electrodes are prepared by electrochemical deposition at – 0.475 V vs. MSE in 0.1 M H_2SO_4 + 1 mM $PtCl_4$ for a) 2.5, b) 5, and c) 7.5 s deposition onto HOPG-O_3. First sweep (_____) shows the electro-oxidation of CO_{ads}, second (_ _ _) sweep shows the back ground CV.

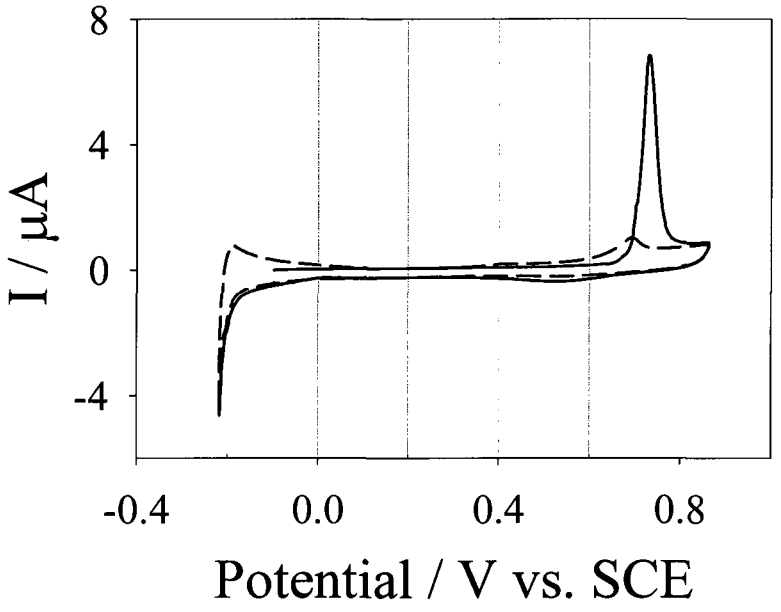

Figure 6.4 CO_{ads} stripping voltammograms recorded at 10 mV s^{-1} in 0.5 M H_2SO_4. Pt/HOPG electrodes are prepared by electrochemical deposition at – 0.475 V vs. MSE in 0.1 M H_2SO_4 + 1 mM $PtCl_4$ for 7.5 s deposition onto HOPG-E. First sweep (_____) shows the electro-oxidation of CO_{ads}, second (_ _ _) sweep shows the back ground CV.

Due to the highly reproducible nature of electrochemical deposition onto ozone oxidized HOPG, the catalytic activity of these electrodes were studied as a function of deposition time. From Figure 6.3 and Table 6.1 it is apparent that increasing the Pt loading, by increasing the deposition time, does not affect the onset potential or the peak width at half height in a systematic fashion. That is to say, although there are differences in the onset potential for the Pt/HOPG-O_3 electrodes prepared using different deposition times, increasing the deposition time does not cause the onset potential to either decrease or increase. Figure 6.3, however, nicely shows the effect of increasing the platinum loading on the measured stripping charge (obtained by integrating the current associated with the electro-oxidation of CO_{ads}): As the platinum loading increases, the surface area of platinum increases, and thus, the amount of CO_{ads} increases resulting in a larger stripping charge. Figure 6.3 clearly illustrates how the magnitude of the CO_{ads} oxidation, and hence the magnitude of the measured CO_{ads} stripping charge reflects the available surface area of the platinum catalysts. This fact is utilized in Chapter Seven to study the electrochemical

stability of the prepared Pt/HOPG electrodes. That is to say, by measuring changes in CO_{ads} stripping charge information regarding changes in the Pt catalyst surface area is determined.

Table 6.1 Summary of CO_{ads} oxidation characteristics of Pt deposited* onto freshly cleaved (Pt/HOPG-FC), ozone oxidized (HOPG-O_3), and electrochemically oxidized (HOPG-E) HOPG.

	Deposition time / s	CO_{ads}† peak onset potential / V	CO_{ads}† peak width at half height / V
Pt/HOPG-FC	7.5	0.55 ± 0.04	0.08 ± 0.02
Pt/HOPG-O_3	2.5	0.53 ± 0.03	0.12 ± 0.02
	5.	0.59 ± 0.06	0.06 ± 0.02
	7.5	0.57 ± 0.03	0.06 ± 0.01
Pt/HOPG-E	7.5	0.64 ± 0.01	0.04 ± 0.
Polycrystalline Pt Foil	n/a	0.39	0.06

* Pt was deposited at – 0.475 V vs. MSE in a 0.1 M H_2SO_4 + 1 mM $PtCl_4$ solution.

† The CO_{ads} stripping voltammograms were carried out at 10 mV s^{-1} in 0.5 M H_2SO_4. The potentials are reported vs. the SCE.

Characteristics of the CO_{ads} stripping voltammograms of Pt/HOPG prepared by electrochemical deposition (Figure 6.2, Figure 6.3, Figure 6.4) are listed in Table 6.1. From Figure 6.2, Figure 6.3, Figure 6.4, and Table 6.1 the notable characteristics of the CO_{ads} stripping voltammograms for Pt/HOPG electrodes prepared by electrochemical deposition can be summarized as: A) CO_{ads} electro-oxidation peak shape, i.e., a single CO_{ads} electro-oxidation peak is observed. (B) The CO_{ads} stripping charge decreases with successive CO_{ads} stripping voltammograms. (C) The characteristic $H_{ads/des}$ peaks are not as well resolved as in the case of polycrystalline Pt foil. (D) It is seen that the CO_{ads} stripping peaks are shifted to more positive potentials compared to polycrystalline platinum foil. (Each of these points will be discussed sequentially below).

A) CO_{ads} electro-oxidation peak shape.

Oxidation of CO_{ads} on Pt/HOPG electrodes prepared by electrochemical deposition was found to result in a single CO_{ads} oxidation peak, i.e., there was no pre-peak. The presence of

a small pre-peak is frequently observed when the platinum surface is saturated with CO at adsorption potentials below 0.3 V vs. RHE (as was done in this work).[98] The pre-peak corresponds to a small fraction of CO molecules which are more weakly bound to platinum compared to the remaining bound CO_{ads}.[98] Thus, the absence of a pre-peak indicates a more uniform CO_{ads} layer on the Pt/HOPG electrodes compared to Pt foil.

B) The CO_{ads} stripping charge decreases with successive CO_{ads} stripping voltammograms.

Figure 6.2 shows series of subsequent CO_{ads} stripping experiments carried out on the same Pt/HOPG-FC prepared by electrochemical deposition. It is seen (Figure 6.2a) that the CO_{ads} stripping charge, Q_{COads}, continually decreases with the number of stripping voltammograms carried out. The second CO_{ads} oxidation experiment (Figure 6.2a) indicates a 49 % decrease in Q_{COads} compared to the first experiment, and the third experiment shows a further decreases in Q_{COads} of 54 %. The Q_{COads} value is proportional to the surface area of the Pt catalyst. Therefore, the lower Q_{COads} values observed here indicate a decrease of Pt surface area with CO_{ads} stripping experiments, thus indicating that the platinum particles are not electrochemically stable. Effective Pt surface area can be lost due to dissolution (as a result of potential cycling), agglomeration, or Ostwald ripening. It is unlikely that agglomeration is the sole cause since it has been observed that aggregation causes a shift in the CO_{ads} oxidation onset potential to lower values[99] and this is not observed in the present study. All Pt/HOPG electrodes prepared by electrochemical deposition (onto either freshly cleaved or oxidized HOPG) lost stripping charge with successive stripping experiments. The electrochemical stability of these electrodes are discussed in detail in Chapter Seven.

C) The characteristic $H_{ads/des}$ peaks are not well resolved.

The typical $H_{ads/des}$ peaks, particularly the one associated with the more strongly bound hydrogen, are not clearly resolved on the Pt/HOPG samples. It is possible that impurities adsorbed onto the platinum particles are blocking adsorption and sequential desorption of hydrogen. However, XPS analysis did not indicate the presence of chloride or other impurities on the surface of Pt/HOPG samples. Nevertheless, methods to clean the Pt catalysts were tested. As discussed above, potential cycling (which is commonly used to clean platinum surfaces) cannot be employed for the Pt/HOPG samples as it results in excessive platinum dissolution, therefore alternative cleaning techniques were investigated. The Pt/HOPG samples were placed in a tube furnace and exposed to (1) cycling flows of H_2

and air at 130 °C, (2) reduction under H_2 at 250 °C, and (3) cycling flows of H_2 and air at 130 °C followed by reduction under H_2 at 250°C. Unfortunately, Pt was also lost during these procedures.

Suppression of $H_{ads/des}$ peaks on small platinum nanoparticles has been previously observed, i.e., the suppression of $H_{ads/des}$ peaks may not be linked to impurities.[99,100] Another reason for the suppression of the $H_{ads/des}$ peaks could be related to the ratio of surface atoms located in the {100} and {111} terraces to atoms occupying edge and corner sites of platinum nano-catalysts. As platinum nanoparticles decrease in size, the ratio of atoms in the {100} and {111} crystal planes to atoms at edge and corner sites also decreases.[101] The two hydrogen peaks of a typical polycrystalline platinum foil correspond to more strongly and less strongly adsorbed hydrogen which correspond to hydrogen adsorbing onto the {100} and {111} crystal planes, respectively.[102] Previous work has shown that the intensity of $H_{ads/des}$ peaks, particularly the one associated with the more strongly bound hydrogen, decreases with decreasing particle size and this decrease in intensity is associated with the decrease of the relative number of atoms located within the {100} and {111} crystal planes compared to atoms at edge and corner sites.[100] Thus, the suppression of $H_{ads/des}$ on Pt/HOPG samples, may relate to a surface structure different from the {100} and {111} structures.

D) Positive shift in the CO_{ads} electro-oxidation onset potential.

The CO_{ads} oxidation onset potentials of the Pt deposits formed in this study are shifted to more positive potentials compared to polycrystalline platinum foil.[99] The positive potential shift of the CO_{ads} oxidation peak suggests that it is more difficult to initiate the oxidation process on the Pt/HOPG electrodes than on polycrystalline platinum. Previous work has shown positive potential shifts of the CO_{ads} oxidation peak for annealed Pt surfaces compared to their respective 'pre-annealed' CO_{ads} oxidation potential.[103] It was found[104] that annealing the Pt surface significantly improved the domain size of the $p(2\times2)$–3CO structure, formed on Pt(111) at low potentials; i.e., annealing the Pt surface decreased the number of defect sites. It has been proposed that OH_{ads} formation (Equation 6.2) occurs at defect and step sites on the Pt crystal.[106,105] It therefore follows that the annealed surfaces from the previous study, with fewer irregularities, had positive shifts in the CO_{ads} oxidation peak since it was difficult for $Pt(OH)_{ads}$ to form on the platinum surface with fewer defects. It is possible that the observed positive shift in the CO_{ads} oxidation peak in this work could be at

least partially due to the difficulty in forming $Pt(OH)_{ads}$. Consequently, the positive shift in onset potential of the CO_{ads} oxidation peak for the electrodeposited Pt samples, compared to polycrystalline platinum foil, could be taken as an indication that the prepared deposits have a surface with fewer defects. However, it has been shown that Pt nano-catalysts generally have a comparatively defective surface, and thus, form $Pt(OH)_{ads}$ more easily than polycrystalline Pt foil. It may be that the catalyst prepared by electrochemical deposition onto HOPG can form $Pt(OH)_{ads}$ relatively easily but the overall kinetics of the electro-oxidation of CO_{ads} are slowed by either the recombination reaction (Equation 6.3) or the surface diffusion of CO_{ads} (Equation 6.4). In fact, it has been reported that the CO_{ads} oxidation kinetics decrease with decreasing particle size because the mobility of CO_{ads} on the Pt surface (Equation 6.4), as well as the recombination rate (Equation 6.3), decrease as the platinum particle size decreases.[106]

It should be noted that previous studies have reported that agglomeration of Pt nanoparticles shifts the CO_{ads} oxidation reaction to less anodic potentials compared to polycrystalline Pt foil.[99,107] It is believed that this results from the unusual physical properties of nanostructured materials that can occur during agglomeration.[108] The fact that the CO_{ads} oxidation reaction is shifted to more positive potentials compared to polycrystalline platinum foil, may indicate that the Pt catalysts prepared in this work behave, at least electrochemically, as individual nanoparticles, and not as agglomerates.

6.4.3 Stripping Voltammetry of CO_{ads} onto Electrochemically Deposited Pt using Long Deposition Times.

Analysis of the CO_{ads} stripping voltammograms presented in Figure 6.2, Figure 6.3, and Figure 6.4 is complicated by the concurrent decrease in Pt surface area; i.e., while the voltammograms are recorded, not only is CO_{ads} on the Pt deposits electrochemical oxidized, but there is also a substantial loss in Pt surface area (discussed in detail in Chapter Seven). Thus, from Figure 6.2, Figure 6.3, and Figure 6.4, it is an oversimplification to assign the positive shift in CO_{ads} oxidation onset to the surface specific kinetics of electro-oxidation of CO_{ads} (Equations 6.2 – 6.4) as it cannot be ascertained whether or not the loss of Pt is also causing a positive shift in the CO_{ads} oxidation onset. To determine what role Pt loss plays in causing the positive shift of the CO_{ads} oxidation peak onset of Pt/HOPG electrodes prepared

by electrochemical deposition using short times, electrodes were prepared using significantly longer deposition times, i.e., 100 and 900 s. The longer deposition times of 100 and 900 s were selected since these deposition times result in Pt/HOPG-O_3 electrodes for which Pt surface area losses have minimal effect. Ozone oxidized HOPG substrates were used as they facilitate reproducible electrochemical deposition.

SEM images of the Pt/HOPG electrodes are presented in Figure 6.5. Cyclic voltammograms of these electrodes were recorded and are shown in Figure 6.6. Additionally, the catalytic activity of these electrodes towards electrochemical oxidation of CO_{ads} was tested by stripping voltammetry. The overall stripping charge, $Q_{CO_{ads}}$, estimated for a particular sample, is used to normalize the y-axis, $i/Q_{CO_{ads}}$, in these voltammograms to allow for easy comparison of the data. Figure 6.7a and Figure 6.7b show three successive CO_{ads} stripping voltammograms for Pt/HOPG-O_3 electrodes prepared with 100 and 900 s of deposition time, respectively. Included for comparison in Figure 6.7 is the stripping voltammogram for CO_{ads} on polycrystalline Pt foil. CO_{ads} stripping characteristics, such as average CO_{ads} peak width at half height and average CO_{ads} peak onset potential, are summarized in Table 6.2.

From Figure 6.5, it is evident that even at long deposition times of 100 and 900s, platinum is deposited as large clusters, i.e. a Pt film has not formed. The average diameter of the deposits are 98 ± 35 and 148 ± 41 nm for the samples prepared using 100 and 900 s, respectively. Curiously, the Pt deposits are not significantly larger than the deposits formed using short, < 10 s, deposition times. However, there is a dramatic increase in Pt deposit density, observed for the long deposition times, > 10 s, as seen when comparing Figure 4.9 and Figure 6.5.

Analysis of the cyclic voltammograms recorded for the Pt/HOPG-O_3 electrodes, prepared by electrochemically depositing Pt for long times (Figure 6.6), gives insight into the nature of the deposited platinum. Both samples prepared by electrochemically depositing for long times have the characteristic $H_{ads/des}$ peaks as well as Pt oxidation and platinum oxide reduction peaks compared to that of polycrystalline Pt foil.

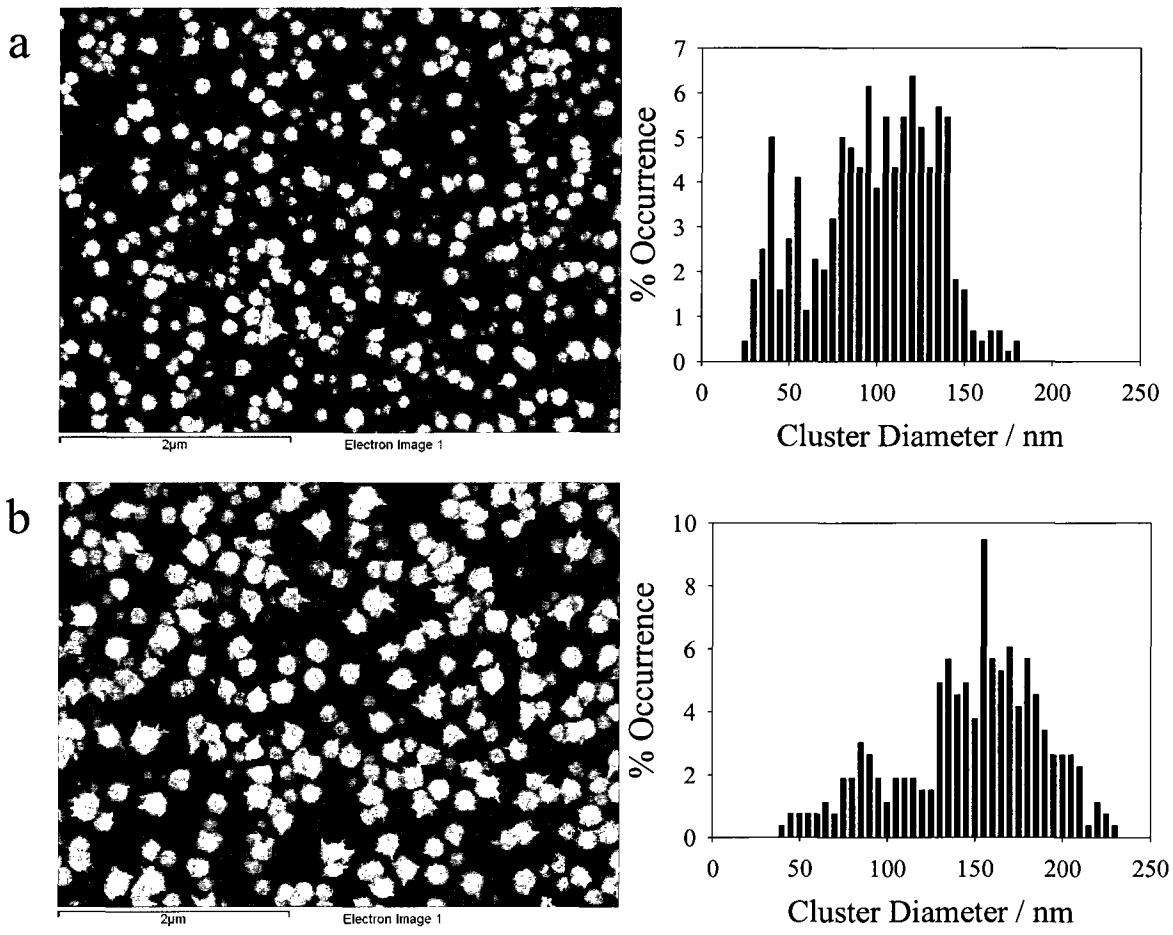

Figure 6.5 Scanning electron images of Pt electrochemically deposited onto ozone oxidized HOPG for a) 100 s and b) 900 s. Reduction occurred at – 0.475 V vs. MSE in 1 mM $PtCl_4$ + 0.1 M H_2SO_4. HOPG was oxidized in 0.15 ppm O_3 for 15 min. at 300 °C. Magnification of SEM images is 25000 times.

Examination of Figure 6.7a, and Figure 6.7b, shows that the measured current changes very little for the three successive experiments. Note that after one CO_{ads} stripping experiment (which comprises three cyclic voltammograms), analysis of CO_{ads} stripping charges indicates that 1 and 4 % of the charge is lost for the samples prepared by electrochemical deposition times of 100 and 900 s, respectively. However, the precision of measuring stripping charge was found to be 5 % for polycrystalline Pt foil, thus changes of less than 5 % are not significant. What is important to note is that although the observed decrease in CO_{ads} stripping charge for the Pt/HOPG-O_3 electrodes prepared by 100 and 900 s of deposition time are similar in magnitude, the CO_{ads} stripping characteristics for these two

samples are very different, as illustrated in Figure 6.7a and Figure 6.7b. This suggests that the observed CO_{ads} oxidation characteristics, specifically the oxidation onset potential, for the Pt/HOPG-O_3 electrodes prepared by depositing Pt for 100 and 900 s are not dominated by Pt loss, but, more likely differences in the Pt structure. It is shown in Figure 6.7 and Table 6.2 that the CO_{ads} oxidation onset for the sample prepared by electrochemically depositing Pt for 100 s is shifted to more positive potentials than polycrystalline Pt foil, while the sample prepared by electrochemically depositing Pt for 900 s is shifted to more negative potentials than polycrystalline Pt foil. Thus, the results in Figure 6.7 suggest that Pt loss is not causing the positive shift in the onset potential for CO_{ads} oxidation.

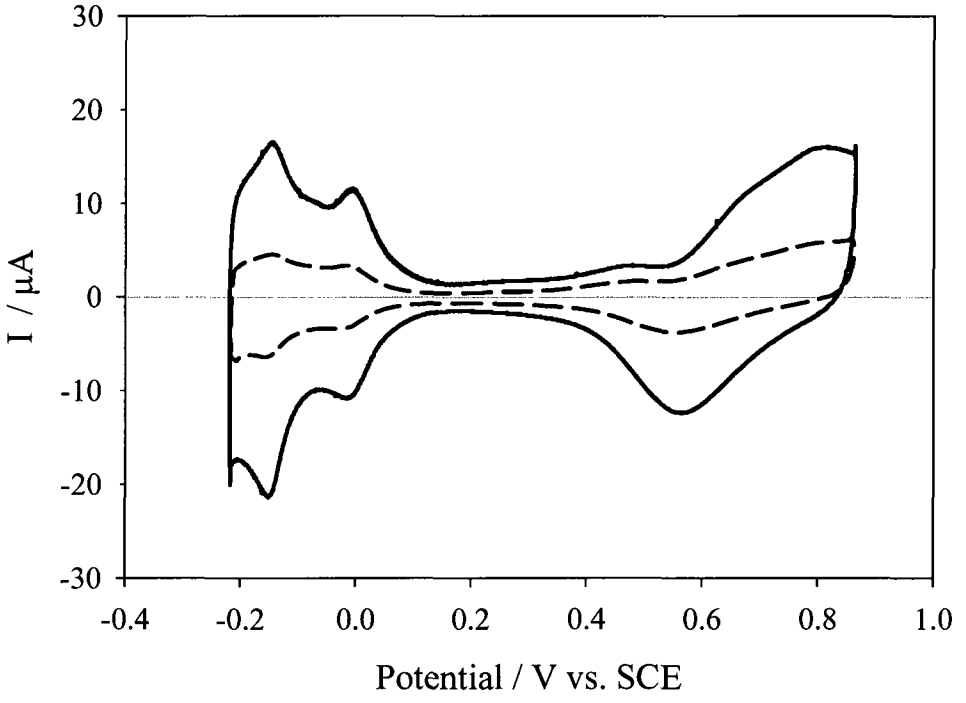

Figure 6.6 Cyclic voltammograms recorded at 10 mV s^{-1} in 0.5 M H_2SO_4. _ _ _ 100 and ——— 900 s at – 0.475 V vs. MSE onto O_3 oxidized HOPG (15 min., 300 °C, 0.15 ppm O_3) in 0.1 M H_2SO_4 + 1 mM $PtCl_4$. The positive potential limit is set to 0.86 V so that a monolayer of $Pt(OH)_{ads}$ is formed for polycrystalline Pt foil.

It is interesting to note that while there is no trend in the CO_{ads} electro-oxidation onset potential of Pt/HOPG electrodes when comparing short times, i.e. 2.5, 5., 7.5 s (see Table 6.1), when comparing the onset potentials of Pt/HOPG electrodes prepared at short

deposition times, i.e. < 10 s, to 100s, and finally to 900 s there is an overall trend that the onset potential becomes less anodic for the longer the deposition time. While Pt/HOPG electrodes prepared using short deposition times and 100 s deposition time show slower kinetics compared to polycrystalline Pt foil, the kinetics of CO_{ads} electro-oxidation of the Pt/HOPG electrodes prepared with 900 s of deposition time has faster kinetics compared to polycrystalline foil. Unfortunately, stripping voltammetry does not provide information to determine with any certainty which step in the electrochemical oxidation of CO_{ads} is the rate determining step (RDS). That is to say, it is not known if the adsorption of activated water (Equation 6.2), the recombination reaction (Equation 6.3), or the surface diffusion of CO_{ads} (Equation 6.4) is the RDS. Thus, we cannot say if there is a shift of the rate determining step (RDS) from one reaction to another, or if the RDS remains the same but the kinetics of the RDS increase.

Table 6.2 Summary of CO_{ads} oxidation characteristics of Pt deposited* for long times onto O_3 oxidized (Pt/HOPG-O_3) HOPG.

	Deposition time / s	CO_{ads}† peak onset potential / V	CO_{ads}† peak width at half height / V
Pt/HOPG-O_3	100	0.47 ± 0.01	0.03 ± 0.
	900	0.33 ± 0.02	0.06 ± 0.
Polycrystalline Pt Foil	n/a	0.39	0.06

* Pt was deposited at – 0.475 V vs. MSE in 0.1 M H_2SO_4 + 1 mM $PtCl_4$ solution.

† The CO_{ads} stripping voltammograms were carried out at 10 mV s^{-1} in 0.5 M H_2SO_4. The potentials are reported vs. the SCE.

Electrochemical deposition of Pt onto HOPG is a versatile deposition technique. Chapter Four showed how modifications to the HOPG surface can modify the electrode morphology, even making the deposition process much more reproducible. This sections has shown that the catalytic activity of the Pt/HOPG electrode towards the electrochemical oxidation of CO_{ads} can be improved by controlling the deposit size which is easily controlled by the deposition time.

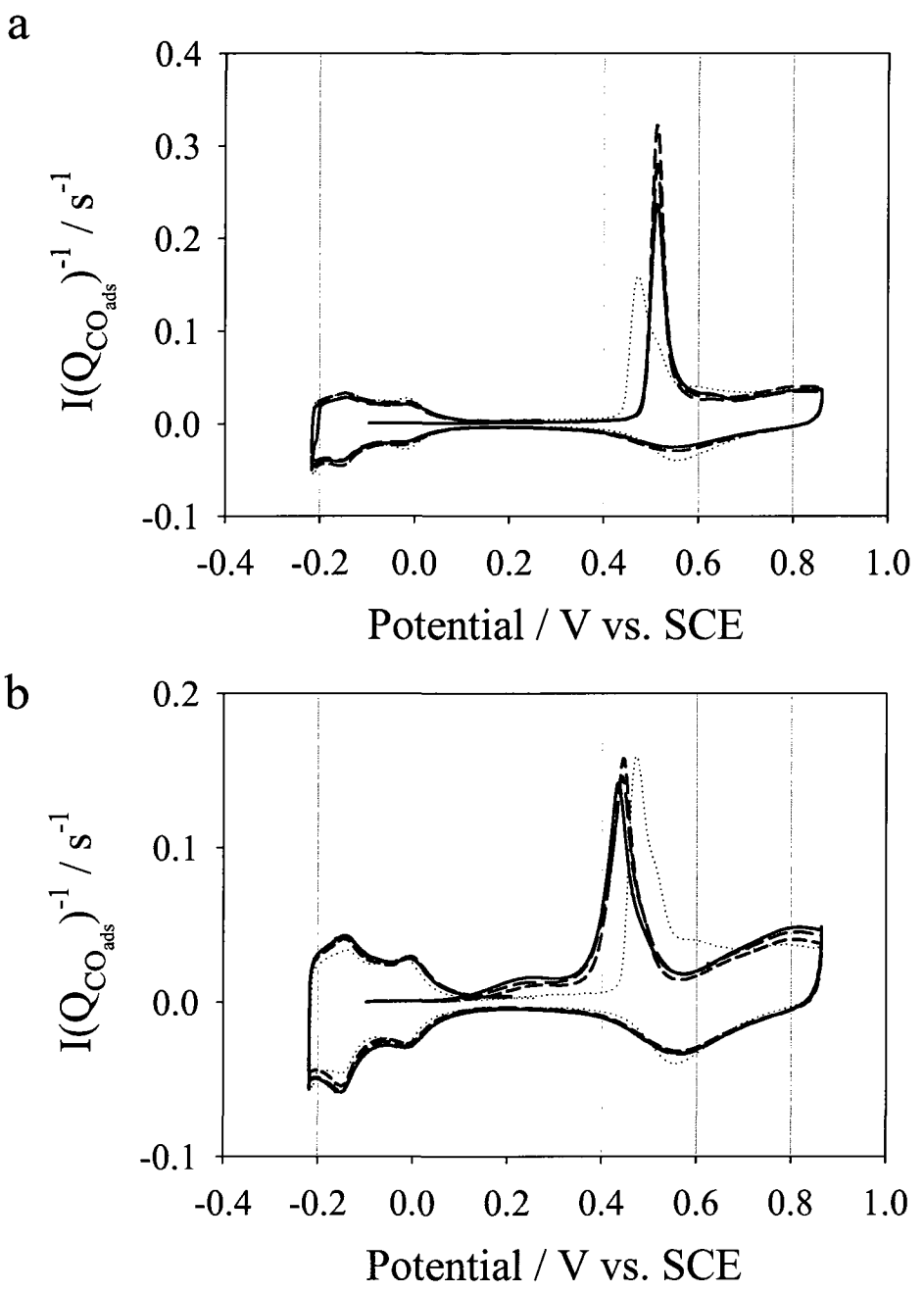

Figure 6.7 CO_{ads} stripping voltammograms recorded at 10 mV s^{-1} in 0.5 M H_2SO_4. a) 100 b) 900 s at – 0.475 V vs. MSE deposition onto O_3 oxidized HOPG (15 min., 300 °C, 0.15 ppm O_3) in 0.1 M H_2SO_4 + 1 mM $PtCl_4$. First (_____), second (_ _ _), and third (_ _ _ _ _) CO_{ads} stripping voltammograms. The CO_{ads} stripping CV for polycrystalline platinum foil is included for comparison. ..... The positive potential limit is set to 0.86 V so that a monolayer of $Pt(OH)_{ads}$ is formed for polycrystalline Pt foil.

6.4.4 Stripping Voltammetry of CO_{ads} onto Impregnated and Thermally Decomposed Pt.

Figure 6.8 shows the stripping voltammograms for Pt/HOPG electrodes prepared by impregnation followed by thermal decomposition onto a) freshly cleaved, b) ozone oxidized, and c) electrochemically oxidized HOPG. The overall stripping charge, $Q_{CO_{ads}}$, estimated for a particular sample, is used to normalize the y-axis, $i/Q_{CO_{ads}}$, in these voltammograms to allow for easy comparison of the data. As with the stripping voltammetry data for Pt/HOPG electrodes prepared by electrochemical deposition, both the first and second sweeps are plotted (see Figure 6.8). The first sweep in a CO_{ads} stripping voltammogram experiment gives insight into the electrochemical activity of the catalyst towards oxidizing CO_{ads}. The second sweep, which is conducted to ensure that all of the CO_{ads} was oxidized in the first sweep, also generates an 'electrochemical spectrum' indicating the potentials at which electrochemical processes occur.

When considering the data presented in Figure 6.8, a number of generalizations can be made. In particular, the oxidation characteristics for the three samples made by impregnation and thermal decomposition, Figure 6.8a-c, are remarkably similar to one another despite the different pre-treatments of the HOPG substrates and notably different from the oxidation characteristics corresponding to the electrochemically deposited Pt catalysts (see Figure 6.2, Figure 6.3, and Figure 6.4). The observed differences between the two methods of Pt nano-catalyst preparation and the observed similarities for a particular preparation method on differently pre-treated HOPG indicates that substrate pre-treatment does not play a significant role in defining the electro-catalytic behaviour of the platinum nano-catalysts towards electrochemically oxidizing CO_{ads}; rather, the method of nano-catalyst preparation appears to be important. It should be emphasized that the differences in CO_{ads} stripping characteristics between Pt catalysts prepared by electrochemical deposition vs. impregnation followed by thermal decomposition are not due to differences in platinum loading. The CO_{ads} stripping charge for the Pt/HOPG electrodes prepared by impregnation and thermal decomposition are of the same order of magnitude as the CO_{ads} stripping charges measured for the Pt/HOPG electrodes prepared by electrochemical deposition.

The main points of difference in the CO_{ads} oxidation characteristics for the two preparation methods can be summarized as; (A) the hydrogen adsorption/desorption, $H_{ads/des}$,

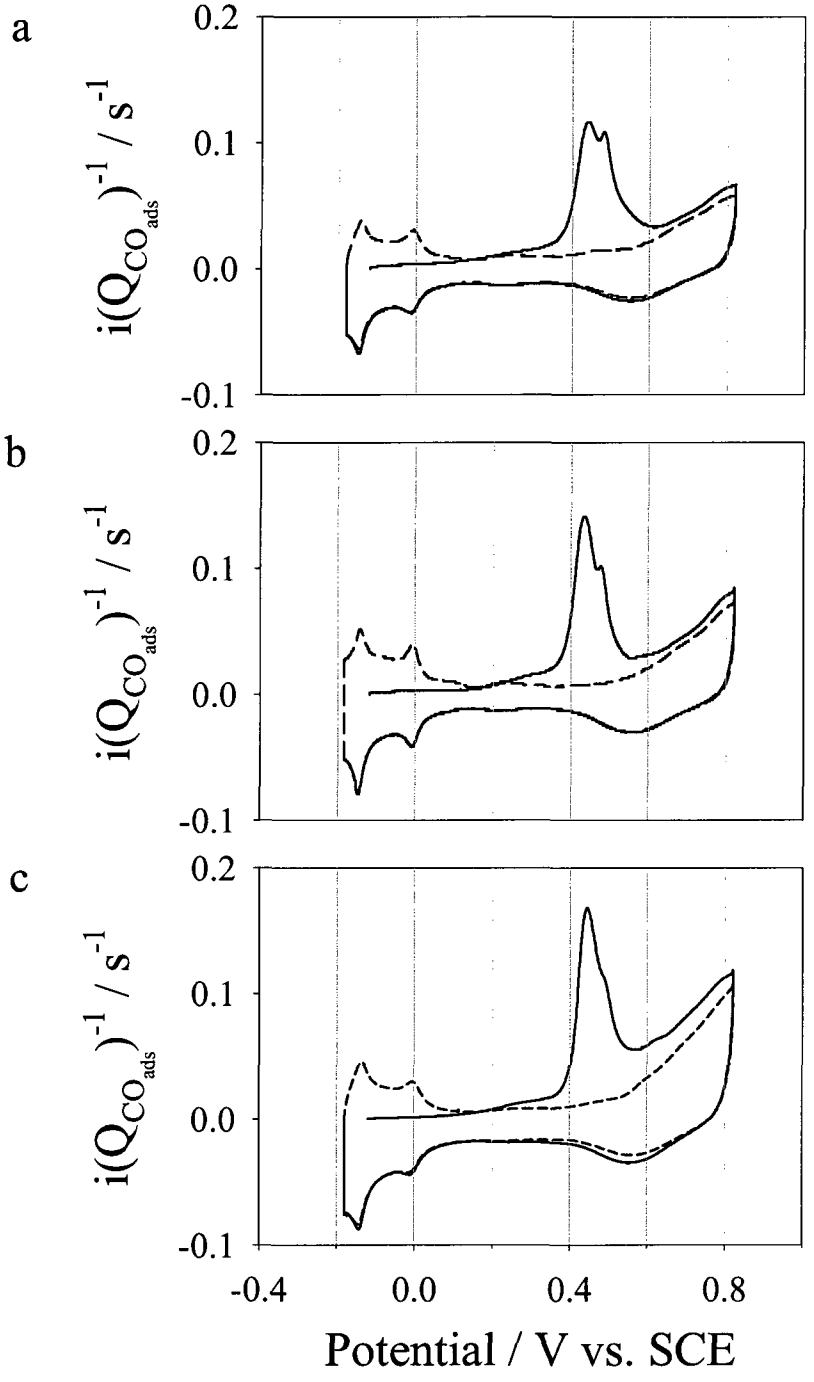

Figure 6.8 CO_{ads} stripping voltammograms recorded at 10 mV s^{-1} in 0.5 M H_2SO_4 for Pt precursor salts (250 µL of 2.6×10^{-4} M H_2PtCl_4 + 6.4 $\times 10^{-4}$ M HCl) decomposed thermally onto a) HOPG-fc and b) HOPG-O_3 ; and c) (250 µL of 2.6×10^{-5} M H_2PtCl_4 + 6.5 $\times 10^{-5}$ M HCl) thermally decomposed onto HOPG-E. First sweep (_____) shows the electro-oxidation of CO_{ads}, second (_ _ _) sweep shows the back ground CV.

peaks for the thermally decomposed Pt/HOPG samples are clearly resolved while they are not for the electrochemically deposited Pt clusters prepared at short times, < 10 s; (B) the CO_{ads} oxidation onset is shifted to less anodic potentials for the thermally decomposed Pt nano-catalysts compared to the electrochemically deposited Pt clusters prepared at short times, < 10 s, and to polycrystalline platinum foil; C) CO_{ads} electro-oxidation for Pt/HOPG electrodes prepared by impregnation followed by thermal decomposition show either two peaks or a single peak with a distinct shoulder. In the following, each point of difference will be discussed sequentially.

A) $H_{ads/des}$ peaks in the second sweep of the stripping voltammogram.

$H_{ads/des}$ peaks are not clearly resolved on Pt nano-catalysts prepared by electrochemical deposition onto freshly cleaved and oxidized HOPG while they are for Pt/HOPG electrodes prepared by impregnation followed by thermal decomposition. Assuming impurities are not the cause of the $H_{ads/des}$ suppression, it is likely that the nano-catalysts prepared by electrochemical deposition at short times, < 10 s, under the conditions presented in Chapters Three and Four do not adsorb hydrogen at two distinctly different sites (with two distinct adsorption energies) as observed on polycrystalline Pt foil. Pt nano-catalysts prepared by impregnation and thermal decomposition show well defined $H_{ads/des}$ peaks typical of polycrystalline platinum. This indicates that impregnation and thermal decomposition results in the formation of Pt with two distinct H_{ads} sites similar to polycrystalline Pt foil.

B) CO_{ads} oxidation onset potential.

The onset of the CO_{ads} oxidation reaction on Pt nano-catalysts prepared by impregnation and thermal decomposition (Figure 6.8a-c) occurs at less anodic potentials compared to the onset for the CO_{ads} oxidation on Pt nano-catalysts prepared by electrochemical deposition at short times (< 10 s) (Figure 6.2, Figure 6.3, and Figure 6.4) or for polycrystalline platinum foil (Figure 6.1), see Table 6.2 and Table 6.3 for comparison. The negative potential shift indicates that the CO_{ads} oxidation reaction initiates more easily on the Pt nano-catalysts prepared by impregnation and thermal decomposition than on polycrystalline Pt foil or electrochemically deposited Pt clusters.

The fact that $Pt(OH)_{ads}$ formation occurs at defect and edge sites on the Pt crystals,[106,105] combined with the high resolution TEM results (Chapter Five, Figure 5.2) that indicate that the thermally decomposed particles are irregular in shape and not faceted (i.e. highly

defective), strongly suggest that the adsorption of activated water is facile on these electrodes, and therefore, this reaction may not be the rate determining step (RDS) for electro-oxidation of CO_{ads} on Pt catalysts prepared in by thermal decomposition. However, this is purely speculative and cannot be said with certainty. Moreover, even if the adsorption of activated water is not the RDS for the electro-oxidation of CO_{ads} on thermally decomposed catalysts, the fact that the onset potential is shifted to more anodic potentials for Pt/HOPG electrodes prepared by electrochemical deposition does not indicate that the adsorption of activated water is the RDS for these electrodes. For example, it is possible that $Pt(OH)_{ads}$ forms at less anodic potentials than the onset potential for Pt/HOPG electrodes prepared by electrochemical deposition, yet the recombination reaction or the surface diffusion of CO_{ads} is slow enough that one of these reactions are the RDS.

Table 6.3 Summary of CO_{ads} oxidation characteristics, taken from Figure 6.8, of Pt thermally decomposed onto freshly cleaved (Pt/HOPG-FC), ozone oxidized (Pt/HOPG-O_3), and electrochemically oxidized (Pt/HOPG-E).

	CO_{ads} oxidation pre-peak onset / V vs. SCE	CO_{ads} oxidation main peak onset / V vs. SCE
Pt/HOPG-FC	0.12	0.29
Pt/HOPG-O_3	0.12	0.31
Pt/HOPG-E	0.12	0.31
Polycrystalline Pt foil	0.	0.39

Close analysis of Figure 6.8 indicates that the CO_{ads} oxidation onset occurs at approximately 0.12 V vs. SCE for the Pt/HOPG electrodes prepared by impregnation and thermal decomposition. Analysis of the second cyclic voltammogram for these electrodes indicates that a reversible surface reaction is also initiated at 0.12 V vs. SCE. This reversible reaction maximizes at approximately 0.22 V vs. SCE for all Pt/HOPG electrodes prepared by impregnation and thermal reduction in this work. The exact nature this redox-reaction is unknown, however the potential at which it occurs, combined with its reversible nature, indicates that it may be a quinone/hydroquinone-type reaction.[109] It is interesting that only the Pt/HOPG electrodes prepared by impregnation and thermal decomposition have this

quinone/hydroquinone reaction. The formation of a quinone-group on HOPG results from HOPG oxidation. As it is well known that platinum will catalyze the oxidation on HOPG,[92,93,94] one can conclude that Pt which is thermally decomposed onto HOPG oxidizes the HOPG substrate more easily than if the Pt is electrochemically deposited onto the substrate. Thus, the formation of a quinone-group on Pt/HOPG electrodes prepared by impregnation and thermal decomposition indicates that there is a stronger interaction between the thermally decomposed Pt nano-catalysts and the HOPG substrate compared to the electrochemically deposited Pt clusters and HOPG.

To test if the presence of quinone-groups on the HOPG substrate would help to initiate the oxidation of CO_{ads} on Pt, hydroquinone was added to Pt/HOPG electrodes prepared by electrochemical deposition. This was achieved by two different methods. In the first method, Pt was deposited onto freshly cleaved HOPG by applying a 5 s deposition pulse at – 0.475 V vs. MSE in a solution of 1 mM $PtCl_4$ + 0.1M H_2SO_4; subsequently a 150 µL aliquot of 1 mM hydroquinone in H_2O was deposited onto the Pt/HOPG substrate and allowed to dry. The second method was simply a reversal of the first, i.e., a 150 µL aliquot of the 1 mM hydroquinone solution was placed onto freshly cleaved HOPG and, once the solution had dried, a 5 s deposition pulse at – 0.475 V vs. MSE in a solution of 1 mM $PtCl_4$ + 0.1M H_2SO_4 was applied. CO was then adsorbed onto both samples and electrochemically oxidized in the usual fashion. The presence of hydroquinone did not have an apparent effect on the electrochemical activity of the Pt nano-catalysts prepared in these manners towards oxidizing CO_{ads}, and thus it is unlikely that the formation of a quinone/hydroquinone-type group on Pt/HOPG electrodes prepared by impregnation and thermal decomposition helps to initiate the electrochemical oxidation of CO_{ads}.

C) CO_{ads} electro-oxidation peak shape.

As mentioned previously, the CO_{ads} stripping voltammograms for Pt nano-catalysts prepared by impregnation and thermal decomposition (Figure 6.8) clearly shows a shoulder on the positive potential side of the oxidation peak. The occurrence of two oxidation peaks, or a single peak with a pronounced shoulder, has been reported in the literature and a variety of explanations have been proposed. For example, it was found that Pt/carbon electrodes that contained a mixture of nano-catalysts and agglomerates of nano-catalysts show two CO_{ads} oxidation peaks. Agglomerated nano-catalysts are expected to show a CO_{ads} oxidation

peak at lower overpotentials compared to non-agglomerated particles.[99] However, this is not a possible explanation as TEM analysis did not reveal particle agglomeration on samples prepared by impregnation and thermal decomposition. Moreover, Pt/HOPG electrodes prepared by electrochemical deposition show a single CO_{ads} oxidation peak on the first CO_{ads} stripping voltammogram, despite the fact that TEM analysis clearly showed Pt particle agglomeration (see Chapters Three and Four).

Another study found a single CO_{ads} oxidation peak for Pt samples prepared by impregnation on chemically oxidized Vulcan support whereas two distinct CO_{ads} oxidation peaks were observed for samples prepared in the same fashion on untreated Vulcan support.[110] It was suggested that oxidizing the carbon support homogenized the carbon surface which in turn homogenized the nature of the deposited platinum. Although that explanation appears appropriate for that work, it is not a possible explanation for this work as CO_{ads} characteristics are the same regardless of the HOPG oxidation pretreatment.

It has been suggested that multiple CO_{ads} oxidation peaks represent different groups of particle sizes and CO_{ads} oxidation peaks have been deconvoluted into multiple peaks that may represent groups of different particle sizes.[15] It is likely that Pt nano-catalysts of different sizes have different CO_{ads} oxidation characteristics. However, these differences can be described more directly by considering changes in terrace and edge sites or changes in crystal faces that correspond to changes in particle size.[101] For example, CO bonds more strongly onto edges sites than to terrace sites. It has therefore been suggested that CO_{ads} oxidation peaks that are found at higher overpotentials correspond to CO_{ads} on edge sites while CO_{ads} oxidation peaks found at lower overpotentials correspond CO_{ads} on terrace sites.[111]

Single crystal studies have shown that the main CO_{ads} electro-oxidation peak differs for different single crystal planes; i.e., the peak maximum position becomes more anodic in the order Pt(110) < Pt(111) << Pt(100).[112,113] Polycrystalline Pt electrodes are found to show two CO_{ads} oxidation peaks. Studies performed at the same experimental conditions, i.e., the same supporting electrolyte and the same sweep rate, have shown that the CO_{ads} oxidation peak found at less anodic potentials for polycrystalline Pt occurs at approximately the same potential as the CO_{ads} oxidation peaks for single crystals Pt(110) and Pt(111). Also, it appears that the more anodic CO_{ads} oxidation peak for polycrystalline Pt corresponds to the

CO_{ads} oxidation peak for the single crystal Pt(100). It is tempting to assign the two CO_{ads} oxidation peaks observed for thermally decomposed Pt as representing CO_{ads} on the different single crystals, especially when considering the strong $H_{ads/des}$ peaks that indicate a highly crystalline Pt deposit. However, neither the position of the first or second CO_{ads} oxidation peak observed for thermally decomposed Pt lie at the same potential as the doublet observed for polycrystalline platinum foil measured at the same experimental conditions, thus, one cannot conclude that the crystallinity of the thermally decomposed Pt is the same as the crystallinity of the different crystal faces in the polycrystalline platinum foil measured in this work.

Despite the discrepancy between the onset of the CO_{ads} oxidation peak for thermally decomposed Pt and polycrystalline Pt foil, the CO_{ads} oxidation peak at less anodic potentials may still represent oxidation of CO_{ads} on Pt(110) and Pt(111) crystal faces and the oxidation peak at more anodic potentials may represent the oxidation of CO_{ads} on Pt(100), i.e. thermally decomposed deposits may be composed of these three low index crystal planes. The fact that the onset for the oxidation of CO_{ads} on thermally decomposed Pt deposits occurs at less anodic potentials may simply indicate that the thermally decomposed deposits are sufficiently altered to allow for faster overall kinetics. For example, they may be rougher and have more defects than polycrystalline platinum and therefore form $Pt(OH)_{ads}$ more easily than polycrystalline platinum, (this is supported by the HRTEM images presented in Chapter Five; see e.g. Figure 5.2). Other possibilities are that the surface may allow for faster CO_{ads} surface diffusion, or the surface structure may favor the recombination reaction.

6.5 CONCLUSIONS

The activity of six different types of Pt/HOPG electrodes towards the electrochemical oxidation of CO_{ads} was tested. It was found that the methods of substrate pre-treatment studied in this work (freshly cleaved, ozone oxidized, or electrochemically oxidized) did not affect the activity of the electrodes to the electro-oxidation of CO_{ads}. In general it was found that Pt/HOPG electrodes prepared by electrochemical deposition using short deposition times (< 10 s) were less active, i.e. they showed slower kinetics, than polycrystalline Pt foil or electrodes prepared by impregnation followed by thermal decomposition.

The onset potential for the electro-oxidation of CO_{ads} was shifted to more anodic potentials for electrodes prepared by electrochemical deposition using short deposition times. The slower kinetics may have resulted from the slow adsorption of activated water, $Pt(OH)_{ads}$, the slow surface diffusion of CO_{ads}, or the slow recombination reaction of $Pt(OH)_{ads}$ with $Pt(CO)_{ads}$. Unfortunately stripping voltammetry does not provide sufficient information to determine which step is the rate determining step. The typical $H_{ads/des}$ peaks normally found on polycrystalline Pt foil were present, but not as well resolved on the Pt/HOPG electrodes prepared by electrochemical deposition. This may result from the presence of impurities, or it may reflect the surface structure of the catalysts indicating that two different H_{ads} sites with distinct adsorption energies are not present on the Pt deposits prepared by electrochemical deposition.

Complicating the analysis of this reaction is the fact that during the stripping voltammetry experiment Pt is lost from the electrode surface. To determine if the loss of Pt is the cause of the positive shift in the onset potential, Pt/HOPG electrodes were prepared by electrochemical deposition using long deposition times, i.e. 100 and 900 s. Neither of these electrodes showed significant loss of Pt, thus their kinetics towards the electro-oxidation of CO_{ads} is not complicated by the simultaneous loss of Pt. The Pt/HOPG electrodes prepared using short deposition times, < 10 s, and the electrodes prepared using 100 s of deposition time also showed slower kinetics than polycrystalline foil. Thus, the slow kinetics results from the unique surface structure of the Pt deposits, and not the loss of Pt from the electrode. Interestingly, the $H_{ads/des}$ peaks for both electrodes prepared using long deposition times were well resolved as they are on polycrystalline Pt foil. This indicates that the cause of the unique $H_{ads/des}$ observed Pt/HOPG electrodes using short deposition times does not directly affect the CO_{ads} oxidation kinetics.

A trend of improving CO_{ads} oxidation kinetics was observed when comparing the Pt/HOPG electrodes prepared at short times, < 10 s, to the electrode prepared using 100 s, to the electrode prepared with 900 s of deposition time. In fact, the Pt/HOPG electrode prepared with 900 s of deposition time had faster kinetics towards the electro-oxidation of CO_{ads} than polycrystalline Pt foil. This result illustrates the versatile nature of electrochemical deposition as a method to prepared electrodes; by varying a parameter as

simple as deposition time, catalysts of varying activity towards the electro-oxidation of CO_{ads} can be prepared.

The electrodes prepared by impregnation followed by thermal decomposition showed improved kinetics towards the electro-oxidation of CO_{ads} compared to the electrodes prepared by electrochemical deposition using short deposition times, < 10 s. This was demonstrated by the shift of the electro-oxidation onset to less anodic potentials. The cathodic shift did not appear to be caused by quinone groups found on these electrodes. From the stripping voltammogram it appears that the Pt deposits on the Pt/HOPG electrodes prepared by impregnation followed by thermal decomposition are polycrystalline. For example, the oxidation peak show a peak doublet (or shoulder) typical of polycrystalline foil and the second sweep of the stripping voltammograms show the typical $H_{ads/des}$ and Pt oxidation reduction peaks of polycrystalline Pt foil.

Chapter Seven

Stabilization of Platinum Nano-Catalysts on HOPG

7.1 ABSTRACT

The short-term electrochemical stability of Pt/HOPG electrodes prepared by electrochemical deposition or impregnation followed by thermal decomposition onto freshly cleaved, ozone oxidized, or electrochemically oxidized HOPG was tested. The stability was determined by comparing the loss in CO_{ads} stripping charge measured with successive CO_{ads} stripping voltammograms. For a given substrate, Pt/HOPG electrodes prepared by impregnation followed by thermal decomposition proved to be more electrochemically stable than Pt/HOPG electrodes prepared by electrochemical deposition. For both methods of deposition, oxidizing HOPG electrochemically stabilized the particles in comparison to freshly cleaved HOPG; ozone oxidation was the superior substrate pre-treatment method stabilizing the electrodes to the greatest extent. The Pt/HOPG electrode which showed the least amount of CO_{ads} stripping charge loss, i.e. the electrode which was the most electrochemically stable, was prepared by impregnation followed by thermal decomposition onto ozone oxidized HOPG. The chemical interaction between the Pt catalyst and the carbon substrate was determined by XPS analysis. It was found that Pt 4f spectra of all six of the Pt/HOPG electrodes were shifted to higher binding energies indicating that Pt was interacting with the HOPG defects possibly forming platinum-carbon bonds. For a given support, the Pt/HOPG electrodes prepared by impregnation followed by thermal decomposition showed a greater interaction between the Pt and the carbon support compared to Pt/HOPG electrodes prepared by electrochemical deposition. Of the six electrodes, the Pt/HOPG electrode prepared by impregnation followed by thermal decomposition onto ozone oxidation showed the greatest interaction between Pt and the carbon support. The XPS results indicate that the electrochemical stability is positively influenced by the interaction between the catalyst and the carbon support.

7.2 INTRODUCTION

When studying the electrochemical activity of a catalyst, it is imperative that the catalyst does not change during the testing process. For example, if spectroscopic analysis performed before catalytic activity testing, such as transmission electron microscopy (TEM), indicates that the catalyst particles are of a particular size, and then the catalyst's activity towards a

particular reaction is tested, it is premature to then conclude that the catalyst's activity can be associated with the measured pre-test size. A more thorough analysis requires that the particle size be measured again after the catalytic activity testing. This is important because if the catalyst changes size during the testing procedure, then one cannot say whether it is the initial size, the final size, or some in-between size which is responsible for the measured activity. The same logic can be applied to a number of catalyst characteristics such as crystal structure, dispersion, and loading. There are many processes that can occur when a catalyst is in solution that may result in changes in the morphology of the catalyst. The three main processes are Ostwald ripening, dissolution, and agglomeration. While some of these mechanisms can be minimized or eliminated, some (as discussed in the following) are unfortunate and unavoidable consequences of electrochemical systems.

Ostwald ripening, in general terms, is the growth of larger particles at the expense of smaller particles. It is a thermodynamically driven process which lowers the overall energy of the catalyst system. Ostwald ripening has been highlighted as a probable cause of Pt loss in polymer electrolyte membrane fuel cells.[114,115,116] With the use of *in situ* electrochemical scanning tunnelling microscopy (in situ STM), Ostwald ripening can be imaged in real time. In situ STM analysis revealed that Ostwald ripening of Pt islands on a Pt film occurs while holding the electrode at potentials in the double layer region.[117] Atomic resolution *in situ* STM analysis indicated that the islands which grew during Ostwald ripening were predominantly of the Pt(111) crystal structure.[117] This indicates that Ostwald ripening can alter the surface crystal structure in addition to changing Pt island size. Other work by the same group indicated that Ostwald ripening of Pt islands was limited to the double layer region.[118] It was postulated that hydrogen adsorption prevented the release of surface Pt atoms and platinum oxidation passivated the Pt surface. Ostwald ripening, therefore, can be eliminated by not cycling or holding the potential of the catalyst in the double layer region. However, this condition seriously limits the electrochemical tests that can performed on the catalysts. For example, cyclic voltammetry between $Pt(H)_{ads}$ and Pt oxide formation and CO_{ads} stripping voltammetry both involve cycling the Pt catalyst through the region where only double layer charging occurs. Despite the fact that Ostwald ripening cannot be eliminated for the above mentioned tests, it can be minimized by minimizing the amount of time that the potential of the catalyst is held within the double layer region. For example,

Ostwald ripening studied by *in situ* STM occurred over the time period of hours, while in a typical CO_{ads} stripping experiment presented in this thesis the potential is held in the double layer region for only 4 min..[i] Thus, during one CO_{ads} stripping voltammetry, the extent of Ostwald ripening is minimal. Generally, minimizing the time at which the Pt catalyst potential is held in the double layer region will minimize the extent of Ostwald ripening.

Ostwald ripening is initiated by the release of an atom from the parent structure followed by redeposition onto another structure. This can occur via two mechanisms; adatoms can be emitted and diffuse along the film surface to larger islands; or a dissolution-redeposition process, where atoms randomly detach and reattach at the solid/liquid phase, can occur.[117] Dissolution of Pt into solution can greatly change the catalyst electrode since, in addition to Ostwald ripening, it can lead to Pt loading loss. For example, in polymer electrolyte fuel cells, platinum redeposition can occur in the membrane of the fuel cell, thus becoming effectively lost to the electrode.

Platinum can dissolve into solution electrochemically

$$Pt(s) \rightleftarrows Pt^{2+}(aq) + 2e^- \tag{7.1}$$

Using the Nernst equation, we can see that the electrochemical dissolution of Pt is dependent on both the potential and temperature.

$$E = E° - \frac{RT}{2F} ln(C_{Pt^{2+}}) \tag{7.2}$$

Where the activity coefficient of Pt^{2+} ions is assumed to be 1 and $C_{Pt^{2+}}$ is the Nernstain concentration of Pt^{2+} ions under the applied potential E. Rearrangement of Equation 7.2 gives

$$C_{Pt^{2+}} = exp\left[\frac{RT}{2F}(E - E°)\right] \tag{7.3}$$

---

[i] On a Pt film, the double layer region spans 400 mV (see Chapter Two, Section 2.3.1). As each CO_{ads} stripping experiment comprises three cyclic voltammogram which pass through the double layer region we can calculate the amount of time that the potential is held within the double layer region as:

$$t = 400\frac{mV}{sweep} \times 2\frac{sweeps}{cycle} \times 3\ \frac{cycles}{COads\ experiment} \times \frac{1}{10}\frac{s}{mV} \times \frac{1}{60}\frac{min}{s} = 4\ \frac{min}{COads\ experiment}$$

From Equation 7.3 it is evident that as the temperature increases, the concentration of dissolved Pt will also increase. This is mainly due to the temperature term in the numerator of the exponential term, but also because the value of $E°$ decreases with increasing temperature.[114] Equation 7.3 also predicts that as the applied potential increases, the solubility of Pt will also increase.

In general terms, experimental evidence supports the trends predicted by the Nernst equation.[115,119,120,121,122] This is to say that the concentration of dissolved ions is found to increase with increasing temperature and increasing potential. However, the potential dependence and the magnitude of Pt solubility deviates considerably from Nernstian behaviour. The major discrepancies between observed solubility of Pt and the values predicted by Equation 7.3 can be summarized as: (i) Pt solubility plateaus or even decreases at potentials $\geq$ 1.1 V vs. RHE; (ii) the slope of Pt^{2+} concentration vs. the logarithm of potential is less than predicted by the Nernst equation ($2.3RT/2F$); (iii) at voltages lower than 0.95 V vs. RHE, concentrations of Pt^{2+} are considerably higher than predicted by the Nernst equation.

It has been proposed that Pt dissolution is prevented at potentials $\geq$ 1.1 V vs. RHE because at these oxidizing potentials the growth and place-exchange of Pt oxide atomic layers can passivate the Pt surface and reduce Pt dissolution.[123,124] The discrepancy between the measured slope of Pt^{2+} concentration vs. the logarithm of potential, and the slope predicted by the Nernst equation, is hypothesized[114] to be caused by variations in surface morphologies and particle size effects that (i) influence the thermodynamics and the kinetics of Pt dissolution if less than one monolayer of Pt is dissolved, and (ii) are caused by the unique surface energies of nanoparticles.

The larger than predicted concentrations of Pt^{2+} measured at potentials lower than 0.95 V vs. RHE are proposed to result from a combination of electrochemical and chemical reactions that can lead to the dissolution of Pt into solution.[125] For example, once platinum is oxidized electrochemically

$$Pt(s) + H_2O \rightleftarrows PtO(s) + 2H^+ + 2e^- \qquad (7.4)$$

it can then dissolve into solution via a chemical reaction

$$PtO(s) + 2H_3O^+ \longrightarrow Pt^{2+} + 3H_2O \quad (7.5)$$

This proposed method of Pt dissolution explains the measured pH dependence of Pt dissolution. Although Pt dissolution cannot be prevented, it can be minimized during catalytic activity testing by testing at room temperature and minimizing testing times.

In addition to Ostwald ripening and dissolution, agglomeration of the catalyst results in Pt surface area losses. Agglomeration refers to the migration of catalyst particles along the surface of the carbon support resulting in coalescence when two or more particles meet. Agglomeration is identified as occurring when particle size distribution is log-normal with respect to volume and shows a distinctive tail at large particle sizes.[126] Additionally, rates of cluster growth that are dependent on particle loading also indicate agglomeration.[127] Agglomeration occurs due to weak adhesion of the particle to the support. Thus, agglomeration can be minimized if the adhesion of Pt particles to the support is increased. Of the different processes which result in Pt surface area loss, Ostwald ripening and dissolution, cannot be eliminated but can only be minimized. Agglomeration itself can be prevented by increasing the adhesion between the Pt catalyst and the carbon support.

In this chapter, the electrochemical stability of the Pt/HOPG electrodes prepared by electrochemical deposition or impregnation, followed by thermal decomposition of Pt onto freshly cleaved, ozone oxidized, or electrochemically oxidized HOPG, will be tested. Electrochemical stability will be determined by comparing changes of Pt surface area caused by successive adsorbed CO (CO_{ads}) stripping voltammetry. X-ray photoelectron spectroscopy analysis of the six different Pt/HOPG electrodes is conducted to determine which electrode has the greatest platinum-support interaction.

7.3 EXPERIMENTAL

7.3.1 Solutions, Cells, and Electrodes.

Chapter Two, Section 2.2 describes the solutions, cells, and electrodes used in this work. A Hg/Hg_2SO_4, 0.5 M H_2SO_4 (MSE) electrode was used as the reference electrode for

electrochemical deposition of Pt and electrochemical oxidation of HOPG. A Hg/Hg_2Cl_2, sat. KCl (SCE) was used for the CO_{ads} stripping voltammetry.

7.3.2 Substrate Pre-Treatments.

Grade SPI-1 HOPG from SPI supplies were used as substrates in all experiments. Pt was deposited onto freshly cleaved (denoted HOPG-FC), ozone-oxidized (denoted HOPG-O_3), and electrochemically oxidized (denoted HOPG-E) HOPG.

HOPG was freshly cleaved using the adhesive-tape method.

Ozone oxidation of the HOPG is described in detail in Chapter Four Section 4.3.2. Ozone oxidized HOPG substrates discussed in this chapter were oxidized at 300 °C for 15 min in 0.15 ppm O_3.

HOPG was electrochemically oxidized in a 0.1 M H_2SO_4 solution at + 1.55 V for 30 s.

7.3.3 Platinum Deposition Method.

Electrochemical deposition occurred at – 0.475 V vs. MSE for 7.5 s in 1 mM $PtCl_4$ + 0.1 M H_2SO_4. Details of the deposition procedure are described in Chapter Three, Section 3.3.3.

Impregnation and thermal decomposition was carried out as described in Chapter Five, details of the deposition procedure are described in Chapter Five, Section 5.3.3.

7.3.4 Adsorbed CO Stripping Voltammetry.

Adsorbed CO (CO_{ads}) stripping voltammetry is used as a test reaction to determine if the electrode morphology changes after electrochemical use. Chapter Six, Section 6.3.4 describes the method of CO_{ads} stripping voltammetry and Section 6.4.1 describes the process of electrochemical oxidation of CO_{ads} onto polycrystalline Pt foil.

7.3.5 XPS Analysis.

The Pt 4f position of Pt foil was corrected to silver ($3d_{5/2}$ at 368.26 eV). The Pt & Ag foils were analyzed on the same day under the same conditions. Pt 4f XPS Spectra were deconvoluted using the same parameters as used by Bancroft et. al.[128] Specifically a good fit was achieved by setting the spin-orbit coupling to 3.3 eV, the ratio of the areas of the $4f_{7/2}$ to $4f_{5/2}$ peaks to 1.33 eV, and keeping the FWHM the same for the $4f_{7/2}$ and $4f_{5/2}$ peaks. The Gaussian-Lorentzian fraction was set to 0.5 for all peaks in all spectra. See Section 2.4.4.2 for further details.

7.4 RESULTS AND DISCUSSIONS

7.4.1 Stability During Electrochemical Testing.

A key aspect of a Pt catalyst system appropriate for catalytic activity testing is that the catalyst must be stable during the testing process, i.e., the catalyst particles must not agglomerate together or excessively dissolve into solution during catalytic activity testing. A good measure of the electrochemical stability of Pt deposits is to measure the Pt surface area before and after electrochemical testing. If the catalysts agglomerate together or dissolve into solution during the testing, then the measured Pt surface area after testing will be smaller than the surface area before testing. A standard method of measuring Pt surface area is to measure the charge associated with hydrogen adsorbed (H_{ads}) onto the Pt surface, or hydrogen desorption (H_{des}) from the Pt surface (see Chapter Two, Section 2.3.1). However, measuring changes in the $H_{ads/des}$ peaks is not an appropriate method in this work since the Pt/HOPG electrodes prepared by electrochemical deposition Pt do not have well defined H_{ads} or H_{des} peaks. An alternative method of measuring the surface area of Pt catalyst is to measure the charge associated with the electrochemical oxidation of CO adsorbed (CO_{ads}) on Pt catalysts (see Chapter Six, Section 6.4.1). This method is feasible assuming that the CO_{ads} coverage does not change during electrochemical CO_{ads} stripping voltammetry, which is a reasonable assumption if the crystal structure of the Pt catalysts do not change during CO_{ads} stripping voltammetry.

To test the electrochemical stability of the Pt catalysts, five successive CO_{ads} oxidation stripping voltammograms were run on each of the six different Pt/HOPG electrodes. The CO_{ads} stripping charge was measured for each experiment. From the measured CO_{ads} stripping charge, the percent of remaining CO_{ads} stripping charge, $Q_{CO_{ads}}$, was calculated as follows:

$$\%\, Q_{CO_{ads}}\text{remaining} = \frac{Q_n}{Q_1} \times 100\% \tag{7.6}$$

where n, $1 \leq n \leq 5$, is the number of subsequent CO_{ads} stripping voltammograms on a particular sample, Q_1 is the $Q_{CO_{ads}}$ value measured in the 1st stripping cyclic voltammogram, and Q_n is the $Q_{CO_{ads}}$ value measured in the n^{th} stripping cyclic voltammogram. Table 7.1 lists

the average percentage remaining $Q_{CO_{ads}}$ with each successive stripping voltammogram; Figure 7.1 is a plot of the data from Table 7.1.

Table 7.1 Stability of Pt nano-catalysts on HOPG substrates: Measured by changes in $Q_{CO_{ads}}$ over five successive stripping voltammograms.

HOPG pre-treatment	Pt nano-catalysts Preparation	% $Q_{CO_{ads}}$ remaining*			
		2nd	3rd	4th	5th
HOPG-FC	Electrochemical deposition†	43 ± 16	24 ± 20	3 ± 6	1 ± 2
HOPG-FC	Impregnation and thermal decomposition ††	81 ± 14	61 ± 9	36 ± 10	36 ± 5
HOPG-E‡	Electrochemical deposition †	67 ± 19	49 ± 18	35 ± 2	32 ± 4
HOPG-E‡	Impregnation and thermal decomposition ††	83 ± 12	76 ± 10	73 ± 7	65 ± 4
HOPG-O_3**	Electrochemical deposition §	73 ± 26	57 ± 30	51 ± 26	45 ± 24
HOPG-O_3**	Impregnation and thermal decomposition ††	95 ± 4	94 ± 8	90 ± 9	94 ± 12

* $\%\ Q_{CO_{ads}}\text{remaining} = \frac{Q_n}{Q_1} \times 100\%$

† Pt was deposited at – 0.475 V vs. MSE in 0.1 M H_2SO_4 + 1 mM $PtCl_4$ solution for 7.5 s.

‡ 30s electrochemical oxidation at 1.55 V vs. MSE in 0.1 M H_2SO_4.

§ Pt was deposited at – 0.475 V vs. MSE in 0.1 M H_2SO_4 + 1 mM $PtCl_4$ solution for 5 s.

** HOPG was oxidized at 300 °C for 15 min in 0.15 ppm O_3.

†† 250 μL of 2.6×10^{-4} M H_2PtCl_4 + 6.4×10^{-4} M HCl.

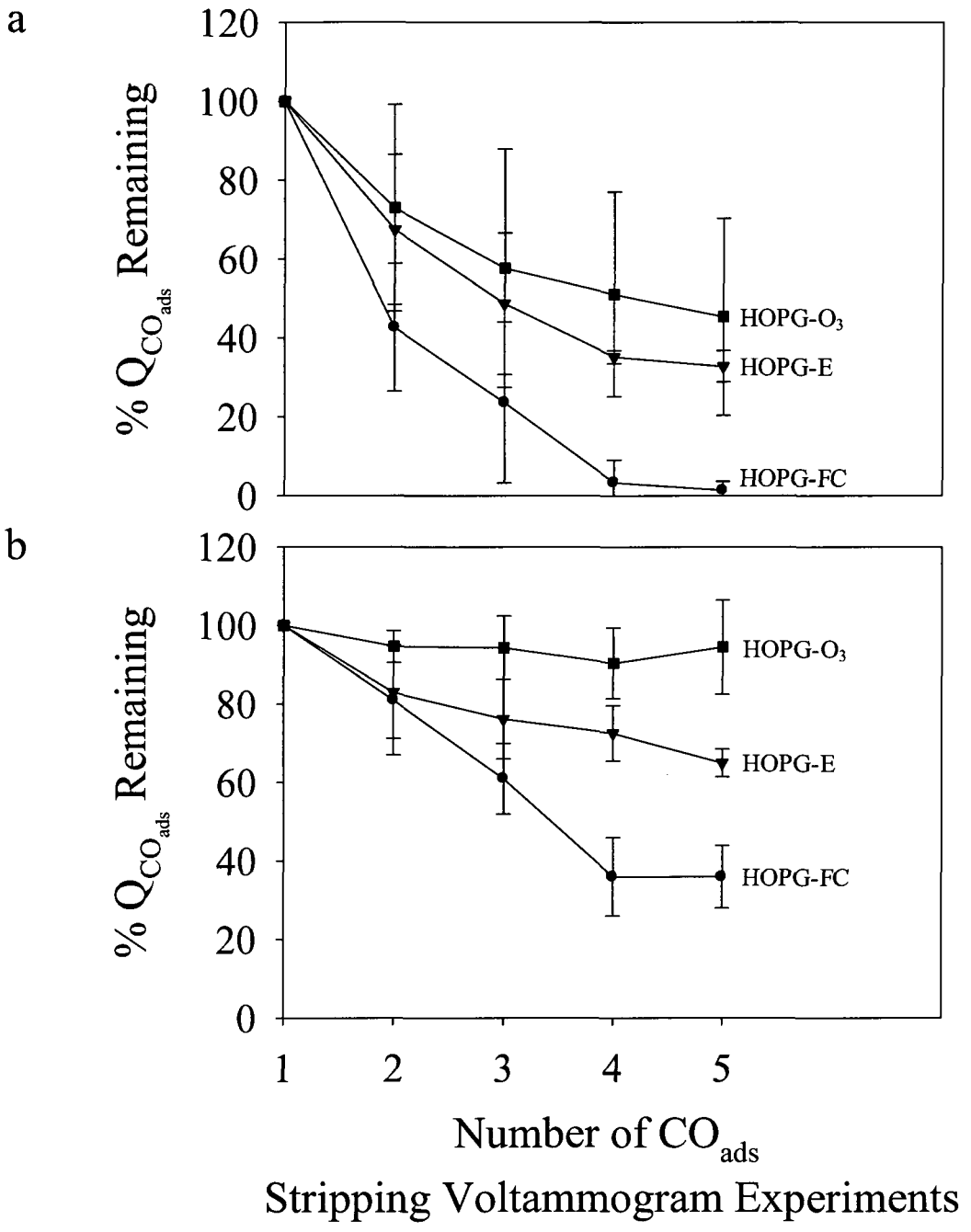

Figure 7.1 Stability of Pt nano-catalysts on HOPG substrates. Plot of % $Q_{CO_{ads}}$ remaining (calculated using Equation 7.6) over five successive stripping voltammograms. a) Pt/HOPG electrodes prepared by electrochemical deposition; b) Pt/HOPG electrodes prepared by impregnation and impregnation and thermal decomposition. Freshly cleaved (●), ozone oxidized (■), and electrochemically oxidized (▲) HOPG.

The Pt/HOPG electrode prepared by electrochemically depositing Pt onto freshly cleaved HOPG has the lowest electrochemical stability. For example, less than 50 % of the original stripping charge remains when comparing the second stripping voltammogram to the first. This indicates that more than 50 % of the Pt surface area is lost (due to agglomeration, dissolution, Ostwald ripening, or a combination there of) during the first CO_{ads} stripping experiment that comprises of three successive cyclic voltammograms. By the fifth stripping voltammogram almost all of the stripping charge is lost, indicating that almost all of the deposited Pt has dissolved into solution since agglomeration alone is unlikely to cause such a dramatic decrease in Pt surface area.

Oxidizing the HOPG substrate improves the stability of Pt/HOPG electrodes prepared by electrochemical deposition. For example, after each CO_{ads} stripping experiment there is more remaining CO_{ads} stripping charge for the electrode prepared by electrochemical deposition onto electrochemically oxidized HOPG compared to the sample prepared by electrochemical deposition onto freshly cleaved HOPG. Oxidizing HOPG with ozone gas has an improved stabilizing effect compared to electrochemical oxidation of HOPG. Comparison of the three electrodes prepared by impregnation followed by thermal decomposition displays the same trend; ozone oxidation is the most effective pre-treatment for stabilizing HOPG followed by electrochemical oxidation, and freshly cleaved HOPG is the least effective.

From Table 7.1 it is evident that Pt/HOPG electrodes prepared by impregnation followed by thermal decomposition are significantly more stable than Pt/HOPG electrodes prepared by electrochemical deposition. For example, after the fifth experiment 36 ± 5 % of the stripping charge remains for the electrode prepared by impregnation followed by thermal decomposition onto freshly cleaved HOPG, compared to almost no stripping charge that remains for the electrode prepared by electrochemical deposition onto the same substrate. Comparing the samples prepared on electrochemically oxidized HOPG by electrochemical deposition versus impregnation followed by thermal decomposition, it is clear that for this substrate the Pt nano-catalysts prepared by impregnation followed by thermal decomposition are almost twice as stable (65 ± 4 % $Q_{CO_{ads}}$ remaining after five CO_{ads} stripping voltammograms) as the catalyst prepared by electrochemical deposition (32 ± 4 % $Q_{CO_{ads}}$ remaining after five CO_{ads} stripping voltammograms).

The sample prepared by impregnation followed by thermal decomposition of Pt onto ozone oxidized HOPG has the greatest amount of % $Q_{CO_{ads}}$ remaining over the course of the five successive CO_{ads} stripping voltammograms. In fact, within the calculated standard deviation there is almost no Pt loss. From this electrochemical stability data, it is clear that the most promising method of preparing Pt nano-catalysts on HOPG is to thermally decompose the Pt precursor salt onto ozone oxidized HOPG.

7.4.2 X-ray Photoelectron Spectroscopy Analysis of Pt/HOPG Electrodes.

7.4.2.1 Comparison of Pt 4f spectra for all Pt/HOPG electrodes.

The electrochemical stability testing indicates that the most stable Pt/HOPG electrode is prepared by impregnation and thermal decomposition of Pt onto ozone oxidized HOPG. This stability could result from either a physical or chemical interaction between the Pt catalyst prepared by impregnation and thermal decomposition and the ozone oxidized HOPG substrate. For example, TEM analysis of a Pt/HOPG-O_3 sample prepared by impregnation and by thermal decomposition, prepared using the same experimental conditions as the Pt/HOPG-O_3 sample which was tested for electrochemical stability by multiple CO_{ads} stripping voltammograms (see Table 7.1), showed that the Pt nano-catalyst had an average particle size of 2.83 ± 0.8 nm. The average particle size is not much smaller than the average pit size of 3.8 ± 0.9 nm, which results from the ozone oxidation procedure. Thus, it is conceivable that the particles have formed inside the pit and are physically stabilized by the walls of the pit. Figure 7.2 and Figure 7.3 are high resolution transmission electron microscopy (HRTEM) images of Pt/HOPG electrodes prepared by impregnation and thermal decomposition onto ozone oxidized HOPG. Figure 7.2 shows both the deposited particles and the pits that result from ozone oxidation. The ozone oxidized pits are highlighted in Figure 7.2b. As can be seen from Figure 7.2, the carbon is disordered at the edges of the ozone oxidized pits. Figure 7.3 highlights a single particle on the ozone oxidized HOPG surface. Figure 7.3 shows that the carbon structure surrounding the platinum particles is disordered, indicating that the platinum particle is indeed located within the pit, explaining the enhanced stability for Pt/HOPG electrodes prepared by impregnation and thermal decomposition onto ozone oxidized HOPG. However this does not explain why Pt/HOPG electrodes prepared by impregnation followed by thermal decomposition of electrochemically oxidized HOPG are more stable than electrodes prepared by the same

method on freshly cleaved HOPG. Moreover, it does not explain why Pt/HOPG electrodes prepared by impregnation followed by thermal decomposition are more stable than electrodes prepared by electrochemical deposition on the same substrate. Thus there must be another factor that influences the stability of the Pt/HOPG electrodes.

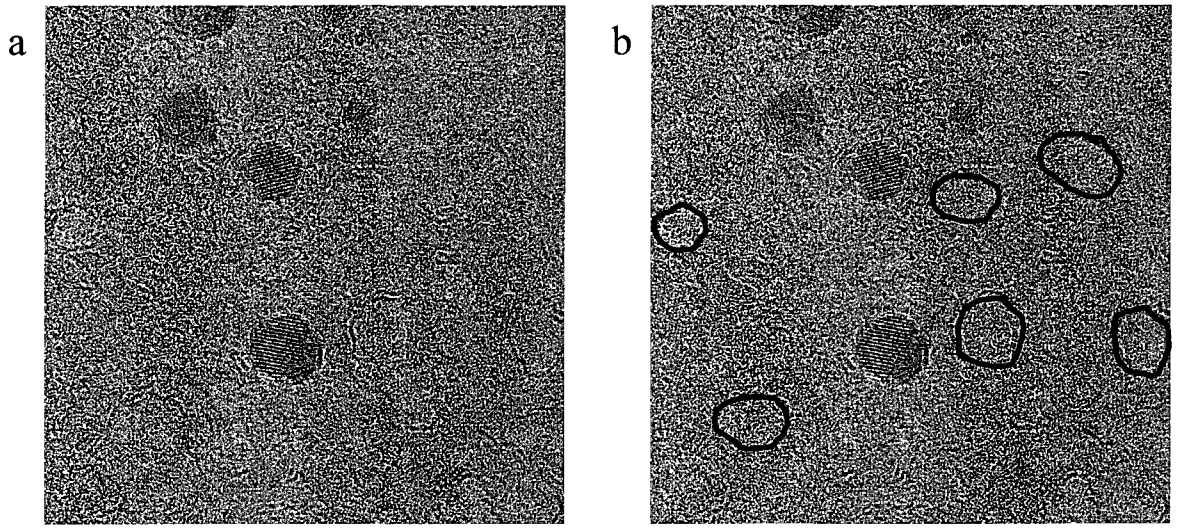

Figure 7.2 a) High resolution TEM image which has been filtered by local convolution to enhance the edges of the pits; b) same as a, however, some of the edges of the pits are emphasized with black lines. Note the disorder in the carbon at the edges of the pits.

One possible explanation for the observed trends in the stability data is that the observed enhanced electrochemical stability, is that the stability results from a chemical effect. That is to say during the deposition process a platinum-carbon chemical bond forms and stabilizes the catalysis. This theory can be tested with the use of X-ray photoelectron spectroscopy (XPS).

XPS analysis was conducted to determine if there are any measurable differences in the electronic states of Pt for the different types of prepared Pt/HOPG electrodes. Figure 7.4 shows the Pt 4f spectra for Pt/HOPG electrodes prepared by electrochemical deposition or impregnation followed by thermal decomposition onto freshly cleaved (Figure 7.4a), ozone-oxidized (Figure 7.4b), and electrochemically-oxidized (Figure 7.4c) HOPG. Table 7.2

summarizes the Pt 4f peak widths, positions, and shifts compared to polycrystalline platinum foil.

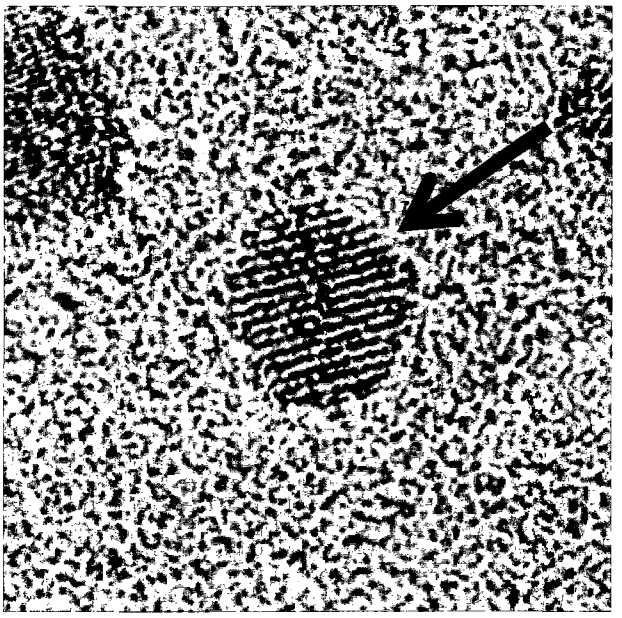

Figure 7.3 High resolution TEM image which has been filtered by local convolution to enhance the edges of the pits. The disorder in the carbon at the particle edge is similar to that observed for pits (see Figure 7.2) indicating that the particles are sitting in the pits of the ozone oxidized HOPG.

The Pt 4f spectra for all prepared Pt/HOPG electrodes are significantly wider than that of Pt metal. The exact cause of the Pt 4f signal broadening is not immediately apparent. It may be due to the less effective screening of the core hole states that occurs in small clusters compared to bulk metal.[129,130] Or it may be caused by surface platinum oxide formation that could form on the Pt catalysts surface during the time period between preparation of the samples and when they were put into the XPS vacuum chamber for analysis. It is quite possible that the Pt 4f broadening results from a combination of the two above mentioned possible causes.

The Pt $4f_{7/2}$ peak maxima for all the prepared samples are shifted to more positive binding energies compared to bulk platinum metal, which occurs at 71.2 eV (see Figure 7.4 and Table 7.2). It is possible that the positive shift in binding energy results from platinum oxide formation either during sample preparation or during the time between sample preparation and XPS analysis. To test this possibility, a sample (prepared by impregnation

followed by thermal decomposition) was electrochemically reduced and transferred under argon from the electrochemical cell to the XPS instrument. This sample showed a similar shift in binding energy (0.7 eV compared to platinum foil) as the sample prepared in the same fashion, but not electrochemically reduced (0.6 eV compared to platinum foil).

Table 7.2 Summary of experimental X-ray photoelectron spectroscopy data of Pt $4f_{7/2}$ spectrum.

Pt nano-catalysts Preparation	HOPG pre-treatment	BE	BE shift compared to Pt foil	FWHM $4f_{7/2}$
			eV	
Electrochemical Deposition*	Freshly Cleaved HOPG	71.5	0.3	1.525
Electrochemical Deposition*	Electrochemically Oxidized†	71.5	0.3	1.29
Electrochemical Deposition*	Ozone Oxidized‡	71.6	0.4	1.746
Impregnation and thermal decomposition§	Freshly Cleaved HOPG	71.5	0.3	1.031
Impregnation and thermal decomposition§	Electrochemically Oxidized†	71.7	0.5	1.544
Impregnation and thermal decomposition§	Ozone Oxidized‡	71.8	0.6	1.21
Impregnation and thermal decomposition§ followed by electrochemical deposition.††	Ozone Oxidized‡	71.9	0.7	1.195
Polycrystalline Pt foil**		71.2	n/a	0.947

* Pt was deposited at – 0.475 V vs. MSE in 0.1 M H_2SO_4 + 1 mM $PtCl_4$ solution for 5 s.

† 180 s electrochemical oxidation at 1.55 V vs. MSE in 0.1 M H_2SO_4.

‡ HOPG was oxidized at 300 °C for 15 min in 0.15 ppm O_3.

§ 250 µL 2.6×10^{-5} M H_2PtCl_4 + 6.5×10^{-5} M HCl

** Prior to analysis, Pt foil was sputtered in vacuum for 5 minutes using a Ar ion gun at an accelerating voltage of 4kV and emission of 10 mA.

†† Electrochemical deposition was achieved by cycling the electrode between 0.2 to – 0.22 V vs. SCE 10 times at 100 mV s^{-1}

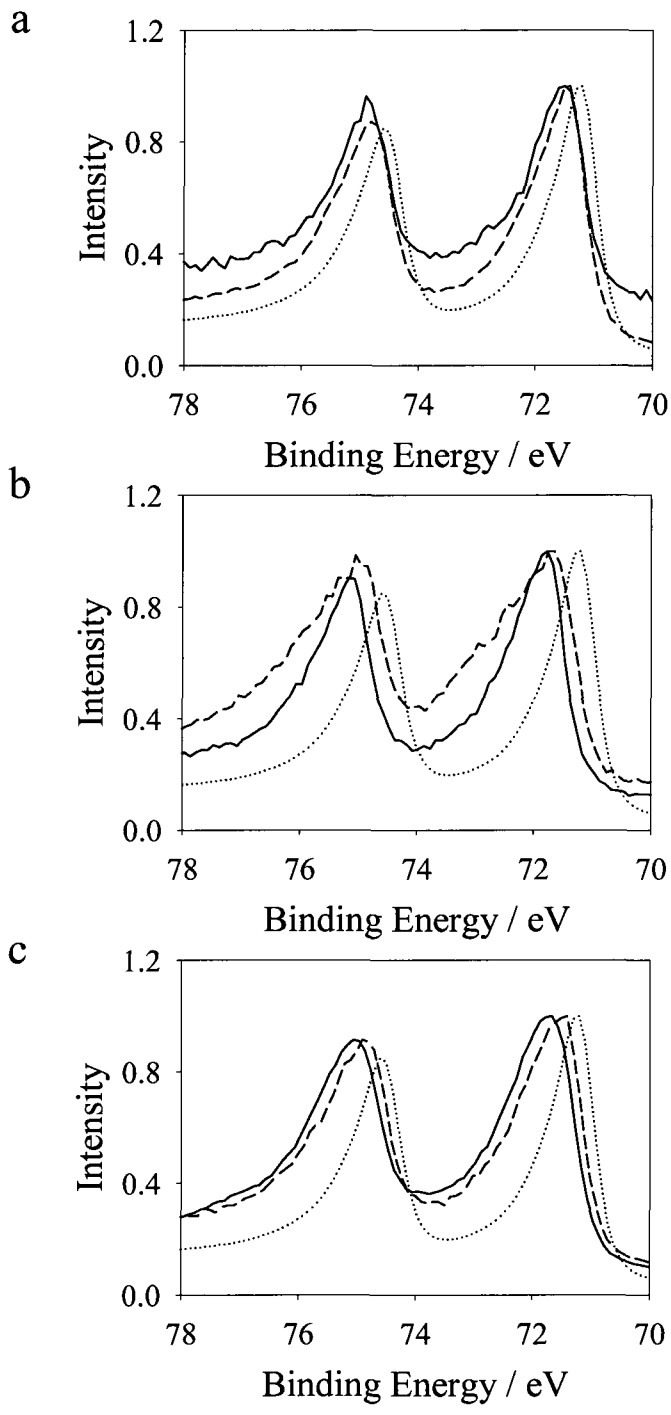

Figure 7.4 Platinum 4f spectra of Pt nano-catalysts electrochemically deposited (— — —) or thermally decomposed (———) onto a) freshly cleaved, b) ozone oxidized, and c) electrochemically oxidized HOPG. The Pt 4f spectrum for polycrystalline bulk platinum metal is included for comparison (.....).

The positive shift in the binding energy of the Pt 4f peak for all samples indicates that the platinum particles have similar electronic environments to one another, which is different from bulk Pt metal, regardless of their deposition method or the pre-treatment of the HOPG substrate that they are deposited onto. This is particularly remarkable as some of the nano-catalysts have formed clusters, while others exist as individual nano-catalysts less than 5 nm in size. Previous work has shown a positive shift in metal binding energies for Pt sputter-deposited onto HOPG.[130] The positive binding energy shift is attributed to a final state effect caused by a slow relaxation of the core hole created by photoemission, which is due to the small size of the deposited clusters and the poor coupling of the deposited metal with the graphite substrate.[130] It is possible that the same final state effect is occurring with the samples prepared in this work.

A more probable cause of the positive shift in binding energy is the interaction between the deposited metal and defect sites on the HOPG surface.[131] In another study,[131] experiments were performed where Pt adatom and Pt_8 cluster mobility on the basal plane was significantly reduced by pre-adsorption of a monolayer of argon. This allowed comparison between the Pt 4f photoelectron spectra of adatoms/clusters on the basal plane to the Pt 4f spectra of adatoms that have diffused to the step edges of HOPG. It was found that the binding energies of the Pt 4f photoelectron spectra for adatoms/clusters on the basal plane of HOPG are similar to that of bulk Pt. Conversely, the Pt 4f photoelectron spectra of the adatoms located along step edges has a large shift, 0.75 eV, to higher binding energies.[131] These studies suggest that the positive shift in binding energy associated with small clusters is due to interactions between Pt and defect sites, possibly due to the formation of platinum-carbon bonds, and is not caused by final state effects.

A closer analysis of the Pt 4f spectra shows that the Pt $4f_{7/2}$ maximum for the particles prepared by impregnation followed by thermal decomposition onto electrochemically-oxidized HOPG is shifted by 0.2 eV more positive than Pt prepared by electrochemical deposited onto electrochemically-oxidized HOPG. Similarly, the Pt $4f_{7/2}$ maximum for Pt prepared by impregnation followed by thermal decomposition onto ozone-oxidized HOPG is shifted by 0.2 eV more positive than electrodes prepared by electrochemical deposition onto ozone-oxidized HOPG. Conversely, for the two samples prepared on freshly cleaved HOPG,

the Pt $4f_{7/2}$ spectra for both the samples, regardless of the deposition technique are shifted 0.3 eV positive compared to platinum foil.

For both samples prepared on oxidized HOPG, the Pt 4f spectra for Pt nano-catalysts prepared by impregnation followed by thermal decomposition are shifted positively compared to Pt prepared by electrochemical deposition. TEM results (see Chapters Four and Five) indicate that the electrochemical deposition conditions used in this work result in the formation of large clusters regardless of the substrate pre-treatment. Within a cluster only a fraction of the Pt nano-catalysts can make contact with defect sites on the oxidized HOPG substrate. Conversely, the majority of Pt nano-catalysts prepared by impregnation followed by thermal decomposition reside at defect sites. The positive shift in binding energy of the Pt 4f spectra for samples prepared by impregnation followed by thermal decomposition, compared to electrochemical deposition, indicates that there is a stronger interaction between the thermally decomposed deposits and the HOPG substrate.

Of all the Pt/HOPG samples studied, the sample with the greatest positive shift in the Pt 4f spectra (0.6 eV compared to polycrystalline Pt foil) is the sample prepared by impregnation followed by thermal decomposition onto ozone oxidized HOPG; this sample also has the greatest electrochemical stability. Thus, there is a correlation between nano-catalyst stability and the strength of the interaction between the nano-catalysts and the support. The XPS results clearly indicate that increasing the chemical interaction between the Pt catalyst and the carbon substrate increases the Pt/HOPG electrode stability. However, the overall stability for the Pt/HOPG-O_3 electrodes prepared by impregnation and thermal decomposition is a cumulative effect of chemical interactions (Pt-C bond formation) and physical interactions (Pt is physically stabilized within the pits).

In the introduction of this chapter different mechanisms of Pt loss were discussed. These methods are: Ostwald ripening, dissolution (electrochemical or chemical), and agglomeration. Increasing the interactions, chemical or physical, between the Pt catalyst and the HOPG support will not prevent either Ostwald ripening or dissolution. However, increasing the interactions between the platinum and HOPG will decrease the extent of surface diffusion of the platinum catalysts and thus decrease the extent of agglomeration.

7.4.2.2 Analysis of Pt–C bond formation during impregnation and thermal decomposition.

To determine at what point the Pt-C interactions begin to form, XPS analysis was conducted during various stages of the impregnation and thermal reduction process. The following three samples were analyzed by XPS: (1) K_2PtCl_4 powder placed on HOPG; this analysis determines the chemical environment of Pt(II) in K_2PtCl_4; (2) A Pt/HOPG-O_3 electrode prepared by depositing 250 μL of 2.6 x 10^{-5} M K_2PtCl_4 + 6.5 x 10^{-5} M HCl on to an ozone oxidized (0.15 ppm O_3 at 300 °C for 15 min) HOPG substrate and allowing the solution to dry in air; this analysis will determine if Pt(II) changes during the impregnation step; (3) A Pt/HOPG-O_3 electrode prepared like sample (2) followed by a reduction step (2 h at 250 °C under 8 % H_2 in Ar); this analysis will determine the electronic state of Pt after reduction. The Pt 4f spectrum of all three samples are shown in Figure 7.5.

The spectra of K_2PtCl_4 powder, Figure 7.5a, can be deconvoluted into contributions from Pt(II) and Pt(IV). The majority of Pt 4f signal represents Pt(II) with only 11 % of the signal representing Pt(IV). This small amount of Pt(IV) likely results from air oxidation of the powder and not a disproportionation reaction since there is no Pt(0) signal. The binding energy for Pt(II) $4f_{7/2}$ signal, 73.2 eV, is on par with previous studies of K_2PtCl_4.[i,132,133] This binding energy is 0.8 eV higher than what is expected for Pt(II)O. This positive shift in binding energy reflects the larger net electronegative force that the four chlorine atoms, compared to the single oxygen atom, generate on the central platinum atom.

Figure 7.5b shows the Pt 4f spectra of a K_2PtCl_4 and HCl solution which was allowed to air dry on an ozone oxidized HOPG substrate. There are two notable differences between this spectrum and the spectrum for K_2PtCl_4 powder. Firstly, while both spectra in Figure 7.5a and b can also be deconvoluted into a Pt(II) and a Pt(IV) spectra, the spectra shown in Figure 7.5b has a considerably larger Pt(IV) contribution. Approximately 30 % of the Pt found on the air dried sample is in the Pt(IV) state, indicating that the process of air drying the Pt salt solution causes some of the Pt(II) to oxidize to Pt(IV). This is not unexpected as during air drying the Pt salt is exposed to oxygen from the air.

---

[i] There was sufficient K_2PtCl_4 powder on the HOPG substrate that the typically narrow C 1s signal of the HOPG substrate was not detected. Instead a wider C 1s signal, typical of carbon contamination from the air, was measured. Thus, correction for charging on this sample (and only this sample) was achieved by setting the C1s signal to 285 eV.

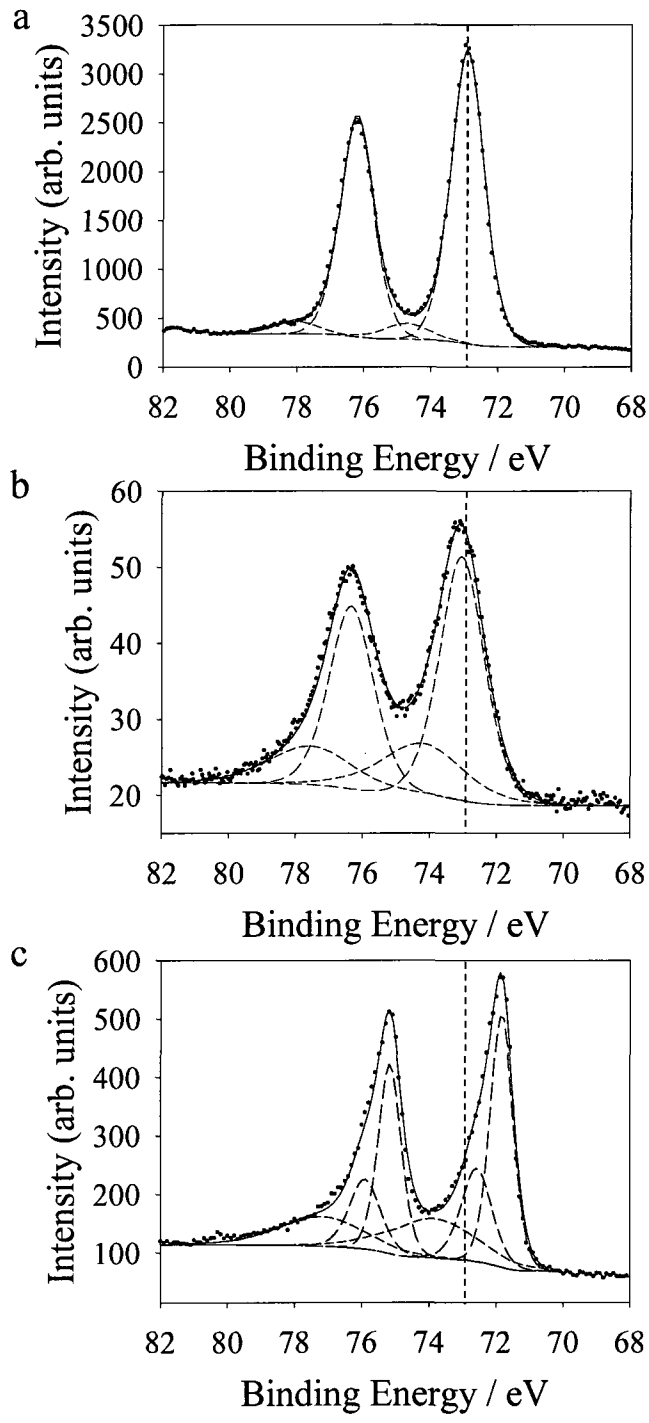

Figure 7.5 Platinum 4f spectra a) K_2PtCl_4, b) 250 µL of 2.6 x 10^{-5} M K_2PtCl_4 + 6.5 x 10^{-5} M HCl air dried on ozone oxidized HOPG, and c) 250 µL of 2.6 x 10^{-5} M K_2PtCl_4 + 6.5 x 10^{-5} M HCl air dried and reduced (2 h at 250 °C under 8% H_2 in Ar) on ozone oxidized HOPG. Ozone oxidation of HOPG occurred in 0.15 ppm O_3 at 300 °C for 15 min..

The second difference between Figure 7.5a and b is that the spectrum in Figure 7.5b is shifted 0.1 eV more positive compared to the spectrum in Figure 7.5a. XPS analysis of the sample prepared by air drying the K_2PtCl_4 + HCl solution on the ozone oxidized HOPG did not reveal the presence of chlorine. Although there may be trace amounts of chlorine (i.e. amounts below the detection limit of the instrument) remaining on the surface, the majority of chlorine was removed. This can be said with confidence because although the sensitivity factor for chlorine is 6.7 times less than that for platinum, given the concentrations of K_2PtCl_4 and HCl used, there is 6.5 times more chlorine in the solution than platinum. Thus, despite the differences in sensitivity factors between chlorine and platinum, the area under the intensity signal for the chlorine signal should be similar to the measured area under the intensity signal for Pt. Since chlorine is absent from the HOPG surface, the positive binding energy shift observed in Figure 7.5b is not influenced by interactions between platinum and chlorine. However, it is still shifted positive by 0.9 eV to Pt(II)O. This observed positive shift is taken as an indication that a Pt-C bond has formed during the impregnation step.

The spectrum of Pt impregnated and thermally decomposed onto ozone oxidized HOPG is shown in Figure 7.5c. The platinum spectrum is deconvoluted into a Pt(0), Pt(II), and Pt(IV) spectra. Despite the good fit generated by deconvoluting the spectrum into three different species, as mentioned previously, the width of the Pt 4f peak may also be due to the less effective screening of the core hole states that occurs in small clusters compared to bulk metal.[129,130] Regardless, it should be noted that both the Pt(0) peak and the Pt $4f_{7/2}$ maximum are shifted positive to bulk Pt metal and negative to the spectrum of Figure 7.5b, indicating that some Pt-Pt bonds form at the expense of some Pt-C bonds.

The XPS analysis provides convincing evidence that platinum is forming a chemical bond with carbon and that this bond increases the binding energy of the Pt 4f electrons. A positive shift in the Pt 4f binding energy has been observed for many Pt nano-catalyst systems.[129,131,130,134,135,136] The mechanism of Pt(II) impregnation and thermal decomposition is not well studied, however, $H_2Pt(IV)Cl_6$ impregnation and reduction has been extensively studied.

It is generally accepted that impregnation involves two steps[137]; partial reduction,

$$H_2Pt(IV)Cl_6 + \equiv C\text{-}H + H_2O \longrightarrow Pt(II)Cl_4^{2-} + 2Cl^- + \equiv C\text{-}O^- + 5H^+ \qquad (7.7)$$

followed by attachment to the carbon support

$$Pt(II)Cl_4^{2-} + S \longrightarrow PtCl_3S^- + Cl^- \quad (7.8)$$

where S denotes ligand sites, principally C=C and oxygen-containing functional groups. The formation of platinum metal occurs via

$$PtCl_3S^- + R \longrightarrow Pt(0) + 3Cl^- + S + O \quad (7.9)$$

Where R denotes the reducing agent and O denotes the oxidized form of the reducing agent.

Within the work presented in this thesis, impregnation and thermal decomposition is achieved using a $K_2Pt(II)Cl_4$. Consistent with the above mechanism and the XPS results that suggest the formation of a Pt–C bond, we propose that the impregnation reaction involves interaction of Pt(II) with a ligand site via

$$Pt(II)Cl_4^{2-} + S \longrightarrow Pt(II)S^{2+} + 4Cl^- \quad (7.10)$$

and the reduction step is suggested to follow

$$Pt(II)S^{2+} + R \longrightarrow (1\text{-}a)Pt(0) + aPt(O)S + S + O \quad (7.11)$$

In Equation 7.11 the coefficient a; $0 < a < 1$, reflects the fact that not all of the platinum is chemically bound to the substrate. As the decomposition of $PtCl_4^{2-}$ takes place during the impregnation step, in this work, the method would more accurately be referred to as "impregnation followed by thermal reduction" instead of "impregnation followed by thermal decomposition".

The interaction between platinum and the carbon support is suggested to be analogous to the interaction between platinum and olefins. The Dewar-Chatt-Duncanson model can be used to explain the binding of transition metals to olefins.[138,139] Olefins bind to transition

metals via their π orbitals by donating electron density into an empty metal d-orbital (see Figure 7.6a). The bond is stabilized by the donation of electron density from an occupied metal d-orbital to the olefin's π^* orbital (see Figure 7.6b). This bond formation can occur by ligand substitution, reduction, or by metal atom synthesis (evaporation of the metal under high vacuum and co-condensation of the metal vapour with potential ligands). Considering that this work was conducted at atmospheric pressure, and that there is evidence of platinum-carbon bond formation before the platinum is reduced, it is reasonable to infer that the platinum-carbon bond forms by a ligand substitution reaction releasing chlorine from the platinum complex as illustrated in Equation 7.10. The positive shift in the Pt 4f binding energy indicates that platinum is acting as an electron donor to the HOPG. Thus, back donation from the occupied d orbitals of platinum into the carbon-carbon π^* orbital appears to be more significant than π donation from the carbon support to empty d orbitals in the Pt(II) atom.

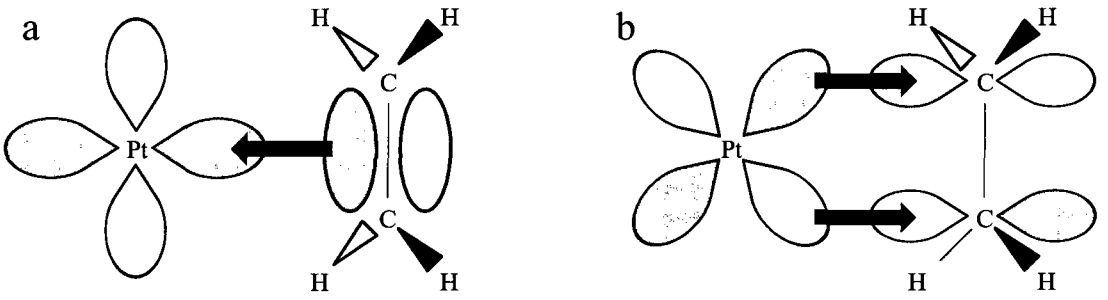

Figure 7.6 Dewar-Chatt-Duncanson model of bonding between transition metals and olefins, a) π donation, and b) back-donation into olefin π^* orbitals.

7.5 CONCLUSIONS

The electrochemical stability of Pt/HOPG electrodes was tested. The electrodes were prepared by electrochemical deposition or impregnation followed by thermal decomposition onto freshly cleaved, ozone oxidized, or electrochemically oxidized HOPG, resulting in six different electrodes. Stability against Pt surface area loss was determined by comparing successive CO_{ads} stripping charges. It was found that for a given substrate pre-treatment, the

electrodes prepared by impregnation followed by thermal decomposition were more stable than the electrode prepared by electrochemical deposition, regardless of the substrate pre-treatment. For a given deposition technique, ozone oxidation showed the best stabilizing effect , followed by electrochemical oxidation, and finally freshly cleaving the HOPG (which was the least effective at stabilizing Pt nanoparticles). Of all six electrodes prepared and tested, the electrode prepared by impregnation followed by thermal decomposition onto ozone oxidized HOPG had the greatest short-term electrochemical stability.

High resolution TEM analysis indicated that Pt nano-catalysts on ozone oxidized HOPG prepared by impregnation followed by thermal decomposition resided within the pits generated by ozone oxidation.

The six different electrodes were analyzed by X-ray photoelectron spectroscopy. The XPS Pt 4f spectra of all six prepared Pt/HOPG electrodes were shifted to higher binding energies compared to bulk Pt metal. This positive shift indicates that prepared catalysts are interacting with defect sites on the HOPG surface probably through the formation of Pt-C bonds. For electrodes prepared on oxidized HOPG, the Pt 4f spectra of the electrodes prepared by impregnation followed by thermal decomposition where shifted to higher binding energies than the Pt 4f spectra of the electrode prepared by electrochemical deposition. Of the three samples prepared by impregnation followed by thermal decomposition, the Pt 4f spectra of the Pt/HOPG-O_3 electrode displayed the highest shift in binding energies compared to Pt/HOPG-E or Pt/HOPG-FC electrodes. This indicates that of the six electrodes prepared, the Pt/HOPG-O_3 electrode prepared by impregnation followed by thermal decomposition had the greatest amount of interaction with the carbon support, probably in the form of platinum-carbon bonds. The XPS results indicate that the superior electrochemical stability of the thermally decomposed Pt/HOPG-O_3 electrodes results from the chemical interaction between the Pt catalyst and the carbon substrate and the physical interactions between the Pt particle and the pit which it is contained within.

The impregnation and reduction pathway was determined by XPS analysis of the various samples, prepared to represent the various stages of the impregnation and thermal decomposition process. From this analysis, it was determined that during impregnation, Pt^{2+} ions interact with C=C ligand sites forming Pt–C bonds. XPS analysis shows that chlorine is not present on the sample after the impregnation or reduction steps, indicating that chloride

ions are volatilized possibly as chlorine gas. During the reduction step, Pt–Pt bonds form at the expense of some of the Pt–C bonds. However, some Pt–C bonds remain, as indicated by the positive shift of the Pt 4f spectra for Pt/HOPG electrodes prepared by impregnation followed by thermal decomposition.

Chapter Eight

Conclusion

This thesis examines the preparation and characterization of various "Pt-on-carbon" electrodes. The motivation for this work is to study the effects of particle deposition techniques and substrate pre-treatment on the morphology, activity towards electro-oxidation of adsorbed carbon monoxide, and the electrochemical stability of the prepared electrodes. With this goal in mind, Pt catalyst electrodes were prepared by two different methods; electrochemical deposition or impregnation followed by thermal decomposition. Highly

ordered pyrolytic graphite, HOPG, was selected as the support, since it is catalytically inert for the test reactions studied in this thesis and because it has a well defined surface structure with a high stability against corrosion. To test the effect of defect sites on Pt catalyst nucleation, the HOPG surface was oxidized either electrochemically or with the use of ozone gas. The combination of two different deposition methods (electrochemical deposition or impregnation followed by thermal decomposition) and three different types of substrates (freshly cleaved, electrochemically oxidized, or ozone oxidized HOPG) results in six different electrodes that were studied with respect to their particle morphology, their activity towards electro-oxidation of adsorbed carbon monoxide (CO_{ads}), and their electrochemical stability. In this chapter some of the main conclusions of this work are highlighted. As well, future work of interest in this field of catalysis are proposed.

8.1 PLATINUM DEPOSITS PREPARED BY ELECTROCHEMICAL DEPOSITION ONTO HOPG

Pt was electrochemically deposited onto freshly cleaved, electrochemically, or ozone oxidized HOPG. Scanning tunnelling microscopy showed that ozone oxidation introduces randomly distributed nano-pits, < 10 nm in diameter, on the basal plane of HOPG, whereas, scanning electron microscopy revealed large pits, 85 – 127 nm in diameter, originating at defect sites on the electrochemically oxidized HOPG surface. In conjunction with the spectroscopic analysis, electrochemically determined roughness factors indicate that electrochemical oxidation is a much more severe oxidation process compared to ozone oxidation. As the number of naturally occurring defect sites and step edges differ for each HOPG substrate, electrochemical oxidation (which occurs at naturally occurring defect sites and step edges) amplifies the differences between different HOPG samples. Conversely, as ozone oxidation creates defects, it minimizes the differences between HOPG samples.

Electrochemical deposition at the conditions presented in this work resulted in the formation of Pt clusters onto HOPG, regardless of the substrate pre-treatment, i.e. oxidizing HOPG electrochemically or with ozone gas did not prevent clusters from forming. High resolution transmission electron microscopy (HRTEM) indicates that the clusters consist of smaller nanoparticles that form by agglomeration.

Current-time analysis indicates that Pt deposit growth occurred via a 3D nucleation process on freshly cleaved and ozone oxidized HOPG. Reduced variable plots indicate that the nucleation process on freshly cleaved HOPG is highly variable; in some cases nucleation occurred instantaneously, in other cases progressive nucleation was observed. Analysis of deposition charges indicate variations in the amount of Pt deposited which supports the finding of an inconsistent deposition process on freshly cleaved HOPG. Oxidizing the substrate with ozone gas shifts the nucleation process from progressive towards instantaneous. Instantaneous nucleation is favoured since it results in a narrower particle size distribution. Nucleation analysis was not possible for the electrochemical deposition onto electrochemically oxidized HOPG. However, it was found that the amount of Pt deposited increased with increased extent of electrochemical oxidation.

TEM analysis reveals the important role that nucleation sites play in causing the observed inconsistency in the Pt deposition process on freshly cleaved HOPG. It was found that the Pt deposits were nucleating almost exclusively along step edges on freshly cleaved HOPG. As the number of step edges on an HOPG substrate changes each time the substrate is cleaved, the number of nucleation sites also changes. It was concluded that the variability in the number of step edges, and thus the number of nucleation sites, is the cause of the variability in the observed nucleation methods and amount of platinum deposited. Oxidizing HOPG with either ozone gas or electrochemical methods results in Pt depositing on the basal plane of the substrate. Electrochemically depositing onto ozone oxidized HOPG resulted in an increase in deposition reproducibility compared to freshly cleaved HOPG. Conversely, electrochemical deposition onto electrochemically oxidized HOPG proved to be highly irreproducible as is was greatly dependent on the extent of electrochemical oxidation which is in turn dependant on the number of step edges and defects found on the HOPG substrate.

8.2 IMPREGNATION AND THERMAL DECOMPOSITION OF PLATINUM ONTO HOPG

Impregnation and thermal decomposition was studied as a alternative method to electrochemical deposition to form Pt nano-catalysts without the use of stabilizers. The nano-catalysts were prepared on freshly cleaved, ozone oxidized, and electrochemically oxidized HOPG. Impregnation and thermal decomposition of the Pt precursor salt onto

freshly cleaved and oxidized HOPG produced well dispersed nano-catalysts that did not agglomerate during the deposition process. Pt nano-catalysts were confined to step edges on the freshly cleaved HOPG while they were distributed over the basal plane on the oxidized HOPG. This confirms our previous finding, when studying electrochemical deposition on freshly cleaved and oxidized HOPG, that oxidation of HOPG produces nucleation site on the basal plane. TEM analysis after CO_{ads} stripping voltammetry of Pt nano-catalysts formed onto freshly cleaved and electrochemically oxidized HOPG indicates that the catalysts were larger compared to the "as-prepared" samples. This suggests that either the catalyst agglomerated during CO_{ads} stripping voltammetry or deposition is not a reproducible process on freshly cleaved and electrochemically oxidized HOPG. Impregnation and thermal decomposition onto ozone oxidized HOPG, however, produced Pt nano-catalysts that are stable against agglomeration during CO_{ads} stripping voltammetry. Impregnation and thermal decomposition onto ozone oxidized HOPG is also a reproducible nano-catalysts preparation technique.

8.3 ACTIVITY OF THE PREPARED ELECTRODES TOWARDS THE ELECTROCHEMICAL OXIDATION OF ADSORBED CARBON MONOXIDE

The activity of six different types of Pt/HOPG electrodes towards the electrochemical oxidation of CO_{ads} were tested. It was found that the methods of substrate pre-treatment studied in this work (freshly cleaved, ozone oxidized, or electrochemically oxidized) did not affect the activity of the electrodes to the electro-oxidation of CO_{ads}. In general it was found that Pt/HOPG electrodes prepared by electrochemical deposition using short deposition times (< 10 s) were less active, i.e. they showed slower kinetics, than polycrystalline Pt foil or electrodes prepared by thermal decomposition.

The onset potential for the electro-oxidation of CO_{ads} was shifted to more anodic potentials for electrodes prepared by electrochemical deposition using short deposition times. The slower kinetics may have resulted from the slow adsorption of activated water, $Pt(OH)_{ads}$, the slow surface diffusion of CO_{ads}, or the slow recombination reaction of $Pt(OH)_{ads}$ with $Pt(CO)_{ads}$. Unfortunately stripping voltammetry does not provide sufficient information to determine which step is the rate determining step. Complicating the analysis of this reaction is the fact that during the stripping voltammetry experiment Pt is lost from

the electrode surface. To determine if the loss of Pt is the cause of the positive shift in the onset potential, Pt/HOPG electrodes were prepared by electrochemical deposition using long deposition times, i.e. 100 and 900 s. Neither of these electrodes showed significant loss of Pt, thus their kinetics towards the electro-oxidation of CO_{ads} is not complicated by the simultaneous loss of Pt. The Pt/HOPG electrode prepared using short deposition times, < 10 s, and the electrode prepared using 100 s of deposition time also showed slower kinetics than polycrystalline foil. Thus clearly showing the slow kinetics results from the unique surface structure of the Pt deposits, and not the loss of Pt from the electrode.

A trend of improving CO_{ads} oxidation kinetics was observed when comparing the Pt/HOPG electrodes prepared at short times, < 10 s, to the electrode prepared using 100 s, to the electrode prepared with 900 s of deposition time. In fact, the Pt/HOPG electrode prepared with 900 s of deposition time had faster kinetics towards the electro-oxidation of CO_{ads} than polycrystalline Pt foil. This result illustrates the versatile nature of electrochemical deposition as a method to prepared electrodes; by varying a parameter as simple as deposition time catalysts of varying activity towards the electro-oxidation of CO_{ads} can be prepared.

The electrodes prepared by impregnation followed by thermal decomposition showed improved kinetics towards the electro-oxidation of CO_{ads} compared to the electrodes prepared by electrochemical deposition using short deposition times, < 10 s. This was demonstrated by the shift to less anodic potential of the electro-oxidation onset. From the stripping voltammogram it appears that the Pt deposits on the Pt/HOPG electrodes prepared by impregnation followed by thermal decomposition are polycrystalline. For example, the oxidation peak shows a peak doublet (or shoulder) typical of polycrystalline foil and the second sweep of the stripping voltammograms show the typical $H_{ads/des}$ and Pt oxidation reduction peaks of polycrystalline Pt foil.

8.4 ELECTROCHEMICAL STABILITY OF THE PREPARED ELECTRODES

The electrochemical stability of six different Pt/HOPG electrodes were tested. Stability against Pt surface area loss was determined by comparing successive CO_{ads} stripping charges. It was found that for a given substrate pre-treatment, the electrodes prepared by impregnation and thermal decomposition were comparatively more stable than the electrodes

prepared by electrochemical deposition, regardless of the substrate pre-treatment. For a given deposition method, the sample prepared on ozone oxidized HOPG proved to be the most stable, followed by electrochemical oxidation, and finally freshly cleaved HOPG was the least.

High resolution TEM analysis showed that the Pt particles formed by impregnation followed by thermal decomposition onto ozone oxidized HOPG are located in the pits generated by ozone oxidation. The Pt catalysts for these electrodes are in part stabilized by a physical interaction between the particles and the pit in which they are situated.

Interactions between the deposited platinum and the substrate for the six different electrodes were analyzed by X-ray photoelectron spectroscopy, (XPS). The XPS Pt 4f spectra of all six prepared Pt/HOPG electrodes were shifted to higher binding energies compared to bulk Pt metal. This positive shift indicates that the prepared catalysts are interacting with defect sites on the HOPG surface, probably through the formation of Pt-C bonds. For the electrodes prepared using oxidized HOPG, the Pt 4f spectra of the electrodes prepared by impregnation and thermal decomposition where shifted to higher binding energies than the Pt 4f spectra of the electrodes prepared by electrochemical deposition. Of the three samples prepared by impregnation and thermal decomposition, the Pt 4f spectra of Pt/HOPG-O_3 electrode displayed the highest shift in binding energies compared to Pt/HOPG-E or Pt/HOPG-FC electrodes. Of the six electrodes prepared, the Pt/HOPG-O_3 electrode prepared by impregnation and thermal decomposition had the greatest amount of interaction between the deposited Pt and the carbon support, probably in the form of Pt-C bonds. The XPS results indicate that the superior electrochemical stability of the thermally decomposed Pt/HOPG-O_3 electrodes results from the chemical interaction between the Pt catalyst and the carbon substrate.

Impregnation and reduction pathways were determined by XPS analysis of various samples prepared to represent the various stages of the impregnation and thermal decomposition process. From this analysis, it was determined that during impregnation, Pt^{2+} ions interact with C=C ligand sites forming Pt–C bonds. XPS analysis shows that chloride is not present on the sample after the impregnation and/or reduction steps indicating that chloride ions are volatilized, possibly as Cl_2. During the reduction step, Pt–Pt bonds form at the expense of some of the Pt–C bonds. However, some Pt–C bonds remain as indicated by

the positive shift of the Pt 4f spectra for Pt/HOPG electrodes prepared by impregnation followed by thermal decomposition.

8.5 FUTURE WORK

8.5.1 HRTEM analysis of Pt/HOPG electrodes prepared by impregnation followed by thermal decomposition after electrochemical testing.

One of the unique results of the Pt/HOPG electrodes prepared by impregnation followed by thermal decomposition is that the "formed particles" are irregular in shape. This contrasts with findings in the literature that platinum nanoparticles are generally truncated octahedral, due to this shape having a minimum surface energy.[89] It would be interesting to determine by HRTEM if the particles maintain their irregular shape, or if they change to the truncated octahedral shape during electrochemical testing.

Successive stripping voltammograms of carbon monoxide adsorbed (CO_{ads}) to Pt/HOPG electrodes prepared by impregnation followed by thermal decomposition have similar onset potentials and stripping peak shapes. This indicates that the surface of the Pt nanoparticles do not change during the successive experiments, at least not in a manner that effects the electro-oxidation of CO_{ads}. The consistency in the CO_{ads} stripping voltammograms leads one to hypothesize that the HRTEM results would not show a great change in particle shape after successive CO_{ads} stripping voltammograms. However, since Ostwald ripening is most prevalent in the double layer region, it could be hypothesized that the particles would change shape and size if the potential were held within this region for several hours.

8.5.2 Electrochemical deposition of Pt(II) complexes onto HOPG.

The results presented in this thesis indicate that Pt/HOPG electrodes prepared by impregnation followed by thermal decomposition are more stable than Pt/HOPG electrodes prepared by electrochemical deposition. This enhanced stability is partially due to the platinum - carbon bond established in the impregnation step. The Pt(II)–C bond is best described by the Dewar-Chatt-Duncanson model.[138] Olefins bind to transition metals via their π orbitals by donating electron density into an empty Pt d-orbital. The bond is stabilized by the donation of electron density from an occupied Pt d-orbital to the olefin's π^* orbital.

Electrochemical deposition of Pt onto HOPG presented in this thesis was achieved using $Pt(IV)Cl_4$. It is probable that during electrochemical deposition, the Pt(II) intermediate does not exist sufficiently long for the formation of Pt(II)–C bond. Using $K_2Pt(II)Cl_4$ as the platinum source for electrochemical deposition may allow for the formation of Pt(II)–C bond before reduction, which may in turn result in a more stable Pt/HOPG electrode. Disproportionation reactions should not be an issue at sufficiently dilute platinum salt concentrations since the X-ray photoelectron spectroscopy analysis of K_2PtCl_4 impregnated on HOPG, presented in Chapter Seven, shows that Pt(0) does not form in solution. However the application of a protective potential, applied before the reduction potential to ensure that platinum does not spontaneously deposit onto HOPG, may prevent the interaction of $Pt(II)Cl_4^{2+}$ with the HOPG surface. Experimental conditions may need to be modified.

8.5.3 Test the activity of Pt/HOPG electrodes towards oxygen reduction.

The oxygen reduction reaction, ORR, requires optimization to allow for commercialization of low temperature fuel cell. For example, the US Department of Energy has set Pt loading targets that require a four-fold increase in activity towards the ORR, compared to present Pt/C catalyst, to maintain high energy conversion efficiency at medium to low power levels.[140] It would be interesting to compare the activity of all six Pt/HOPG electrodes towards the ORR. These experiments would be complicated by the instability of the Pt/HOPG electrodes prepared by electrochemical deposition. For example, it is expected that the reduction current will decrease with time for the Pt/HOPG electrodes prepared by electrochemical deposition because the platinum is lost from the electrode surface.

Chapter Nine

Claims to Original Research

The following claims are made to original research which have been discussed in this thesis.

1) The effect of oxidizing HOPG on the electrochemical deposition of platinum was studied extensively in this work. Two different mechanism of oxidizing HOPG were compared and contrasted; ozone oxidation and electrochemical oxidation. It was found that since ozone oxidation generated defects on the HOPG surface it homogenized the number of nucleation sites from one sample to the next, thus, increasing electrochemical deposition reproducibility. Whereas, electrochemical oxidation, which occurred at naturally occurring defects and step edges, amplified the differences in the number of nucleation sites from one sample to the next, thus, decreasing electrochemical deposition reproducibility. The amount of Pt electrodeposited onto electrochemically oxidized HOPG was found to be dependent on the extent of HOPG oxidation, i.e. oxidation charge, and was not directly related to oxidation time.
2) Electrochemical deposition of Pt onto HOPG was found to form platinum clusters regardless of the substrate pre-treatment (i.e. freshly cleaved, ozone oxidized, or

electrochemically oxidized HOPG. HRTEM analysis found that the deposits formed by agglomeration of particles.

3) The adsorbed carbon monoxide (CO_{ads}) electro-oxidation kinetics of Pt/HOPG electrodes prepared by electrochemical deposition were easily controlled by controlling the deposition time. For example, electrodes prepared using very short deposition times, < 10 s, have CO_{ads} oxidation onset potentials shifted to more anodic potentials compared to polycrystalline Pt foil. Increasing the deposition time to 100 s resulted in an electrode with CO_{ads} oxidation onset potentials shifted anodically to polycrystalline foil, but not shifted as greatly as for the electrodes prepared with deposition times < 10 s. Furthermore, the CO_{ads} oxidation onset potential is sifted *less* anodically, compared to polycrystalline Pt foil, for electrodes prepared using very long deposition times, 900 s. Thus, the kinetics for the CO_{ads} electro-oxidation reaction can be controlled by controlling the deposition time.
4) Pt/HOPG electrodes prepared by impregnation and thermal decomposition onto HOPG formed individual nano-catalyst regardless of the substrate pre-treatment. It was found that oxidation of the HOPG surface was required to allow for nucleation of Pt on the basal plane of HOPG. Impregnation and thermal decomposition onto ozone oxidized HOPG proved to be a reproducible method of preparing a Pt/HOPG electrode. Conversely, freshly cleaved and electrochemically oxidized HOPG either did not allow for a reproducible deposition technique or did not stabilize the catalyst against agglomeration during CO_{ads} stripping voltammetry.
5) CO_{ads} stripping characteristics for Pt/HOPG electrodes were very different for Pt/HOPG electrodes prepared by impregnation and thermal decomposition compared to electrodes prepared by electrochemical deposition. The substrate pre-treatment did not appear to influence the activity of the prepared catalyst towards electro-oxidation of CO_{ads}. For all Pt/HOPG electrodes prepared by impregnation followed by thermal decomposition, the CO_{ads} oxidation onset potential was shifted to less anodic potentials compared to polycrystalline Pt foil, indicating faster oxidation kinetics.
6) Short-term electrochemical stability of the six different types of Pt/HOPG electrodes were studied by comparing successive CO_{ads} stripping charges. It was found that Pt/HOPG electrodes prepared by impregnation followed by thermal decomposition

were more stable than electrodes prepared by electrochemical deposition. For a given deposition technique, it was found that ozone oxidation was the most effective HOPG pre-treatment at stabilizing the Pt catalysts, followed by electrochemical oxidation, and freshly cleaved HOPG was found to be the least effective. X-ray photoelectron spectroscopy (XPS) analysis indicated that the Pt 4f spectra for all Pt/HOPG were shifted to higher binding energies. However, the extent of the positive binding energy shift mirrored the stability results. That is to say, Pt 4f spectra for Pt/HOPG electrodes prepared by impregnation and thermal decomposition onto oxidized HOPG were shifted to higher binding energies than electrodes prepared by electrochemical deposition onto oxidized HOPG. For a given deposition technique, Pt/HOPG electrodes prepared on ozone oxidized HOPG had the greatest positive Pt 4f binding energy shift, followed by electrochemical oxidation, and finally freshly cleaved HOPG (which had the smallest positive binding energy shift). The electrode with the greatest shift was the one prepared by impregnation followed by thermal decomposition onto ozone oxidized HOPG, this electrode was also the electrode with the greatest short-term electrochemical stability. The positive shift in binding energy is attributed to the formation of Pt-C bonds via the Dewar-Chatt-Duncanson model. It is the extent of this chemical interaction between the Pt catalysts and the HOPG substrate that is responsible for the short-term electrochemical stability.

7) The impregnation and thermal decomposition pathway was proposed based on analysis of XPS Pt 4f spectra of; (1) K_2PtCl_4, (2) Pt/HOPG samples after impregnation with K_2PtCl_4 + HCl, and (3) after thermal decomposition of K_2PtCl_4 + HCl. It was concluded that during impregnation Pt(II) forms a chemical bond with a ligand site on HOPG (principally C=C). This reactions is a substitution reaction that releases Cl^- from the precursor salt as Cl_2. Reduction of platinum results in some Pt-C bonds breaking to allow for the formation of Pt-Pt bonds.

Chapter Ten

References

1 R. L. Burwell, *ACS Symposium Series 222*, B. H. Davis and W. P. Hettinger, Editors, p. 3-12. American Chemical Society, USA (1983).

2 C. H. Bartholomew and R. J. Farrauto, *Fundamentals of Industrial Catalytic Processes*, p. 5, Wiley, New Jersey, (2006).

3 Ref. 2, p. 11.

4 Ref. 2, p. 570.

5 Ref. 2, p. 489.

6 Ref. 2, p. 575.

7 Ref. 2, p. 710.

8 A. Krishna, C. Hsieh, A. E. English, T. Pecoraro and C. Kuehler, *Hydrocarb. Proc.*, **Nov**, 59, (1991).

9 T. Zalioubovskaia, A. Gedeon, J. Fraissard, E. Fadchenko and B. Nefedow, in *Fluid Catalytic Cracking , Materials and Processes, ACS Symposium Series* M.L Occelli

and P. O'Connor, Editors, p. 139, American Chemical Society, Washington DC (1994).

10 W. Vielstich, in *Handbook of Fuel Cells; Fundamentals, Technology, and Applications*, Vol. 1, W. Vielstich, A. Lamm and H. A. Gasteiger, Editor, p. 28, Wiley, Italy (2003).

11 N. Alonso-Vante, *Fuel Cells*, **06**, 182 (2006).

12 T. Teranishi, M. Hosoe, T. Tanaka, M. Miyake, *J. Phys. Chem. B*, **103**, 3818 (1999).

13 T. Vad, H.-G. Haubold, N. Waldoèfner and H. Boènnemann, *J. Appl. Crystallogr.*, **35**, 459 (2002).

14 O. V. Cherstiouk, P. A. Simonov, V. I. Zaikovskii and E. R. Savinova, *J. Electroanal. Chem.*, **554-555**, 241 (2003).

15 F. Maillard, M. Eikerling, O. V. Cherstiouk, S. Schreier, E. Savinova and U. Stimming, *Faraday Discuss.*, **125**, 357 (2004).

16 H. Liu, C. Song, L. Zhang, J. Zhang, H. Wang, D. Wilkinson and H. Liu, *J. Power Sources*, **155**, 95 (2006).

17 P. Gélin and M. Primet, *Appl. Catal., B*, **39**, 1 (2002).

18 A. J. Dickinson, L. P. L. Carrette, J. A. Collins, K. A. Friedrich and U. Stimming, *Electrochim. Acta*, **47**, 3733 (2002).

19 F. J. Rodriguez, P. J. Sebastian, O. Solorza and R. Perez, *Int. J. Hydrogen Energy*, **23**, 1030 (1998).

20 Y. Zhang and C. Erkey, *J. Supercrit. Fluids*, **38**, 252 (2006).

21 P. W. Atkins, *Physical Chemistry*, p. 706, 4th ed., Oxford University Press, Oxford (1990).

22 S. Eriksson, U. Nylen, S. Rojas and M. Boutonnet, *Appl. Catal., A*, **265**, 207 (2004).

23 V. Uskoković and M. Drofenik, *Adv. Colloid Interface Sci.*, **vol**, page (2007).

24 I. Lisieck and M. P. Pileni, *J. Am. Chem. Soc.*, **115**, 3887 (1993).

25 L. Xiong and A. Manthiram, *Solid State Ionics*, **176**, 385 (2005).

26 D. R. M. Godoi, J. Perez and H. M. Villullas, *J. Electrochem. Soc.*, **154**, B474 (2007).

27 J. Kizling, *PhD Thesis*, Royal Institute of Technology, Stockholm (1991).

28 M. Yang, Y. Yang, Y. Liu, G. Shen and R.Yu *Biosens. Bioelectron.* **21**, 1126 (2006).

29 I. E. Ko, *Preparation of Solid Catalysts*, G. Ertl, J. Weitkamp and H. Knözinger, Editors, p. 85–98, Wiley-VCH, Weinheim (1999).

30 L. M. Bronstein, *Top. Curr. Chem.*, **226**, 55 (2003).

31 E. J. McLeod and V. I. Birss. *Electrochim. Acta.*, **51**, 684 (2005).

32 J. Marie, S. Berthon-Gabry, P. Achard, M. Chatenet, A. Pradourat and E. Chainet, *J. Non-Cryst. Solids*, **350**, 88, (2004).

33 K. Shimazu, D. Weisshaar and T. Kuwana, *J. Electroanal. Chem.*, **223**, 223 (1987).

34 J. V. Zoval, J. Lee, S. Gorer and R. M. Penner, *J. Phys. Chem. B*, **102**, 116 (1998).

35 G. Lu and G. Zangari, *J. Phys. Chem. B*, **109**, 7998 (2005).

36 O. Antoine and R. Durand, *Solid-State Lett.*, **4**, A55 (2001).

37 Z. He, J. Chen, D. Liu, H. Tang, W. Deng and Y. Kuang, *Mater. Chem. Phys.*, **85**, 396 (2004).

38 N. Georgolios, D. Jannakoudakis and P. Karabinas, *J. Electroanal. Chem.*, **264**, 235 (1989).

39 E. Budevski, G. Staikov and W. J. Lorenz, *Electrochemical Phase Formation and Growth*, R. C. Alkire, H. Gerischer, D. M. Kolb and C. W. Tobias, Editors, p. 1, VCH, New York (1996).

40 R. Greef, R. Peat, L. M. Peter, D. Pletcher and J. Robinson, *Instrumental Methods in Electrochemistry*, T. J. Kemp, Editor, p. 283, Ellis Horwook Limited, New York, (1985).

41 X. Xue, C. Liu, W. Xing and T. Lu, *J. Electrochem. Soc.*, **153**, E79 (2006).

42 P. S. Patil, *Mater. Chem. Phys.*, **59**, 185 (1999).

43 R. Mueller, L. Mädler and S. E. Pratsinis, *Chem. Eng. Sci.*, **58**, 1969 (2003).

44 R. Jairath, A. Jain, R. D. Tolles, M. J. Hampden-Smith and T. T. Kodas, *The Chemistry of Metal CVD*, T. T. Kodas and M. J. Hampden-Smith, Editors, p. 30, VCH, . New York (1994).

45 P. Sivakumar, R. Ishak and V. Tricoli, *Electrochim. Acta*, **50**, 3312 (2005).

46 T. T. Kodas and M. J. Hampden-Smith, *The Chemistry of Metal CVD*, T. T. Kodas and M. J. Hampden-Smith, Editors, p. 432, VCH, . New York (1994).

47 E. Antolini, J. R. C. Salgado, R. M. dda Silva and E. R. Gonzalez, *Mater. Chem. Phys.*, **101**, 395 (2007).

48 K. S. S. Harsha, *Principles of Physical Vapor Deposition of Thin Films*, p. 381, Elsevier, New York (2006).

49 D. Zhong, B. Mishra, J. J. Moore and A. Madan, *Surf. Eng.*, **20**, 196 (2004).

50 R. Woods, *Electroanalytical Chemistry*, Vol. 9, A. J. Bard, Editor, p. 1, Marcel Dekker, New York, (1980).

51 D. Chescoe and P. J. Goodhew, *The Operation of the Transmission Electron Microscope*, Oxford University Press, Oxford (1984).

52 Ref 21, p. 286.

53 J. Tersoff and D. R. Hamann, *Phys. Rev. B*, **31**, 805 (1985).

54 S. J. Schmieg and D. N. Belton, *Surf. Sci. Spectra* **1**, 333 (1993).

55 R. I. Masel, *Chemical Kinetics and Catalysis*, p. 876, Wiley-Interscience, Toronto (2001).

56 J. L. Zubimendi, L. Vazques, P. Ocón, J. M. Vara, W. E. Triaca, R. C. Salvarezza and A. J. Arvia, *J. Phys. Chem.*, **97**, 5095 (1993).

57 I. Lee, K.-Y. Chan and D.L. Phillips, *Appl. Surf. Sci.*, **136**, 321 (1998).

58 G. Lu and G. Zangari, *Electrochim. Acta*, **51,** 2531 (2006).

59 S. C. Roy, P. A. Christensen, A. Hamnett, K. M. Thomas and V. Trapp, *J. Electrochem. Soc.*, **143**, 3073 (1996).

60 P. K. Shen and A. C. C. Tseung, *J. Electrochem. Soc.*, **141**, 3082 (1994).

61 B. Scharifker and G. Hills, *Electrochim. Acta*, **28**, 879 (1983).

62 L. Heerman and A. Tarallo, *J. Electroanal. Chem.*, **470,** 70 (1999).

63 B. R. Scharifker and J. Mostany, *J. Electroanal. Chem.*, **177**, 13 (1984).

64 M. E. Hyde and R. G. Compton, *J. Electroanal. Chem.*, **549,** 1 (2003).

65 H. Halvorsen, C. Bock, B. MacDougall and D. Wang. *ECS Transactions - Washington, DC*,**11**, (2008).

66 A. Tracz, G. Wegner and J. P. Rabe, *Langmuir*, **19**, 6807 (2003).

67 H. Chang and A. J. Bard, *J. Am. Chem. Soc.*, **112**, 4598 (1990).

68 B. Zhang and E. Wang, *Electrochim. Acta*, **40**, 2627 (1995).

69 K. W. Hathcock, J. C. Brumfield, C. A. Goss, E. A. Irene and R. W. Murray, *Anal. Chem.*, **67**, 2201 (1995).

70 B. Zhang and E. Wang, *J. Electroanal. Chem.*, **399**, 83 (1995).

71 C. A. Goss, J. C. Brumfield, E. A Irene and R. W. Murray, *Anal. Chem.*, **65**, 1378 (1993).

72 H-X You, N. M. D. Brown and K. F. Al-Assadi, *Surf. Sci.*, **284**, 263 (1993).

73 M. J. Nowakowski, J. M. Vohs and D. A. Bonnell, *Surf. Sci. Lett.*, **271**, L351 (1992).

74 I. Lopez-Salido, D. C. Lim and Y. D. Kim, *Surf. Sci.*, **588**, 6 (2005).

75 J. Fournier, D. Miousse, L. Brossard and H. Menard, *Mater. Chem. Phys.*, **42**, 181 (1995).

76 E. A. Eklund, E. J. Snyder and R. S. Williams, *Surf. Sci.*, **285**, 157 (1993).

77 A. Stabel, K. Eichhorst-Gerner, J. P. Rabe and A. R. Gonzalez-Elipe, *Langmuir*, **14**, 7324 (1998).

78 W. R. Salaneck and C. F. Brucker, *Phys. Rev. B*, **24**, 5037 (1981).

79 M. Wahlqvist and A. Shchukarev, *J. Electron. Spectrosc. Relat. Phenom.*, **156-158**, 310 (2007).

80 G. Beamson and D. Briggs, *High Resolution XPS of Organic Polymers; The Scienta ESCA 300 Database*, p. 281, John Wiley & Sons, Toronto (1992).

81 E. Gileadi, *Electrode Kinetics for Chemists, Chemical Engineers, and Materials Scientists*, p. 6, Wiley–VCH, New York (1993).

82 Y. Song, Y-B. Jiang, H. Wang, D. A. Pena, Y. Qiu, J. E. Miller and J. A. Shelnutt, *Nanotechnology*, **17**, 1300 (2006).

83 S. R. de Miguel, O. A. Scelza, M. C. Roman-Martinez, C. Salinas-Martinez de Lecea, D. Cazorla-Amorosand and A. Linares-Solano, *Appl. Catal., A.* **170**, 93 (1998).

84 P. A. Simonov, A. V. Romanenko, I. P. Prosvirin, G. N. Kryukova, A. L. Chuvilin, S. V. Bogdanov, E. M. Morozand and V. A. Likholobov, *Stud. Surf. Sci. Catal*, **118**, 15 (1998).

85 M. Herberkhold, *Metal π-Complexes Vol. 2: Complexes with Mono-Olefinic Ligands*, p. ##, Elsevier, Amsterdam (1972).

86 C. N. R. Rao, H. K. N. Aiyer, T. Arunarkavalli and G. U. Kulkarni, *Catal. Lett.*, **23**, 37 (1994).

87 S. Lee, H. Permana and K. Y. S. Ng, *J. Vac. Sci. Technol. B*, **10**, 561 (1992).

88 K. L. Yeung and E. E. Wolf, *Catal. Lett.*, **23**, 213 (1992).

89 W. Romanowski, *Surf. Sci.* **18**, 373 (1969).

90 B. MacDougall and M. Gattrell, in *Handbook of fuel cells : fundamentals, technology, and applications*, Vol. 2 Electrocatalysis, W. Vielstich, A. Lamm and H. A. Gasteiger, Editors, p. , Wiley, New York, (2003).

91 B. Beden, C. Lamy, N. R. De Tacconi and A. J. Arvia, *Electrochim. Acta*, **35**, 691 (1990).

92 E. R. Savinova, N. P. Levedeva, P. A. Simonoc and G. N. Kryukova, *Russ. J. Electrochem.* **36**, 952 (2000).

93 Z. Siroma, K. Ishii, K. Yasuda, Y. Mayazaki, M. Inaba and A. Tasaka, *Electrochem. Commun.* **7**, 1153 (2005).

94 K. Kinoshita, *Carbon: Electrochemical and Physioco-chemical Properties*, p. 187, Wiley, New York (1988).

95 B. Adreaus and M. Eikerling, *J. Electroanal. Chem.*, **607**, 121 (2007).

96 M. T. M. Koper, T. E. Shubina and R. A. Van Santen, *J. Phys. Chem. B*, **106**, 686 (2002).

97 S. Gilman, *J. Phys. Chem.*, **66**, 2657 (1962).

98 T. Iwasita, *Handbook of Fuel Cells – Fundamentals, Technology and Applications* V2: *Electrocatalysis*, W. Vielstich, H. A. Gasteiger and A. Lamm, Editors, p. 603, Wiley, New York (2003).

99 F. Maillard, S. Schreier, M. Hanzlik, E. R. Savinova, S. Weinkauf and U. Stimming, *Phys. Chem. Chem. Phys.*, **7**, 385 (2005).

100 Y. Takasu, Y. Fujii, K. Yasuda, Y. Iwanaga and Y. Matsuda, *Electrochim. Acta*, **34,** 453 (1989).

101 R. V. Hardeveld and F. Hartog, *Surf. Sci.*, **15,** 189 (1969).

102 K. Yamamoto, D. M. Kolb, R. Kotz and G. Lehmpfuhl, *J. Electroanal. Chem.*, **96**, 233 (1979).

103 M. Arenz, K. J. J. Mayrhofer, V. Stamenkovic, B. B.Bilzanac, T. Tomoyuki, P. N. Ross and N. M. Marković, *J. Am. Chem. Soc.*, **127**, 6819 (2005).

104 N. M. Marković and P. N. Ross, Jr., *Surf. Sci. Rep.*, **45**, 117 (2002).

105 N. M. Marković, T. J. Schmidt, B. N. Grgur, H. A. Gasteiger, R. J. Behm and P. N. Ross, *J. Phys. Chem. B*, **103**, 8568 (1999).

106 B. Andreaus, F. Maillard, J. Kocylo, E. R. Savinova and M. Eikerling, *J. Phys. Chem. B*, **110**, 21028 (2006).

107 O. V. Cherstiouk, P. A. Simonov and E. R. Savinova, *Electrochim. Acta*, **48**, 3851 (2003).

108 H. Gleiter, *Nanostruct. Mater.*, **1**, 1 (1992).

109 K. Kano and B. Uno, *Anal. Chem.*, **65**, 1088 (1993).

110 J. L. Gómez de la Fuente, S. Rojas, M. V. Martínez-Huerta, P. Terreros, M. A. Peña and J. L. G. Fierro, *Carbon,* **44**, 1919 (2006).

111 S. Guerin, B. E. Hayden, C. E. Lee, C. Mormiche, J. R. Owen, A. E. Russell, B. Theobald and D. Thompsett, *J. Comb. Chem.*, **6**, 149 (2004).

112 B. Beden, S. Bilmes, C. Lamy and J.M. Leger, *J. Electroanal. Chem.*, **149**, 295 (1983).

113 J-M. Leger, B. Beden and C. Lamy *J. Electroanal. Chem.*, **170**, 305 (1984).

114 Y. Shao-Horn, W. C. Sheng, S. Chen, P. J. Ferreira, E. F. Holby and D. Morgan, *Top Catal*, **46**, 285 (2007).

115 P. J. Ferreira, G. J. la O', Y. Shao-Horn, D. Morgan, R. Makharia, S. Kocha and H. A. Gasteiger, *J. Electrochem. Soc.*, **152**, A2256 (2005).

116 A. V. Virkar and Y. Zhou, *J. Electrochem. Soc.*, **154**, B540 (2007).

117 Q. Xu, T. He and D. O. Wipf *Langmuir* **23**, 9098 (2007).

118 Q. Xu, E. Kreidler, D. O. Wipf and T. He, *J. Electrochem. Soc.* **155** B228 (2008).

119 X. P. Wang, R. Kumar and D. J. Myers, *Elecytrochem. Solid-State Lett.*, **9**, A225 (2006).

120 X. P. Wang, R. Kumar, N. Kariuki and D. J. Mayers, *J. Electrochem. Soc.* (unpublished)

121 A. Honji, T. Mori, K. Tamura and Y. Hishinuma, *J. Electrochem. Soc.*, **135**, 355 (1988).

122 P. Bindra, S. J. Clouser and E. Yeager, *J. Electrochem. Soc.*, **126**, 1631 (1979).

123 G. Jerkiewicz, G. Vatankhah, J. Jessard, M. P. Soriaga and Y. S. Park, *Electrochimica Acta*, **49**, 1451 (2004).

124 M. Alsabet, M. Grden and G. Jerkiewicz, *J. Electroanal. Chem.*, **589**, 120 (2006).

125 K-I. Ota, Y. Koizumi, S. Mitsushima and N. Kamiya, *ECS Trans*, **3**, 619 (2006).

126 C. C. Granqvist and R. A. Buhrman, *J. Catal*, **42**, 477 (1976).

127 E. Ruckenstein and B. Pulvermacher, *J. Catal*, **29**, 224 (1973).

128 G. M. Bancroft, I. Adams, L. L. Coatsworth, C. David Bennewitz, J. D. Brown and W. Westwood. *Anal. Chem.* **47**, 586 (1975).

129 G. K. Wertheim, S. B. Di Cenzo and D. N. E. Buchanan *Phys. Rev., B* **33**, 5384 (1986).

130 P. Marcus and C. Hinnen, *Surf. Sci.*, **392**, 134 (1997).

131 K. Fauth, M. Heßler, D. Batchelor and G. Schutz, *Surf. Sci.*, **529**, 397 (2003).

132 J. Escard, B. Pontvianne, M. T. Chenebaux and J. Cosyns *Bull. Soc. Chim. Fr.*, 2400 (1975).

133 J. P. Contour, G. Mouvier, M. Hoogewijs and C. Leclere *J. Catal.*, **48**, 217 (1977).

134 Sh. K. Shaikhutdinov, M. Schildenberger, M. Noeske and G. Mestl *React. Kinet. Catal. Lett*, **67**, 129 (1999).

135 D-Q. Yang, G.-X. Zhang, E. Sacher, M. José-Yacamán and N. Elizondo *J. Phys. Chem. B*, **110**, 8348 (2006).

136 A. Howells, T. Harris, K. Sashikata, G. S. Chottiner and D. A. Scherson *Solid State Ionics*, **94**, 115 (1997)

137 H. E. van Dam and H. Van Bekkum *J. Catal.*, **131**, 335 (1991).

138 M. Dewar *Bull. Soc. Chim. Fr.*, **18**, C79 (1951).

139 J. Chatt and L. A. Duncanson, J. Chem. Soc., 2939 (1953).

140 C. He, S. Desai, G. Brown and S. Bollepalli, *Electrochem. Soc. Interface*, **3**, 41 (2005).